# Von Hippel-Lindau-Protein, cAMP-responsives Element-bindendes Protein- und Hypoxie-abhängige Veränderungen im Metabolismus des Nierenzellkarzinoms

Dissertation

zur Erlangung des

Doktorgrades der Naturwissenschaften (Dr. rer. nat.)

der

Naturwissenschaftlichen Fakultät I – Biowissenschaften –

der Martin-Luther-Universität

Halle-Wittenberg,

vorgelegt

von Frau Sandra Leisz

geb. am 02.09.1983 in Schkeuditz

Gutachter/in:

1. PD Dr. Hans-Hinrich Kaatz, Institut für Zoologie, Martin-Luther-Universität Halle-Wittenberg
2. Prof. Dr. Barbara Seliger, Institut für Medizinische Immunologie, Martin-Luther-Universität Halle-Wittenberg
3. Prof. Dr. Marina Kreutz, Klinik und Poliklinik für Innere Medizin III, Universität Regensburg

Öffentliche Verteidigung: 13.10.2021

„Dass ich erkenne, was die Welt im Innersten zusammenhält"
Johann Wolfgang von Goethe

„Keine Krankheit kann in einem basischen Milieu existieren. Nicht einmal Krebs."
Otto Warburg

gewidmet meiner Familie

**Abbildungs- und Tabellenverzeichnis ..... I**
**Abkürzungsverzeichnis ..... II**
**1 Einleitung ..... 1**
1.1 Charakteristika und Therapie des Nierenzellkarzinoms ..... 1
1.2 Molekulare Pathogenese des NZK ..... 2
1.3 Der Transkriptionsfaktor HIF ..... 5
1.4 Der Transkriptionsfaktor CREB ..... 6
1.5 Veränderungen des Metabolismus im Tumor ..... 6
1.5.1 Der „Warburg Effekt“ ..... 6
1.5.2 Auswirkungen des „Warburg Effekts“ auf die Immunantwort ..... 9
1.6 Identifizierung von intra- und extrazellulären Biomarkern des NZK ..... 10
**2 Ziele der Arbeit ..... 12**
**3 Beschreibung der publizierten Manuskripte ..... 13**
3.1 „Distinct von Hippel-Lindau gene and hypoxia-regulated alterations in gene and protein expression patterns of renal cell carcinoma and their effects on metabolism“ ..... 13
3.2 „VHL-dependent alterations in the secretome of renal cell carcinoma: Association with immune cell response?“ ..... 15
3.3 „Hypoxia-mediated alterations and their role in the HER-2/neu-regulated CREB status and localization“ ..... 17
3.4 „Linking CREB function with altered metabolism in murine fibroblast-based model cell lines” ..... 19
**4 Manuskripte ..... 21**
4.1 „Distinct von Hippel-Lindau gene and hypoxia-regulated alterations in gene and protein expression patterns of renal cell carcinoma and their effects on metabolism“ ..... 21
4.2 „VHL-dependent alterations in the secretome of renal cell carcinoma: Association with immune cell response?“ ..... 32
4.3 „Hypoxia-mediated alterations and their role in the HER-2/neu-regulated CREB status and localization“ ..... 50
4.4 „Linking CREB function with altered metabolism in murine fibroblast-based model cell lines” ..... 74
**5 Diskussion ..... 99**
5.1 Diskrepanz und Konvergenz des VHL-, CREB-, und Sauerstoff-gesteuerten Expressionsmusters ..... 100
5.2 Der Einfluss von VHL, CREB und Hypoxie auf die Glykolyse ..... 106
5.3 Differentieller Einfluss von VHL, CREB und Hypoxie auf die Atmungskette und die mitochondriale Aktivität ..... 109
5.4 VHL-abhängige Reduktion des Aminosäuremetabolismus ..... 110

5.5 Die Rolle von VHL und Hypoxie im Abbau und Transport von Fettsäuren ..... 112
5.6 VHL-, CREB- und Hypoxie-abhängiger Abbau reaktiver Sauerstoffspezies ..... 113
5.7 Die Auswirkung von VHL-Defizienz, verstärkte CREB-Aktivität oder Hypoxie auf das TME und die Zellen des Immunsystems ..... 116
**6 Zusammenfassung ..... 120**
**7 Ausblick ..... 123**
**8 Literaturverzeichnis ..... 124**
**9 Eigenständigkeitserklärung ..... 140**
**10 Lebenslauf ..... 141**
10.1 Persönliche Daten ..... 141
10.2 Wissenschaftlicher Werdegang ..... 141
10.3 Schulausbildung ..... 142
**11 Publikationen, Vorträge und Fortbildungen ..... 143**
11.1 Publikationen ..... 143
11.2 Ausgewählte Poster ..... 144
11.3 Ausgewählte Vorträge ..... 145
11.4 Auszeichnung ..... 145
11.5 Fortbildungen ..... 145
**12 Danksagung ..... 147**
**13 Anhang ..... 148**

# Abbildungs- und Tabellenverzeichnis

**Abbildung 1: Klassifizierung des Nierenzellkarzinoms (NZK).... 2**
**Abbildung 2: VHL- und Hypoxie-abhängige Funktion des Hypoxie-induzierbaren Faktors.... 3**
**Abbildung 3: Häufigkeit mutierter Gene im kzNZK.... 4**
**Abbildung 4: Einfluss des „Warburg Effektes“ auf das Tumormikromilieu.... 10**
**Abbildung 5: Schematische Übersicht der publizierten Untersuchungen zu den VHL-, Hypoxie-, und CREB-abhängigen Veränderungen im Zellmetabolismus.... 100**
**Abbildung 6: Funktionen der TGM2.... 103**
**Abbildung 7: Validierung der TGM2-Transkript- und Proteinmenge unter Normoxie und Hypoxie.... 104**
**Abbildung 8: Einfluss von Hypoxie und HIF2α-Proteinmenge auf die TGM2-mRNA-Expression.... 105**
**Abbildung 9: VHL-, CREB- und Hypoxie-abhängige differenziell exprimierte Enzyme der Glykolyse.... 109**
**Abbildung 10: VHL-, Hypoxie- und CREB-mediierter ROS-Abbau.... 116**
**Abbildung 11: Interaktion zwischen heterogenen Tumorbereichen mit unterschiedlichem glykolytischen Phänotyp.... 118**
**Abbildung 12: Schematische Zusammenfassung der VHL-, Hypoxie-, und CREB-gesteuerten Deregulation des Zellmetabolismus.... 122**
**Anhang Abbildung 1: Kaplan-Meier-Überlebenskurven.... 148**
**Anhang Abbildung 2: SOD2-Expressionsanalyse.... 148**

**Tabelle 1: Charakteristika von HIF1α und HIF2α.... 5**
**Tabelle 2: Einfluss verschiedener Onkogene und Tumorsuppressorgene auf den Zellmetabolismus.... 8**
**Tabelle 3: Darstellung des prozentualen Eigenanteils der zusammengefassten Manuskripte.... 20**
**Tabelle 4: Auswirkung der Ansäuerung des TME auf Immunzellen.... 117**

# Abkürzungsverzeichnis

| | |
|---|---|
| 2D | Zweidimensional |
| ACC | Acetyl-CoA-Carboxylase |
| ACO | Aconitase |
| ADP | Adenosindiphosphat |
| ALDO | Aldolase |
| Akt | Proteinkinase B |
| AS | Aminosäure |
| ATP | Adenosintriphosphat |
| BAP1 | BRCA1 assoziiertes Protein-1 |
| β2M | Beta-2-Mikroglobulin |
| BRCA | *Breast cancer* |
| CA9 | Carboanhydrase IX |
| cAMP | Cyclisches Adenosinmonophosphat |
| CBP | CREB-bindendes Protein |
| CD | *Cluster of differentiation* |
| CEST | *Chemical exchange saturation transfer* |
| COSMIC | *Catalogue of Somatic Mutations in Cancer* |
| CPT | Carnitin-Palmityltransferase |
| CREB | *cAMP response element-binding protein* |
| CTLA | *Cytotoxic T-lymphocyte-associated protein* |
| CXCR4 | *C-X-C chemokine receptor type 4* |
| DNA | Desoxyribonukleinsäure |
| DST | Dystonin |
| ECHS1 | *Enoyl-CoA hydratase, short chain 1* |
| ELISA | *Enzyme-linked immunosorbent assay* |
| Elk | *Ets like-1 protein* |
| EMT | Epithelial-mesenchymale Transition |
| ENO | Enolase |
| ERK | *Extracellular-signal Regulated Kinases* |
| Ets | *E26 transformation-specific* |
| EV | Extrazelluläre Vesikel |
| FABP | *Fatty acid-binding protein* |
| FAD | Flavinadenindinukleotid |
| FASN | Fettsäuresynthase |
| FH | Fumerathydratase |
| FIH | *Factor inhibiting HIF* |
| FLCN | Folliculin |
| fwd | *Forward* |
| GCS | Glutamyl-Cystein-Synthetase |
| GDP | Guanosindiphosphat |
| GEO | *Gene Expression Omnibus* |
| GLUT1 | Glukosetransporter 1 |
| GMP | Guanosinmonophosphat |
| GPX | Glutathionperoxidase |
| GR | Glutathionreduktase |
| GSH | Glutathion |
| GSS | Glutathionsynthetase |
| GSSG | Glutathiondisulfid |
| GSTP1 | Glutathion-S-Transferase P1 |
| GTP | Guanosintriphosphat |
| h | Stunden |
| HAF | Hypoxie-assoziierter Faktor |

| | |
|---|---|
| HER-2/neu | Humaner epidermaler Wachstumsfaktorrezeptor 2 |
| HIF | Hypoxie-induzierbarer Faktor (*Hypoxia-inducible factor*) |
| HK | Hexokinase |
| HLA | *Human leukocyte antigen* |
| HNF | Hepatozytärer nuklearer Faktor |
| HRE | *Hypoxia-responsive element* |
| Hsp | Hitzeschockprotein |
| ICER | *Inducible cyclic adenosine monophosphate early repressor* |
| IFN | Interferon |
| IHC | Immunhistochemie |
| IL | Interleukin |
| Kat | Katalase |
| KIRC | *Kidney Renal Clear Cell Carcinoma* |
| kzNZK | Klarzelliges Nierenzellkarzinom |
| LDH | Laktatdehydrogenase |
| LRP | Leucin-reiches Protein |
| MCT | Monocarboxylattransporter |
| MDH | Mitochondriale Dehydrogenase |
| MHC | *Major histocompatibility complex* |
| miR | Mikro-Ribonukleinsäure |
| MMP | Matrixmetalloproteinase |
| mRNA | Boten-Ribonukleinsäure |
| MRT | Magnetresonanztomographie |
| mTOR | *Mechanistic target of Rapamycin* |
| MUC | Mucin |
| NAD | Nicotinamidadenindinukleotid |
| NADP | NAD-Phosphat |
| NCBI | *National Center for Biotechnology Information* |
| NEMO | NFκB-essentieller Modulator |
| NFκB | *Nuclear factor k-light-chain-enhancer of activated B cells* |
| NID2 | Nidogen 2 |
| NK-Zellen | Natürliche Killerzellen |
| NZK | Nierenzellkarzinom |
| OXPHOS | Oxidative Phosphorylierung |
| PBMC | *Peripheral blood mononuclear cells* |
| PD-1 | *Programmed cell death protein 1* |
| PDGF | *Platelet-derived growth factor* |
| PET | Positronenemissionstomographie |
| PGAM | Phosphoglucomutase |
| PGK | Phosphoglyceratkinase |
| pH | *Potentia Hydrogenii* |
| PHD | Prolylhydroxylase |
| PI3K | Phoshatidylinositol-3-Kinase |
| PKM | Pyruvatkinase M |
| PP2A | Proteinphosphatase 2A |
| PPARγ | Peroxisom-Proliferator-aktivierter Rezeptor Gamma |
| PPARGC1a | PPAR Gamma Coaktivator 1 alpha |
| PRBM1 | Polybromo 1 |
| PRDX | Peroxiredoxin |
| PTEN | Phosphatase- und Tensinhomolog |
| qPCR | Quantitative Echtzeit-Polymerase-Kettenreaktion |
| RAB | *RAS-related in brain* |
| K-RAS | *Kirsten Rat sarcoma* |
| rev | *Reverse* |
| ROS | Reaktive Sauerstoffspezies (*reactive oxygen species*) |
| SBFI | *Stony Brook fatty acid-binding protein inhibitor* |

| | |
|---|---|
| SDH | Succinatdehydrogenase |
| SETD2 | *SET-domain containing 2* |
| SFMBT1 | *Scm-like with four malignant brain tumor domains 1* |
| shRNA | *Short hairpin ribonucleic acid* |
| siRNA | *Small interfering ribonucleic acid* |
| SOD | Superoxiddismutase |
| STAT | *Signal Transducers and Activators of Transcription* |
| SUMO | *Small ubiquitin-like modifier* |
| TAM | Tumorassoziierte Makrophagen |
| TCA | Tricarbonsäure (*tricarboxylic acid*) |
| TCGA | *The Cancer Genom Atlas* |
| TGF | *Transforming growth factor* |
| TGM | Transglutaminase |
| TIGAR | *TP53-induced glycolysis and apoptosis regulator* |
| TIL | Tumor-infiltrierender Lymphozyt |
| TME | Tumormikromilieu (*tumor microenvironment*) |
| TKI | Tyrosinkinaseinhibitor |
| TPI | Triosephosphatisomerase |
| TSC | *Tuberous sclerosis complex* |
| TTN | Titin |
| Trx | Thioredoxin |
| TXNR | Thioredoxinreduktase |
| VEGF | Vaskulärer endothelialer Wachstumsfaktor |
| VHL | Von Hippel-Lindau Protein |
| VHLdb | *VHL data base* |
| WB | *Western Blot* |

# 1 Einleitung

## 1.1 Charakteristika und Therapie des Nierenzellkarzinoms

Das Nierenzellkarzinom (NZK) umfasst eine heterogene Gruppe von Tumoren, deren Ursprung in epithelialen Nierentubuluszellen liegt[1]. Es gehört mit ca. 2 % der Gesamtkrebsdiagnosen und ca. 400.000 neuen Fällen im Jahr 2018 zu den 10 häufigsten Krebsarten weltweit[2,3]. Dabei sind das klarzellige[4] (ca. 70-80 %), papilläre[5] (ca. 10-15 %) und chromophobe NZK[6] (ca. 3-5 %) die häufigsten Subtypen des NZK[7,8] (**Abbildung 1**). Im Jahr 2013 wurde die histopathologische Klassifizierung durch die Internationale Gesellschaft für Urologische Pathologie modifiziert und die Diagnostik von folgenden fünf neuen Tumorentitäten empfohlen: tubulozystisches NZK, NZK assoziiert mit einer erworbenen zystischen Nierenerkrankung, klarzelliges papilläres NZK, Translokations-assoziiertes NZK und hereditäre Leiomyomatose-assoziertes NZK[3,9]. Die Einteilung in Tumorgrade (*Grading*) erfolgt beim klarzelligen und papillären NZK aufgrund der Eosinophilie sowie der nukleolären Prominenz für Grad 1-3, während Grad 4 durch nukleäre Anaplasie (Riesenzellen, sarkomatoide Differenzierung und/oder rhabdoide Morphologie) gekennzeichnet ist[9,10]. Die Tumorklassifikation (*Staging*) erfolgt nach dem TNM-System (*Tumor, Node, Metastasis*), wobei nach Größe und Ausbreitung des Tumors (T) sowie dem Vorhandensein von örtlichen Lymphknotenmetastasen (N) und/oder Fernmetastasen (M) unterschieden wird[11].

Das metastasierende klarzellige Nierenzellkarzinom (kzNZK) geht mit der höchsten Mortalitätsrate und der schlechtesten Prognose beim NZK einher[12,13]. Eine Reihe Krebsgenomuntersuchungen zeigten eine starke intra-[14-16] und intertumorale[17] Heterogenität des kzNZK, welche die Behandlung zusätzlich erschwert[18]. Lokal abgegrenzte NZK werden mittels partieller oder radikaler Nephrektomie entfernt[19]. Eine weitere Möglichkeit der Tumorentfernung stellt die Ablation dar[20]. Trotz der Tumorresektion entwickeln etwa 30 % der Patienten Metastasen, die mit einer hohen Mortalitätsrate assoziiert sind und zahlreiche weitere zielgerichtete Therapien erfordern[21-23]. Die Hauptrisikofaktoren, ein NZK zu entwickeln sind neben dem steigenden Alter[24], Übergewicht, Bluthochdruck und Rauchen auch übermäßiger Alkoholkonsum, chronische Nierenerkrankungen, Nierenzysten und Diabetes[25-27]. Männer sind häufiger betroffen sind als Frauen (2:1)[28,29]. Trotz der Fortschritte der letzten Jahrzehnte in der Behandlung des metastasierenden NZK mit Zytokinen wie Interleukin-2 (IL-2) und Interferon $\alpha$ (IFN$\alpha$)[30], Stammzelltransplantation, antitumorale Antikörpertherapie, Tumorvakzinierungen oder Rezeptor-Tyrosinkinase-Inhibitoren (TKI) z. B. mit Sunitinib, Pazopanib und Sorafinib sowie mTOR-Inhibitoren wie Temsirolismus und Everolismus lag die 5-Jahres-Überlebensrate in fortgeschrittenen Tumorstadien (Stadium 4) bei unter 20 %[12]. Erst mit der Zulassung der sogenannten „Checkpoint-Inhibitoren“ (CI) z. B. Nivolumab (anti-*Programmed cell death protein 1* (PD-1) Antikörper) nach vorheriger anti-angiogener TKI-Therapie (zugelassen seit 2015) und der Kombinationstherapie aus Nivolumab und Ipilimumab

(anti-*cytotoxic T-lymphocyte-associated protein 4* (CTLA4) Antikörper) in den letzten Jahren konnte ein Ansprechen von bis 60 % der Grad 4 NZK erreicht werden. Sowohl nach der „Leitlinie für Diagnostik, Therapie und Nachsorge des Nierenzellkarzinoms“(08/2020), als auch nach der „*Society for Immunotherapy of Cancer*“ richtet sich die empfohlene Therapie des metastasierenden NZK mit TKI und/oder CI nach dem Risikoprofil des Patienten (günstiges Risiko: keine Risikofaktoren, intermediäres Risiko: 1-2 Risikofaktoren, ungünstiges Risiko: >2 Risikofaktoren), wobei je nach Risikomodell Faktoren wie z. B. ein niedriger Hämoglobinwert, eine erhöhte Serumkalziumkonzentration sowie erhöhte Neutrophilen- und Trombozytenanzahl (*International Metastatic Renal Cell Carcinoma Database Consortium Score*) einbezogen werden[31-34].

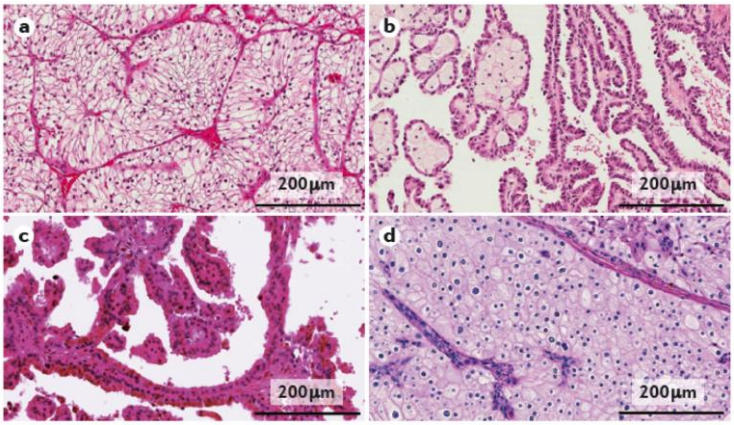


**Abbildung 1: Klassifizierung des Nierenzellkarzinoms (NZK).**
Ca. 75 % aller NZKs gehören zum klarzelligen Subtyp (**a**). Das papilläre NZK tritt in ≈15 % aller Fälle auf und wird in den basophilen (**b**) und eosinophilen (**c**) Subtyp unterteilt. Das chromophobe NZK repräsentiert mit ca. 5 % den dritthäufigsten Subtyp (**d**). Hämatoxylin-Eosin-Färbung, verändert nach Hsieh *et* al., 2017[3].

## 1.2 Molekulare Pathogenese des NZK

NZK treten hauptsächlich sporadisch auf. Nur bei etwa 3-5 % aller NZK ist ein hereditäres Syndrom wie z. B. das Von Hippel-Lindau-Syndrom, welches durch eine Keimbahnmutation im Von Hippel-Lindau (*VHL*)-Tumorsuppressorgen ausgelöst wird, oder das Birt-Hogg-Dubé-Syndrom ursächlich[35]. Derzeit sind 11 Gene bekannt (*BAP1, FLCN, FH, MET, PTEN, SDHB, SDHC, SDHD, TSC1, TSC2 und VHL*) deren Mutation an der Progression des NZK beteiligt sind[17,36-40]. Bei sporadischen kzNZK kommt es mit einer Häufigkeit von ca. 80 % zu einem Funktionsverlust des *VHL*-Tumorsuppressorgens durch Mutationen, Deletionen in der Chromosom 3p25-Region oder epigenetischer Genstilllegung[41-47]. Ursprünglich wurden zwei Isoformen des Proteins identifiziert. Mit 213 Aminosäuren (AS) besitzt das Volllängen-Protein ein Molekulargewicht von 24 kDa, während bei der kürzeren 18 kDa-Isoform die ersten 53 AS aufgrund eines alternativen Translationsstart fehlen[48-50]. Beide Isoformen sind biologisch aktiv und können über die Bindung von Elongin B und C sowie Cullin 2 einen E3-Ubiquitinligasekomplex bilden, welcher zur Ubiquitinierung und zum proteasomalen Abbau

des Hypoxie-induzierbaren Faktors (HIF)α führt[51-55]. Zusätzlich wurde eine dritte VHL-Isoform mit unbekannter Funktion beschrieben.

Der Verlust der VHL-Proteinfunktion z. B. durch Mutationen führt zu einer konstitutiven Stabilisierung von HIFα, was die Transkription einer Reihe von Zielgenen wie dem vaskulären endothelialen Wachstumsfaktor (VEGF) oder der Carboanhydrase IX (CA9)[56-58] (**Abbildung 2)** aktiviert. In Zellen mit funktionellem VHL wird der HIFα-Abbau durch Hypoxie verhindert, indem die Prolylhydroxylasen (PHD) mit sinkendem Sauerstoffgehalt durch Konformationsänderung inaktiviert werden[59-64]. Da in Tumoren fortschreitender Größe die Versorgung mit Sauerstoff über die Blutgefäße schlechter wird, findet häufig in Karzinomen ohne VHL-Verlust ebenfalls eine partielle reversible HIFα-Stabilisierung statt[65].

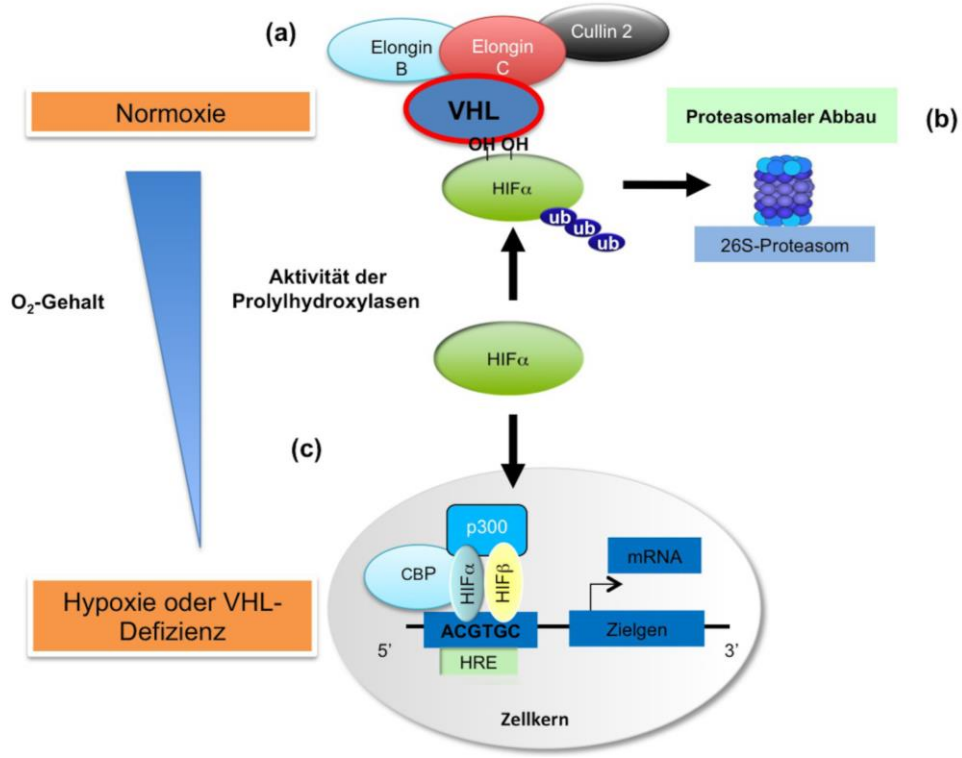


**Abbildung 2: VHL- und Hypoxie-abhängige Funktion des Hypoxie-induzierbaren Faktors.**
Unter Normoxie wird der Hypoxie-induzierbare Faktor (HIF) an zwei Prolylresten hydroxyliert (**a**). Damit kann das Von Hippel-Lindau-Protein (VHL) an HIFα binden und einen E3-Ubiquitinligasekomplex mit Elongin B, Elongin C und Cullin 2 rekrutieren. Durch die Ubiquitinierung von HIF wird der Transkriptionsfaktor im 26S-Proteasom abgebaut. Dabei beträgt die HIF-Halbwertszeit etwa fünf Minuten (**b**). Unter hypoxischen Bedingungen sind die Prolylhydroxylasen inaktiv, so dass HIFα in den Zellkern transloziert. Im Zellkern dimerisiert HIFα mit der HIFβ-Untereinheit, um mit verschiedenen Cofaktoren, wie z. B. p300 oder dem CREB-bindenden Protein (CBP), an ein spezifisches DNA-Motiv das *Hypoxia-responsive element* (HRE), mit der Konsensussequenz ACGTGC zu binden, wodurch die Transkription verschiedener Zielgene gestartet wird (**c**). Liegt in der Zelle kein funktionelles VHL vor, wird HIFα wie unter sauerstoffarmen Bedingungen nicht abgebaut und die Transkription der HIF-Zielgene ist konstitutiv aktiv. Verändert nach Befani und Liakos[66].

Trotz allem reicht der alleinige funktionelle Verlust von VHL nicht aus, die kzNZK-Entstehung zu initiieren, was darauf schließen lässt, dass eine weitere genetische oder epigenetische Prädisposition vorliegen muss, um ein kzNZK hervorzurufen (*two-hit* Modell)[67-70]. In den letzten

Jahren identifizierten großangelegte Krebsgenomprojekte neue kzNZK-Mutationen z. B. im Polybromo 1- *(PRBM1), SET domain containing 2- (SETD2)* und BRCA1-assoziiertes Protein 1 *(BAP1)*-Gen (**Abbildung 3**), welche für Chromatin- und Histon-regulierende Tumorsuppressorproteine codieren und in der Nähe des *VHL*-Gens auf dem Chromosom 3p21 lokalisiert sind[36,38,39,71]. Nach *VHL* ist *PRBM1* ist das am häufigsten mutierte Gen im kzNZK. Im Mausmodell führt die renale Kodeletion von *VHL* und *PBRM1* zu bilateralen, multifokalen kzNZK[72]. Weiterhin wurde beim kzNZK eine negative Korrelation zwischen *PBRM1*-Mutationen und *BAP1*-Mutationen nachgewiesen. Jedoch sind Tumore mit *BAP1*-Mutationen mit einem höheren Tumorgrad, gesteigerter Aggressivität und einer kürzeren Patientenüberlebensrate im Vergleich zu *PBRM1*-defizienten Tumoren assoziiert. Darüber hinaus weisen *BAP1*-defiziente Tumore eine höhere *mechanistic target of Rapamycin complex 1* (mTORC1)-Aktivierung auf[73]. Während z. B. *PBRM1*-Mutationen subtypspezifisch ausschließlich beim papillären NZK mit einem kürzerem Patientenüberleben verbunden sind, wurde für alle NZK-Subtypen eine gesteigerte DNA-Hypermethylierung (CpG-Insel-Methylator-Phänotyp), *CDKN2A*-Mutationen und eine gesteigerte Typ-2-T-Helferzell-mediierte Immunantwort nachgewiesen, was jeweils mit einer schlechteren Prognose einherging[71,74].

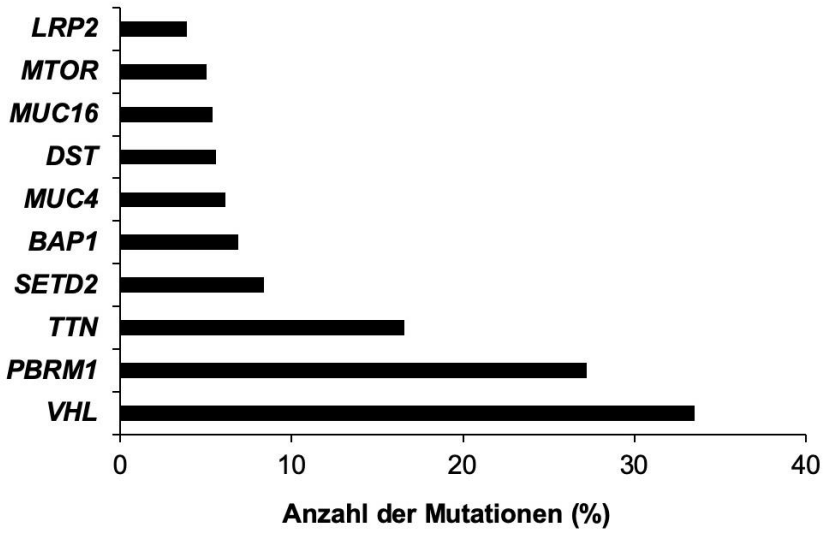


**Abbildung 3: Häufigkeit mutierter Gene im kzNZK.**
Die Genarray-Daten des Krebsgenomatlas (*The Cancer Genome Atlas, TCGA*) zeigen die zehn am häufigsten mutierten Gene aus 537 untersuchten kzNZK (Projekt *TCGA-Kidney Renal Clear Cell Carcinoma*, Stand 04.10.2020). Die Gene *VHL, PBRM1, TTN, SETD2* und *BAP1* sind auf dem Chromosom 3p lokalisiert.

VHL ist nicht ausschließlich am proteasomalen Abbau von HIF$\alpha$ beteiligt, sondern besitzt zusätzlich weitere proteolytische und nicht-proteolytische Funktionen, die allerdings noch nicht vollständig charakterisiert sind[75]. Erst kürzlich wurde gezeigt, dass VHL die Ubiquitinierung und den Abbau des onkogenen Proteins *Scm-like with four malignant brain tumor domains 1* (SFMBT1) steuert[76]. Zusätzlich sind HIF-unabhängige VHL-Funktionen bekannt, wie die

Regulation des Tumorsuppressors p53, die Beteiligung an der DNA-Reparatur und des Abbaus von oxidativem Stress[77-80].

### 1.3 Der Transkriptionsfaktor HIF

HIF steuert 1-5 % der humanen Gene direkt oder indirekt und ist damit in zahlreiche Vorgänge der Tumorentstehung wie Metastasierung, Invasion, Zellüberleben, Tumorangiogenese und Epithelial-mesenchymale Transition (EMT) involviert[81].

HIF1α und HIF2α binden an ein identisches DNA-Motiv (**Abbildung 2**) und besitzen eine Aminosäureübereinstimmung von 48 %[82]. Es unterscheiden sich aber partiell ihre Proteininteraktionspartner und Zielgene (**Tabelle 1**). Die HIF-Expression stellt nicht nur im NZK, sondern ebenfalls in zahlreichen anderen soliden Tumoren, einen wichtigen prognostischen Faktor dar, welcher mit einer schlechten Patientenprognose einhergeht[83]. Dabei werden Tumore, welche ausschließlich HIF2 exprimieren (H2-Tumor) von Tumoren, die eine Überexpression von HIF1 und HIF2 (H1H2-Tumore) besitzen, unterschieden[83].

Im Gegensatz zum Brustkrebs ist im NZK HIF1α häufig nicht exprimiert, während HIF2α die Funktionen des Transkriptionsfaktors übernimmt[84,85]. Eine HIF2α-Überexpression wurde bereits in einer Vielzahl von Tumorentitäten, einschließlich des nichtkleinzelligen Lungenkarzinoms[86], des Endometriumkarzinoms[87], des Plattenepithelkarzinoms[88], des Astrozytoms[89], des Kolorektalkarzinoms[90] und des Gallenblasenkarzinoms[91], beschrieben, wobei die HIF2α-Expression dieser vaskularisierten Tumore mit der Expression angiogener Faktoren wie VEGF korreliert.

**Tabelle 1: Charakteristika von HIF1α und HIF2α.**

| Eigenschaft | HIF1α | HIF2α |
|---|---|---|
| Hydroxylierung | Prolylrest 402 und 564 | Prolylrest 405 und 531 |
| Regulation | HAF, FIH-1, Hsp70, Hsp90 | FIH-1, Hsp90 |
| Proteininteraktion | HNF-4 | Ets1, Elk1, NEMO |
| Expression | Ubiquitär | Begrenzt auf Endothelium, Leber, Hirn, Niere, Lunge und Herz |
| Pathophysiologie | Assoziiert mit Brustkrebs | Assoziiert mit Nierenzellkarzinom |

Elk, *ETS like-1 protein*; Ets, *E26 transformation-specific*; FIH, HIF-inhibierender Faktor; HAF, Hypoxie-assoziierter Faktor; HNF, Hepatozytärer nuklearer Faktor; Hsp, Hitzeschockprotein; NEMO, NFκB-essentieller Modulator. Zusammengefasst nach Befani und Liakos, 2018[66].

## 1.4 Der Transkriptionsfaktor CREB

Neben VHL und HIF spielt der Transkriptionsfaktor *Cyclic adenosin monophosphate (cAMP)-response element-binding protein* 1 (CREB), welcher die Expression von zahlreichen Genen reguliert, in der Progression des NZK eine Rolle. Zusätzlich wird die adaptive Reaktion des Sauerstoffverlustes (Hypoxie) im Tumorgewebe durch HIF und CREB gesteuert.

Die Aktivierung des CREB-Proteins erfolgt über die Phosphorylierung der Serinseitenketten durch Kinasen der Zellsignalwegskomponenten, wobei die Phosphorylierung des Serinrestes 133 am besten charakterisiert ist[92,93]. Der aktivierte Transkriptionsfaktor transloziert in den Zellkern und bildet ein Homodimer oder Heterodimer (ATF-1, CREM)[94]. Gleichzeitig interagiert das Dimer, ebenfalls wie HIF (**Abbildung 2**), mit CBP sowie einer Histonacetyltransferase zu einem Transkriptionsinitiationskomplex. Dabei wird ein spezifisches DNA-Element mit der Konsensussequenz TGACGTCA, genannt *cAMP-responsive element* (CRE), gebunden, um die CREB-abhängige Gentranskription zu initiieren[95,96]. Mittels spezifischer Modifikation und zellulärer Lokalisation steuert CREB eine Reihe zellulärer Prozesse, wie die Proliferation und das Zellüberleben, und treibt in Tumoren die maligne Transformation voran[97-100]. In zahlreichen Studien wurde gezeigt, dass eine verstärkte Aktivierung von CREB bei akuter myeloischer Leukämie[101,102], nichtkleinzelligen Lungenkarzinomen[103,104], Leberzellkarzinomen[105], Brustkrebs[106], und Melanomen[107] die Tumorprogression fördert. In Xenograft-Modellen des Leberzellkarzinoms wurde die Hypoxie-induzierte Ausbildung der tumorversorgenden Blutgefäße sowohl durch shRNA-mediierte verminderte Expression von CREB als auch von HIF reduziert[108].

Weiterhin wurde eine verstärkte CREB-Phosphorylierung am Serinrest 133 sowie eine erhöhte CREB-Expression in kzNZK-Zelllinien und -Geweben nachgewiesen[109,110]. Die Reduktion der CREB-Expression mittels siRNA bzw. die Hemmung der Phosphorylierung führte *in vitro* zu verringertem Wachstum, weniger Migration und Invasion sowie zur Herunterregulation von Matrixmetallopeptidasen[110,111], deren Expression mit der Fähigkeit zur Metastasierung assoziiert sind[112,113]. Die Hemmung der CREB-Phosphorylierung unterdrückte das NZK-Wachstum im Mausmodell nahezu komplett[109]. Zusätzlich zeigten *in vivo* Daten, dass eine verstärkte CREB-Expression mit einer höheren Überlebensrate von NZK-Patienten einhergeht[114].

## 1.5 Veränderungen des Metabolismus im Tumor

### 1.5.1 Der „Warburg Effekt“

Bereits in den 1920er Jahren beobachtete Otto Warburg, die Fähigkeit von Tumorzellen den Metabolismus zur aeroben Glykolyse umzustellen[115-118]. Der sogenannte „Warburg Effekt“, welcher mit einer hohen Laktatproduktion der Zellen einhergeht, unterscheidet Tumorzellen von gutartigen Zellen, deren Glukoseverbrauch unter atmosphärischen

Sauerstoffbedingungen durch die Inhibierung der Glykolyse gehemmt ist (Pasteur-Effekt). Dieser Effekt wurde mittels Positronenemissionstomographie (PET) bewiesen, wobei die Methode mit einer über 90-prozentigen Sensitivität und Spezifität heute noch zur Detektion von Metastasen eingesetzt wird[119]. Die Energiegewinnung gesunder Zellen über die oxidative Phosphorylierung (OXPHOS) produziert 18-mal mehr ATP, als die aerobe Glykolyse, welche zu einem hohen Glukoseverbrauch und einer verstärkten Produktion reaktiver Sauerstoffspezies (ROS) der Tumorzellen führt[120]. Weiterhin wurde beschrieben, dass die Überexpression des Enzyms Laktatdehydrogenase (LDH), erhöhte Glutaminolyse und mitochondriale Dysfunktionen zum „Warburg Effekt" in Tumoren beiträgt. Glykolyse-Enzyme wie Triosephosphatisomerase (TPI1), Enolase (ENO) 1 und Pyruvatkinase M (PKM) 2 werden verstärkt im NZK exprimiert[121,122]. Eine Reihe von Onkogenen wie HER-2/neu bzw. der Verlust von Tumorsuppressorgenen wie VHL sind assoziiert mit einer Aktivierung des Phosphatidylinositol-3-Kinase (PI3K/Proteinkinase B)-Signalweges. Diese Aktivierung führt zur Translokation von vesikulären Glukosetransportern zur Zelloberfläche, aktiviert das Enzym Hexokinase (HK), inhibiert die Glykogensynthase-Kinase 3 (Gsk3) und erreicht damit die Glukoseabhängigkeit der Zellen. Aufgrund dessen wird die Proteinkinase B (Akt) ebenfalls als „Warburg-Kinase" bezeichnet[123]. Zusätzlich wurde erst kürzlich gezeigt, dass die Herunterregulation von Proteinen der Atmungskette wie das *Ubiquinol-Cytochrome C Reductase Hinge* Protein, welches den Elektronentransfer im Komplex III der Elektronentransportkette beeinflusst, zur Verstärkung des „Warburg Effekts" im NZK beiträgt[124].

Zahlreiche HIF-Zielgene sind in den Zellmetabolismus involviert und beeinflussen die Glykolyse, Laktatproduktion, Angiogenese, Metastasierung und den Eisenmetabolismus. Zu diesen Zielgenen gehören z. B. Glukosetransporter (GLUT1), glykolytische Enzyme (HK, Aldolase A, ENO1, PKM2) und die LDHA sowie der Laktattransporter MCT4[81,125]. Durch die verstärkte Laktatproduktion und –sekretion kommt es bei VHL-defizienten oder hypoxischen Tumorzellen zu einer Ansäuerung (Azidose) des extrazellulären Raums bzw. des Tumormikromilieus, wobei dieser Effekt durch die Anreicherung von Protonen ($H^+$) verstärkt wird. Zusätzlich führt die verstärkte Akt-Aktivierung zur Azidose[123].

Zusammenfassend wird der „Warburg Effekt" in Tumorzellen durch verschiedene Onkogene, Hypoxie und Verlust von Tumorsuppressorgenen ausgelöst (**Tabelle 2**) und verschafft dem Tumor bessere Bedingungen zur verstärkten Proliferation, Angiogenese, Invasion und Metastasierung. Außerdem beeinflusst der Laktatspiegel und der extrazelluläre pH-Wert die tumorale Immunantwort[126].

**Tabelle 2: Einfluss verschiedener Onkogene und Tumorsuppressorgene auf den Zellmetabolismus.**

| Onkogen | Tumorentität | Auswirkung | Referenz |
|---|---|---|---|
| PI3K | Eierstock-, Magen-Kolonkarzinom, | CPT1A↑ GLUT1↑ | 127, 132 |
| Akt | Eierstock-, Brustkarzinom | FASN↑ Aktiviert mTOR | 128 |
| HER-2/neu | Brustkarzinom | FASN↑ ACCα↑ Aktiviert mTOR | 129 |
| Tyrosinkinasen | Mehrere Entitäten, z. B. NZK | Inaktivieren PKM2 | 130 |
| K-RAS | Pankreas-, Kolonkarzinom | GLUT1↑ Glutamin↑ | 131 |
| MYC | Burkitt Lymphom, kzNZK | PDK1↑ Glutaminolyse↑ | 132 |
| **Tumorsuppressor** | **Tumorentität** | **Auswirkung** | **Referenz** |
| VHL | kzNZK | HIFα-Abbau | 133 |
| p53 | Mehrere Entitäten, z. B. Kolonkarzinom | TIGAR↓ PGAM↓ | 134-136 |
| PTEN | Prostatakarzinom | Inhibiert PI3K | 133 |
| FH | Papilläres NZK | Inhibiert PHD | 137 |
| SDH | Phäochromozytom | Inhibiert PHD | 137 |

↑, verstärkte Expression; ↓, verminderte Expression; ACCα, Acetyl-CoA-Carboxylase alpha; CPT1A, Carnitin-Palmityltransferase 1A; FASN, Fettsäuresynthase; FH, Fumerathydratase; HIF, *Hypoxia-inducible factor*; K-RAS, *Kirsten Rat sarcoma*; kzNZK, klarzelliges Nierenzellkarzinom; mTOR, *mechanistic target of Rapamycin*; PGAM, Phosphoglucomutase; PHD, Prolylhydroxylasen; PKM, Pyruvatkinase M; PI3K, Phosphoinositol-3-Kinase; PTEN, Phosphatase- und Tensinhomolog; SDH, Succinatdehydrogenase; TIGAR: *TP53-induced glycolysis and apoptosis regulator*; VHL, Von Hippel-Lindau.

### 1.5.2 Auswirkungen des „Warburg Effekts“ auf die Immunantwort

Die Auswirkungen der Stoffwechselveränderungen im Tumor auf die Umgebung sind vielfältig. Einerseits wird durch die Stabilisierung des Transkriptionsfaktors HIF die Expression und Sekretion von VEGF und die Laktatakkumulation verstärkt, was zur Neubildung von Blutgefäßen und damit zur besseren Versorgung des Tumors mit Glukose und Nährstoffen führt (**Abbildung 4a**). Andererseits ist der Tumorstoffwechsel mit verminderten Arginin-, Tryptophan-, Glutamin- und Glukosespiegel im Mikromilieu assoziiert (**b**). Diese Nährstoffreduktion, die Akkumulation von Laktat und die Azidose wirken hemmend auf die Proliferation und Aktivität von Immunzellen. In Makrophagen wird die Glykolyse und die OXPHOS vermindert, während es bei T-Zellen zur Reduktion der Interferon (IFN)γ-Produktion kommt. Oxidative Tumorzellen werden durch die verstärkte Sezernierung von Laktat und Wachstumsfaktoren der glykolytischen Zellen zur Proliferation angeregt (**c**)[138-140]. Die Wechselwirkungen der malignen Zellen mit dem Mikromilieu führen zu einem Vorteil bei der Metastasierung, Proliferation und Hemmung der Apoptose des Tumors[138,140].

Nachdem die Mechanismen der Tumorzellen, der Erkennung durch das körpereigene Immunsystem (z. B. durch die Herunterregulation von MHC-Molekülen[141,142] oder der Expression von HLA-G[143,144]) zu entgehen in den letzten Jahren besser aufgeklärt wurden, hat das Interesse an zielgerichteten Immuntherapien zur Krebsbekämpfung stark zugenommen. Zahlreiche Studien zeigten, dass das Tumormikromilieu die Effektivität von onkologischen Therapien beeinflusst[126,140]. Das Tumorstroma besteht aus verschiedenen Zellpopulationen wie z. B. T- und Natürliche Killer (NK)-Zellen, Makrophagen, dendritische Zellen, Fibroblasten und Endothelzellen. Tumor-infiltrierende lymphatische (TIL) Zellen können abhängig von ihrer Dichte und Aktivität das Tumorwachstum kontrollieren und sind in höherer Dichte mit einer besseren Prognose assoziiert. Für das NZK ist eine Korrelation des verstärkten Glukosestoffwechsels im Tumor mit einer geringeren CD8-positiven T-Zell-Infiltration beschrieben[145,146]. In weiteren Studien wurde die Modulation der Immunzellfunktion durch Laktat in Assoziation mit verstärkter Tumorprogression und Metastasierung gezeigt[147,148]. Laktat verstärkt die IL-23-Produktion in Monozyten und Makrophagen, induziert eine M2-Polarisation in Tumor-assoziierten Makrophagen (TAM) und inhibiert die Aktivität von T- sowie NK-Zellen[149,150]. Für Melanom-Patienten wurde ein Zusammenhang zwischen der LDHA-Expression, T-Zellaktivität, IFNγ-Expression der TIL und dem damit verbundenen verstärkten Tumorwachstum sowie einer immunsuppressiven Wirkung von Laktat nachgewiesen[151].

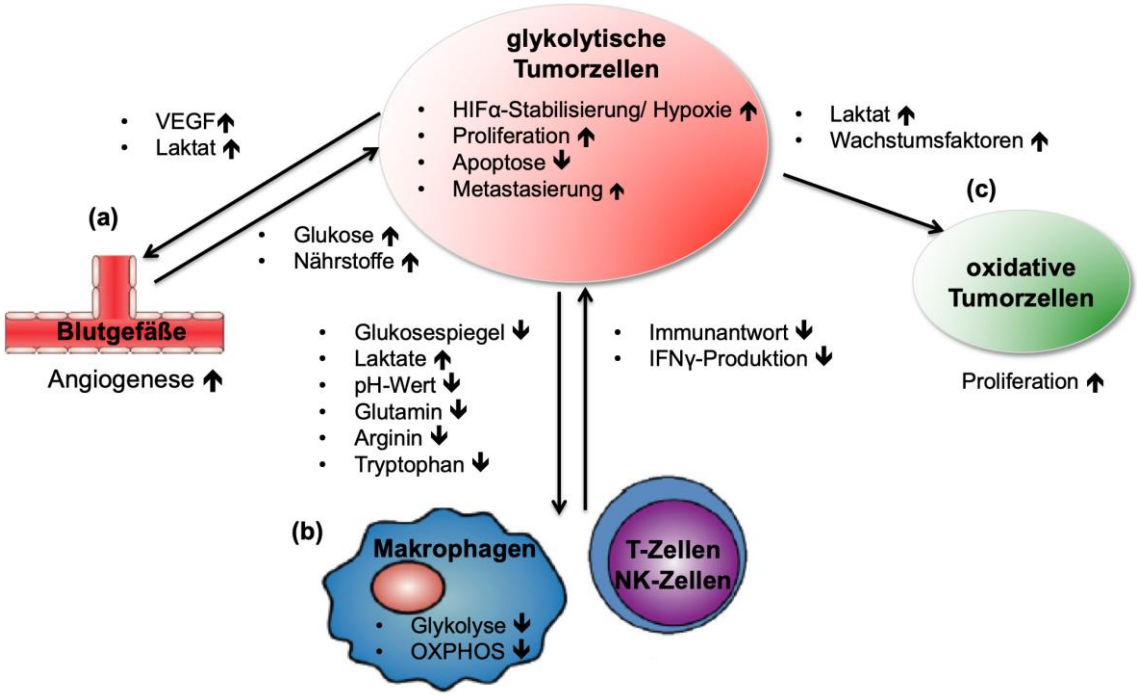


**Abbildung 4: Einfluss des „Warburg Effektes“ auf das Tumormikromilieu.**
↑, verstärkt; ↓, vermindert; IFN, Interferon; OXPHOS, oxidative Phosphorylierung; NK-Zellen, natürliche Killerzellen; VEGF, vaskulärer endothelialer Wachstumsfaktor.

### 1.6 Identifizierung von intra- und extrazellulären Biomarkern des NZK

In den letzten Jahren führte eine Reihe von *Microarray*-[45], Proteom-[74] und Genomanalysen[71] zur Identifizierung einer Vielzahl von differentiell exprimierten Genen und Proteinen in NZK-Läsionen im Vergleich zu gesunden Nierenepithelzellen, die mit der Metastasierung und dem Überleben der Patienten korrelierten[152-154]. Dies waren z. B. Komponenten des Zytoskeletts sowie der Signaltransduktionswege, der Zellproliferation und -motilität, der Expressionskontrolle, der Immunantwort und am Zellmetabolismus beteiligte Gene/Proteine. Besonders vielversprechend erwiesen sich Serumbiomarker für das metastasierende NZK wie C-reaktives Protein, VEGF, ALDOA, CA9, *Tissue Inhibitor of Metalloproteinase* (TIMP) 1, RAS p21 und IL-6[153,155-159]. Ebenfalls wurde zirkulierende Tumor-DNA (*VHL, BAP1 und PRBM1)* detektiert[160]. Weiterhin wurden Tumorstammzellmarker, vor allem Zelloberflächenproteine wie *C-X-C chemokine receptor type* 4 (CXCR4), CD105, CD133 und CD44, als prognostische oder therapeutische Marker diskutiert[161].

Durch die zunehmende Bedeutung der Modulation des Tumormikromilieus wurde die Zusammensetzung von extrazellulären Membranvesikeln (Exosomen, EV) und anderen sekretierten tumoralen Proteinen untersucht. Für das NZK wurde eine Vielzahl von exosomalen Proteinen wie z. B. CA9 und HLA-G sowie mRNA von VEGF, MMP2 und MMP9 identifiziert. Zusätzlich konnten zahlreiche Mikro-RNA (miR) wie die miR-183, deren Expression mit der Metastasierung, Angiogenese und der Herunterregulation der Immunantwort im NZK assoziiert war, in Exosomen nachgewiesen werden[162]. Die extrazelluläre Abgabe von Exosomen beeinflusst die Immunantwort[163] und die

Tumormetastasierung[164], wodurch EV, welche aus den meisten Körperflüssigkeiten isoliert werden können, als Quelle für potentielle diagnostische Biomarker des NZK gelten[165-167].

Im NZK gehen metabolische Veränderungen mit einer erhöhten Expression von Glykolyse- und Glutaminolyse-Enzymen sowie einer verminderten Expression verschiedener an der Atmungskette sowie an der Glukoneogenese beteiligter Enzyme einher. Dabei sind die metabolischen Alterationen abhängig vom Tumorgrad[168]. Ebenfalls wurden subtypspezifische differenzielle metabolische Signaturen detektiert, welche das kzNZK und das papilläre NZK vom chromophoben unterscheiden[71,169].

Einige dieser putativen molekularen Marker wurden vergleichend zu bestehenden prognostischen Parametern analysiert oder in bestehende Prognosescores integriert und zeigten eine Verbesserung der Prognosebewertung[71,170,171]. Jedoch wurde bisher keiner dieser Marker in der Klinik etabliert, da Studien zur unabhängigen oder prospektiven Validierung fehlen.

# 2 Ziele der Arbeit

Der zelluläre Stoffwechsel hat sich als kritische Determinante für die Lebensfähigkeit und Funktion sowohl von NZK-Zellen als auch der Zellen des Tumormikromilieus herausgestellt. Um den enormen anabolen Bedarf aufrechtzuerhalten, unterscheidet sich der Tumormetabolismus stark von dem somatischer Zellen. Der tumorale Stoffwechsel führt zu einer Mikroumgebung, die häufig sauer, hypoxisch und/oder verarmt an kritischen Nährstoffen ist, welche von Immunzellen benötigt werden. In diesem Zusammenhang kann der veränderte Tumorstoffwechsel zur Verminderung der immunvermittelten Tumorerkennung führen. Der direkte Einfluss von VHL, CREB und Hypoxie auf den Tumormetabolismus sowie das Tumormikromilieu war zum Zeitpunkt der Erstellung dieser Dissertation weitgehend unbekannt. Von daher sollte im Rahmen der vorliegenden Arbeit das VHL-, CREB- und Hypoxie-abhängige Expressionsprofil im NZK und onkogentransformierten Zellmodellen mittels *Microarray*- und/oder Proteomanalysen charakterisiert werden, die Auswirkungen auf den Zellmetabolismus untersucht und die funktionelle Bedeutung dieser Prozesse sowie ihr Einfluss auf die antitumorale Immunantwort aufgeklärt werden. Dabei wurden folgende Forschungsschwerpunkte bearbeitet:

i. Charakterisierung der Transkriptmengen, des Gesamtproteoms und Sekretoms in VHL-negativen und VHL-positiven NZK-Zelllinien unter Normoxie und Hypoxie,
ii. Identifizierung und Validierung von VHL-, HIF-, CREB-, und Hypoxie-abhängigen am Metabolismus beteiligten Genen/Proteinen,
iii. Einfluss von VHL-Defizienz, CREB-Überexpression und Sauerstoffreduktion auf spezifische Vorgänge und Komponenten des Energiestoffwechsels,
iv. Einfluss definierter Komponenten des Sekretoms auf die Immunantwort.

Diese Studien sollten nicht nur zu einem besseren Verständnis der Rolle des Tumorenergiestoffwechsels und der Biologie von CREB, HIF und VHL in diesem Prozess führen, sondern ebenfalls dessen Einfluss auf die Immunantwort charakterisieren und NZK-Kandidatentumormarker identifizieren, welche zur Etablierung prognostischer bzw. therapeutischer Strategien genutzt werden können. Das Verständnis der unterschiedlichen Stoffwechselbedürfnisse der verschiedenen Zellen, bietet die Möglichkeit, die Funktion der Immunzellen gezielt zu regulieren. Die Charakterisierung des Tumorstoffwechsels könnte metabolische Schwachstellen und somit langfristig Ansätze für eine verbesserte Immuntherapie aufdecken.

# 3 Beschreibung der publizierten Manuskripte

## 3.1 „Distinct von Hippel-Lindau gene and hypoxia-regulated alterations in gene and protein expression patterns of renal cell carcinoma and their effects on metabolism“

**Sandra Leisz**, Kristin Schulz, Susanne Erb, Peter Oefner, Katja Dettmer, Dimitrios Mougiakakos, Ena Wang, Francesco M. Marincola, Franziska Stehle, Barbara Seliger

*Oncotarget* (2015), 6(13):11395-406

Das Wissen über die molekularen Mechanismen der zellulären Anpassung an den Funktionsverlust des VHL-Proteins und die tumorale Hypoxie im NZK hat in den letzten Jahren zugenommen. Jedoch gab es bisher nur wenige Informationen über die Überschneidungen und Unterschiede in der Gen-/Proteinexpression beider Prozesse. Ziel dieser Studie war es daher, VHL- und Hypoxie-regulierte Veränderungen im Stoffwechsel des humanen NZK mittels Transkriptom- und Proteomanalysen zu untersuchen. Die Auswirkung der VHL- und Hypoxie-regulierten veränderten Gen-/Proteinexpressionsmuster auf den zellulären Stoffwechsel wurde durch die Bestimmung der Glukoseaufnahme, der Laktatsekretion, des extrazellulären pH-Wertes, der Laktatdehydrogenase-Aktivität, des Aminosäuregehaltes und des ATP-Spiegels analysiert. Unter Verwendung von $VHL^-$/$VHL^+$-NZK-Zellen, welche unter normoxischen und hypoxischen Bedingungen kultiviert wurden, konnten VHL-abhängige, HIF-abhängige sowie VHL-/HIF-unabhängige Signaturen in den Gen- und Proteinexpressionsmustern identifiziert und anschließend in anderen NZK-Zelllinien validiert werden. Etwa 30 % der unter diesen unterschiedlichen Bedingungen differenziell exprimierten Gene/Proteine waren am zellulären Stoffwechsel beteiligt, was mit einem veränderten Metabolismus sowie mit VHL-abhängigen Veränderungen des intrazellulären Aminosäuregehaltes einherging. Zusammenfassend zeigt die Studie Überschneidungen, aber auch Unterschiede in der Expression, welche durch VHL-Funktionalität und Hypoxie kontrolliert werden, und demonstriert damit Unterschiede in der metabolischen Umschaltung des NZK. Weiterhin wurden potentielle neue Markerproteine für das VHL-defiziente oder hypoxische NZK identifiziert.

Beiträge der Autoren: Sandra Leisz hat das Manuskript zusammen mit Barbara Seliger konzipiert und geschrieben sowie folgende Experimente durchgeführt: Zellkultur und Hypoxie-Inkubation, 2D-Gelanalysen mit anschließender Proteinidentifizierung, Expressionsanalysen (qPCR, *Western Blots* (WB)), sämtliche Stoffwechselanalysen mit Ausnahme der Aminosäuremessung, die gesamte Auswertung der Analysen inklusive der statistischen Auswertung. Franziska Stehle und Kristin Schulz waren an der Etablierung und Durchführung der 2D-Gelelektrophorese sowie an der Proteinidentifizierung beteiligt. Susanne Erb hat das Zellsystem und die Hypoxie-Analysen etabliert. Peter Oefner und Katja Dettmer haben die Aminosäuremessung durchgeführt. Dimitrios Mougiakakos hat den „Seahorse Analyzer“ und die für die Messung benötigten Verbrauchsmaterialien zur Verfügung gestellt. Francesco Marincola und Ena Wang haben die *Microarray*-Analyse durchgeführt.

## 3.2 „VHL-dependent alterations in the secretome of renal cell carcinoma: Association with immune cell response?“

Franziska Stehle, **Sandra Leisz**, Kristin Schulz, Nicolle Schwurack, Nico Weber, Chiara Massa, Jana Kalich, Corinna Fahldieck, Barbara Seliger

*Oncotarget* (2015), 6(41):43420-37

Proteine der extrazellulären Matrix modulieren die Interaktion zwischen Tumor, Stroma und Immunzellen innerhalb der Tumormikroumgebung und können damit ein immunsuppressives Tumormikromilieu aufbauen. Um die Sekretom-vermittelte, VHL-mediierte Interaktion zwischen Tumorzellen und T-Lymphozyten zu bestimmen, wurden periphere mononukleäre Blutzellen (*Peripheral blood mononuclear cells*, PBMC) von gesunden Spendern entweder in konditioniertem Medium einer VHL-defizienten NZK-Zelllinie (786-0 $VHL^-$) bzw. den VHL-transfizierten Zellen dieser NZK-Zelllinie (786-0 $VHL^+$) oder direkt mit einer der beiden Zelllinien kokultiviert. Dabei wurde bei 786-0 $VHL^+$-konditioniertem Medium eine höhere T-Zell-Proliferation festgestellt. Durch die Anwendung eines quantitativen proteombasierten Ansatzes mittels differentieller Gelelektrophorese und anschließender Massenspektrometrie wurden 14 Proteine identifiziert, die im Sekretom der 786-0 $VHL^-$-Zellen im Vergleich zu den 786-0 $VHL^+$-Zellen differentiell exprimiert vorlagen. Alle identifizierten Proteine waren an tumorassoziierten biologischen Funktionen, einschließlich der Immunantwort, beteiligt. Funktionelle Studien zur verstärkten Superoxiddismutase 2 (SOD2)-Sekretion zeigten, dass diese ein Regulator der T-Zell-Aktivierung und des Zelltods ist. Die Inkubation der T-Zellen mit solublem SOD2 führte ebenfalls zu einer verminderten T-Zellaktivierung und IL-2-Sekretion, was auf eine kritische Rolle der extrazellulären SOD2-Spiegel für die T-Zellproliferation und -aktivierung hinweist. Folglich konnten diese Daten erstmals eine direkte Assoziation des VHL-Verlustes mit der Reduktion der T-Zellaktivität nachweisen.

Beiträge der Autoren: Sandra Leisz war an der Etablierung der Hypoxie-Experimente, der Proteinidentifizierung, der mRNA-Validierung und am Schreiben des Manuskriptes beteiligt. Franziska Stehle hat das Manuskript zusammen mit Barbara Seliger konzipiert und geschrieben. Kristin Schulz hat die *enzyme-linked immunosorbent assays* (ELISA) durchgeführt und war an der Proteinidentifizierung beteiligt. Nico Weber hat die 2D-Gelelektrophorese des Sekretoms im Rahmen seiner Diplomarbeit durchgeführt. Nicolle Schwurack führte im Rahmen ihrer Bachelorarbeit die T-Zellanalysen durch. Chiara Massa beteiligte sich an der Etablierung der ELISA-Experimente. Corinna Fahldieck und Jana Kalich haben die FACS- und WB-Analysen durchgeführt.

## 3.3 „Hypoxia-mediated alterations and their role in the HER-2/neu-regulated CREB status and localization“

André Steven, **Sandra Leisz**, Katharina Sychra, Bernhard Hiebl, Claudia Wickenhauser, Dimitrios Mougiakakos, Rolf Kiessling, Carsten Denkert, Barbara Seliger

*Oncotarget* (2016), 7(32):52061-52084

Der Transkriptionsfaktor CREB ist an der Entwicklung von HER-2/neu-überexprimierenden murinen und humanen Tumoren beteiligt. Dabei wurde der Zusammenhang zwischen der HER-2/neu-vermittelten CREB-Aktivierung, der posttranslationalen Modifikation und Lokalisation von CREB und Veränderungen im zellulären Metabolismus aufgrund einer veränderten Tumormikroumgebung bisher nicht untersucht. In der vorliegenden Studie wurde gezeigt, dass das shRNA-vermittelte *Silencing* von CREB in HER-2/neu-transformierten Zellen zu einer verminderten Tumorbildung führte, sowie mit einer reduzierten Angiogenese und der Zunahme nekrotischer und hypoxischer Bereiche im Tumor einherging. In HER-2/neu-transformierten Zellen wurde durch Hypoxie die Phosphorylierung von CREB am Serin 133, aber nicht am Serin 121 induziert. Dies war verbunden mit einer Hochregulation der Hypoxie-induzierbaren Gene GLUT1 und VEGF, erhöhter Zellmigration und Matrix-Metalloproteinase-vermittelter Invasion. Die Behandlung der HER-2/neu$^+$-Zellen mit Signaltransduktionsinhibitoren, welche insbesondere die HER-2/neu-vermittelten Signalwege hemmten, konnte die Hypoxie-gesteuerte CREB-Aktivierung revertieren. Zusätzlich zu den Veränderungen in der Phosphorylierung verursachte Hypoxie in HER-2/neu$^+$-Zellen eine transiente Ubiquitinierung und *small ubiquitin-like modifier*(SUMO)ylierung von CREB sowie eine Kolokalisation des nukleären CREB in der mitochondrialen Matrix. Eine mitochondriale Lokalisation von CREB wurde ebenfalls in hypoxischen Bereichen von HER-2/neu-positiven Mammakarzinomen nachgewiesen, was *in vitro* mit einem veränderten Genexpressionsmuster, einer veränderten Aktivität und einem veränderten Metabolismus der Mitochondrien assoziiert war und zu einer erhöhten Atmungsrate, oxidativen Phosphorylierung sowie einem erhöhten mitochondrialen Membranpotential führte. Diese Daten weisen darauf hin, dass die HER-2/neu-vermittelte CREB-Aktivierung, welche durch eine hypoxische Tumormikroumgebung verursacht wird, auf verschiedenen Ebenen zum neoplastischen Phänotyp von HER-2/neu-transformierten Zellen beiträgt.

Beiträge der Autoren: Sandra Leisz hat die extrazelluläre Flussmessung durchgeführt und ausgewertet. Weiterhin war sie an der Durchführung der Mausexperimente, der Etablierung der Hypoxie-Versuche, der ATP- und LDH-Messung und dem Schreiben des Manuskriptes beteiligt. André Steven hat gemeinsam mit Barbara Seliger das Projekt konzipiert und das Manuskript geschrieben. André Steven hat die gesamten Experimente mit Ausnahme der immunhistochemischen (IHC) Untersuchungen und der extrazellulären Flussmessung mit dem „Seahorse Analyzer“ durchgeführt. Katharina Synchra, Claudia Wickenhauser und Carsten Denkert führten die IHC-Analysen durch und stellten das humane Tumormaterial zur Verfügung. Bernhard Hiebl war an den Mausexperimenten beteiligt. Dimitrios Mougiakakos stellte den „Seahorse Analyzer“ sowie das Verbrauchsmaterial für die extrazelluläre Flussmessung zur Verfügung. Rolf Kiessling stellte die humanen HER-2/neu-Zellmodelle zur Verfügung.

### 3.4 „Linking CREB function with altered metabolism in murine fibroblast-based model cell lines"

André Steven, **Sandra Leisz**, Claudia Wickenhauser, Kristin Schulz, Dimitrios Mougiakakos, Rolf Kiessling, Carsten Denkert, Barbara Seliger

*Oncotarget* (2017), 8(57):97439-97463

CREB ist häufig in Tumoren unterschiedlicher Histologie überexprimiert und verstärkt aktiviert, was zu erhöhter Proliferation, Migration, Invasion, Angiogenese sowie reduzierter Apoptose der Tumorzellen führt. Für die deregulierte Expression sind sowohl transkriptionelle als auch posttranskriptionelle Regulationsmechanismen ursächlich. Die vorliegende Studie zeigt, dass deregulierte CREB-Expressionsspiegel und -Aktivierung mit Veränderungen im zellulären Metabolismus assoziiert sind. Mittels vergleichender Proteomanalyse wurde ein differentielles Expressionsmuster, der am zellulären Stoffwechsel beteiligten Proteine bei CREB-herunterregulierten HER-2/neu-transfizierten Zellen identifiziert. Dies war mit einem verminderten GLUT1-Expressionsniveau, reduzierter Glukoseaufnahme und reduzierter Expression glykolytischer Enzyme im Vergleich zu HER-2/neu$^+$-Zellen verbunden. Weiterhin führte die Hypoxie-induzierte CREB-Aktivierung zu Veränderungen des Stoffwechsels in HER-2/neu-transfizierten Zellen. Der verminderte pH-Wert im Zellkulturüberstand von HER-2/neu$^+$-Zellen war mit einer verstärkten intrazellulären LDH-Expression und Laktatsekretion assoziiert, wobei sich eine Reversion des Effektes durch die Herunterregulation von CREB zeigte. Darüber hinaus ging die Hypoxie-mediierte erhöhte CREB-Phosphorylierung am Serinrest 133 mit einer verminderter ERK-Aktivität und der verstärkten Aktivierung der Proteinkinase B einher. Zusätzlich wurde gezeigt, dass CREB die Entgiftung von ROS durch die verstärkte Katalase-Expression fördert und somit die mitochondriale Aktivität unter oxidativem Stress schützt. Diese Daten charakterisieren den Zusammenhang zwischen der CREB-Funktion und dem veränderten Stoffwechsel in HER-2/neu-transformierten Zellen. Somit könnten die veränderten Stoffwechselwege einen therapeutischen Ansatz für die Behandlung von Patienten mit HER-2/neu-überexprimierenden Tumoren darstellen.

Beiträge der Autoren: Sandra Leisz hat die extrazelluläre Flussmessung und die massenspektrometrischen Proteinidentifizierung durchgeführt. Außerdem war sie am Schreiben des Manuskriptes beteiligt. André Steven hat gemeinsam mit Barbara Seliger das Projekt konzipiert und das Manuskript geschrieben. André Steven hat die Experimente mit Ausnahme der 2D-Gel-Analysen und der extrazellulären Flussmessung durchgeführt. Kristin Schulz realisierte die 2D-Gel-Analysen. Claudia Wickenhauser, Rolf Kiessling und Carsten Denkert waren am Schreiben des Manuskriptes beteiligt. Dimitrios Mougiakakos stellte den „Seahorse Analyzer“ sowie das Verbrauchsmaterial für die extrazelluläre Flussmessung zur Verfügung.

**Tabelle 3: Darstellung des prozentualen Eigenanteils der zusammengefassten Manuskripte.**

| **Manu-skript** | **Journal** | **Erscheinungs-jahr** | ***Impact Factor**** | **Eigenanteil** | |
|---|---|---|---|---|---|
| | | | | Experimenteller Anteil (%) | Anfertigung des Manuskriptes (%) |
| 1 | *Oncotarget* | 2015 | 5,008 | ca. 90 % | ca. 85 % |
| 2 | | 2015 | 5,008 | ca. 20 % | ca. 20 % |
| 3 | | 2016 | 5,168 | ca. 30 % | ca. 30 % |
| 4 | | 2017 | 4,849 | ca. 20 % | ca. 20 % |

Bei *Oncotarget* handelt es um ein *Peer Review Open Access* Journal mit den Schwerpunkten Onkologie und Zellbiologie. *, übernommen von der Datenbank *Journal Citation Reports* und *scijournal.org (Impact Factor 2017)*.

# 4 Manuskripte

## 4.1 „Distinct von Hippel-Lindau gene and hypoxia-regulated alterations in gene and protein expression patterns of renal cell carcinoma and their effects on metabolism“

www.impactjournals.com/oncotarget/ Oncotarget, Vol. 6, No. 13

### Distinct von Hippel-Lindau gene and hypoxia-regulated alterations in gene and protein expression patterns of renal cell carcinoma and their effects on metabolism

**Sandra Leisz[1], Kristin Schulz[1], Susanne Erb[1], Peter Oefner[2], Katja Dettmer[2], Dimitrios Mougiakakos[3], Ena Wang[4], Francesco M. Marincola[4], Franziska Stehle[1], Barbara Seliger[1]**

[1]Institute of Medical Immunology, Martin Luther University Halle-Wittenberg, 06112 Halle (Saale), Germany

[2]Institute of Functional Genomics, University of Regensburg, 93053 Regensburg, Germany

[3]Department of Internal Medicine 5, University of Erlangen, 91054 Erlangen, Germany

[4]Sidra Medical and Research Center, PO Box 26999, Doha, Qatar

**Correspondence to:**
Barbara Seliger, **e-mail:** Barbara.Seliger@uk-halle.de

***Keywords:*** *hypoxia, von Hippel Lindau gene, renal cell carcinoma, cell metabolism, aerobic glycolysis*

***Received:*** *February 03, 2015* ***Accepted:*** *February 25, 2015* ***Published:*** *March 27, 2015*

## ABSTRACT

**During the last decade the knowledge about the molecular mechanisms of the cellular adaption to hypoxia and the function of the "von Hippel Lindau" (VHL) protein in renal cell carcinoma (RCC) has increased, but there exists little information about the overlap and differences in gene/protein expression of both processes. Therefore the aim of this study was to dissect VHL- and hypoxia-regulated alterations in the metabolism of human RCC using ome-based strategies. The effect of the VHL- and hypoxia-regulated altered gene/protein expression pattern on the cellular metabolism was analyzed by determination of glucose uptake, lactate secretion, extracellular pH, lactate dehydrogenase activity, amino acid content and ATP levels. By employing $VHL^-/VHL^+$ RCC cells cultured under normoxic and hypoxic conditions, VHL-dependent, HIF-dependent as well as VHL-/HIF-independent alterations in the gene and protein expression patterns were identified and further validated in other RCC cell lines. The genes/proteins differentially expressed under these distinct conditions were mainly involved in the cellular metabolism, which was accompanied by an altered metabolism as well as changes in the abundance of amino acids in VHL-deficient cells. In conclusion, the study reveals similarities, but also differences in the genes and proteins controlled by VHL functionality and hypoxia thereby demonstrating differences in the metabolic switch of RCC under these conditions.**

## INTRODUCTION

Renal cell carcinoma (RCC) represents approximately 2–3% of all cancers worldwide. It is a heterogeneous disease with an increasing incidence and more than 100.000 deaths per year [1]. While localized RCC can be cured by surgery, inoperable RCC is resistant to chemotherapy and radiotherapy and about 15% of patients respond to immunotherapy. Angiogenesis plays an important role in RCC development and progression as evidenced by the molecular genetics of the autosomal dominant von Hippel Lindau (VHL) syndrome and the clear cell RCC (ccRCC) subtype. Drugs targeting angiogenic factors have revolutionized the therapy of ccRCC and led to a marked survival benefit in patients with metastatic disease [2]. However, RCC patients often develop resistances to these drugs.

The ccRCC is often associated with a loss of the VHL gene function due to its deletion on chromosome 3p, loss of heterozygosity, promoter methylation or missense mutations. VHL mutations occur in approximately 50% of sporadic ccRCC, which prevent the VHL-mediated degradation of the hypoxia-inducible factor (HIF)α under normoxic conditions. This is also the case by hypoxia, which prevents binding of the prolylhydroxylase (PHD) to HIFα, thereby leading to the induction of HIF targets. More

than 2% of human genes are directly or indirectly regulated by HIF [3]. These HIF targets modulate transcriptional regulation, cell proliferation, survival, apoptosis, motility, cytoskeletal structure, cell adhesion, angiogenesis and cellular metabolism [4]. In ccRCC, HIF1α is often not expressed, while HIF2α adopts its function [5]. Lack of VHL function or hypoxia cause a metabolic switch to aerobic glycolysis [6]. This is associated with a high glucose influx, a decreased gluconeogenesis and an increased lactate concentration in the tumor microenvironment, which is associated with an impaired immune recognition [7, 8] due to changes in the activity and function of T cells, NK cells and dendritic cells (DC) [9–12].

Generally, loss of VHL function or hypoxia has been postulated to cause identical alterations in gene/protein expression and function. However, this study identified differences in the VHL- and hypoxia-induced pathways by determining the mRNA and protein expression pattern of $VHL^-$ RCC cell lines and their VHL transfectants in the presence and absence of hypoxia using cDNA microarrays, 2DE-based proteomics, and metabolomics. Selected differentially expressed genes and proteins were further validated and subjected to functional analysis.

## RESULTS

### Characterization of the different VHL model systems

The mRNA and protein expression levels of VHL were determined under both normoxic and hypoxic conditions in the $VHL^-$ cell lines 786-O, RCC4 and RCC10 and their VHL transfectants using qPCR (Figure 1A) and Western blot analysis (Figure 1B), respectively. Expression of VHL protein was only detectable in VHL transfectants and did not significantly differ between normoxia and hypoxia. Over-expression of VHL led to a degradation of HIF2α protein during normoxia and to its stabilization under hypoxia (Figure 1B). Subsequently, transcription levels of the HIF2α target gene GLUT 1 were reduced by 2.1 to 5-fold under normoxia in the $VHL^+$ RCC cells when compared to $VHL^-$ RCC cells. In contrast, hypoxia caused a 3.5 to 5.9-fold up-regulation of GLUT1 expression in $VHL^+$ RCC cells when compared to normoxia (Figure 1C).

### Identification of VHL- and hypoxia-induced genes

The gene expression pattern of $VHL^-$ and $VHL^+$ 786-O cells was determined under normoxic and hypoxic conditions. The levels of gene expression significantly differed between the cell systems and culture conditions used (Table S2). Some genes were down-regulated up to approximately 60-fold (NID2), while others were up-regulated to approximately 25-fold (RAB31) depending on the conditions analysed.

The most differentially expressed transcripts with $n = 1202$ and $n = 1292$, respectively, were found upon comparison of $VHL^+$ with $VHL^-$ cells under normoxia and hypoxia (Table S3). The overlapping genes (662 genes, Figure S1, Table S4) of these groups represent putative VHL-regulated genes.

The greatest proportion of differentially expressed genes mediated by VHL expression (24%; Figure 2A) and hypoxia (28%; Figure 2B) exert a metabolic function. Figure 2C summarizes the hierarchical clustering of the differentially expressed metabolic genes in VHL-deficient vs. VHL-expressing cells under normoxia and/or hypoxia ($p < 0.05$). The number of VHL-independent, hypoxia-regulated genes (194 regulated cDNAs) was much lower (Table S2), but the lowest number was found for putative HIF2α–regulated genes (28 genes, Table S4). These data indicated distinct VHL-, hypoxia- as well as HIF-independent regulated processes.

### Identification of VHL- and hypoxia-regulated targets

In order to identify differentially expressed proteins caused by a distinct VHL status and hypoxic environment, 2DE-based proteomics of $VHL^-$ and $VHL^+$ 786-O cells cultured under normoxia or hypoxia was performed leading to 76 differentially expressed proteins identified by MALDI-TOF/MS analysis (Table S3, Table S5). These included VHL-independent, but hypoxia-dependent as well as VHL-dependent and hypoxia-independent and HIF2α-dependent targets, respectively. Figure 2D shows identified differentially expressed proteins on a representative 2-DE gel of $VHL^-$ vs. $VHL^+$ 786-O cells during hypoxia. Although the differentially expressed proteins were associated with distinct functions, approximately 30% of VHL-regulated proteins and 38% of hypoxia-regulated proteins belong to metabolic processes (Figure 2E, 2F). There exists a significant overlap in differentially expressed proteins by comparing $VHL^-$ vs. $VHL^+$ 786-O protein profiles to that of 786-O cells under normoxic versus hypoxic conditions, whereas only a few proteins were found to be differentially expressed in normoxic vs. hypoxic 786-O cells ($n = 13$) and $VHL^+$ 786-O cells ($n = 2$), respectively (Table S5).

### Impact of VHL- and hypoxia-dependent alterations on the cellular metabolism

In order to validate the differentially expressed genes and proteins, modulated by VHL, hypoxia or a combination of both, qPCR, Western blot analyses and enzymatic activity assays of selected targets were performed.

The glucose consumption of the $VHL^{-/+}$ RCC model system was investigated via the uptake of fluorescent dye labelled glucose. The $VHL^+$ RCC cells showed a

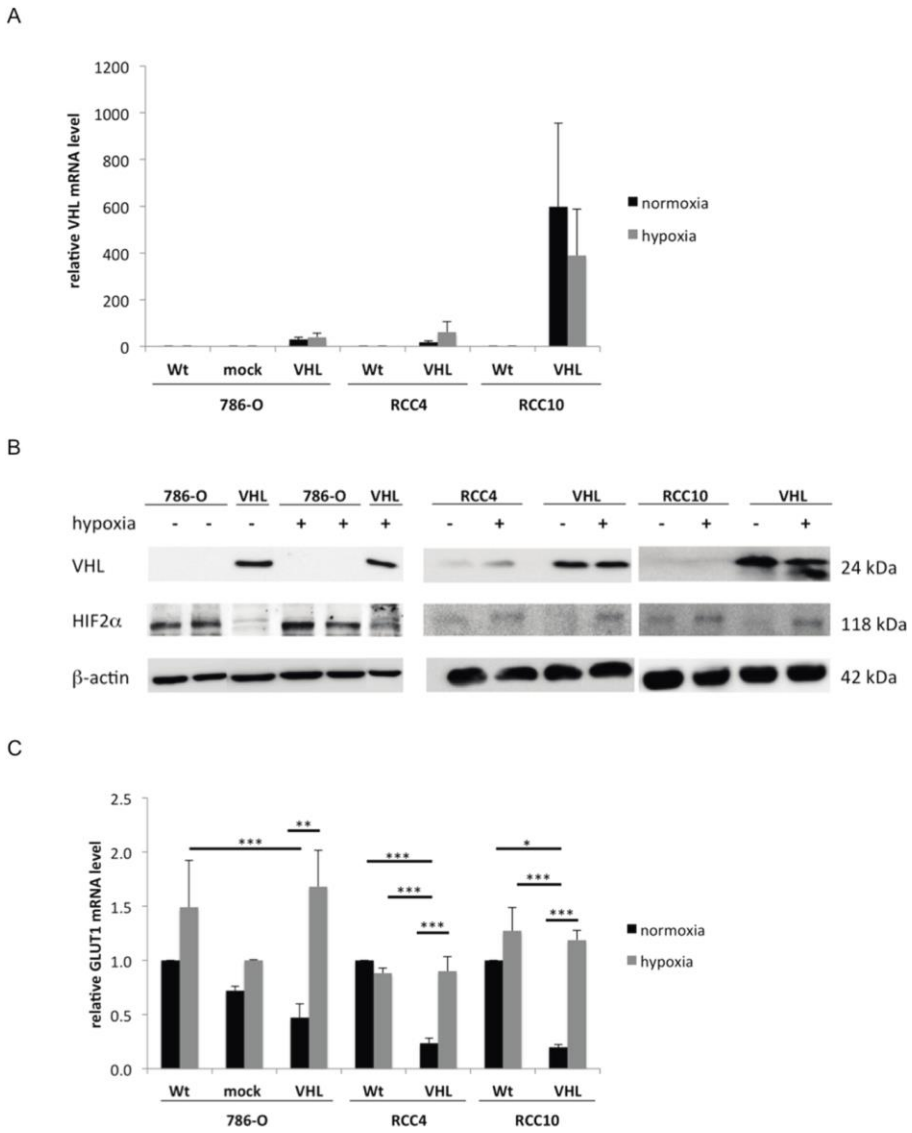


**Figure 1: Restoration of functional VHL expression in 786-O, RCC4 and RCC10 cells. (A)** VHL$^-$ cells were stably transfected with a VHL overexpression vector or vector backbone. The bulk cultures were analysed for VHL mRNA expression after 24 h incubation during normoxia or hypoxia (1% $O_2$) conditions using qPCR. The data was normalized to β-actin expression and the expression of wild type cells incubated under normoxia was set to 1. **(B)** Western blot analysis of VHL and HIF2α protein in wt 786-O, RCC4, and RCC10 cells and their respective transfectants during normoxia and hypoxia. Immunostaining was performed with a VHL- and HIF2α-specific antibody as described in the experimental procedures. Equal amount of protein loading was controlled by immunostaining using β-actin-specific antibody. A representative result of three independent biological replicates is shown. **(C)** mRNA expression of HIF2α target gene GLUT1 in VHL$^-$ and VHL$^+$ cells during normoxia and hypoxia oxygen conditions was measured by qPCR and normalized to β-actin. The expression level of wt RCC cells was set to 1.

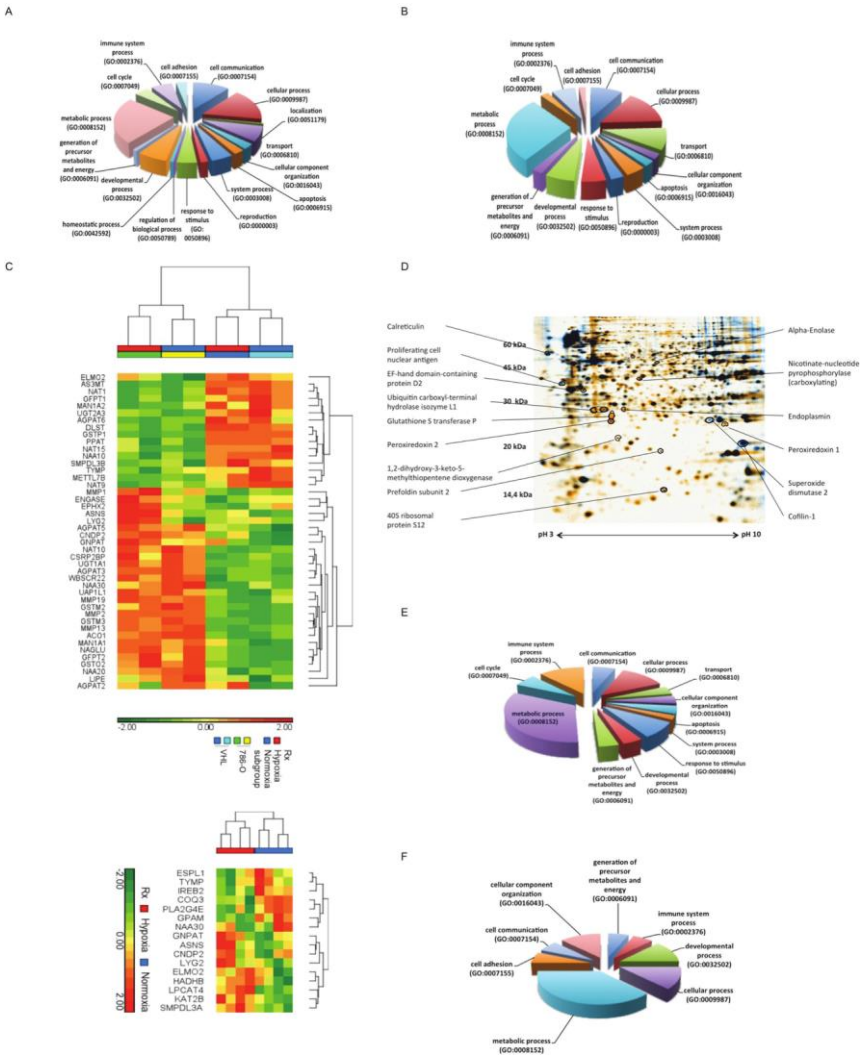


**Figure 2: Functional classification of VHL- and hypoxia-dependent regulated genes and proteins. (A and B)** The cDNA microarray analysis was performed with Trizol-prepared total RNA as described in experimental procedures. For the classification of data in biological processes the PANTHER classification system according to gene ontology criteria was employed. The pie chart shows representative classifications for (A) $VHL^+$ vs. $VHL^-$ 786-O cells, and (B) wt cells incubated during hypoxia (1% $O_2$) vs. normoxia. **(C)** Hierarchical clustering of "ome"-based data. Using the hierarchical clustering differentially expressed genes associated with metabolic function ($p$ <0.05) identified by one way ANOVA among $VHL^+$, $VHL^-$ 786-O under hypoxia or normoxia (top heat map) and hypoxia- vs. normoxia-specific metabolic function related genes independent of VHL status ($t$ test, $p$ < 0.05, bottom heat map) were visualized. **(D)** Identified differentially expressed proteins were marked on a representative 2-DE gel of $VHL^-$ vs. $VHL^+$ 786-O cells during hypoxia. **(E and F)** The pie charts demonstrate the classification of differentially expressed proteins, which were identified by 2DE followed by peptide mass fingerprint. The classification of proteins was performed with PANTHER software and is representatively demonstrated for E) $VHL^+$ vs. $VHL^-$ 786-O cells and F) wt cells incubated under normoxic and hypoxic (1% $O_2$) conditions.

statistically significant 2-fold reduced glucose uptake compared to the VHL-deficient RCC cells (Figure 3A), which was accompanied by an altered expression of many glycolytic enzymes (Table S6). In addition, extracellular flux analysis was performed to assess the ECAR. As shown in Figure 3B, VHL expression significantly decreased glycolysis and glycolytic activity. A VHL-dependent down-regulation of pyruvate kinase (PK)M2, γ-enolase (ENO2) and triosephosphate isomerase (TPI)1 was detected, while ENO2, TPI1 and aldolase (ALDO)A were hypoxia-dependently up-regulated (Table S6). Over-expression of VHL caused a 2- to 2.5-fold reduction in the expression of TPI1 under normoxic conditions in comparison to VHL-deficient RCC cells, while its expression was enhanced 2- to 3.9-fold under hypoxia in the $VHL^+$ RCC cells when compared to normoxic conditions (Figure 3C). In $VHL^-$ 786-O and RCC4 cells, the expression of ALDOA is hypoxia-dependent 1.7- to 2-fold up-regulated, while in RCC10 cells a 2.5-fold VHL-mediated down-regulation of ALDOA was observed, which could be restored by hypoxia (Figure 3D). Furthermore, the intracellular ATP levels were up to 67% decreased in $VHL^+$ when compared to $VHL^-$ RCC cells (Figure 3E).

### Association of VHL expression with an induction of the citric acid cycle and the mitochondrial respiratory chain

To further analyse the VHL status-dependent metabolic changes, the tricarboxylic acid cycle (TCA) and the mitochondrial respiratory chain activity was determined in $VHL^-/VHL^+$ model systems. Despite a VHL-dependent suppression of glycolysis and ATP production, the expression of the enzymes of the TCA and, consequently, of the mitochondrial respiratory chain were increased (Table S6). Interestingly, the SDHA transcription was neither dependent on VHL nor on hypoxia (Figure 4A). In contrast, the protein expression of SDHA was approximately 2-fold up-regulated in $VHL^+$ RCC cells (Figure 4B, 4C). The mitochondrial respiration was assessed in $VHL^-/VHL^+$ RCC cells using the extracellular flux assay. An increase of basal oxygen associated with an increased respiration and respiratory reserve was found in $VHL^+$ compared to $VHL^-$ RCC cells (Figure 4D). This was associated with a 1.5 to 2-fold increase of the mitochondrial dehydrogenase activity upon VHL overexpression (Figure 4E).

### VHL-dependent regulation of lactate secretion and pH regulation

Since VHL could regulate the lactate dehydrogenase (LDH) expression [18, 19], the intracellular LDH activity of the $VHL^-$ and $VHL^+$ cells was determined. When compared to $VHL^-$ RCC cells, LDH activity was down-regulated between 30% to 66% in VHL transfectants (Figure 5A), which was associated with an up to 55% lower extracellular lactate concentration (Figure 5B) and an altered pH in the cell culture supernatant (Figure 5C). In contrast, hypoxia restored the VHL-mediated reduction of LDH activity and lactate secretion, which is accompanied by a drop in the extracellular pH of the VHL transfectants (Figure 5).

### Altered VHL-dependent amino acid content in RCC cell lines

In order to investigate whether the amino acid metabolism is also altered by the VHL status, the content of 20 free amino acids was measured in the 786-O VHL model system under normoxic conditions. In comparison to VHL-deficient 786-O cells, the overall content of free amino acids was reduced about 25% in $VHL^+$ RCC cells, with the highest down-regulation of 2.5-fold for serine (Figure 6). In contrast, the arginine concentration was not altered in the presence or absence of VHL.

## DISCUSSION

Major advances have been made in our understanding of the molecular mechanisms of cellular adaption to hypoxia and the function of VHL. Nevertheless, little information exists about the overlap and differences of VHL-dependent/independent and hypoxia-dependent alterations in gene and protein expression patterns and their effects on the cellular metabolism. Therefore, the aim of the study was to dissect both the VHL- and/or hypoxia-induced pathways, which might lead to the identification of candidate biomarkers for disease progression and novel therapeutic targets. Using a tandem approach of cDNA microarrays and 2-DE-based proteome analyses, a large number of differentially expressed genes and/or proteins could be detected in $VHL^+$ versus $VHL^-$ RCC cells as well as under normoxic and/or hypoxic conditions. Despite a high frequency of genes/proteins concordantly regulated by loss of VHL function and hypoxia, a number of differentially expressed genes/proteins demonstrating a VHL-dependent, VHL-independent, hypoxia-dependent, and hypoxia-independent regulation, respectively, of the gene and protein expression profiles was identified. qPCR and/or Western blot validation further confirmed the differential gene and protein expression profiles in the $VHL^-$ and $VHL^+$ RCC model systems analysed in the absence or presence of hypoxia. Reflecting the biology and molecular features of RCC, the differentially expressed genes/proteins were mainly involved in the cell metabolism and were localized in the cytoplasm. In most cases there exists a concordant expression of these molecules at the mRNA and protein level, although some genes appear to be post-transcriptionally controlled, such as SDHA. These data are in line with the proteome analysis of primary RCC lesions and patient-matched normal kidney epithelium demonstrating an altered glycolysis and gluconeogenesis

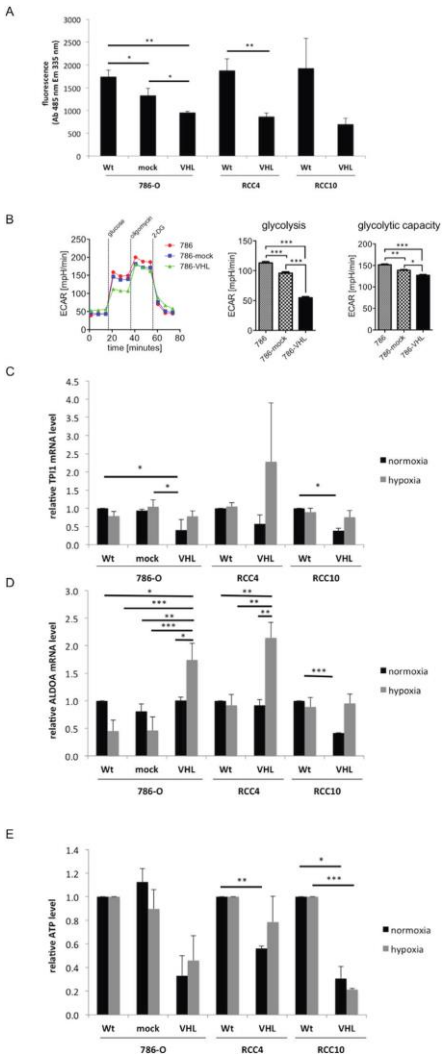


**Figure 3: VHL-dependent changes in glucose uptake and glycolysis. (A)** 1 × $10^4$ cells/cell line were seeded and the glucose uptake was measured by incorporation of fluorescently labelled deoxyglucose (2-NBDG) at absorption and emission wavelengths of 485 nm and 535 nm, respectively. The fluorescence signal of wild type (wt) cells was set to 1. The figure shows the mean values and standard derivations of three independent assays. **(B)** The extracellular acidification rate of wt, mock- and VHL-transfected 786-O cells is measured in response to the indicated substrates and inhibitors. ECAR is predominantly the result of anaerobic glycolysis. ECAR levels upon administration of glucose are indicative for basal glycolysis and upon administration of oligomycin for the cells' glycolytic capacity. A representative analysis as well as the mean values for glycolysis and the glycolytic capacity is shown. Bars indicate the standard error mean. Abbreviations: p, *p*-value; *, $p < 0.05$; **, $p < 0.005$; ***, $p < 0.001$. **(C and D)** Analyses of TPI1 (C) and ALDOA (D) mRNA expression are shown. qPCR analyses of wt and VHL-transfected 786-O, RCC4 and RCC10 cells were performed using oligo-dT primed cDNA and normalized to β-actin mRNA expression. The expression levels of parental cells were set to 1 and the diagram shows the means with S.D. of three biological replicates. **(E)** ATP levels were measured by the Cell Titer Glo luminescence cell viability assay as described in experimental procedures. The $VHL^-$ RCC cells were set to 1.

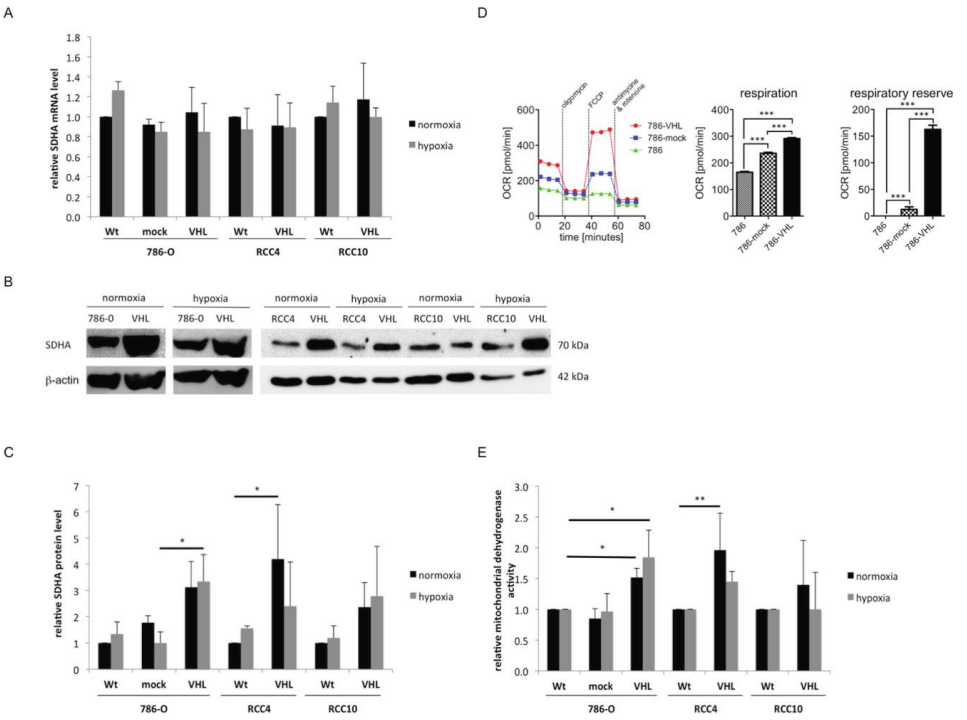


**Figure 4: Induction of TCA and mitochondrial respiratory chain through VHL overexpression.** **(A)** The transcription level of SDHA was determined using oligo-dT primed cDNA and specific primer via qPCR. Expression of wt cells was set to 1. **(B)** 50 µg protein/cell line was separated by 10% SDS-PAGE, transferred onto a nitrocellulose membrane before immunostaining was performed with a SDHA-specific antibody as described in experimental procedures. Equal protein loading was controlled by subsequent immunostaining using an anti-β-actin-specific antibody. A representative result of three independent biological replicates is shown. **(C)** Densitometric analysis of SDHA expression in $VHL^-$ and $VHL^+$ 786-O, RCC4 and RCC10 cells incubated during normoxia and hypoxia (1% $O_2$) is shown. Areas of immunoblot signals were integrated using AIDA image analyser software and normalized to β-actin. The graphic showed the means and S.D. of three independent experiments. **(D)** The baseline oxygen consumption rate (OCR) was measured by an XFe96 flux analyzer in wt, mock-, and VHL-transfected 786-O cells. OCR is an indicator of mitochondrial respiration. Respiration (OCR) is measured under basal conditions and in response to the indicated substances. Changes after application of the uncoupling agent FCCP are indicative for the respiratory reserve. A representative analysis as well as the mean values for basal respiration and the respiratory reserve is shown. Bars indicate the standard error mean. Abbreviations: p, *p*-value; ***, $p < 0.001$. **(E)** $5 \times 10^3$ cells/well were seeded in triplicates in 96-well plates and incubated for 72 h at 37°C and 5% $CO_2$ during normoxia and hypoxia. The activity of mitochondrial dehydrogenases was measured trough the turnover of the tetrazolium salt XTT to formazan by the OD of 490 nm.

[20, 21]. This study here extended these results by analysing the VHL and hypoxia dependence or independence demonstrating a link between VHL loss and hypoxia, but also a distinction between both pathways. This is mediated by an altered gene and protein expression pattern, which also modulates the tumor microenvironment thereby differentially affecting the metabolic switch of RCC.

Heterogeneous, but increased expression of ALDOA was found in RCC subtypes when compared to normal kidney cortex [22] as well as in the serum of RCC patients and have been used for tumor staging [23]. These data were extended by demonstrated an up-regulation of ALDOA expression associated with hypoxic conditions and loss of VHL expression suggesting a link between ALDOA, VHL and hypoxia. Thus, ALDOA might represent a suitable and potential target irrespective of the VHL status and oxygen conditions.

Several reports have demonstrated a direct correlation between the loss of VHL expression and alterations in the cellular metabolism, leading to an altered tumor microenvironment, such as high lactate concentrations and low pH value [24]. This was

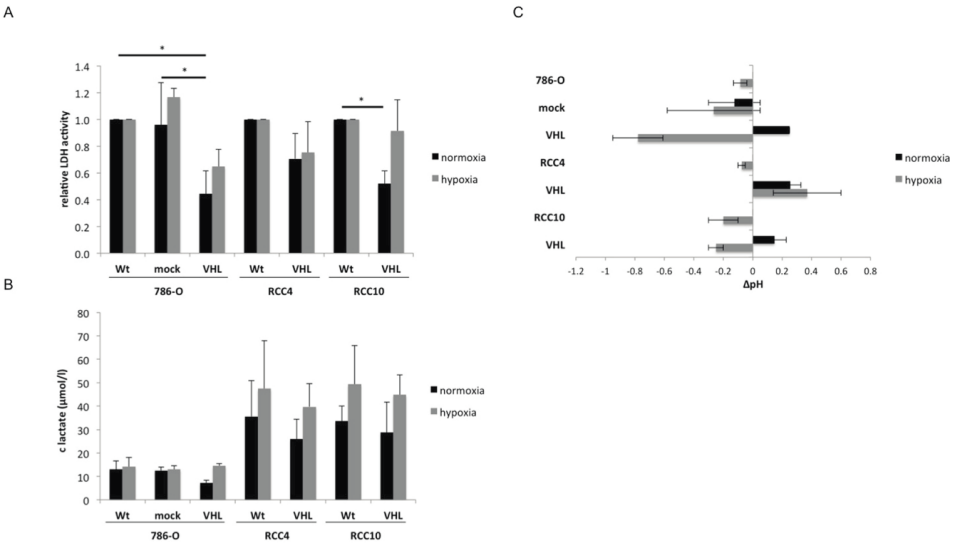


**Figure 5: VHL-dependent alterations of lactate dehydrogenase activity, lactate secretion and extracellular pH as a function of oxygen tension.** Five × $10^3$ $VHL^-/VHL^+$ cells were seeded in triplicate in 96-well plates and incubated for 48 h under both normoxic and hypoxic conditions. Shown are the means and standard derivations of three independent assays **(A)** The intracellular lactate dehydrogenase activity was determined by the CytoTox96 Non-Radioactive Cytotoxicity Assay (Promega). The LDH activity of wt RCC cells was set to 1. **(B)** Extracellular lactate levels in the cell culture supernatants of $VHL^-$ and $VHL^+$ RCC cells under both normoxic and hypoxic conditions. **(C)** Changes in the pH value of supernatants in relation to the respective VHL-deficient RCC cell line under normoxia.

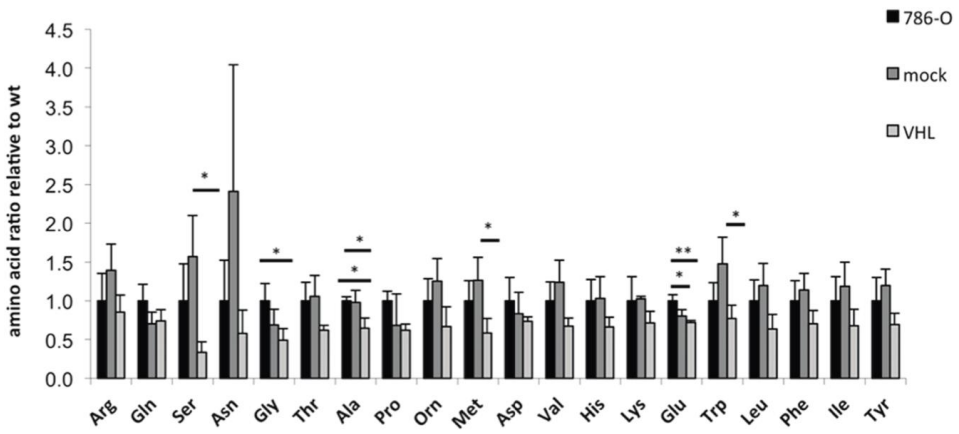


**Figure 6: Intracellular free amino acid levels of wt, $VHL^+$ and $VHL^-$ 786-O cells.** Amino acid concentrations are expressed as ratios relative to the wt, which was set to one. A one-way ANOVA followed by Tukey post hoc test was performed to test for significant differences (*$p \leq 0.05$, **$p \leq 0.01$).

also confirmed in this study by reversible hypoxia- and VHL loss-mediated changes of the intracellular lactate dehydrogenase levels, extracellular lactate concentrations and extracellular pH, as well as the differential expression of genes/proteins involved in changes of the tumor microenvironment. These alterations could lead to an immune suppressive tumor microenvironment [25] although a correlation of the VHL status with the immune cell infiltration has not yet been determined in detail.

Metabolome analysis demonstrated an altered metabolite and amino acid content in $VHL^-$ vs. $VHL^+$ cells (Figure S2), thus supporting their distinct metabolism and was further strengthened by recent work of Gameiro and co-authors describing reduced intracellular citrate levels in VHL mutant versus VHL wt RCC cells due to the presence of HIF thereby linking VHL and hypoxia and sensitizing VHL-deficient cells to glutamine deprivation [26]. Citrate levels could be restored by silencing PDK-1 and ACLY, which was accompanied by suppression of RCC. Furthermore, HIF rendered VHL-deficient cells sensitive to glutamine deprivation *in vitro*, while systemic treatment with glutaminase inhibitors suppressed the *in vitro* and *in vivo* growth of RCC cells.

## MATERIALS AND METHODS

### Cell lines and hypoxia incubation

The RCC cell lines RCC4 and RCC4 VHL were obtained from Health Protection Agency Culture Collections (Salisbury, UK). The RCC cell lines 786-O and RCC10, and their respective stable VHL transfectants were kindly provided by Prof. Wiesener (Erlangen) and were authenticated by DNA profiling. All cell lines were maintained in DMEM supplemented with 10% fetal calf serum (Gibco), 2 mM glutamine (Biochrom AG), 1 mM pyruvate (Gibco), 100 U/mL penicillin and 100 µg/mL streptomycin (PAA). Cells were cultivated for 24 to 72 h either under normal oxygen conditions or at 1% oxygen (hypoxia incubator, Binder) at 37°C and 5% $CO_2$. All experiments were carried out during the logarithmic growth phase of the cells.

### Microarray analysis

Total RNA was extracted from $3 \times 10^6$ cells using Trizol reagent (Invitrogen), reverse transcribed and amplified with the WT expression kit (Invitrogen) according to the manufacturer's manual. Fragmented cDNA was end-labeled using the Affymetrix terminal labeling kit and hybridized onto Human GeneChip 1.0 ST arrays (Affymetrix). The chips were stained and washed following standard procedure and scanned on a GeneChip Scanner 3000 7G (Affymetrix).

### Two-dimensional gel electrophoresis

Protein was isolated from $5 \times 10^7$ $VHL^-/VHL^+$ 786-O cells incubated for 48 h under normoxic or hypoxic conditions. 550 µg/protein lysate were loaded onto IPG strips (pH 3–10, non-linear, Amersham Biosciences) followed by an isoelectric focusing and second-dimension SDS-PAGE separation (13%) and staining with colloidal Coomassie as described [13]. The gels were analyzed using the Delta2D software package (Decodon). Proteins found to be at least two-fold regulated (factor $\geq 2.0$ or $\leq 0.50$; $p \leq 0.05$) were subjected to mass spectrometric identification. The two-dimensional gel electrophoresis was carried out in three independent experiments using five gels for each condition.

### In-gel digestion and mass spectrometric analysis

Differentially regulated protein spots were excised from the gels using the Spothunter (Herolab), destained with 50% acetonitrile (v/v) over night and subjected to in-gel digestion with 8 µg/mL porcine trypsin (Promega). Tryptic digests were subjected to MALDI-TOF mass spectrometry (Ultraflex, Bruker). Protein identification was performed as previously described [13].

### RNA isolation and real time quantitative PCR

Total cellular RNA was isolated using the NucleoSpin RNA II kit (Macherey & Nagel). Two µg of total RNA were reverse transcribed into cDNA using the Revert H Minus First Strand cDNA synthesis kit (Fermentas) and oligo(dT)18 primer according to the manufacturer's instructions. Comparative quantification of gene expression was performed as previously described [14]. The target-specific primers used for qPCR are listed in the Supplementary Table S1.

### Western blot analysis

Cells were harvested as previously described [13] and protein isolated according to Laemmli [15]. Fifty µg protein/lane were subjected to Western blot analysis as recently described [13]. Membranes were incubated over night at 4°C with the primary monoclonal antibodies (mAb) directed against succinate dehydrogenase complex subunit A (SDHA; Cell Signaling), HIF2α (Novus) and β-actin (Sigma-Aldrich), followed by incubation for 1 h with horseradish peroxidase-linked secondary antibody and developed using the ECL method. Chemoluminescence signals were detected using a CCD camera (LAS3000, Raytest). For quantification of the SDHA protein expression the respective area of the signal was integrated using an AIDA image analyser (Raytest) and subsequently normalized to β-actin.

Halle-Wittenberg, Department of Legal Medicine) for authentication of RCC cell lines and Fabian Bull (Martin Luther University Halle-Wittenberg, Department of Bioinformatics) for the help with microarray data. This work was sponsored by the Mildred Scheel Krebshilfe (109247), the Sander Stiftung (2010–002.1), the German Research Foundation (KFO262), and the intramural Roux program of the medical faculty of the Martin Luther University Halle-Wittenberg.

## CONFLICTS OF INTEREST

No potential conflicts of interest were disclosed.

### Abbreviations

2-NBDG; 2-[N-(7-nitrobenz-2-oxa-1, 3-diazol-4-yl)amino]-2-deoxy-D-glucose, 2DE: two-dimensional gel electrophoresis, ACO; aconitase ccRCC, clear cell renal cell carcinoma, ALDOA; aldolase A, AKR1B1; aldose reductase, DMEM; Dulbecco's Modified Eagle's Medium, ECAR; extracellular acidification rate, ECL; electrochemiluminescence, ECHS1; enoyl-CoA hydratase short chain 1, ENO; enolase, FCS; fetal calf serum, GLUT; glucose transporter, HIF; hypoxia inducible factor; HRE; hypoxia responsible element, LDH; lactate dehydrogenase, MALDI-TOF; matrix-assisted laser desorption/ionization time-of-flight, MAPK; mitogen-activated protein kinase, MCT; monocarboxylate transporter, OCR; oxygen consumption rate, p; *p*-value, PBS; phosphate-buffered saline, PKM; pyruvate kinase, RCC; renal cell carcinoma, SDH; succinate dehydrogenasem, SDHA; succinate dehydrogenase complex subunit A, TCA; tricarboxylic acid cycle, TPI; triose-phosphate isomerase, VHL; von Hippel-Lindau Wt, wild type.

## REFERENCES

1. Gupta K, Miller JD, Li JZ, Russell MW, Charbonneau C. Epidemiologic and socioeconomic burden of metastatic renal cell carcinoma (mRCC): a literature review. Cancer treatment reviews. 2008; 34:193–205.
2. Rini BI, Campbell SC, Escudier B. Renal cell carcinoma. Lancet. 2009; 373:1119–1132.
3. Manalo DJ, Rowan A, Lavoie T, Natarajan L, Kelly BD, Ye SQ, Garcia JG, Semenza GL. Transcriptional regulation of vascular endothelial cell responses to hypoxia by HIF-1. Blood. 2005; 105:659–669.
4. Ke Q, Costa M. Hypoxia-inducible factor-1 (HIF-1). Molecular pharmacology. 2006; 70:1469–1480.
5. Kaelin WG Jr. The von Hippel-Lindau tumour suppressor protein: O2 sensing and cancer. Nature reviews Cancer. 2008; 8:865–873.
6. Gordan JD, Thompson CB, Simon MC. HIF and c-Myc: sibling rivals for control of cancer cell metabolism and proliferation. Cancer cell. 2007; 12:108–113.
7. Gottfried E, Kreutz M, Mackensen A. Tumor metabolism as modulator of immune response and tumor progression. Seminars in cancer biology. 2012; 22:335–341.
8. Semenza GL. Tumor metabolism: cancer cells give and take lactate. The Journal of clinical investigation. 2008; 118:3835–3837.
9. Fischer K, Hoffmann P, Voelkl S, Meidenbauer N, Ammer J, Edinger M, Gottfried E, Schwarz S, Rothe G, Hoves S, Renner K, Timischl B, Mackensen A, Kunz-Schughart L, Andreesen R, Krause SW, et al. Inhibitory effect of tumor cell-derived lactic acid on human T cells. Blood. 2007; 109:3812–3819.
10. Gottfried E, Kunz-Schughart LA, Ebner S, Mueller-Klieser W, Hoves S, Andreesen R, Mackensen A, Kreutz M. Tumor-derived lactic acid modulates dendritic cell activation and antigen expression. Blood. 2006; 107:2013–2021.
11. Husain Z, Huang Y, Seth P, Sukhatme VP. Tumor-derived lactate modifies antitumor immune response: effect on myeloid-derived suppressor cells and NK cells. Journal of immunology. 2013; 191:1486–1495.
12. Mendler AN, Hu B, Prinz PU, Kreutz M, Gottfried E, Noessner E. Tumor lactic acidosis suppresses CTL function by inhibition of p38 and JNK/c-Jun activation. International journal of cancer Journal international du cancer. 2012; 131:633–640.
13. Recktenwald CV, Mendler S, Lichtenfels R, Kellner R, Seliger B. Influence of Ki-ras-driven oncogenic transformation on the protein network of murine fibroblasts. Proteomics. 2007; 7:385–398.
14. Wulfaenger J, Niedling S, Riemann D, Seliger B. Aminopeptidase N (APN)/CD13-dependent CXCR4 down-regulation is associated with diminished cell migration, proliferation and invasion. Molecular membrane biology. 2008; 25:72–82.
15. Laemmli UK. Cleavage of structural proteins during the assembly of the head of bacteriophage T4. Nature. 1970; 227:680–685.
16. Recktenwald CV, Leisz S, Steven A, Mimura K, Muller A, Wulfanger J, Kiessling R, Seliger B. HER-2/neu-mediated down-regulation of biglycan associated with altered growth properties. The Journal of biological chemistry. 2012; 287:24320–24329.
17. van der Goot AT, Zhu W, Vazquez-Manrique RP, Seinstra RI, Dettmer K, Michels H, Farina F, Krijnen J, Melki R, Buijsman RC, Ruiz Silva M, Thijssen KL, Kema IP, Neri C, Oefner PJ, Nollen EA. Delaying aging and the aging-associated decline in protein homeostasis by inhibition of tryptophan degradation. Proceedings of the National Academy of Sciences of the United States of America. 2012; 109:14912–14917.

18. Lichtenfels R, Kellner R, Atkins D, Bukur J, Ackermann A, Beck J, Brenner W, Melchior S, Seliger B. Identification of metabolic enzymes in renal cell carcinoma utilizing PROTEOMEX analyses. Biochimica et biophysica acta. 2003; 1646:21–31.
19. Semenza GL. Targeting HIF-1 for cancer therapy. Nature reviews Cancer. 2003; 3:721–732.
20. Lichtenfels R, Dressler SP, Zobawa M, Recktenwald CV, Ackermann A, Atkins D, Kersten M, Hesse A, Puttkammer M, Lottspeich F, Seliger B. Systematic comparative protein expression profiling of clear cell renal cell carcinoma: a pilot study based on the separation of tissue specimens by two-dimensional gel electrophoresis. Molecular & cellular proteomics : MCP. 2009; 8:2827–2842.
21. Unwin RD, Craven RA, Harnden P, Hanrahan S, Totty N, Knowles M, Eardley I, Selby PJ, Banks RE. Proteomic changes in renal cancer and co-ordinate demonstration of both the glycolytic and mitochondrial aspects of the Warburg effect. Proteomics. 2003; 3:1620–1632.
22. Craven RA, Hanrahan S, Totty N, Harnden P, Stanley AJ, Maher ER, Harris AL, Trimble WS, Selby PJ, Banks RE. Proteomic identification of a role for the von Hippel Lindau tumour suppressor in changes in the expression of mitochondrial proteins and septin 2 in renal cell carcinoma. Proteomics. 2006; 6:3880–3893.
23. Takashi M, Zhu Y, Nakano Y, Miyake K, Kato K. Elevated levels of serum aldolase A in patients with renal cell carcinoma. Urological research. 1992; 20:307–311.
24. Haase VH. The VHL/HIF oxygen-sensing pathway and its relevance to kidney disease. Kidney international. 2006; 69:1302–1307.
25. Singer K, Kastenberger M, Gottfried E, Hammerschmied CG, Buttner M, Aigner M, Seliger B, Walter B, Schlosser H, Hartmann A, Andreesen R, Mackensen A, Kreutz M. Warburg phenotype in renal cell carcinoma: high expression of glucose-transporter 1 (GLUT-1) correlates with low CD8(+) T-cell infiltration in the tumor. International journal of cancer Journal international du cancer. 2011; 128:2085–2095.
26. Gameiro PA, Yang J, Metelo AM, Perez-Carro R, Baker R, Wang Z, Arreola A, Rathmell WK, Olumi A, Lopez-Larrubia P, Stephanopoulos G, Iliopoulos O. *In vivo* HIF-mediated reductive carboxylation is regulated by citrate levels and sensitizes VHL-deficient cells to glutamine deprivation. Cell metabolism. 2013; 17:372–385.



„*Supplementary tables and figures*“ siehe Anhang auf CD

## 4.2 „VHL-dependent alterations in the secretome of renal cell carcinoma: Association with immune cell response?“

www.impactjournals.com/oncotarget/ Oncotarget, Vol. 6, No. 41

# VHL-dependent alterations in the secretome of renal cell carcinoma: Association with immune cell response?

**Franziska Stehle[1], Sandra Leisz[1], Kristin Schulz[1], Nicolle Schwurack[1], Nico Weber[1], Chiara Massa[1], Jana Kalich[1], Corinna Fahldieck[1], Barbara Seliger[1]**

[1]Martin Luther University Halle-Wittenberg, Institute of Medical Immunology, 06112 Halle (Saale), Germany

**Correspondence to:**
Barbara Seliger, **e-mail:** barbara.seliger@uk-halle.de

**Keywords:** *VHL, renal cell carcinoma, tumor microenvironment, secretome, manganese superoxide dismutase 2*

***Received:*** *August 04, 2015* ***Accepted:*** *September 29, 2015* ***Published:*** *October 12, 2015*

## ABSTRACT

**Secreted proteins could modulate the interaction between tumor, stroma and immune cells within the tumor microenvironment thereby mounting an immunosuppressive tumor microenvironment. In order to determine the secretome-mediated, von Hippel Lindau (VHL)-regulated cross-talk between tumor cells and T lymphocytes peripheral blood mononuclear cells (PBMC) from healthy donors were either cultured in conditioned media obtained from normoxic and hypoxic human VHL-deficient renal cell carcinoma (RCC) cell line (786-0$^{VHL-}$) and its wild type (wt) VHL-transfected counterpart (786-0$^{VHL+}$) or directly co-cultured with both cell lines. An increased T cell proliferation was detected in the presence of 786-0$^{VHL+}$-conditioned medium. By applying a quantitative proteomic-based approach using differential gel electrophoresis followed by mass spectrometry fourteen proteins were identified to be differentially expressed within the secretome of 786-0$^{VHL-}$ cells when compared to that of 786-0$^{VHL+}$ cells. All proteins identified were involved in multiple tumor-associated biological functions including immune responses. Functional studies on manganese superoxide dismutase 2 (MnSOD2) demonstrated that it was a regulator of T cell activation-induced oxidative signaling and cell death. Direct effects of soluble MnSOD2 on the growth properties and interleukin 2 (IL-2) secretion of T cells could be demonstrated underlining the critical role of extracellular MnSOD2 levels for T cell proliferation and activation.**

## INTRODUCTION

Despite the recent advances in the detection as well as treatment of metastatic renal cell carcinoma (RCC) the overall 5 year's survival rate of RCC patients with metastatic disease is still low suggesting a poor prognosis and worse clinical outcome of this disease. While RCC are refractory to standard therapies and only showed an approximately 15 – 20% response rate to cytokine treatment, targeted therapies using tyrosine kinase inhibitors (TKI) have shown promising results in advanced RCC, but their clinical efficacy is limited due to the development of resistances to these drugs. Therefore, a suitable therapeutic strategy might be the combination of anti-angiogenic and immune-based treatment as first-line therapy this disease [1]. Prior to implementing such combinatorial therapeutic concepts, it is important to understand how the tumor microenvironment generates systemic immune suppression in RCC patients. Angiogenesis and immune suppression have been shown to support each other in the RCC microenvironment. The high pro-angiogenic status of RCC is associated with an accumulation of regulatory T cells (Tregs) and myeloid-derived suppressor cells (MDSC) in the local tumor microenvironment [2], in particular in the tumor invasion zone. Thus, the high frequency of Tregs and MDSC might allow RCC cells to evade immune surveillance thereby promoting disease progression [3]. The impaired anti-tumor immune response in RCC involves T cells, natural killer (NK) cells, dendritic cells (DCs), macrophages and MDSC [4, 5]. The complex interplay between various cell types of the immune system, tumor cells and the tumor microenvironment is reflected by a high dynamic range of the immune cell infiltrate as well as soluble

and physical factors and therefore should be carefully accounted for the timing and selection of anti-cancer strategies, especially immunotherapy. For example, the activation of DC subpopulations at early RCC stages is counterbalanced by the co-appearance of Tregs, whereas later stages are characterized by an accumulation of neutrophils at the tumor site [6]. The presence of tumor-associated macrophages (TAMs) and high serum levels of IL-1β in RCC patients correlate with advanced disease. The presence of IL-1β in the tumor microenvironment promotes the development of aggressive RCC by inducing the expression of matrix metalloproteinase (MMP) 1, MMP3, MMP10 and MT1-MMP via activation of the transcription factor CCAAT enhancer binding protein β (CEBPβ) [7]. Macrophages that infiltrate human RCC display significantly enhanced expression levels and activity of 15-lipoxygenase-2 (15-LOX2) resulting in stimulation inflammation and immune dysfunction [8, 9].

Furthermore, the characteristics of the tissue microenvironment including metabolic changes play an integral role in supporting the proliferation of cancer cells [10, 11] suggesting that metabolic reprogramming might affect tumor growth [12, 13]. Indeed, glucose metabolism and growth control are tightly linked in proliferating cells and involve signal transduction cascades including the PI3K/Akt/mTOR pathway [14]. The "Warburg effect" describes cells exhibiting a metabolic shift toward aerobic glycolysis supporting an increased production of biomass, in particular amino acids and nucleic acids [15]. However, the metabolic signatures of cancer cells are not passive responses to damaged mitochondria, but result from oncogene-directed metabolic reprogramming required for the alterations of the composition of cellular constituents and soluble factors within the tumor microenvironment, which is accompanied by changes of the tumor growth characteristics. Recent evidence suggests that metabolites can be oncogenic by altering cell signaling and blocking cellular differentiation [13]. Moreover, the inefficient production of ATP associated with the Warburg effect results in selective advantages mediated by intracellular metabolic shifts, which have also an impact on the extracellular tumor microenvironment supporting tumor cell growth and survival [11]. This includes an increased adenosine concentration, which is involved in impaired T cell-mediated tumor rejection and support of angiogenesis [11].

Mutation, loss or methylation of both *von Hippel-Lindau* (VHL) alleles has been reported in sporadic RCC of the clear cell type (ccRCC) and in the inherited VHL syndrome. The lack of VHL protein function caused metabolic alterations, which lead to a switch from oxidative phosphorylation to aerobic glycolysis, increased glycogen synthesis along with a switch from glucose to glutamine as the major substrate for fatty acid synthesis resulting in tumor progression and therapy resistance [16]. The VHL gene product is a critical component of a multi-protein ubiquitin ligase complex targeting the regulatory hypoxia-inducible factor (HIF)-α subunits for oxygen-dependent proteolysis [17, 18]. The broad metabolic reprogramming is coordinated at the transcriptional level by HIF-1, which functions as a master regulator to balance oxygen supply and demand [16] and activates the transcription of > 100 genes involved in a variety of physiological cell processes, such as e.g. vascular endothelial growth factor (VEGF), glucose transport (glucose transporters), glycolysis (glycolytic enzymes), and cell survival (insulin-like growth factor 2) [19, 20]. Furthermore, the VHL-induced gene regulation can also occur independent of hypoxia [20, 21]: Cells defective for the VHL gene product constitutively overexpress HIF target genes irrespective of the environmental oxygen concentration [22] due to the stabilization of HIF-α subunits [23]. Using various ome-based approaches a number of studies demonstrated a differential gene and protein expression pattern in $VHL^-$ and $VHL^+$ RCC cells, which is partially overlapping, but also distinct from that induced by hypoxia [24–27]. However, so far it has not been determined whether and how the loss of VHL function affects the secretome of RCC cells thereby also modulating the immune cell response. In order to study the VHL-mediated changes within the tumor microenvironment a pair of RCC cell lines that are either defective or expressing the wild-type (wt) VHL gene product were used to generate conditioned media under normoxic and hypoxic conditions and in co-culture experiments with peripheral blood mononuclear cells (PBMC). The effect of the conditioned media or of the co-cultivation with $VHL^-/VHL^+$ RCC cell lines on the proliferation rate as well as the expression of distinct activation markers was determined. The results demonstrate VHL-dependent alterations of the RCC secretome, which modulate the T cell activation by negatively interfering with T cell proliferation and cytokine secretion. This could be linked to changes in the extracellular manganese superoxide dismutase (MnSOD2) concentration. Thus MnSOD2 plays an important role in the cross talk between tumor and immune cells within the tumor microenvironment of RCC.

## RESULTS

### Reduction of T cell proliferation and activation marker (CD25) expression in the presence of 786-$0^{VHL-}$-conditioned media

To determine whether the VHL reconstitution has direct effects on CD3/CD28- or PHA-M stimulated immune effector cells, PBMC from healthy donors were cultured in media conditioned under normoxic (21% $O_2$, 48 h) or hypoxic (1% $O_2$, 48 h, balanced $N_2$)

conditions from 786-0$^{VHL-}$ versus 786-0$^{VHL+}$ cells and subsequently analyzed with respect to proliferation, composition and function of immune cell subpopulations. As shown in Figure 1, PBMC were analyzed by flow cytometry using covalent CFSE staining (A / B) thereby demonstrating an inhibition of cell proliferation in the presence of 786-0$^{VHL-}$-conditioned medium. The reduced immune cell proliferation in 786-0$^{VHL-}$ normoxic conditioned media was independent of the stimulation method used for activation (Figure 1A). The inhibition of T cell proliferation was detected in both conditioned media alone (Figure 1A) and upon co-culture with 786-0$^{VHL-}$ cells in the pre-conditioned medium (Figure 1B). Under hypoxic conditions the effects on cell proliferation in the presence of 786-0$^{VHL-}$ cells and 786-0$^{VHL-}$-conditioned media were increased (Figure 1B). Furthermore, cells were grown for 72 h under normoxic conditions and analyzed by flow cytometry for the lymphocyte repertoire using seven-color staining. Flow cytometry revealed a VHL-dependent increase in the percentage of peripheral blood CD4$^+$ CD25$^+$ T cells within the total CD4$^+$ T cell population as well as the percentage of blood CD8$^+$ CD25$^+$ T cells within the total CD8$^+$ T cell population (Figure 1C). In contrast, other markers analyzed were not altered in dependence of VHL and hypoxia (data not shown).

### Identification of differentially secreted proteins in 786-0$^{VHL-}$ versus 786-0$^{VHL+}$ conditioned media

To determine VHL-dependent differentially secreted proteins the protein pattern of 786-0$^{VHL-}$ and 786-0$^{VHL+}$ conditioned media was compared by 2DE-based proteome analysis. Differentially secreted protein spots of the 786-0$^{VHL-}$ versus 786-0$^{VHL+}$ model system (Figure 2A) were then subjected to mass spectrometric analysis. Overall, 64 distinct proteins were found differentially secreted and identified by mass spectrometry. The vast majority of proteins (46 proteins) were differentially secreted within normoxic conditioned media of 786-0$^{VHL-}$ versus 786-0$^{VHL+}$ cells. 24 proteins were detected to be differentially secreted in the presence of hypoxic conditioned media of 786-0$^{VHL-}$ versus 786-0$^{VHL+}$ cells (Figure 2B). 6 proteins were identified upon culture in normoxic and hypoxic conditioned media, including aldose reductase (AKR1B1), cofilin-1 (CFL1), glutathione synthetase (GSS), plasminogen activator inhibitor 1 (Serpine1), superoxide dismutase (MnSOD2) and metalloproteinase inhibitor 2 (TIMP2). As listed in Table 1, 14 proteins were constantly detected as differentially secreted in 3 individual experiments (Figure 2C) upon VHL overexpression: 9 proteins were down-regulated and 5 proteins were up-regulated in conditioned media of 786-0$^{VHL-}$ versus 786-0$^{VHL+}$ cells.

### Functional annotation cluster analysis

To categorize the biological processes that are altered in 786-0$^{VHL+}$ conditioned media all differentially expressed proteins (fold change ≥2.0) were classified using the Functional Annotation Cluster (FAC) tool available in the Database for Annotation, Visualization and Integrated Discovery (DAVID) [http://david.abcc.ncifcrf.gov/home.jsp]. DAVID FAC analysis of 46 regulated proteins identified using normoxic conditioned media generated a total of 11 and 3 functional clusters for up-regulated and down-regulated proteins, respectively using default parameters. DAVID FAC analysis of the 24 regulated proteins identified using hypoxic conditioned media generated a total of 5 functional clusters for down-regulated proteins, respectively using default parameters. The Gene ontology (GO) terms "Biological Process", "Cellular Component" and "Molecular Function" were used for annotations. The GO terms with highest significance and statistically significant *p*-values from the resulting functional clusters are listed in Tables 2 and 3 for hypoxic and normoxic conditioned media, respectively. Regarding there classification all identified differentially secreted proteins are involved in multiple tumor-associated biological functions and the regulation in the 786-0$^{VHL+}$ conditioned media coincides with the reduced aggressiveness in the presence of VHL protein (Figure 3).

### Gene ontology analysis using GOMiner

Gene ontology (GO) terms for repeatedly identified proteins were extracted, and overrepresented functional categories for differentially abundant proteins were determined by the high throughput GOMiner tool (National Cancer Institute, http://discover.nci.nih.gov/gominer/) [28]. Proteins involved in regulation of immune system processes include beta-2-microglobulin (B2M), plasminogen activator inhibitor 1 (SERPINE 1), mitochondrial superoxide dismutase (MnSOD2) and ubiquitin-conjugating enzyme E2 N (UBE2N). The proteins B2M and SERPINE 1 were up-regulated in the media conditioned by 786-0$^{VHL+}$ cells, whereas MnSOD2 and the UBE2N were down-regulated in the respective cell culture supernatants.

### Validation of representative differentially secreted proteins in 786-0$^{VHL-}$ versus 786-0$^{VHL+}$ conditioned media

The up-regulation of B2M and SERPINE 1 as well as the down-regulation of MnSOD2 and UBE2N in the cell culture supernatants were validated by qPCR using oligo-(dT)18 primed cDNA of 786-0$^{VHL-}$ and 786-0$^{VHL+}$ cells incubated for 48 h under normoxic and hypoxic conditions (Figure 4). Furthermore, the up-regulation of B2M and the down-regulation of MnSOD2 in the cell

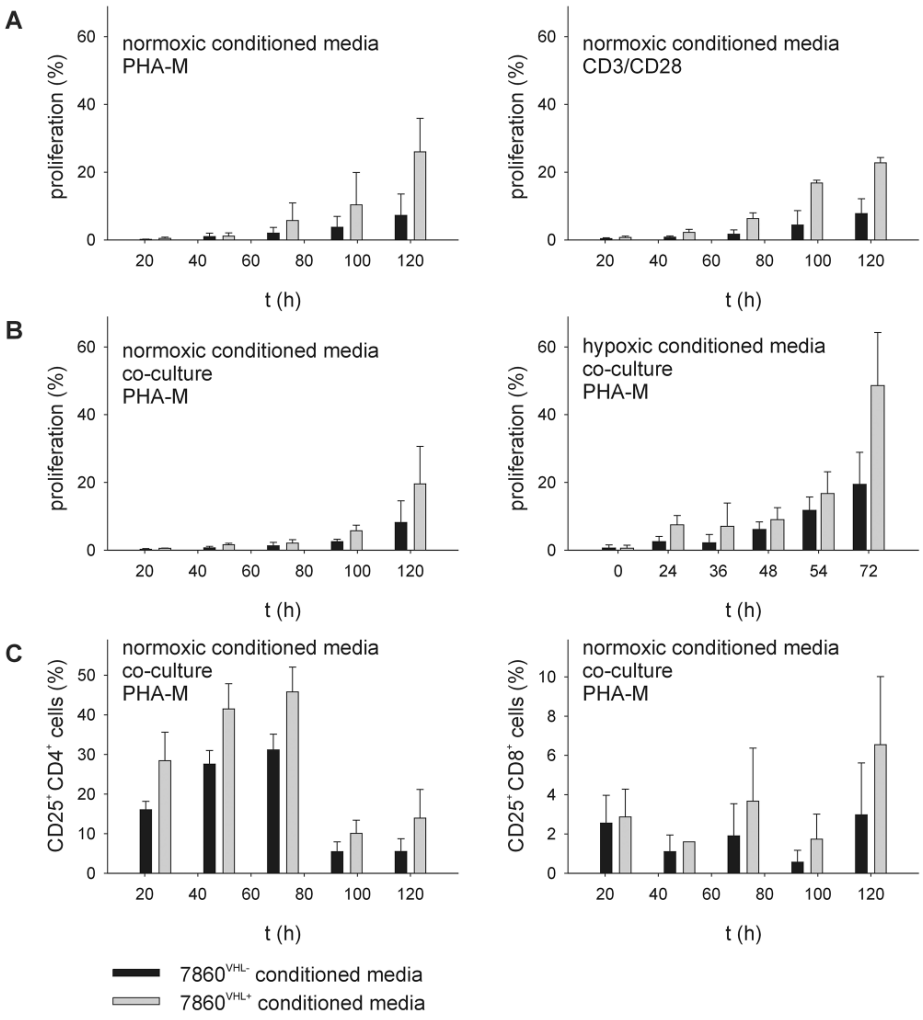


**Figure 1: Reduction of T cell proliferation and CD25 expression within 786-0$^{VHL-}$ conditioned media.** PBMC from healthy donors were prepared by Ficoll density gradient centrifugation and stimulated directly with anti-CD3 and anti-CD28 antibodies (mouse anti-human, BD, 1 µg/ml each) or PHA-M (Sigma-Aldrich, 4 µg/ml) and IL-2 (100 U/ml). "Cells were grown up to 6 days in 786-0VHL- or 786-0VHL+ conditioned media **(A)** or in the presence of 786-0VHL-/VHL+ cells **(B)**, respectively. Cells were analyzed via flow cytometry using covalent CFSE staining (Invitrogen) according to the manufacturer's protocol." Cells were grown for 6 days under normoxic conditions and analyzed via flow cytometry for lymphocyte markers using seven-color staining panels **(C)** Data are represented as mean percentage (%) ± SD based on five independent experiments.

culture supernatants of 786-0$^{VHL+}$ cells were validated by Western blot analysis using freshly prepared conditioned medium (Figure 5A and 6A). B2M is a component of the major histocompatibility complex (MHC) class I involved in the presentation of peptide antigens to the immune system. As intracellular B2M non-covalently associates with the 44 kDa heavy chain of the MHC class I antigen complex, the VHL-dependent expression of B2M and MHC class I antigens (HLA-A, B and C) was also analyzed using flow cytometry. In contrast to the

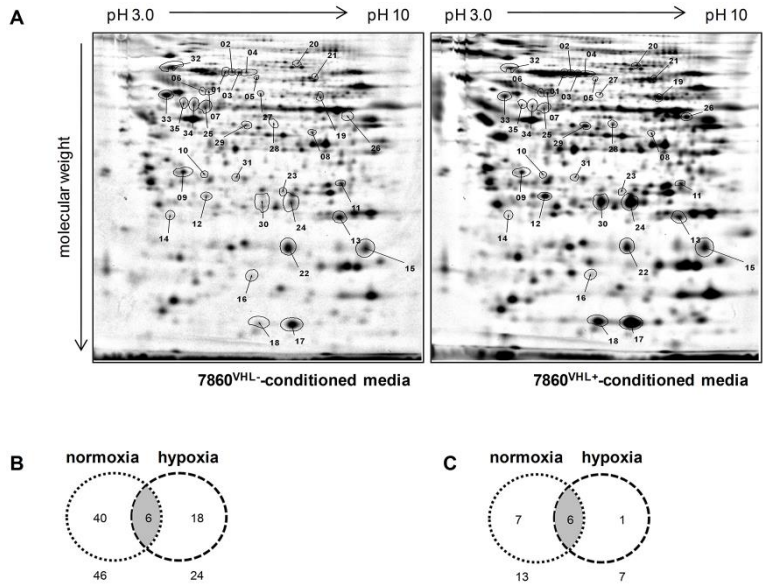


**Figure 2: Comparative profiling of cell culture supernatants upon reconstitution of VHL expression in the 786-0 cell line. (A)** Representative protein expression profiles of media conditioned by the parental cell line 786-0$^{VHL-}$ (left panel) and its VHL-transfected variant (786-0$^{VHL+}$, right panel) under normoxic conditions (21% $O_2$, 48 h) is shown. The respective protein pools were individually labeled with distinct fluorescence dyes (DIGE technology) and than co-separated by 2-DE as described in the Materials and methods section. Differentially expressed proteins are labeled with numbers. Figure B and C show an overview of the conditioned media profiling results. The Venn diagrams display the distribution pattern of all differentially secreted proteins under normoxic and hypoxic conditions **(B)** as well as the repeatedly detected secreted proteins **(C)**.

VHL-dependent 1.7 - and 3.5 - fold up-regulation of B2M ($p < 0.01$) within the cell culture supernatants of 786-0$^{VHL+}$ cells under normoxic or hypoxic conditions, respectively, no increase of intracellular B2M or MHC class I heavy chain was detectable under these conditions (Figure 5B).

With regard to MnSOD2 the supernatants of the 786-0$^{VHL+}$ RCC cells had 3.8 − fold or 2.1 – fold lower MnSOD2 levels compared to the supernatants of the 786-0$^{VHL-}$ cells ($p < 0.01$) under normoxic or hypoxic conditions, respectively (Figure 6A). These data were further confirmed by determination of the MnSOD2 enzyme activity demonstrating a 2.2 − fold or 1.8 – fold lower MnSOD2 activity of 786-0$^{VHL+}$ cells when compared to the supernatants of 786-0$^{VHL-}$ cells ($p < 0.01$) under normoxic or hypoxic conditions, respectively (Figure 6B).

### Inhibition of T cell activation-induced cell proliferation and IL-2 secretion by increased MnSOD2 levels and activity

To determine whether the reduced MnSOD2 secretion as a consequence of the VHL reconstitution caused an increased proliferation of stimulated immune effector cells within the supernatants of 786-0$^{VHL+}$ cells, PBMC from healthy donors were stimulated with anti-CD3 and anti-CD28 antibodies in the absence and presence of recombinant MnSOD2 protein followed by the analysis of their proliferation capacity using CFSE staining. As shown in Figure 7A, an inhibition of cell proliferation in the presence of MnSOD2 protein was detected, which was comparable to the diminished immune cell proliferation in the presence of MnSOD2 within the supernatants of 786-0$^{VHL-}$ cells.

To prove whether the reduced cell proliferation rate could be linked to MnSOD2-mediated alteration of cytokine secretion, the IL-2 concentration was determined using a commercial ELISA assay. Therefore, “day 6” T cells were re-stimulated with anti-CD3 and anti-CD28 antibodies in the absence and presence of recombinant MnSOD2 protein for 20 and 40 h and their IL-2 secretion was subsequently analyzed (Figure 7B). The supernatants of MnSOD2-treated re-stimulated “day 6” T cells showed 1.8 and 2.1 – fold lower IL-2 levels after 20 and 40 h of re-stimulation, respectively when compared to the supernatants lacking recombinant MnSOD2 ($p < 0.01$).

**Table 1: Proteins differentially secreted in media conditioned by 786-0$^{VHL-}$- versus 786-0$^{VHL+}$ cells**

| protein name | gene symbol | UniProtKB ID. | x-fold change | cellular function | cellular compartment |
|---|---|---|---|---|---|
| aldose reductase | AKR1B1 | P15121 | 0.4 ± 0.1 ↓ **N/H** | glyceraldehyde oxidoreductase activity | cytosol, extracellular space, nucleus |
| retinal dehydrogenase 1 | ALDH1A1 | P00352 | 3.5 ± 1.3 ↓ **N** | aldehyde dehydrogenase (NAD) activity | cytosol |
| **beta-2-microglobulin** | **B2M*** | P61769 | 2.9 ± 0.6 ↓ **N** | component of the class I major histocompatibility complex (MHC) | extracellular space, secreted |
| T-complex protein 1 subunit zeta | CCT6A | P40227 | 0.4 ± 0.1 ↓ **H** | chaperone | cytoplasm |
| cofilin-1 | CFL1 | P23528 | 0.4 ± 0.1 ↓ **N/H** | regulation of actin cytoskeleton dynamics | cell membrane, cytoplasm, cytoskeleton, nucleus |
| cathepsin D | CTSD | P07339 | 0.4 ± 0.1 ↓ **N** | acid protease | extracellular space, secreted, lysosome |
| glutathione synthetase | GSS | P48637 | 0.5 ± 0.1 ↓ **N/H** | glutathione biosynthesis | cytosol |
| matrix metalloproteinase-2 (72 kDa type IV collagenase) | MMP2 | P08253 | 0.4 ± 0.1 ↓ **N** | metalloproteinase involved in angiogenesis, tumor invasion, inflammation | cytoplasm, extracellular matrix, membrane, mitochondrion, nucleus, secreted |
| **plasminogen activator inhibitor 1** | **SERPINE1*** | P05121 | 2.2 ± 0.1 ↓ **N/H** | serine protease inhibitor | extracellular space, secreted |
| **superoxide dismutase [Mn], mitochondrial** | **MnSOD2*** | P04179 | 0.4 ± 0.1 ↓ **N/H** | destroys superoxide anion radicals | mitochondrion |
| metalloproteinase inhibitor 2 | TIMP2 | P16035 | 2.7 ± 0.4 ↓ **N/H** | irreversible inactivation of metalloproteinases | extracellular space, secreted |
| triosephosphate isomerase | TPI1 | P60174 | 0.4 ± 0.1 ↓ **N** | gluconeogenesis, glycolysis | cytosol |
| **ubiquitin-conjugating enzyme E2 N** | **UBE2N*** | P61088 | 0.5 ± 0.1 ↓ **N** | polyubiquitination, DNA repair | cytoplasm, nucleus |
| WD repeat-containing protein 1 | WDR1 | O75083 | 2.5 ± 0.1 ↑ **N** | induces disassembly of actin filaments in conjunction with ADF/cofilin family proteins | cytoplasm, cytoskeleton |

Proteins involved in regulation of immune system processes are marked in bold.

## DISCUSSION

To improve treatment of RCC using combinations of anti-angiogenic and immune-based therapy an increased knowledge of the interactions between tumor, stroma and distinct immune cell types are necessary. As secreted proteins are supposed to be involved in the interaction amongst these cells within the tumor microenvironment the VHL-regulated cross talk between tumor cells and T lymphocytes and the involvement of the secretome in this process was analyzed in the present study.

**Table 2: Significantly enriched gene ontology terms detected by FAC in up-regulated and down-regulated proteins after cultivation under hypoxic conditions**

| | No. of AC | GO Term (fold enrichment) | No. of Proteins | *p*-value |
|---|---|---|---|---|
| **up-regulated** | 0 | | | |
| **down-regulated** | 1 | GO:0031988, membrane-bounded vesicle (1.98) | 4 | 0.014 |
| | 2 | GO:0031974, membrane-enclosed lumen (1.28) | 6 | 0.021 |
| | 3 | GO:0043066, anti-apoptosis (1.15) | 3 | 0.016 |
| | 4 | GO:0031012, extracellular matrix (1.14) | 3 | 0.040 |
| | 5 | GO:0006928, cell motion (0.9) | 4 | 0.010 |

**Table 3: Significantly enriched gene ontology terms detected by FAC in up-regulated and down-regulated proteins after cultivation under normoxic conditions**

| | No. of AC | GO Term (fold enrichment) | No. of Proteins | *p*-value |
|---|---|---|---|---|
| **up-regulated** | 1 | GO:0006986, response to unfolded protein (1.69) | 4 | 0.00026 |
| | 2 | GO:0030414, peptidase inhibitor activity (1.60) | 3 | 0.035 |
| | 3 | GO:0031988, membrane-bounded vesicle (1.44) | 5 | 0.015 |
| | 4 | GO:0031400, negative regulation of protein modification process (1.10) | 3 | 0.019 |
| | 5 | GO:0004175, endopeptidase activity (1.02) | 4 | 0.034 |
| | 6 | GO:0042981, regulation of apoptotic process (0.93) | 6 | 0.012 |
| | 7 | GO:0016192, vesicle-mediated transport (0.84) | 5 | 0.018 |
| | 8 | GO:0043161, proteasome-mediated ubiquitin-dependent protein catabolic process (0.79) | 3 | 0.014 |
| | 9 | GO:0005525, GTP binding (0.78) | 3 | 0.016 |
| | 10 | GO:0046907, intracellular transport (0.67) | 5 | 0.027 |
| | 11 | GO:0005576, extracellular region (0.65) | 9 | 0.015 |
| **down-regulated** | 1 | GO:0006732, coenzyme metabolic process (2.53) | 3 | 0.017 |
| | 2 | GO:0031988, membrane-bounded vesicle (2.48) | 5 | 0.0064 |
| | 3 | GO:0043066, anti-apoptosis (0.84) | 3 | 0.030 |

To identify differentially secreted proteins in 786-0$^{VHL-}$ versus 786-0$^{VHL+}$ conditioned media responsible for reduction of T cell proliferation and activation marker (CD25) expression within 786-0$^{VHL-}$ conditioned media (Figure 1), the protein pattern of 786-0$^{VHL-}$ and 786-0$^{VHL+}$ conditioned media was compared using 2DE-based proteome analysis. The secretome study was performed *in vitro* by first culturing 786-0$^{VHL-}$ and 786-0$^{VHL+}$ cells in serum-supplemented medium to obtain a sufficient number of cells. Subsequently cells are washed carefully with sterile phosphate-buffered saline to remove bovine serum proteins followed by incubation in serum-free medium up to 72 hours. Conditioned medium containing cell-secreted proteins was collected and analyzed by 2D gel electrophoresis prior to protein identification by mass spectrometry.

Altogether, 64 proteins were found differentially secreted in dependence of the VHL status from which 14 proteins were constantly found in 3 individual experiments (Figure 2; Table 1).

The relative low number of recurring proteins might be explained by false-positive discoveries due to serum proteins or proteins released by dying cells or as the result of mechanical injury [29]. The incubation of mammalian cells in serum-free medium to avoid interference from serum contaminants might affect the cell secretome profile. In addition, the length of incubation in serum-free medium could also dramatically influence the secretome profiles, as increased cell death correlates with an increased release of intracellular proteins [29].

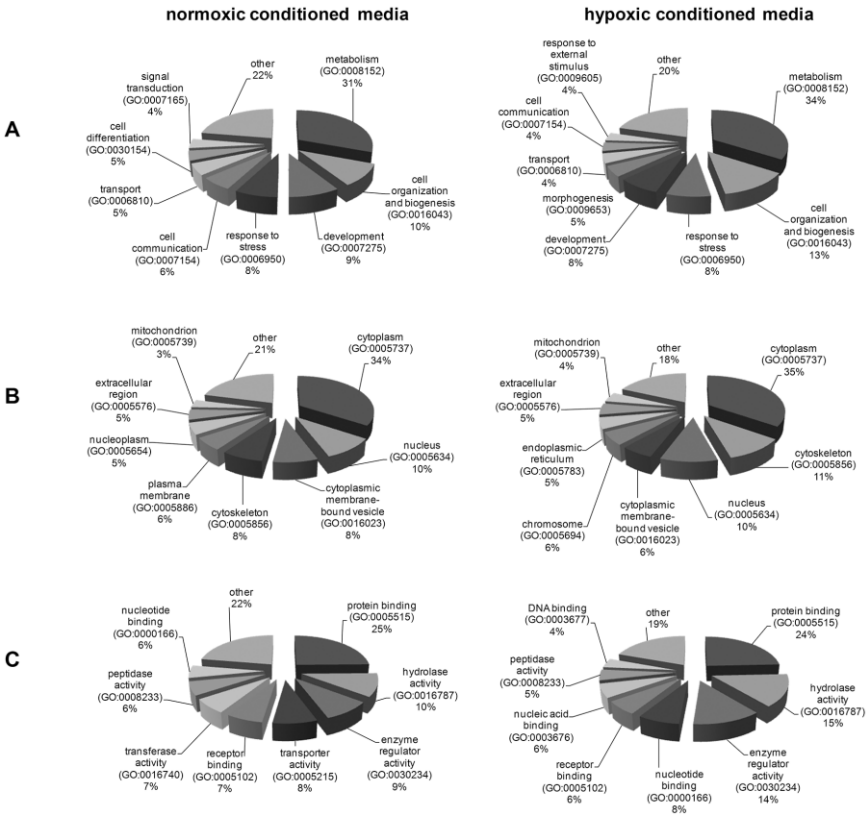


**Figure 3: Classification of the differentially secreted proteins according to their biological processes (A), cellular components (B) and their molecular functions (C).**

The functional annotation cluster analysis of all identified proteins clearly showed an enrichment of proteins localized within membrane-bounded vesicles or in the extracellular region (Table 2 and 3; Figure 3). Furthermore, intracellular proteins like anti-apoptotic proteins or proteins of the unfolded protein response were additionally identified (Table 2 and 3).

Several intracellular proteins are consistently found to be released by cultured mammalian cells into the conditioned medium. Although these intracellular proteins can be released due to cell death or leakage, there is evidence that some of these proteins are secreted via non-classical pathways like vesicles and exosomes [30]. Often these proteins possess additional extracellular functions that are different from their intracellular role. Exosomes are small vesicles with an average size ranging from 30 to 150 nm. They are believed to originate from endosomes and contain a variety of components including mRNA, miRNA and proteins such as carbohydrate and lipid metabolism enzymes, cytoskeletal components and chaperone proteins [31, 32]. Exosomes might play a role in protein turnover, serve as carriers for RNA and miRNA as well as modulate the immune response [33]. The enrichment of proteins that are localized within membrane-bounded vesicles clearly showed the involvement of exosome release for modification of the cell culture supernatants of 786-$0^{VHL-}$ and 786-$0^{VHL+}$ cells. For example, α-enolase (ENO1), a glycolytic enzyme, involved in the synthesis of pyruvate, was detected in significant amounts in the secretome of almost every type of cultured mammalian cell. Additionally, it was down-regulated within the supernatant of 786-$0^{VHL+}$ cells (regulation factor 0.4). Extracellular or cell surface ENO1 was suggested to act as a plasminogen receptor mediating extracellular matrix degradation and cell migration in cancer and to have diagnostic and

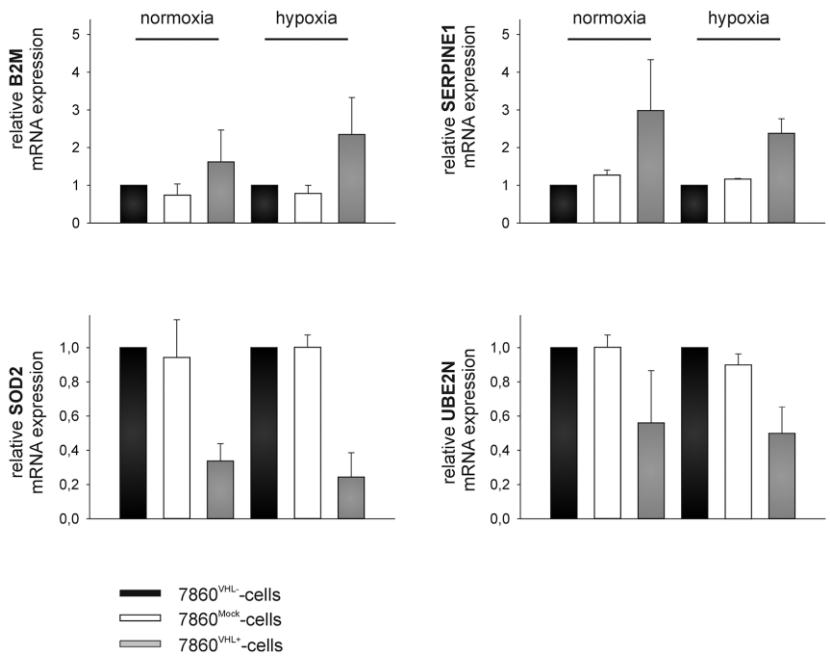


**Figure 4: Representative qPCR-mediated target validation.** 786-0$^{VHL-}$ and 786-0$^{VHL+}$ cells were cultured under normoxic (21% $O_2$, 48 h) and hypoxic (1% $O_2$, 48 h) conditions and subjected to quantitative real-time PCR analysis to determine mRNA levels of B2M, MnSOD2, plasminogen activator inhibitor 1 (SERPINE1), and ubiquitin-conjugating enzyme E2 N (UBE2N) using oligo-(dT)18 primed cDNA. Mean expression of HPRT and PPIA were used for normalization. Data were represented as mean percentage (%) ± SD based on three independent experiments.

prognostic values [34]. Down-regulation of ENO1 within the supernatant of 786-0$^{VHL+}$ cells corresponds with the reduced aggressiveness of the 786-0$^{VHL+}$ cells.

The 14 proteins, which were constantly found regulated in dependence of VHL in 3 individual experiments, were analyzed with respect to their GO terms [28]. The proteins B2M and SERPINE 1 were up-regulated in the media conditioned by 786-0$^{VHL+}$ cells, whereas MnSOD2 and the UBE2N were down-regulated in this cell culture supernatant. The VHL-dependent down-regulation of MnSOD2 as well as the upregulation of B2M was further validated by qPCR, Western Blot analysis as well as MnSOD2 activity assays (Figure 4 and 6). In contrast to MnSOD2, B2M protein was just found up-regulated within the cell culture supernatants of 786-0$^{VHL+}$ cells and not intracellular (Figure 5).

RCC comprises a heterogeneous group of tumors with various molecular and cytogenetic abnormalities and different histological features as cell types and tumor architecture [35]. Untargeted metabolomic analyses of murine ccRCC model demonstrated that HIF1α activates the transcription of genes that cause increased glucose uptake, glycolysis, and lactate production. In addition, it diminishes the flux of pyruvate entering the tricarboxylic acid cycle accompanied with a decreased oxidative phosphorylation identical to those observed in human ccRCC samples [36]. Furthermore, molecular genetic and proteomic tools led to the discovery of potential diagnostic, prognostic and therapeutic biomarkers of this disease. In early studies, the 2-DE expression patterns from whole renal and RCC tissues resulted in a number of differentially expressed proteins associated with RCC. This includes MnSOD2, a mitochondrial enzyme related to the redox cycle, involved in various regulatory functions of cells, which was not present in normal kidney tissue [35, 37, 38]. It is noteworthy that there exists a large diversity of MnSOD2 levels in various human cancers, which is most likely due to the combination of heterogeneity of genomic events and environmental changes [35].

MnSOD2 is an anti-oxidative enzyme responsible for the defense against $O_2^-$ radicals released by the electron chain as a byproduct of respiration. Moreover, MnSOD2 plays a key role in the regulation of human

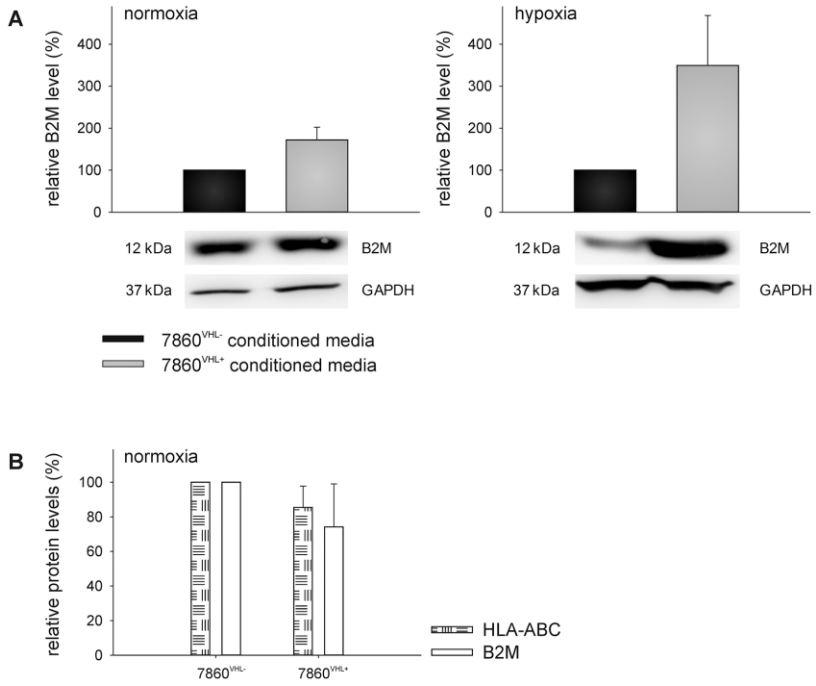


**Figure 5: VHL-mediated up-regulation of B2M in the supernatant of 786-0$^{VHL+}$ cells.** The up-regulation of B2M within the cell culture supernatant was verified at the protein level **(A)** as described within the Materials and Methods section. Blots were probed with an anti-B2M mAb, whereas the immunostaining with the anti-GAPDH mAb served as a loading control. In addition, the intracellular protein levels of B2M as well as HLA-ABC of 786-0$^{VHL-}$ and 786-0$^{VHL+}$ cells were analyzed by flow cytometry after intracellular staining using FITC-conjugated anti-B2M or FITC-conjugated anti-HLA-ABC antibodies (BD) **(B)** Data are represented as mean percentage (%) ± SD based on five independent experiments.

T cell activation since it mediates the first step in the mitochondrial oxidative signal generation. Thus, MnSOD2 represents an important control switch in the process of activation-induced oxidative signal generation in T cells.

The TCR-mediated gene expression strictly depends on the simultaneous activation of oxidation-dependent and calcium-dependent transcription factors. The activation-induced oxidative signal is generated by different enzymes including the NADPH oxidases NOX2 and DUOX1 [39, 40]. Since the mitochondrial respiratory complex I was identified as an essential source of reactive oxygen species (ROS) generation upon TCR stimulation mitochondria could function as oxidative signaling organelles during T cell activation [41, 42]. After the complex I-mediated formation of $O_2^-$ radicals, the transformation into the oxidative signaling molecule $H_2O_2$ occurs within the mitochondrial matrix [43]. $H_2O_2$ diffuses into the cytosol and potentiates TCR signaling via reversible inactivation of negative regulatory phosphatases or direct influence on NF-κB/AP-1 activity or DNA binding occurs [44–46 ]. In order to avoid harmful ROS effects as well as to allow signaling integration, the TCR-induced generation of mitochondrial oxidative signals has to be tightly regulated. Following T cell activation the mitochondrial complex I-mediated release of $O_2^-$ radicals is up-regulated, while MnSOD2 participates in generation of mitochondrial $H_2O_2$ during the signaling phase. In the presence of low MnSOD2 levels, $H_2O_2$ could also be produced by reactions other than $O_2^-$ radical dismutations, which have substrate/product ratios higher than MnSOD2. The resulting increased cytoplasmic $H_2O_2$ levels activate the redox-dependent transcription factors NF-κB- and AP-1. As a consequence the expression of CD95L, IL-2 and MnSOD2 is initiated. The transcriptional upregulation of MnSOD2 results in higher mitochondrial concentrations and activity leading to the inhibition of $H_2O_2$ release. The reduced probability of $O_2^-$ radicals to participate in other $H_2O_2$-generating reactions yielding more $H_2O_2$/single $O_2^-$ radical than the dismutase reaction itself lowers

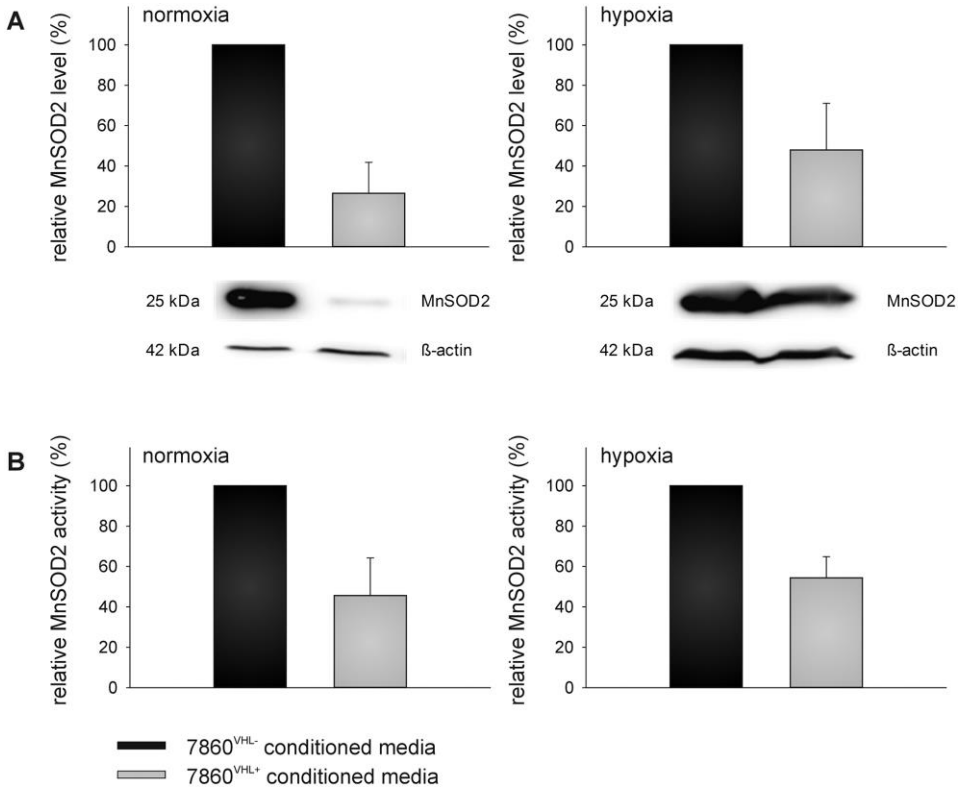


**Figure 6: VHL-mediated down-regulation of extracellular superoxide dismutase (MnSOD2) level and activity.** Down-regulation of superoxide dismutase (MnSOD2) within the cell culture supernatant was also verified at the protein level **(A)** as described within the Materials and Methods section. Blots were probed with anti-MnSOD2 antibodies, whereas the immunostaining with the anti-β-actin mAb served as loading control. In addition, MnSOD2 activity was assessed using the Superoxide Dismutase Activity Colorimetric Assay Kit as described in the Materials and Methods section **(B)**.

cytoplasmic $H_2O_2$ concentrations resulting in a decreased NF-κB/AP1 activation [47–49 ].

In this context it was shown that the TCR-induced oxidative signal generation as well as the NF- κB/AP1-dependent IL-2 gene expression inversely correlates with the protein content of MnSOD2 [48]. Consequently, MnSOD2 over-expression abrogated T cell activation-triggered mitochondrial ROS production as well as NF-κB/AP-1-mediated transcription [48]. In line with this report the proliferation of TCR-stimulated immune effector cells was significantly inhibited in the presence of recombinant MnSOD2 protein ($p < 0.01$) (Figure 7A). Therefore, the VHL-mediated increase of cell proliferation of stimulated immune effector cells within the supernatants of 786-$0^{VHL+}$ cells could at least partly be attributed to decreased extracellular MnSOD2 levels and activity. IL-2 secretion of TCR-stimulated T cells was also slightly, but significantly diminished in presence of recombinant MnSOD2 protein (Figure 7B). Upon the internalization into the mitochondria the increased amount of extracellular MnSOD2 remove $O_2^-$ radicals more efficiently thus mimicking the inhibition of the signal transduction. Consequently, lowered expression of IL-2 resulted in decreased IL-2 secretion in the presence of recombinant MnSOD2 (Figure 7B). Our data underline the critical role of MnSOD2 in T cell response and suggest that MnSOD2 could represent a novel target for (immuno-) therapies.

## MATERIALS AND METHODS

### Chemicals

Recombinant MnSOD2 protein was purchased from Abnova (Pforzheim, Germany). Endotoxins were removed

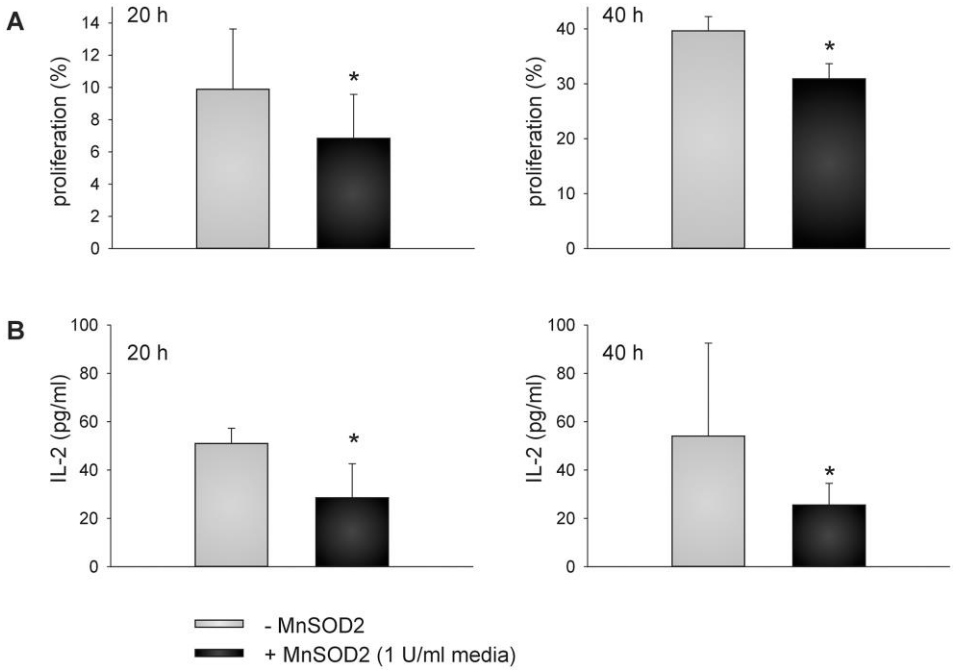


**Figure 7: MnSOD2-induced reduction of T cell proliferation and IL-2 secretion.** PBMC from healthy donors were prepared by Ficoll density gradient centrifugation, labeled with CFSE according to the manufacturer 's instructions, and stimulated directly with anti-CD3 and anti-CD28 antibodies (mouse anti-human, BD, 1 µg/ml each) and IL-2 (100 U/ml). Cells were grown in the absence or presence of MnSOD2 (1U/ml) for 20 and 40 h prior to flow cytometry **(A)**.
IL-2 secretion was analyzed using commercial enzyme-linked immunosorbent assay (ELISA) (eBioscience, Austria) using "day 6" T cells at a density of $1 \times 10^5$ cells/well onto 96-well culture plates in the absence and presence of 1 U/ml MnSOD2 as described in Materials and Methods section **(B)**.
Data are represented as mean percentage (%) ± SD based on five independent experiments.
**p*-value < 0.05

using the Detoxi-Gel™ Endotoxin Removing Gel (Thermo Fisher Scientific, Rockford, IL, USA) according to the manufacturer's instructions prior to sterile filtration using a 0.22 mm syringe filter. MnSOD2 activity was analyzed using the Superoxide Dismutase Activity Colorimetric Assay Kit (Abcam, Cambridge, UK) according to the manufacturer's protocol.

### Cell culture and preparation of conditioned media

The parental ccRCC cell line 786-0 harboring a mutated *VHL* gene (786-$0^{VHL-}$) and its counterpart stably transfected with a HA-tagged wt VHL gene construct (786-$0^{VHL+}$) have been recently described [26]. Both cell lines were grown in Dulbecco's modified Eagle medium (DMEM; Sigma-Aldrich, Munich, Germany) supplemented with 10% fetal calf serum (FCS, PAA Laboratories GmbH, Coelbe, Germany), 2 mM L-glutamine (Lonza, Cologne, Germany), 1% sodium pyruvate (GIBCO, Life technologies, Carlsbad, USA), 1% non-essential amino-acid mixture (GIBCO), and 1% penicillin/streptomycin (PAA).

To prepare conditioned media $1 \times 10^6$ parental 786-$0^{VHL-}$ or 786-$0^{VHL+}$ RCC cells, respectively, were seeded in complete medium under conventional conditions (37°C, humidified atmosphere, containing 5% $CO_2$) for 24 hours. Cells were then washed 3 times with phosphate buffered saline (PBS) before the medium was changed into an FCS-free Roswell Park Memorial Institute Medium (RPMI-1640; Sigma-Aldrich) supplemented with 2 mM L-glutamine (Lonza), 1% sodium pyruvate (GIBCO), 1% non-essential amino-acid mixture (GIBCO), and 1% penicillin/streptomycin (PAA) and exposed to normoxia (21% $O_2$, 5% $CO_2$) or hypoxia (1% $O_2$, 5% $CO_2$, and balanced $N_2$) for 48 h. In addition, the apoptosis rate of the

cells grown under normoxia and hypoxia was determined. Conditioned medium of non-apoptotic cells (apoptosis <5%) was collected, centrifuged at 300 × *g* for 5 min and at 5000 × *g* for 10 min, and finally filtered using a 0.22 mm syringe filter.

PBMC of healthy donors obtained from the local Department of Transfusion Medicine were isolated from heparinized venous blood samples by density gradient centrifugation using Leukosep® (Greiner Bio-One, Germany) and Biocoll Separation Solution (Biochrome, Berlin, Germany). PBMC were either cultured under conventional conditions (37°C, humidified atmosphere, containing 5% $CO_2$, 72 h) in conditioned media supplemented with 10% FCS (PAA) in the presence of 100 U/ml IL-2 (PROLEUKIN, Chiron, Ratingen, Germany) or co-cultured with 786-$0^{VHL-}$ or 786-$0^{VHL+}$ cells in the presence of conditioned media and directly stimulated with plate-bound agonistic anti-CD3 and anti-CD28 antibodies (mouse anti-human, 1 µg/ml each, BD Biosciences, Heidelberg, Germany) or PHA-M (Sigma-Aldrich). For co-culture experiments 2 × $10^6$ PBMC/well were seeded onto six-well culture plates and incubated with conditioned media for 120 or 72 hours under normoxic or hypoxic conditions, respectively. 786-$0^{VHL-}$ or 768–$0^{VHL+}$ cells were added at a density of 3 × $10^5$ on 25-mm Anopore tissue culture plate inserts (0.02 µm pore size; Nalge Nunc International, Thermo Fisher Scientific).

T cells were isolated from PBMC after labeling with allophycocyanine (APC)-conjugated anti-CD3 antibodies using the EasySep™ Human APC Positive Selection Kit according to the manufacturer's instructions (Stemcell Technologies, Grenoble, France). T cells were expanded by stimulation with plate-bound anti-CD3 and anti-CD28 antibodies (mouse anti-human, 1 µg/ml each) and subsequent culture in IL-2-containing (25 U/ml, PROLEUKIN) RPMI-1640 (Sigma-Aldrich) supplemented with 10% FCS (PAA) and 2 mM L-glutamine (Lonza) for 5–6 days ("day 6" T cells).

### Proliferation assay

To evaluate cell proliferation, 1 × $10^7$ PBMC in 10 ml of PBS were labeled with 5,6-carboxyfluorescein succinimidyl ester (CFSE, 0.5 µM, Invitrogen, Eugene, USA) according to the manufacturer's instructions. 2 × $10^6$ cells/well were seeded in 6 well microtiter plates (TPP, Trasadingen, Switzerland) in 5 ml of 786-$0^{VHL-}$ or 786-$0^{VHL+}$ conditioned media or in co-culture with 3 × $10^5$ 786-$0^{VHL-}$ / 786-$0^{VHL+}$ cells/well in the presence of conditioned media followed by direct stimulation with plate-bound anti-CD3 and anti-CD28 antibodies (mouse anti-human, 1 µg/ml each, BD Biosciences) and maintained for 5 days in culture. 10,000 events were analyzed on a BD FACSCanto II flow cytometer in combination with the FACSDiva software package (BD Biosciences) in a time kinetic. The results were expressed as percentage of proliferating cells.

Proliferation assays in the presence of MnSOD2 were analyzed as described above in the absence and presence of 1U/ml recombinant MnSOD2 (Abnova; Pforzheim, Germany) within the culture medium for up to 40 hours.

### Monitoring VHL-dependent alterations in the composition and function of T cell subpopulations

Seven-color flow cytometric staining was used for analyzing VHL-dependent effects on CD3/CD28-stimulated PBMC. Briefly, 2 × $10^6$ cells/well were seeded in 6 well microtiter plates (TPP) in 5 ml of 786-$0^{VHL-}$ or 786-$0^{VHL+}$ conditioned media or in co-culture with 3 × $10^5$ 786-$0^{VHL-}$ / 786-$0^{VHL+}$ cells/well in the presence of conditioned media followed by direct stimulation with plate-bound anti-CD3 and anti-CD28 antibodies (mouse anti-human, 1 µg/ml each, BD Biosciences). After 68 h, BD GolgiPlug™ (5 µl) and IL-2 (100 U/ml) were added to each cell suspension and further incubated for 4 h. The cells were harvested and washed twice with PBS. Surface molecules were directly stained with the fluorescence-conjugated antibodies against CD3, CD4, CD8, CD25 and CD45 as well as the respective fluorescence-labelled lgG controls (all purchased from BD Biosciences) for 15 min at room temperature. Cells were washed with PBS and fixed in PBS containing 1% paraformaldehyde. Three independent experiments were performed.

### Apoptosis assay

To evaluate the VHL-mediated apoptosis induction, 2 × $10^6$ PBMC were cultured in 5 ml of 786-$0^{VHL-}$ or 786-$0^{VHL+}$ conditioned media or in co-culture with 3 × $10^5$ 786-$0^{VHL-}$ / 786-$0^{VHL+}$ cells/well in the presence of conditioned media followed by direct stimulation with plate-bound anti CD3-and anti-CD28 antibodies (mouse anti-human, 1 µg/ml each, BD Biosciences) for 72 h. Apoptosis was determined by flow cytometry after staining of cells with APC-annexin V (BD Phamingen™) and propidium iodide (2 mg/ml, Sigma-Aldrich) according to the manufacturer 's instructions (BD Phamingen™). The stained cells were analyzed using the BD FACSCanto II flow cytometer and the FACSDiva software package (BD).

### cDNA synthesis and qPCR

Total RNA was extracted from the samples using the Nucleospin Extract II kit (Macherey-Nagel, Düren, Germany) according to the manufacturer's instructions. cDNA was synthesized from 3 µg RNA treated with DNase I (Invitrogen GmbH, Karlsruhe, Germany) using oligo dT primers (Fermentas, Mannheim, Germany) and the RevertAid™ H Minus First Strand cDNA synthesis kit (Fermentas, St. Ingbert, Germany) before qPCR was performed with target-specific primers (Table S1)

using Platinum® SYBR® Green qPCR SuperMix-UDG (Invitrogen) and applying the following parameters for 40 cycles; denaturation 95°C, 15 s; annealing/elongation 60°C, 30 s. Relative mRNA expression levels for specific genes were normalized to peptidylprolylisomerase A (PPIA) and hypoxanthine-guanine phosphoribosyl-transferase (HPRT). The transcription levels of 786-$0^{VHL-}$ cells were set to one and the relative expression ratios in 786-$0^{VHL+}$ cells were calculated, respectively.

### NaDOC/TCA precipitation

Proteins of the cell culture supernatants were precipitated using the sodium deoxycholate (NaDOC)/TCA precipitation procedure described by Bensadoun and Weinstein [50], which allows a quantitative recovery of protein samples [51].

The samples were mixed with 10% aqueous NaDOC (1:100, by volume). Then 50% aqueous TCA (1:20, by volume) was added. After incubation at room temperature for 15 min the samples were centrifuged in 50 ml centrifuge tubes (Greiner) at 4,500 *g* and 4°C for 45 min. The supernatant was decanted and the pellet was washed with 20 ml aqueous ethanol (70%). After incubation at −20°C for 15 min, the samples were centrifuged at 4,500 *g* and 4°C for 45 min. The supernatant was decanted and 1 ml aqueous ethanol (70%) was added to the pellet followed by thorough mixing. Then the pellet was transferred into a 1.5 ml cup (Eppendorf). After incubation at −20°C for 15 min, the samples were centrifuged at 21,000 *g* and 4°C for 15 min. The supernatant was decanted and 1 ml aqueous acetone (80%) was added to the pellet followed by thorough vortexing. After incubation at −20°C for 15 min, the samples were centrifuged at 21,000 *g* and 4°C for 15 min. The supernatant was decanted and the pellet was dried under nitrogen.

### Resolubilization of protein pellets

The precipitates of 1 I cell culture supernatant/conditioned media were incubated in 200 µl DIGE lysis buffer (30 mM Tris–HCl buffer, pH 8.5, containing 7 M urea (Applichem, Darmstadt, Germany), 2 M thiourea (Sigma-Aldrich) and 4% (w/v) 3 [(3 cholamidopropyl)-dimethylamino] 1 propane sulfonate (CHAPS; Applichem)) at 25°C for 30 min thereby vortexing thoroughly. Solubilized proteins were then sonicated using two cycles of five impulses (0.5 s/impulse) at 100% power (Bandelin UW 2070 sonicator, MS 73 needle; Bandelin, Berlin, Germany) and total protein concentration of samples was determined as previously described [52].

### Fluorescence labeling of protein pellets

All fluorescence labelings were performed in DIGE lysis buffer using the *Refraction-2D Labeling Kit* according to the manufacturer's instructions (NHDyeAGNOSTICS, Halle (Saale), Germany). Briefly, 25 µg of a mixture composed of equal amounts of proteins precipitated from 786-$0^{VHL-}$- and 786-$0^{VHL+}$-conditioned media were labeled for 30 min on ice with 100 pmol of G-Dye 100 as internal protein standard, whereas 25 µg of individual protein representing either proteins of 786-$0^{VHL-}$- or 786-$0^{VHL+}$-conditioned media were independently labeled with 100 pmol of G-Dye 200 and -300, respectively. The individual labelings were performed in a total volume of 21 µl DIGE lysis buffer, respectively for 30 min on ice. The reaction was stopped by adding 1 µL 10 mM lysine. After an incubation on ice for 10 min, an equal amount of 2 × sample buffer (7 M urea, 2 M thiourea, 0.4M NDSB-256 (Merck Biosciences, Darmstadt, Germany), 4% CHAPS, 2% dithiothreitol (DTT; Applichem), 1% pharmalytes pH 3–10 (Amersham Biosciences, Freiburg, Germany) was added to the mixture before the samples were pooled and subjected to 2-DE separation.

### Two-dimensional gel electrophoresis (2-DE), protein visualization and image analysis

For analytical gels the volume of the labeled protein mix was adjusted with Lysis-buffer (7 M urea, 2 M thiourea, 0.2 M dimethylbenzylammonium propane sulfonate (NDSB 201, Merck, Darmstadt, Germany), 1% dithiothreitol (DTT; Applichem), 4% 3 [(3 cholamidopropyl)-dimethylamino] 1 propane sulfonate (CHAPS; Applichem), 0.5% pharmalytes (Amersham Biosciences, Freiburg, Germany) and a trace of the dye bromophenol blue (Serva Electrophoresis, Heidelberg, Germany) to a final volume of 350 µl, whereas for preparative gels 500 µg protein in a total volume of 350 µl lysis buffer were loaded. Samples were applied to IPG strips (pH 3–10 NL, 18 cm, GE Healthcare, Munich, Germany) by in-gel rehydration and covered with 450 µl Immobiline DryStrip Cover Fluid (GE Healthcare). After 2 h of rehydration, isoelectric focusing (IEF) was carried out at 20°C on an Ettan IPGphor 2 unit (GE Healthcare) at the following settings: 30 V 10 hrs, 500 V 1 h, 1000 V 1 h, 5000 V 1 h, and 8000 V up to a total of 45,000 Vhrs. The IPG strips were subjected to a 2 step strip equilibration procedure, which was performed by incubation the strips first for 15 min in 12 ml equilibration buffer I (6 M urea, 2% SDS, 50 mM Tris HCl (pH 8.8), 30% glycerol, supplemented with 1.5% DTT) followed by 15 min in 12 ml equilibration buffer II (6 M urea, 2% SDS, 50 mM Tris HCl (pH 8.8), 30% glycerol, supplemented with 4.8% iodoacetamide, all chemicals purchased from Applichem). SDS-PAGE separation was performed using a PROTEAN plus Dodeca Cell (Bio-Rad, Munich, Germany) with gels of 1.5 mm thickness and an acrylamide/bisacrylamide matrix of 2.5% C and 13% T (Serva, Heidelberg, Germany). Strips were fixed on vertical SDS-PAGE gels with 1.5% soft melting agarose (BioLine GmbH, Luckenwalde, Germany) and traces of bromophenol blue. Electrophoresis was

performed with constant voltage (20 V, 1 h; 120 V, 15 h) at 10°C.

Gel documentation was accomplished by using a Fuji FLA 5100 fluorescence-scanning device (Fuji Photo Film, Duesseldorf, Germany). The PMT for all scans was set to 50 V below the saturation point of the brightest spot and all gel images were acquired at a resolution of 100 µm.

After 2D separation the preparative gels were stained with colloidal Coomassie Blue staining solution (10% ammonium sulfate (Applichem), 10% phosphoric acid (Merck KGaA), 0.12% Coomassie Brilliant Blue G250 (Applichem), 20% methanol (Merck KGaA); [53], and thereafter destained by extensive washing in $ddH_2O$. Preparative gels were scanned on a conventional scanner (UMAX Image Scanner, GE Healthcare) at a resolution of 600 dpi and stored as TIFF-images.

2D gel image analysis was performed using Delta2D Software version 4.0.8 (DECODON GmbH, Greifswald, Germany). All gel images were matched with the Delta2D software and a synthetic fusion gel was prepared. Final spot detection was performed on the fused gel. The resulting spot pattern was assigned to each of the gels in the experiment. The normalization procedure of the Delta2D software for DIGE experiments is based on the internal protein standard (IPS). The absolute spot volume is divided by the accumulated absolute volume of all spots and subsequently normalized to the corresponding absolute spot volume of the IPS. Furthermore, Student's *t*-test was performed to assess the statistical significance of differentially expressed proteins. Spots whose relative expression is changed at least 2-fold (increase or decrease) at 95% confidence level (*t*-test; $p < 0.05$) were considered to be significant and subsequently subjected to further analysis.

### In-gel digestion and MS

Digestion with trypsin and subsequent spotting of peptide solutions onto the MALDI-targets were performed as previously described [52] with slight modifications. For protein identification the proteins were excised from Colloidal Coomassie Brilliant Blue stained 2D gels using the Herolab spot hunter (Herolab GmbH, Wiesloch, Germany) with a picker head of 1.5 mm diameter and destained by addition of 50% (v/v) ACN. Gel pieces were washed twice with 100 µl 50% (v/v) ACN and once with 100 µl 100% ACN. After drying 5 µl trypsin solution containing 17 ng/µl trypsin (Promega, Madison, WI, USA) in 25 mM $NH_4CO_3$ supplemented with 0.4 mM $CaCl_2$ was added and incubated on ice for 2 h followed by an incubation over night at 37°C. If necessary 5 µl of 25 mM $NH_4CO_3$ supplemented with 0.4 mM $CaCl_2$ were added to keep gel pieces hydrated throughout the digest. Gel pieces were agitated by sonicating in a water bath for 10 min before 1 µl of the supernatant (containing tryptic peptides) were mixed with 1 µl of alpha-cyano-4-hydroxycinnamic acid (HCCA) matrix (saturated at room temperature in 50% ACN, 0.1% TFA) and 1 µl of this solution were directly spotted on the MALDI-target. Prior to the measurement the samples were allowed to dry on the target.

Spectra were calibrated externally using Peptide calibration standard II (Bruker Daltonics Inc, Bremen, Germany). MALDI-TOF-MS was performed on an *ultrafleXtreme*™ mass spectrometer (Bruker Daltonics Inc) in positive reflector mode using an accelerating voltage of 25 kV. Spectra processing was performed with flexAnalysis (3.3.80.0) software for resolution-based peak detection using default settings.

The PMF dataset were analyzed using the MASCOT search engine (http://www.matrixscience.com) with the following parameters: (i) *homo* sapiens sequences; (ii) fixed modification, carbamidomethylation of cysteins; (iii) cleavage enzyme, trypsin; (vi) a maximum of one missed cleavage was allowed; and mass tolerance (monoisotopic), ± 50.0 ppm. Target identification was based on the overall sequence coverage of matching peptide fragments. Proteins were assigned when the MASCOT score exceeded 57 according to the MASCOT-defined significance threshold for false-positive events at $p < 0.05$.

The heterogeneous set of the identified significant differentially expressed proteins was analyzed using gene ontology (GOminer) software [28], which provides information about gene function and cellular localization.

### Functional annotation cluster and pathway analysis DAVID

Functional annotation cluster analysis was performed on the list of up-regulated and down-regulated proteins with a fold change of ≥2.0 [http://david.abcc.ncifcrf.gov/home.jsp]. Only those terms that reported a *p*-value of ≤ 0.05 were selected for analysis. The Gene Ontology (GO) terms of cellular components, molecular function and biological processes in DAVID were employed to categorize enriched biological themes in up- and down-regulated protein lists.

### Western blot analysis

Aliquots of 50 µg of solubilized protein/lane were separated on 12% SDS-PAGE gels and subsequently transferred onto nitrocellulose membranes (Schleicher & Schuell, Dassel, Germany). Membranes were processed as previously described [54] using target protein-specific primary antibodies directed against beta-2-microglobulin (B2M) (kindly provided by Dr. Soldano Ferrone; [55]), MnSOD2 (Abfrontier,

Aachen, Germany), GAPDH (Cell signaling) or β-actin (Sigma-Aldrich) in combination with horse-radish peroxidase (HRP)-conjugated secondary antibodies (Cell Signaling, Frankfurt, Germany). Protein bands were visualized with LumiLight Western Blotting substrate (Roche, Mannheim, Germany) and recorded with a LAS 3000 CCD camera system (FUJIFILM, Duesseldorf, Germany). The co-detection of the GAPDH or β-actin signal, respectively, for each lane on the given blot served as loading control and the relative protein expression level for each target were defined using AIDA software (Raytest, Sprockhoevel, Germany).

### MnSOD2 activity assay

MnSOD2 activity of conditioned media was analyzed using the Superoxide Dismutase Activity Colorimetric Assay Kit (Abcam, Cambridge, UK) according to the manufacturer's protocol using freshly prepared and undiluted 786-$0^{VHL-}$- and 786-$0^{VHL+}$-conditioned media. MnSOD2 activity was analyzed after incubation up to 60 min using a microplate reader (MRX-TC, DYNEX Technologies, Denkendorf, Germany). The absorbance values were expressed as percentage of the supernatant of 786-$0^{VHL-}$ cells.

### Determination cell proliferation and IL-2 secretion in the absence and presence of MnSOD2

IL-2 secretion was analyzed using commercial enzyme-linked immunosorbent (ELISA) assay (eBioscience, Austria) based on the supplier's protocol. Therefore, "day 6" T cells were plated at a density of $1 \times 10^5$ cells/well onto 96-well culture plates in 200µl of RPMI-1640 (Sigma-Aldrich) supplemented with 10% FCS (PAA) and 2 mM L-glutamine (Lonza) in the absence and presence of MnSOD2 (1U/ml, Abnova via Biozol, Eiching, Germany). T cells were directly stimulated with plate-bound anti-CD3 and anti-CD28 antibodies (mouse anti-human, 1 µg/ml each, BD) in a time kinetic fashion (20 h, 40 h). Next, the supernatants were cleared by centrifugation and measurements were performed according the manufacturer's instructions using 100 µl cell culture supernatants.

### Statistical analysis

The results were expressed as mean ± standard deviation of at least three independent experiments. The data were analyzed using the SigmaPlot software (Systat Software, Erkrath, Germany). Differences between groups were examined for statistical significance using the Student's *t* test. A value of $p < 0.05$ was considered as statistically significant.

## Abbreviations

15-LOX2, 15-lipoxygenase-2; B2M, b2-microglobuline; ccRCC, clear cell RCC; CFSE, carboxyfluorescein succinimidyl ester; DC, dendritic cells; ENO1, α-enolase; FAC, Functional annotation cluster GAPDH, glyceraldehyde 3-phosphate dehydrogenase; GO, gene ontology; HIF, hypoxia-inducible factor; HPRT, hypo-xanthine-guanine phosphoribosyl-transferase; IL, interleukin; IPS, internal protein standard; MDSC, myeloid-derived suppressor cells; MMP, matrix metalloproteinase; NK, natural killer; PBMC, peripheral blood mononuclear cells; PPIA, peptidylprolylisomerase A; RCC, renal cell carcinoma; MnSOD, manganese superoxide dismutase; TAM, tumor-associated macrophages; TKI, tyrosine kinase inhibitors; UBE2N, ubiquitin-conjugating enzyme E2 N; VEGF, vascular endothelial growth factor; VHL, von Hippel Lindau; wt, wild-type.

## ACKNOWLEDGMENTS AND FUNDING

We would like to thank Dr. Soldano Ferrone for kindly providing the monoclonal antibody directed against beta-2-microglobulin (B2M). This work was supported by the Mildred Scheel Krebshilfe (109247) and the Deutsche Forschungsgemeinschaft GRK 1591.

## CONFLICTS OF INTEREST

No potential conflicts of interest were disclosed.

## REFERENCES

1. Finke JH, Rayman PA, Ko JS, Bradley JM, Gendler SJ, Cohen PA. Modification of the tumor microenvironment as a novel target of renal cell carcinoma therapeutics. Cancer journal. 2013; 19:353–364.
2. Ning H, Shao QQ, Ding KJ, Gao DX, Lu QL, Cao QW, Niu ZH, Fu Q, Zhang CH, Qu X, Lu JJ. Tumor-infiltrating regulatory T cells are positively correlated with angiogenic status in renal cell carcinoma. Chinese medical journal. 2012; 125:2120–2125.
3. Sell K, Barth PJ, Moll R, Thomas MA, Zimmer N, Oplesch E, Gudo M, Schrader M, Hofmann R, Schrader AJ. Localization of FOXP3-positive cells in renal cell carcinoma. Tumour biology: the journal of the International Society for Oncodevelopmental Biology and Medicine. 2012; 33:507–513.
4. Geissler K, Fornara P, Lautenschlager C, Holzhausen HJ, Seliger B, Riemann D. Immune signature of tumor infiltrating immune cells in renal cancer. Oncoimmunology. 2015; 4:e985082.
5. Santoni M, Berardi R, Amantini C, Burattini L, Santini D, Santoni G, Cascinu S. Role of natural and adaptive

immunity in renal cell carcinoma response to VEGFR-TKIs and mTOR inhibitor. International journal of cancer Journal international du cancer. 2014; 134:2772–2777.

6. Minarik I, Lastovicka J, Budinsky V, Kayserova J, Spisek R, Jarolim L, Fialova A, Babjuk M, Bartunkova J. Regulatory T cells, dendritic cells and neutrophils in patients with renal cell carcinoma. Immunology letters. 2013; 152:144–150.
7. Petrella BL, Vincenti MP. Interleukin-1beta mediates metalloproteinase-dependent renal cell carcinoma tumor cell invasion through the activation of CCAAT enhancer binding protein beta. Cancer medicine. 2012; 1:17–27.
8. Daurkin I, Eruslanov E, Stoffs T, Perrin GQ, Algood C, Gilbert SM, Rosser CJ, Su LM, Vieweg J, Kusmartsev S. Tumor-associated macrophages mediate immunosuppression in the renal cancer microenvironment by activating the 15-lipoxygenase-2 pathway. Cancer research. 2011; 71:6400–6409.
9. Kusmartsev S. Enhanced 5-lipoxygenase activity and elevated eicosanoid production in kidney tumor microenvironment contribute to the inflammation and immune suppression. Oncoimmunology. 2012; 1:249–251.
10. Gatenby RA, Gillies RJ, Brown JS. Of cancer and cave fish. Nature reviews Cancer. 2011; 11:237–238.
11. Mediavilla-Varela M, Luddy K, Noyes D, Khalil FK, Neuger AM, Soliman H, Antonia SJ. Antagonism of adenosine A2A receptor expressed by lung adenocarcinoma tumor cells and cancer associated fibroblasts inhibits their growth. Cancer biology & therapy. 2013; 14:860–868.
12. Sundaram S, Johnson AR, Makowski L. Obesity, metabolism and the microenvironment: Links to cancer. Journal of carcinogenesis. 2013; 12:19.
13. Ward PS, Thompson CB. Metabolic reprogramming: a cancer hallmark even warburg did not anticipate. Cancer cell. 2012; 21:297–308.
14. Yecies JL, Manning BD. mTOR links oncogenic signaling to tumor cell metabolism. Journal of molecular medicine. 2011; 89:221–228.
15. Vander Heiden MG, Cantley LC, Thompson CB. Understanding the Warburg effect: the metabolic requirements of cell proliferation. Science. 2009; 324:1029–1033.
16. Semenza GL. HIF-1 mediates metabolic responses to intratumoral hypoxia and oncogenic mutations. The Journal of clinical investigation. 2013; 123:3664–3671.
17. Cockman ME, Masson N, Mole DR, Jaakkola P, Chang GW, Clifford SC, Maher ER, Pugh CW, Ratcliffe PJ, Maxwell PH. Hypoxia inducible factor-alpha binding and ubiquitylation by the von Hippel-Lindau tumor suppressor protein. The Journal of biological chemistry. 2000; 275:25733–25741.
18. Ivan M, Kondo K, Yang H, Kim W, Valiando J, Ohh M, Salic A, Asara JM, Lane WS, Kaelin WG Jr. HIFalpha targeted for VHL-mediated destruction by proline hydroxylation: implications for O2 sensing. Science. 2001; 292:464–468.
19. Semenza GL. Regulation of mammalian O2 homeostasis by hypoxia-inducible factor 1. Annual review of cell and developmental biology. 1999; 15:551–578.
20. Wykoff CC, Sotiriou C, Cockman ME, Ratcliffe PJ, Maxwell P, Liu E, Harris AL. Gene array of VHL mutation and hypoxia shows novel hypoxia-induced genes and that cyclin D1 is a VHL target gene. British journal of cancer. 2004; 90:1235–1243.
21. Bluyssen HA, Lolkema MP, van Beest M, Boone M, Snijckers CM, Los M, Gebbink MF, Braam B, Holstege FC, Giles RH, Voest EE. Fibronectin is a hypoxia-independent target of the tumor suppressor VHL. FEBS letters. 2004; 556:137–142.
22. Iliopoulos O, Levy AP, Jiang C, Kaelin WG Jr, Goldberg MA. Negative regulation of hypoxia-inducible genes by the von Hippel-Lindau protein. Proceedings of the National Academy of Sciences of the United States of America. 1996; 93:10595–10599.
23. Maxwell PH, Wiesener MS, Chang GW, Clifford SC, Vaux EC, Cockman ME, Wykoff CC, Pugh CW, Maher ER, Ratcliffe PJ. The tumour suppressor protein VHL targets hypoxia-inducible factors for oxygen-dependent proteolysis. Nature. 1999; 399:271–275.
24. Boysen G, Bausch-Fluck D, Thoma CR, Nowicka AM, Stiehl DP, Cima I, Luu VD, von Teichman A, Hermanns T, Sulser T, Ingold-Heppner B, Fankhauser N, Wenger RH, Krek W, Schraml P, Wollscheid B, et al. Identification and functional characterization of pVHL-dependent cell surface proteins in renal cell carcinoma. Neoplasia. 2012; 14:535–546.
25. Craven RA, Hanrahan S, Totty N, Harnden P, Stanley AJ, Maher ER, Harris AL, Trimble WS, Selby PJ, Banks RE. Proteomic identification of a role for the von Hippel Lindau tumour suppressor in changes in the expression of mitochondrial proteins and septin 2 in renal cell carcinoma. Proteomics. 2006; 6:3880–3893.
26. Leisz S, Schulz K, Erb S, Oefner P, Dettmer K, Mougiakakos D, Wang E, Marincola FM, Stehle F, Seliger B. Distinct von Hippel-Lindau gene and hypoxia-regulated alterations in gene and protein expression patterns of renal cell carcinoma and their effects on metabolism. Oncotarget. 2015; 6:11395–11406.
27. Unwin RD, Craven RA, Harnden P, Hanrahan S, Totty N, Knowles M, Eardley I, Selby PJ, Banks RE. Proteomic changes in renal cancer and co-ordinate demonstration of both the glycolytic and mitochondrial aspects of the Warburg effect. Proteomics. 2003; 3:1620–1632.
28. Zeeberg BR, Feng W, Wang G, Wang MD, Fojo AT, Sunshine M, Narasimhan S, Kane DW, Reinhold WC, Lababidi S, Bussey KJ, Riss J, Barrett JC, Weinstein JN. GoMiner: a resource for biological interpretation of

genomic and proteomic data. Genome biology. 2003; 4:R28.

29. Brown KJ, Formolo CA, Seol H, Marathi RL, Duguez S, An E, Pillai D, Nazarian J, Rood BR, Hathout Y. Advances in the proteomic investigation of the cell secretome. Expert review of proteomics. 2012; 9:337–345.
30. Nickel W. Pathways of unconventional protein secretion. Current opinion in biotechnology. 2010; 21:621–626.
31. Keller S, Sanderson MP, Stoeck A, Altevogt P. Exosomes: from biogenesis and secretion to biological function. Immunology letters. 2006; 107:102–108.
32. Pant S, Hilton H, Burczynski ME. The multifaceted exosome: biogenesis, role in normal and aberrant cellular function, and frontiers for pharmacological and biomarker opportunities. Biochemical pharmacology. 2012; 83:1484–1494.
33. Mignot G, Roux S, Thery C, Segura E, Zitvogel L. Prospects for exosomes in immunotherapy of cancer. Journal of cellular and molecular medicine. 2006; 10:376–388.
34. Capello M, Ferri-Borgogno S, Cappello P, Novelli F. alpha-Enolase: a promising therapeutic and diagnostic tumor target. The FEBS journal. 2011; 278:1064–1074.
35. Sarto C, Deon C, Doro G, Hochstrasser DF, Mocarelli P, Sanchez JC. Contribution of proteomics to the molecular analysis of renal cell carcinoma with an emphasis on manganese superoxide dismutase. Proteomics. 2001; 1:1288–1294.
36. Minton DR, Fu L, Chen Q, Robinson BD, Gross SS, Nanus DM, Gudas LJ. Analyses of the transcriptome and metabolome demonstrate that HIF1alpha mediates altered tumor metabolism in clear cell renal cell carcinoma. PloS one. 2015; 10:e0120649.
37. Sarto C, Frutiger S, Cappellano F, Sanchez JC, Doro G, Catanzaro F, Hughes GJ, Hochstrasser DF, Mocarelli P. Modified expression of plasma glutathione peroxidase and manganese superoxide dismutase in human renal cell carcinoma. Electrophoresis. 1999; 20:3458–3466.
38. Sarto C, Marocchi A, Sanchez JC, Giannone D, Frutiger S, Golaz O, Wilkins MR, Doro G, Cappellano F, Hughes G, Hochstrasser DF, Mocarelli P. Renal cell carcinoma and normal kidney protein expression. Electrophoresis. 1997; 18:599–604.
39. Jackson SH, Devadas S, Kwon J, Pinto LA, Williams MS. T cells express a phagocyte-type NADPH oxidase that is activated after T cell receptor stimulation. Nature immunology. 2004; 5:818–827.
40. Kwon J, Shatynski KE, Chen H, Morand S, de Deken X, Miot F, Leto TL, Williams MS. The nonphagocytic NADPH oxidase Duox1 mediates a positive feedback loop during T cell receptor signaling. Science signaling. 2010; 3:ra59.
41. Kaminski M, Kiessling M, Suss D, Krammer PH, Gulow K. Novel role for mitochondria: protein kinase Ctheta-dependent oxidative signaling organelles in activation-induced T-cell death. Molecular and cellular biology. 2007; 27:3625–3639.
42. Kaminski MM, Sauer SW, Klemke CD, Suss D, Okun JG, Krammer PH, Gulow K. Mitochondrial reactive oxygen species control T cell activation by regulating IL-2 and IL-4 expression: mechanism of ciprofloxacin-mediated immunosuppression. Journal of immunology. 2010; 184:4827–4841.
43. Lambert AJ, Brand MD. Reactive oxygen species production by mitochondria. Methods in molecular biology. 2009; 554:165–181.
44. Droge W. Free radicals in the physiological control of cell function. Physiological reviews. 2002; 82:47–95.
45. Gloire G, Legrand-Poels S, Piette J. NF-kappaB activation by reactive oxygen species: fifteen years later. Biochemical pharmacology. 2006; 72:1493–1505.
46. Reth M. Hydrogen peroxide as second messenger in lymphocyte activation. Nature immunology. 2002; 3:1129–1134.
47. Gardner R, Salvador A, Moradas-Ferreira P. Why does SOD overexpression sometimes enhance, sometimes decrease, hydrogen peroxide production? A minimalist explanation. Free radical biology & medicine. 2002; 32:1351–1357.
48. Kaminski MM, Roth D, Sass S, Sauer SW, Krammer PH, Gulow K. Manganese superoxide dismutase: a regulator of T cell activation-induced oxidative signaling and cell death. Biochimica et biophysica acta. 2012; 1823:1041–1052.
49. Liochev SI, Fridovich I. The effects of superoxide dismutase on H2O2 formation. Free radical biology & medicine. 2007; 42:1465–1469.
50. Bensadoun A, Weinstein D. Assay of proteins in the presence of interfering materials. Analytical biochemistry. 1976; 70:241–250.
51. Arnold U, Ulbrich-Hofmann R. Quantitative protein precipitation from guanidine hydrochloride-containing solutions by sodium deoxycholate/trichloroacetic acid. Analytical biochemistry. 1999; 271:197–199.
52. Lichtenfels R, Ackermann A, Kellner R, Seliger B. Mapping and expression pattern analysis of key components of the major histocompatibility complex class I antigen processing and presentation pathway in a representative human renal cell carcinoma cell line. Electrophoresis. 2001; 22:1801–1809.
53. Candiano G, Bruschi M, Musante L, Santucci L, Ghiggeri GM, Carnemolla B, Orecchia P, Zardi L, Righetti PG. Blue silver: a very sensitive colloidal Coomassie G-250 staining for proteome analysis. Electrophoresis. 2004; 25:1327–1333.
54. Leich F, Stohr N, Rietz A, Ulbrich-Hofmann R, Arnold U. Endocytotic internalization as a crucial factor for the cytotoxicity of ribonucleases. The Journal of biological chemistry. 2007; 282:27640–27646.
55. Pellegrino MA, Ng AK, Russo C, Ferrone S. Heterogeneous distribution of the determinants defined by monoclonal antibodies on HLA-A and B antigens bearing molecules. Transplantation. 1982; 34:18–23.



„*Supplementary table S1*“ siehe Anhang auf CD

## 4.3 „Hypoxia-mediated alterations and their role in the HER-2/neu-regulated CREB status and localization“

www.impactjournals.com/oncotarget/ Oncotarget, Vol. 7, No. 32

Research Paper

# Hypoxia-mediated alterations and their role in the HER-2/neu-regulated CREB status and localization

**André Steven[1], Sandra Leisz[1], Katharina Sychra[6], Bernhard Hiebl[2], Claudia Wickenhauser[3], Dimitrios Mougiakakos[4], Rolf Kiessling[5], Carsten Denkert[6], Barbara Seliger[1]**

[1]Institute of Medical Immunology, Martin Luther University Halle-Wittenberg, Halle, Germany
[2]Centre for Basic Medical Research, Martin Luther University Halle-Wittenberg, Halle, Germany
[3]Institute of Pathology, Martin Luther University Halle-Wittenberg, Halle, Germany
[4]Department of Internal Medicine 5, Hematology and Oncology, University of Erlangen-Nuremberg, Erlangen, Germany
[5]Karolinska Institutet, CCK, Stockholm, Sweden
[6]Charité, Institute of Pathology, Berlin, Germany

***Correspondence to:*** *Barbara Seliger,* ***email:*** *Barbara.Seliger@uk-halle.de*

***Keywords:*** *CREB, HER-2/neu, hypoxia, angiogenesis, mitochondria*

***Received:*** *March 11, 2016* ***Accepted:*** *June 17, 2016* ***Published:*** *July 7, 2016*

## ABSTRACT

**The cAMP-responsive element-binding protein (CREB) is involved in the tumorigenicity of HER-2/neu-overexpressing murine and human tumor cells, but a link between the HER-2/neu-mediated CREB activation, its posttranslational modification and localization and changes in the cellular metabolism, due to an altered (tumor) microenvironment remains to be established. The present study demonstrated that shRNA-mediated silencing of CREB in HER-2/neu-transformed cells resulted in decreased tumor formation, which was associated with reduced angiogenesis, but increased necrotic and hypoxic areas in the tumor. Hypoxia induced pCREB$^{Ser133}$, but not pCREB$^{Ser121}$ expression in HER-2/neu-transformed cells. This was accompanied by upregulation of the hypoxia-inducible genes GLUT1 and VEGF, increased cell migration and matrix metalloproteinase-mediated invasion. Treatment of HER-2/neu$^+$ cells with signal transduction inhibitors targeting in particular HER-2/neu was able to revert hypoxia-controlled CREB activation. In addition to changes in the phosphorylation, hypoxic response of HER-2/neu$^+$ cells caused a transient ubiquitination and SUMOylation as well as a co-localization of nuclear CREB to the mitochondrial matrix. A mitochondrial localization of CREB was also demonstrated in hypoxic areas of HER-2/neu$^+$ mammary carcinoma lesions. This was accompanied by an altered gene expression pattern, activity and metabolism of mitochondria leading to an increased respiratory rate, oxidative phosphorylation and mitochondrial membrane potential and consequently to an enhanced apoptosis and reduced cell viability. These data suggest that the HER-2/neu-mediated CREB activation caused by a hypoxic tumor microenvironment contributes to the neoplastic phenotype of HER-2/neu$^+$ cells at various levels.**

## INTRODUCTION

The cAMP-responsive element-binding protein (CREB) belongs to the leucine zipper family of transcription factors. Different mediators, such as growth factors, neurotransmitters, glucose, inflammatory lipids, stress signals as well as factors known to modulate the intracellular cAMP or $Ca^{2+}$ levels can activate CREB through phosphorylation of serine 133 ($Ser^{133}$) by protein kinase A (PKA), protein kinase B (PKB/AKT), mitogen-activated protein kinases (MAPK), calcium-activated calmodulin kinases (CaMKs) and the 90 kD ribosomal S6 kinase. Stress situations like irradiation and UV caused phosphorylation of CREB at serine 121 ($Ser^{121}$) leading to its activation [1-3], while phosphorylation of

CREB at Ser[142] could negatively interfere with CREB activity [2]. The phosphorylated CREB (pCREB) can bind to its transcriptional co-activator (CBP/p300) via the kinase-induced domain (KID) in the cAMP- (CRE) and the KID-interacting domain KIX of CBP [4]. The CREB/CBP complex recruits the transcription machinery to the gene promoter thereby initiating CRE-regulated gene transcription. Upon activation CREB regulates the expression of many genes involved in different physiologic and pathophysiologic processes by binding to the CRE sequence within their promoters [5-9].

In addition, pCREB has been shown to be present and active in mitochondria (mitoCREB): This not only leads to an altered expression pattern of mitochondrial genes [10-13], but also to changes in the mitochondrial function, which could affect cell growth and survival. Although phosphorylation of CREB is the most studied modification, other post-transcriptional modifications (PTMs), like ubiquitination, acetylation and SUMOylation, could also exist. However, the frequency and role of these PTMs for CREB expression and function are incompletely understood [14-17]. Next to the phosphorylation-dependent activation of CREB, the stability of CREB is influenced by hypoxia. In the acute phase of hypoxia CREB can be ubiquitinated and degraded via the ubiquitin/proteasome pathway [18, 19], while SUMOylation of CREB is increased during prolonged hypoxia. The hypoxia-mediated stabilization and activation of CREB results in the induction of various genes [20] leading to an adaptation to hypoxia coupled with a translocation of CREB from the nucleus to the mitochondria [21]. This process caused changes of the mitochondrial function and biogenesis thereby modulating cellular processes including cell survival [13, 22].

A role for CREB in the development of tumors has been suggested since it is often overexpressed and more active in many solid and hematopoietic tumors [23-26]. This could be influenced by the modulation of signalling cascades upstream of CREB as well as the induction of the CRE-dependent gene expression downstream of CREB, e.g. matrix metalloproteinases (MMPs), adhesion molecules and different survival factors [20, 27] leading to an increased tumor growth, prevention of cell death, enhanced metastasis formation and angiogenesis [28]. Furthermore, overexpression of CREB in tumors often correlates with disease progression, poor patient survival and chemotherapy resistance [21, 24-26, 29-31]. On the other hand oxygenation in breast cancer is markedly reduced compared to normal tissue [32]. In mammary carcinoma the CREB pathway is often upregulated [33, 34]. An important role of CREB in breast cancer has been further demonstrated by global profiling of signalling networks in breast cancer stem cells [34]. Recently, a correlation between CREB expression/activation, altered *in vitro* and *in vivo* tumor growth properties and HER-2/neu has been described in both *in vitro* models of HER-2/neu transformation and in HER-2/neu overexpressing human mammary carcinoma [35]. Despite the tumor microenvironment including hypoxia is of critical importance for breast cancer [36], it has not yet been determined whether the HER-2/neu-mediated expression, activation, localization and modification of CREB and upstream signal pathways are altered under hypoxic conditions. Therefore this study analysed the changes of the cellular localization and posttranslational modifications in different HER-2/neu model systems under normoxia and hypoxia in the presence of signal transduction inhibitors.

## RESULTS

### Link between decreased tumorigenicity of CREB-deficient cells and reduced angiogenesis

Recently, a link between HER-2/neu overexpression and CREB activation has been described in parental HER-2/neu$^+$ cells upon silencing of CREB by shRNA without affecting HER-2/neu surface expression [35]. This was accompanied by a decreased tumor growth of CREB-deficient compared to parental HER-2/neu$^+$ cells ([35], Supplementary Figure 1A). In order to determine whether the diminished *in vivo* growth capacity of CREB-deficient HER-2/neu$^+$ cells was associated with a reduced angiogenesis, lesions of parental and shCREB HER-2/neu$^+$ murine tumors were stained with anti-CD31 and anti-HIF-1α antibodies, respectively. As shown in Figure 1A, an altered staining pattern for CD31 and HIF-1α was demonstrated in parental versus CREB-deficient HER-2/neu$^+$ cells with a more than 50% reduced density of blood vessels (Figure 1B), an approximately 2-fold increase of necrotic (Figure 1C) as well as hypoxic areas (Figure 1D) in CREB-deficient tumors when compared to parental HER-2/neu$^+$ tumors. It is noteworthy that the increased HIF-1α expression has been correlated with a worse prognosis of breast cancer patients, while CREB increased the risk of metastases in HER-2/neu$^+$ breast cancer (Supplementary Figure 2 and Supplementary Table 1).

The CREB-mediated regulation of angiogenesis was confirmed *in vitro* by incubating human umbilical vein endothelial cells (HUVEC) with conditioned medium obtained from both parental and CREB-deficient HER-2/neu$^+$ cells. In the presence of supernatants from parental HER-2/neu$^+$ cells morphologic changes of HUVEC were more pronounced with increased numbers of branching points when compared to that from CREB-deficient HER-2/neu$^+$ cells (Figure 1E). To confirm the angiogenic potential of CREB, both parental and CREB-deficient HER-2/neu$^+$ cells were injected with matrigel into the flanks of mice followed by the analysis of tumor growth, hemoglobin content and blood vesel density in these tumors. The matrigel plugs of CREB-deficient HER-2/neu$^+$ cells had a smaller size, a fainter red color (Figure

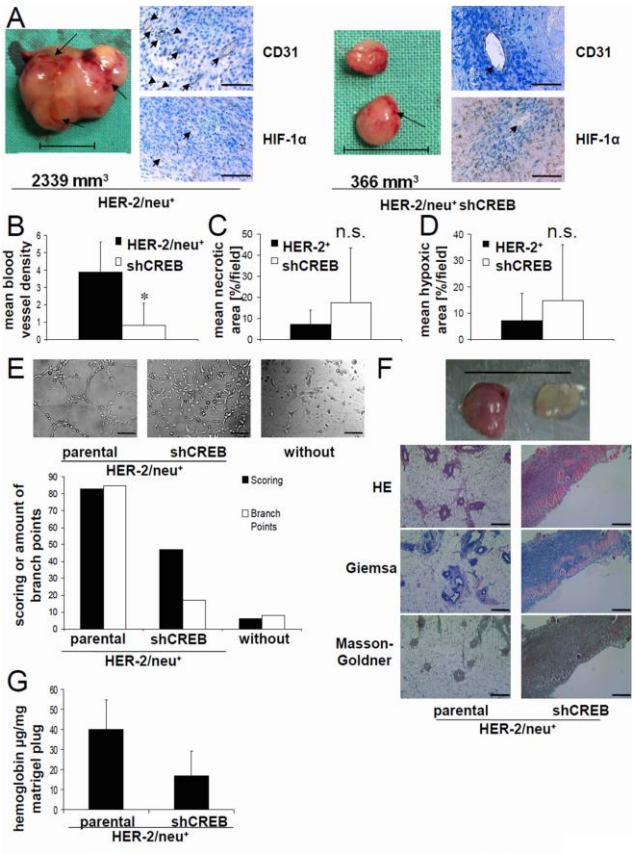


**Figure 1: Link of decreased tumorgenicity of CREB-deficient HER-2/neu⁺ cells and reduced angiogenesis, but enhanced hypoxic areas. A.** DBA-1 mice were injected with parental or CREB-deficient HER-2/neu⁺ cells as described in Materials and Methods and tumors were removed after 42 days. Representative photos of parental and CREB-deficient HER-2/neu⁺ tumors are shown. The arrows indicate the blood vessels on the tumor surface. The tumor volume is given. The bar represents 1 cm (left). 5 µm slices of paraffin-embedded tumors were stained with the indicated primary antibody followed by an anti-rabbit secondary antibody. The detection was performed with the peroxidase substrate DAB. Slides were counterstained with methylene blue. The arrow heads indicate the blood vessels. The bar represents 100 µm; Magnification: 40x (right). **B.** The blood vessel density of the tumors was analysed by counting vessel structures in the anti-CD31 mAb-stained samples (see 1A). Bars represent mean values from four samples/group with four counted fields/sample. **C.** The necrotic area was analysed in the HE-stained samples. Bars represent mean values from four samples/group with four counted fields/sample. **D.** The hypoxic area was analysed in the anti-HIF-1α-stained samples. Bars represent mean values from four samples/group with four counted fields/sample. **E.** 1x10⁴ HUVEC/well were seeded in a 96 well plate on polymerized growth factor reduced matrigel. 100 µl/well fresh medium or cell conditioned medium was added and the cells were incubated for 16 h by 37°C. The morphology of the HUVEC under these distinct culture conditions was compared (left) and the mesh-like structures were quantified (right) as described by Zhang [51]. The bar represents 80 µm; Magnification: 10x. **F.** 1x10⁵ parental and CREB-deficient HER-2/neu⁺ cells resuspended in matrigel were injected into the flank of female DBA-1 mice (n = 8). 7 days after injection the mice were killed and the removed matrigel plugs were photographed. The bar represents 1 cm (up). 5 µm slices of the matrigel plugs from parental and CREB-deficient HER-2/neu⁺ cells were stained as indicated. The bar represents 100 µm; Magnification: 10x (down). **G.** Matrigel plugs from parental and CREB-deficient HER-2/neu⁺ cells were homogenized and their hemoglobin content was analysed as described as in Material and Methods. The bars represent the hemoglobin concentration of each plug from mice injected with the indicated cell line normalized to the weight of the plug. Data demonstrate the results of one out of two independent experiments (with five Matrigel plugs in each experiments) regarding the hemoglobin content/plug from parental and CREB-deficient HER-2/neu⁺ cells.

**Table 1: Influence of CREB knock down on the expression of surface and angiogenesis markers**

| | NIH3T3 | NIH3T3 shCREB | HER-2/neu$^+$ | HER-2/neu$^+$ shCREB |
|---|---|---|---|---|
| Angiopoietin 1 | 1 | 0.56 +/- 0.23 | 4.06 +/- 3.01 | 4.63 +/- 0.41 |
| Angiopoietin 2 | 1 | 1.7 +/- 0.39 * | 0.65 +/- 0.7 | 1.45 +/- 0.44 |
| ICAM-1 | 1 | 0.82 +/- 0.5 | 0.12 +/- 0.03 | 2.07 +/- 1.2 * |
| PECAM1 | 1 | 1.08 +/- 0.54 | 0.28 +/- 0.34 | 0.29 +/- 0.23 |
| VCAM1 | 1 | 0.56 +/- 0.49 | 3.62 +/- 5.63 | 0.18 +/- 0.02 |
| VEGF-A | 1 | 0.87 +/- 0.53 | 2.76 +/- 0.31 | 0.79 +/- 0.49 * |

Cellular RNA isolated from parental and CREB-deficient (shCREB) HER-2/neu$^-$ and HER-2/neu$^+$ cells was subjected to qPCR analysis as described in Materials and Methods. Using gene-specific primers the expression of two angiogenesis markers (VEGF, angiopoetin 1) as well as two adhesion molecules linked with angiogenesis (ICAM-1, VCAM1) was determined. The results represent the mean and SEM from three independent replicates. The expression was normalized to β-actin and the data are expressed as relative mRNA expression by setting the expression levels of NIH3T3 cells to 1.

1F), reduced hemoglobin content and decreased number of blood vessels (Figure 1G). This was accompanied by a downregulation of the mRNA expression levels of VEGF-A and ICAM-1 in CREB deficient cells when compared with parental HER-2/neu$^+$ cells (Table 1).

### Determination of the role of hypoxia on the expression and activation of CREB and its dependence on the HER-2/neu-mediated signaling

Since an oxygen-limited microenvironment (hypoxia) has recently been shown to activate CREB [18, 20], the expression level and phosphorylation status of CREB was compared in HER-2/neu$^-$ NIH3T3 cells and parental HER-2/neu$^+$ cells cultured under normoxic and hypoxic conditions. The induction of hypoxia in these cells was confirmed by an upregulated transcription of VEGF-A and the glucose transporter (GLUT)1 (Figure 2A).

The expression and activation of CREB in the model systems was found to be different both under normoxic and hypoxic culture conditions. A strong upregulation of unphosphorylated CREB and pCREB$^{Ser133}$ was found in hypoxic HER-2/neu$^+$, while expression of pCREB$^{Ser121}$ was unchanged after 24 h hypoxia in these cells (Figure 2B). The increased phosphorylation status of CREB at Ser$^{133}$ was accompanied by an upregulated expression of pERK, but not of ERK, AKT or pAKT in the HER-2/neu$^+$ cell line (Figure 2C), while the cAMP levels were not changed under hypoxic conditions (data not shown) resulting in an unaltered PKA activity. Treatment with the MEK inhibitor trametinib decreased pCREB$^{Ser133}$ but not pCREB$^{Ser121}$ while 5 μM U0126 had no effect (Figure 2D). Blocking PI3K/AKT by LY294002 reduced the phosphorylation of both serine residues. There might be a minor effect of U0126 on the expression of AKT, which does not have an impact on the general results. Analogous to murine parental HER-2/neu$^+$ cells, hypoxia increased pCREB$^{Ser133}$ expression in the breast cancer cell line HTB122 transfected with functional HER-2/neu (E2), but not in HTB122 cells transformed with a signaling-deficient HER-2/neu construct (E2A, Figure 2E). Vice versa the shHER-2/neu-transfected lung carcinoma cell line H125 exhibited a downregulation of pCREB$^{Ser133}$ expression under hypoxic conditions (Supplementary Figure 1B). These data suggested a control of CREB activity by both oncogenic transformation and hypoxia. It is noteworthy that hypoxia did not influence the HER-2/neu surface expression in murine and human HER-2/neu-transformed cells (Figure 2F).

In order to determine whether inhibitors of transduction pathways affect the hypoxia-mediated expression of CREB, hypoxic parental HER-2/neu$^+$ cells were treated with various inhibitors followed by the analysis of the phosphorylation status of CREB. As shown in Figure 2G the tyrosine kinase inhibitor (TKI) lapatinib targeting HER-1 and HER-2/neu had the most significant impact and already 2.5 μM lapatinib caused an 80% downregulation of the expression of pCREB$^{Ser133}$, which could not be further decreased by higher concentrations. In contrast, lapatinib treatment consecutively increased the total CREB expression in a dose-dependent manner.

### Hypoxia-induced post-translational modifications of CREB

In order to dissect the effect of early and late phase hypoxia on the CREB status and its PTMs, time kinetic analyses of parental HER-2/neu$^+$ cells were performed. A transient, but time-dependent upregulation of CREB and pCREB$^{Ser133}$, but not of pCREB$^{Ser121}$ was detected during hypoxia: Already at one hour after hypoxia onset a significant increase in both CREB and pCREB$^{Ser133}$ protein expression was found (Figure 3A). This was accompanied by a transient induction of pCREB$^{Ser133}$ modifications in these cells during the early phase of hypoxia with the

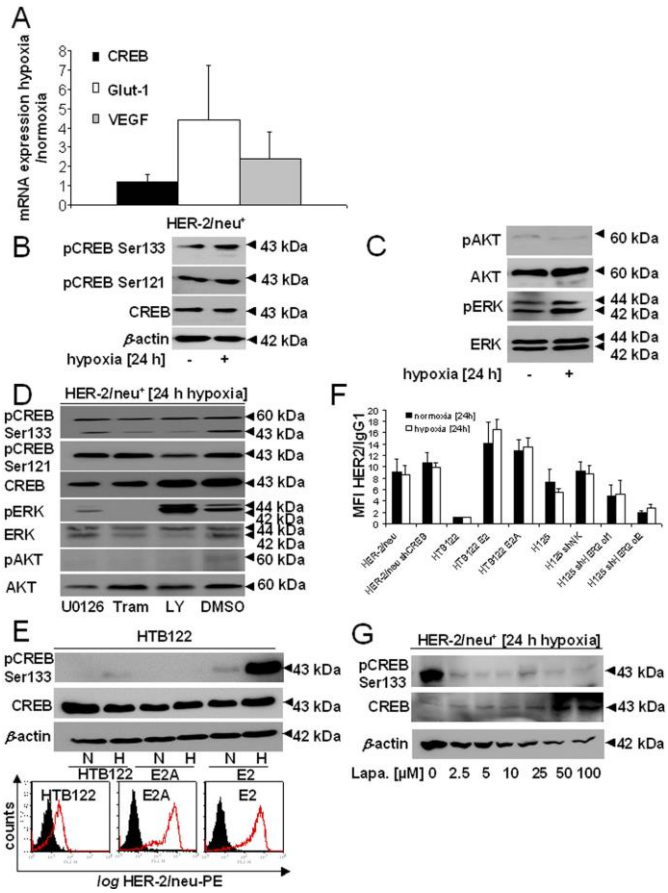


**Figure 2: Hypoxia-induced CREB phosphorylation by induction of the MAPK/ERK signal transduction pathway.** **A.** The transcription of CREB and of hypoxic markers (GLUT1, VEGF) was analysed by qPCR. The bar charts represent the mean values and SEM of three independent experiments. **B.** CREB expression and phosphorylation was compared in HER-2/neu$^+$ NIH3T3 cells under normoxia and hypoxia by Western blot analysis as described in Materials and Methods using an anti-CREB and anti-CREB phosphorylation-specific antibodies. One of three representative Western blots is shown. **C.** The activity/phosphorylation of the AKT and ERK pathway was determined under normoxic and hypoxic conditions by Western blot analysis using total and phosphorylation-specific antibodies, respectively. The data represent one of three biological replicates. **D.** Cells were treated under hypoxia with 5 μM LY294002, 100 nM trametinib or 5 μM U0126 for 24 h. The phosphorylation and total expression of CREB, AKT and ERK was analysed by Western Blot. **E.** Hypoxia-mediated induction of CREB phosphorylation and its dependence on the HER-2/neu status was determined in HTB122 cells and their HER-2/neu-transformed transfectants (E2A: dominant negative mutation in the HER-2/neu kinase domain; E2: wild-type HER-2/neu) either incubated under normoxia or hypoxia for 24 h, respectively, before Western blot analysis was performed as described in Materials and Methods. The results show one of two independent experiments (up). HTB122, E2 and E2A cells were incubated under normoxic conditions for 24 h before the HER-2/neu cell surface expression was determined using flow cytometry. The data are represented as histograms from one out of two representative experiments. The black area represents the IgG control, while the red defined area is the HER-2/neu-PE staining (down). **F.** Cells were incubated for 24 h under normoxia or hypoxia and the presentation of HER-2/neu on the cell surface was determined by flow cytometry as described in Materials and Methods using a PE-labelled anti-HER-/neu mAb. The bars represent the MFI of HER-2/neu compared to an IgG control from two independent experiments. **G.** The effect of inhibition of the HER-2/neu activity by treatment of parental HER-2/neu$^+$ cells with increasing concentrations of lapatinib on CREB phosphorylation was analysed by Western blot. Cells were treated with lapatinib for 24 h under hypoxic conditions.

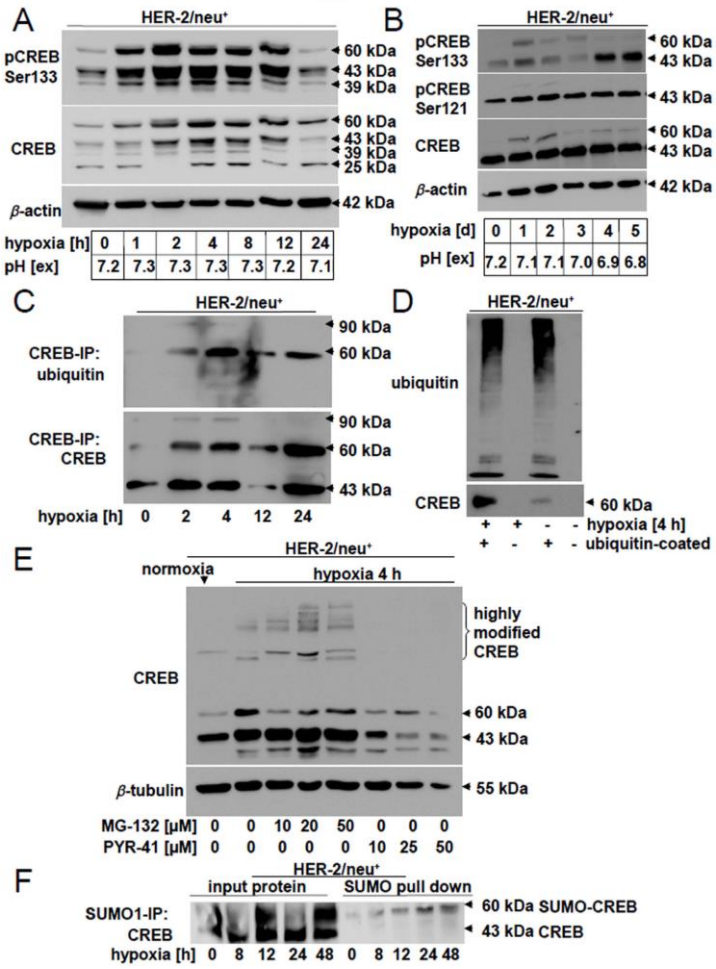


**Figure 3: Hypoxia-mediated post-transcriptional modification and altered distribution of CREB. A.** Comparative analysis of different pCREB and CREB modifications under normoxia and early phase hypoxia (up to 12 h). Western blot analyses were performed as described using CREB and pCREB$^{Ser133}$-specific mAb. The size of the modified CREB protein is given. The blots represent one of three biological replicates. Extracellular pH (pH [ex]) of the cell free media was directly measured with a pH electrode after harvesting the cells. **B.** CREB phosphorylation at serine residue 133 and 121 as well as CREB protein expression was analysed under late phase hypoxia (up to 5 d). The photos represent one of two independent biological replicates. The pH of the culture media was measured with a pH electrode directy after harvesting the cells. **C., D.** Ubiquitination was analysed by CREB immune precipitation (C) and ubiquitin pull down (D) as described in Materials and Methods by loading the complete supernatant on 10% (C) or 12% (D) gels. The proteins were identified by using anti-CREB- or anti-ubiquitin-specific mAb. Results represent data of three (C) or two (D) biological replicates. **E.** Influence of the proteasome inhibitor MG-132 and the ubiquitin inhibitor PYR-41 on CREB modifications. Parental HER-2/neu$^{+}$ cells were either left untreated or treated with different concentrations of MG-132 (10, 25, 50 μM) or PYR-41 (10, 20, 50 μM) for 4 h under hypoxia. Following Western blot analysis using anti-CREB-specific antibodies as described above, the appearance of highly modified CREB molecules was determined. The blot represents one of two biological experiments. **F.** Cells were cultivated under hypoxia for the indicated time and SUMO-1 modified proteins in the cell lysate were precipitated by immunoprecipitation. The proteins were loaded onto a 10% SDS Gel and CREB was detected with specific antibodies.

highest levels at 2 h and their subsequent decline upon prolonged hypoxia (late phase) (Figure 3B). A comparable phosphorylation pattern, but modified CREB forms as demonstrated by two bands at ~90 and ~120 kDa were observed in the HER-2/neu$^+$ breast cancer cell line SKBR3 under hypoxic treatment (Supplementary Figure 1C), while the 60 kDa band was neither visible with CREB nor with pCREB antibodies. In the early phase of hypoxia (up to 48 h) no changes in the pH were measured, but a sligthly more acid pH was observed after 5 d.

Immunoprecipitation with an anti-CREB-specific antibody demonstrated a hypoxia-induced ubiquitination of CREB in parental HER-2/neu$^+$ cells (Figure 3C), which was also confirmed by an ubiquitin pull down assay (Figure 3D). The role of the ubiquitin-dependent proteasomal degradation for CREB expression was further analysed in hypoxic parental HER-2/neu$^+$ cells either left untreated or treated with increasing concentrations of the ubiquitin inhibitor PYR-41 (10, 25, 50 μM) and of the proteasome inhibitor MG-132 (10, 20, 50 μM), respectively. Treatment of hypoxic parental HER-2/neu$^+$ cells with 10 μM PYR-41 abrogated the expression of highly modified CREB, whereas total CREB protein expression was reduced (Figure 3E). In contrast, highly modified CREB expression levels were enhanced in hypoxic cells with increasing concentrations of MG-132. Furthermore, immunoprecipitation of SUMO-1 followed by the detection with CREB-specific antibodies revealed a SUMOylation of CREB after 8 h hypoxia, which further increased during 48 h hypoxia (Figure 3F).

### Hypoxia-induced changes in the localization of CREB in HER-2/neu$^+$ cells

Since stress conditions can cause a translocation of nuclear CREB into mitochondria (mito-CREB) thereby altering the expression of mitochondrial genes including oxidative phosphorylation complexes [7, 37, 38], the subcellular localization of CREB was determined in parental HER-2/neu$^+$ cells under normoxic and hypoxic conditions. As shown in Figure 4A subcellular fractionation revealed a partly translocation of CREB from the nucleus to the mitochondria in hypoxic parental HER-2/neu$^+$ cells. Western blot analysis using antibodies directed against the cytosolic (MEK1) or nuclear (histone H3) compartment served as controls (Figure 4A). These *in vitro* data were confirmed by immunohistochemical analysis of mammary carcinoma lesions demonstrating an increased extracellular localization of pCREB in hypoxic breast cancer areas (Supplementary Figure 3).

The specificity of mitochondrial CREB in hypoxic parental HER-2/neu$^+$ cells was confirmed using the mitochondria-specific dye MitoTracker. A co-localization of CREB into mitochondria of hypoxic, but not of normoxic parental HER-2/neu$^+$ cells was detected with this dye (Figure 4B, ICC pictures), which was accompanied by morphologic changes of hypoxic parental HER-2/neu$^+$ cells towards a more spindle-shaped phenotype (Figure 4B, transmitted light). Under hypoxic conditions nearly 30% of CREB was extra-nuclear localized when compared to ~ 5% under normoxic conditions. The translocation of CREB into mitochondria (mito-CREB) was confirmed by its resistance to digestion with trypsin unless the mitochondria were dissolved by Triton X100 (Figure 4C). Upon sub-fractionating and validation of the purity of the different mitochondrial fractions using specific markers CREB expression was found in the mitochondrial matrix, while the modified form of CREB could be detected in the matrix as well as in the inner and outer mitochondrial membrane (Figure 4D).

The nuclear export of CREB was further shown by treatment of cells with the nuclear translocation blocker leptomycin B. A combination of hypoxia and treatment with 50 ng/ml leptomycin B for 24 h totally abrogated the expression of mito-CREB in parental HER-2/neu$^+$ cells and significantly enriched high molecular weight forms of CREB in the nucleus (Figure 4E). In the presence of leptomycin B the expression of MEK1 shifted in parental HER-2/neu$^+$ cells from the cytosol to the nucleus. A similar CREB expression pattern was detected in the presence of the PI3K inhibitor LY294002 and the E3 ubiquitin ligase inhibitor PYR-41 (Figure 4E).

### Changes in the biogenesis of parental vs. CREB-deficient HER-2/neu$^+$ cells

In order to determine CREB function in the mitochondria the expression of the mitochondrial genes was compared in parental and CREB-deficient HER-2/neu$^+$ cells. As shown in Figure 5A, the mitochondrial genes ND5, COXIII and ATP synthase 6 were downregulated in CREB-deficient HER-2/neu$^+$ cells, whereas the expression of the mitochondrial genes ND1 – 4, ND4L, COXI, COXII and ATP synthase 8 remained unaltered in parental and CREB-deficient HER-2/neu$^+$ cells (data not shown). Changes in the expression pattern of selected mitochondrial genes were not due to alterations of the mitochondrial (mt) DNA content (data not shown). The decreased mitochondrial biogenesis, respiration or incomplete mitophagy was further confirmed by the shCREB-mediated reduction of Ppargc1a transcription (Figure 5B). Since mtDNA contains several putative CRE sites (Figure 5C) the binding of CREB to the D-LOOP of the mtDNA was analyzed, which was enhanced under hypoxia (Figure 5D).

### Hypoxia-mediated changes of the mitochondrial metabolism of parental vs. CREB-deficient HER-2/neu$^+$ cells

The mitochondrial fitness was further investigated by determining the activity of mitochondrial complexes in

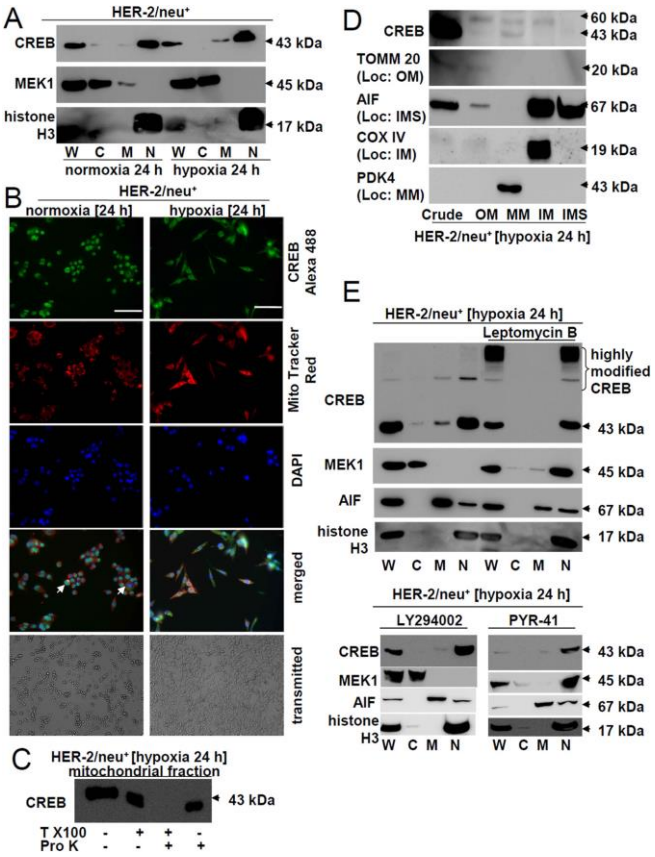


**Figure 4: Increased mitochondrial localization of CREB under hypoxia. A.** The distribution of CREB in different cell fractions was analysed by using a commercial kit for separations followed by Western blot analysis of the distinct fractions. Anti-MEK1 (cytosol) and anti-histone H3 (nucleus) mAb served as markers for the subcellular compartments. "W" marks the whole cell lysate, "C" the cytosolic fraction, "M" the membrane/mitochondrial fraction and "N" the nuclear fraction. The picture represents one of three independent experiments. **B.** Cells were incubated for 24 h under hypoxia or normoxia and 30 min before terminating the cells were stained with 500 nM MitoTracker. After removing the media and fixation with 4% PFA for 20 min the cells were permeabilized with 0.5% Triton X100 in HBBS (HBSS-T) for 30 min. Following incubation with CREB antibody overnight at 4°C the cells were washed three times with HBSS, incubated with the secondary antibody (rabbit-Alexa 488) for 1 h, washed again three times with HBSS and then the nuclei were stained with DAPI. Single and merged colors recorded at a Pathway 855 (BD) are shown. Note the complete loss of nuclear CREB in dividing cells (white arrow heads). The bar represents 100 µm; Magnification: 20x. Morphology of the cells cultivated under normoxia or hypoxia (24 h each) was recorded by microscopic pictures. The pictures were taken on living, non-stained cells (transmitted). **C.** 1 mg isolated intact mitochondria were incubated in 1% Triton X100 and/or 10 U proteinase K in proteinase K buffer and were incubated at 37°C for 30 min and 60°C for 10 min. The reaction was stopped by boiling the probes in Laemmli buffer for 5 min and the stability of CREB was analysed by Western blot using an anti-CREB-specific mAb as described in Materials and Methods. **D.** Mitochondria were sub fractionated into outer membrane (OM), inter membrane space (IMS), inner membrane (IM) and mitochondrial matrix (MM). The purity of the fractions was analysed with marker proteins: TOM20 for OM, AIF for IMS, COXIV for IM, PDK4 for MM. **E.** Cells were cultured in the presence or absence of 50 ng/ml Leptomycin B, 10 µM LY294002 and 10 µM PYR-41 for 24 h under hypoxic conditions. Then cellular proteins were fractionated as described in the Material and Methods section. Additionally to the marker proteins used in (A) AIF served as a marker for the mitochondrial fraction. "W" represents the whole cell lysate, "C" the cytosolic fraction, "M" the membrane/mitochondrial fraction and "N" the nuclear fraction. The picture shows one of two experiments. An accumulation of highly modified CREB and the nuclear translocation of MEK1 and partially of AIF was found under leptomycin B treatment.

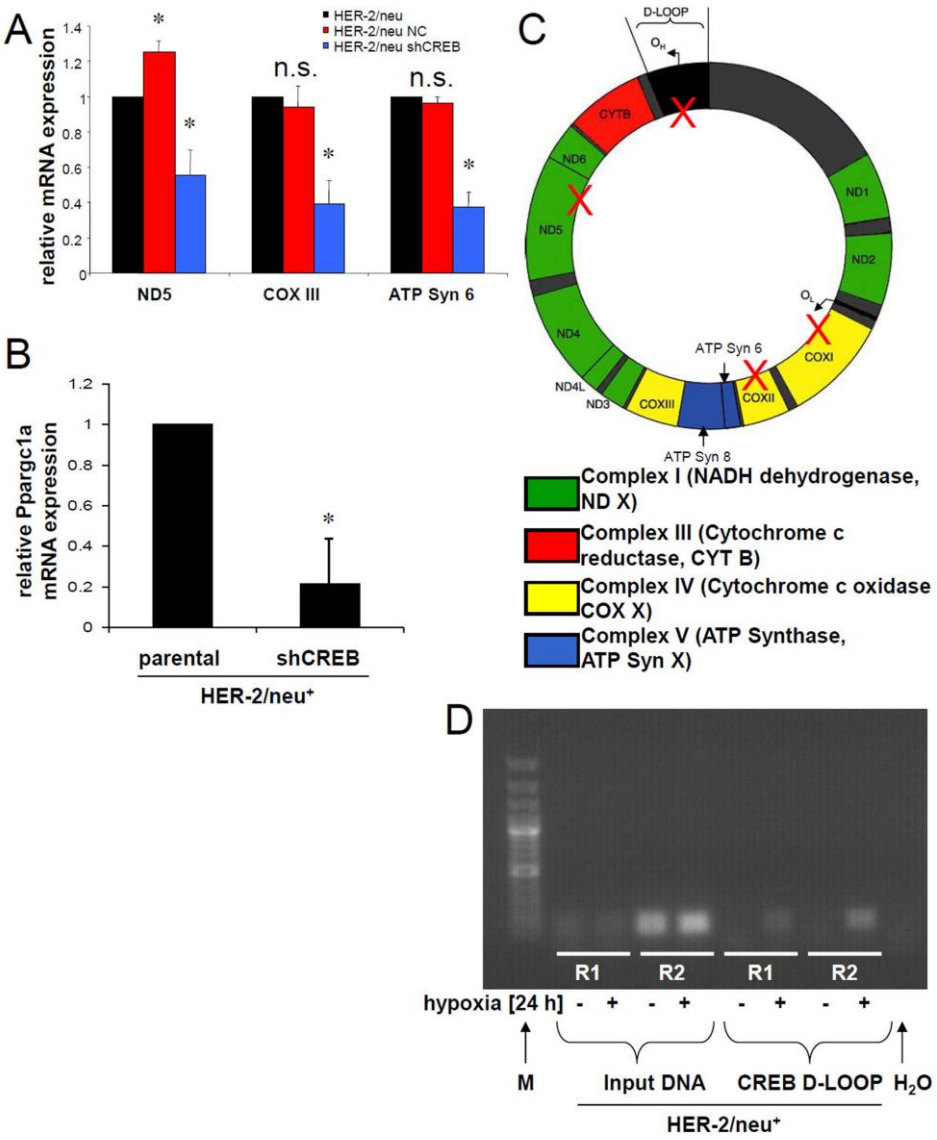


**Figure 5: Regulation of the mitochondrial biogenesis via Ppar1a and CREB binding to mitochondrial elements. A.** mRNA expression of mitochondrial encoded genes was determined by real time PCR using gene specific primer. The bar charts represent the data from two independent experiments. **B.** Expression of Ppargc1a mRNA was quantified by qPCR. The bar charts represent the data from two independent experiments. **C.** Putative CRE motifs were identified in the mtDNA. The mtD-LOOP has 2 CRE elements and in the protein coding regions 3 other CRE elements were identified. These were marked with a red cross. **D.** CREB binding DNA was immunoprecipitated, purified and used in a real time PCR. The products were further analysed by 2% agarose gel electrophoresis. IgG rabbit antibody was used as a control. The gel represents two of three independent experiments.

normoxic and hypoxic CREB-deficient/parental HER-2/neu$^+$ cells. As shown in Figure 6A, NADH dehydrogenase activity (complex I) and complex IV was reduced in hypoxic CREB-deficient HER-2/neu$^+$ cells, which is in line with the cell viability as well as the generation and maintenance of an electrochemical gradient. The increased mitochondrial metabolism/oxidative phosphorylation of parental HER-2/neu$^+$ cells was further underlined by an increased basal respiratory rate (Figure 6B). In addition, the cells' maximal respiratory capacity was determined. Upon addition of the uncoupling agent FCCP a significantly stronger relative increase of the oxygen consumption rate (OCR) in parental HER-2/neu$^+$ cells when compared to CREB-deficient HER-2/neu$^+$ cells was detected. Furthermore, the increased dependency on maintaining the mitochondrial energetic flux was highlighted by the effects of parental HER-2/neu$^+$ cells upon sequential treatment with oligomycin and FCCP, which blocked the mitochondrial function (Figure 6B). Furthermore, shCREB cells had an increased reliance on respiration for producing ATP through ATPase activity. Since PKA was more active in mitochondria upon hypoxia (Figure 6C), a PKA-dependent process was suggested, that can regulate the binding of mitochondrial CREB to the D-LOOP under hypoxia (Figure 5D).

When compared to normoxia a change in the mitochondrial morphology was found in the presence of hypoxia in both parental HER-2/neu$^-$ and HER-2/neu$^+$ cells. Mitochondria undergo mitochondrial fission caused by the accumulation of perinuclear mitochondria (Figure 6D, Supplementary Figure 4) and degradation of dysfunctional mitochondria by mitophagy. To further evaluate the mitochondrial function/dysfunction two types of mitochondria-specific dyes were used that distinguish respiring (MitoTracker Red) from total (MitoTracker Green) mitochondria. HER-2/neu$^+$ cells displayed a stronger signal with MitoTracker Green under hypoxic but not under normoxic conditions when compared to their HER-2/neu$^+$ shCREB counterparts (Figure 6E). Furthermore, parental HER-2/neu$^+$ cells had an increased fraction of respiring (i.e. functional) mitochondria (Figure 6F) when compared to CREB-deficient HER-2/neu$^+$ cells suggesting an enrichment of dysfunctional mitochondria in CREB-deficient cells under hypoxia, which is in line with our functional data for the mitochondrial biogenesis shown in Figure 5B.

### Functional consequences of hypoxia on CREB activity

The hypoxia-induced partly translocation of CREB into mitochondria was accompanied by changes in the mitochondrial membrane potential of parental and CREB-deficient HER-2/neu$^+$ cells. While the JC-1 fluorescence of normoxic parental and CREB-deficient HER-2/neu$^+$ cells was comparable, hypoxia increased the mitochondrial membrane potential of parental HER-2/neu$^+$ cells, but decreased it in CREB-deficient HER-2/neu$^+$ cells (Figure 7A). The altered membrane potential during hypoxia directly correlated with changes in the apoptosis sensitivity: The viability of hypoxic CREB-deficient HER-2/neu$^+$ cells were approximately 20% decreased when compared to hypoxic parental HER-2/neu$^+$ cells (Figure 7B). This was further confirmed by an approximately 30% increased activity of caspase-3 (cleaved form) in normoxic CREB-deficient HER-2/neu$^+$ cells, which was aggravated under hypoxia (Figure 7C). The cellular ATP levels were reduced in hypoxic parental and CREB deficient HER-2/neu$^+$ cells, which were accompanied by a reduced mitochondrial activity. No changes were measured in the CREB deficient NIH3T3 cells between normoxic and hypoxic conditions. Furthermore hypoxia decreased ATP levels and mitochondrial activity in parental/CREB-deficient HER-2/neu$^+$ cells (Figure 7D, 7E).

### Hypoxia-independent induction of cell migration and invasion by CREB activation

During prolonged hypoxia CREB expression and activation was induced thereby affecting the growth properties of cells [20]. Thus, the migration capacity of parental and CREB-deficient HER-2/neu$^-$ and HER-2/neu$^+$ cells was compared under normoxia and hypoxia. As shown in Figure 8A, the migration rate of normoxic HER-2/neu$^-$ and HER-2/neu$^+$ cells was approximately 60 to 70% reduced upon CREB silencing (36). Similar results were obtained in the presence of hypoxia demonstrating a reduced migration rate of CREB-deficient HER-2/neu$^-$ and HER-2/neu$^+$ cells of approximately 60%. A significantly increased invasion capacity of normoxic parental HER-2/neu$^+$ cells compared to normoxic HER-2/neu$^-$ cells was found using transwell assays with matrigel-coated wells. Under these conditions the invasion was 50% inhibited by CREB silencing of HER-2/neu$^+$ cells, while an enhanced invasion was detected in hypoxic parental HER-2/neu$^+$ (Figure 8B). Here the invasion capacity of CREB silenced HER-2/neu$^+$ was highly variable, contrary to the unchanged invasion in the NIH3T3 shCREB cells. This was accompanied by an induction of MMPs in hypoxic parental versus CREB-deficient HER-2/neu$^+$ cells as determined by zymography (Figure 8C) suggesting that the hypoxia-mediated induction of CREB activity affected the regulation of basal MMP expression. MMP9 secretion was further increased under hypoxic but not under normoxic conditions.

## DISCUSSION

CREB has been demonstrated to play a key role in the initiation as well as progression of tumors, since it modulates the expression of genes/proteins involved in cell proliferation, apoptosis, invasion and migration [23-26].

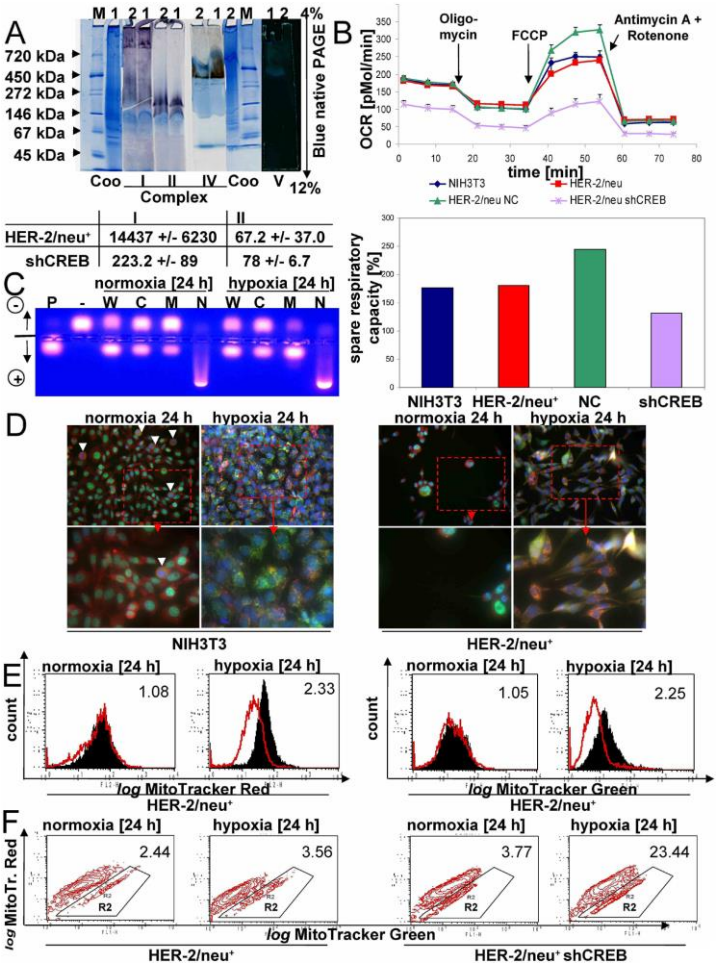


**Figure 6: Regulation of mitochondrial functions by mito-CREB. A.** The activity of mitochondrial complexes was analysed by in gel activity. The numbers in A are the mitochondrial proteins from HER-2/neu$^+$ cells (1) and HER-2/neu$^+$ shCREB cells (2). M: representative molecular weight marker. Coo: Colloidal coomassie staining. The staining of complex V (ATP synthase) was documented in front of a dark background. The data beyond the gel staining represents the spectrometrically analysis of the complex I and II activities from three independent experiments. **B.** Basal oxygen consumption rate (OCR) (an indicator for mitochondrial respiration) was detected using the XF96e Extracellular Flux Analyzer (Seahorse Bioscience). Next, OCR responses towards the application of oligomycin (1 μM), FCCP (2.5 μM), and the combination of antimycin (3 μM), and rotenone (3 μM) (XF Cell Mito Stress Test Kit, Seahorse Bioscience) were evaluated. All experiments were performed in at least hexaplicates. Changes after FCCP application are indicative for the maximal respiratory capacity (up). The spare respiratory capacity was calculated from the results (down). **C.** The PKA activity of the whole cell lysate (W) and the intracellular fraction (C, M, N) was analysed as described in Materials and Methods. Samples (cultivated for 24 h under normoxia or hypoxia), positive (P) and negative (**-**) controls were loaded onto an agarose gel. The gel was photographed under UV irradiation. **D.** The localization of CREB (green), mitochondria (red) and the nucleus (blue) was compared in NIH3T3 and HER-2/neu$^+$ cells under normoxia and hypoxia. White arrows mark dividing cells, which lacks nuclear CREB. Under hypoxic conditions the mitochondrial fission is visible. **E.** HER-2/neu$^+$ cells and CREB-deficient derivatives were incubated under normoxia and hypoxia for 24 hours, before cells were stained with MitoTracker Green and Red, respectively. **F.** In the contour plot the cells in R2 represents mitochondrial dysfunctional cells (pos. for MitoTracker Green, weaker staining for MitoTracker Red). 10.000 cells were analysed by flow cytometry.

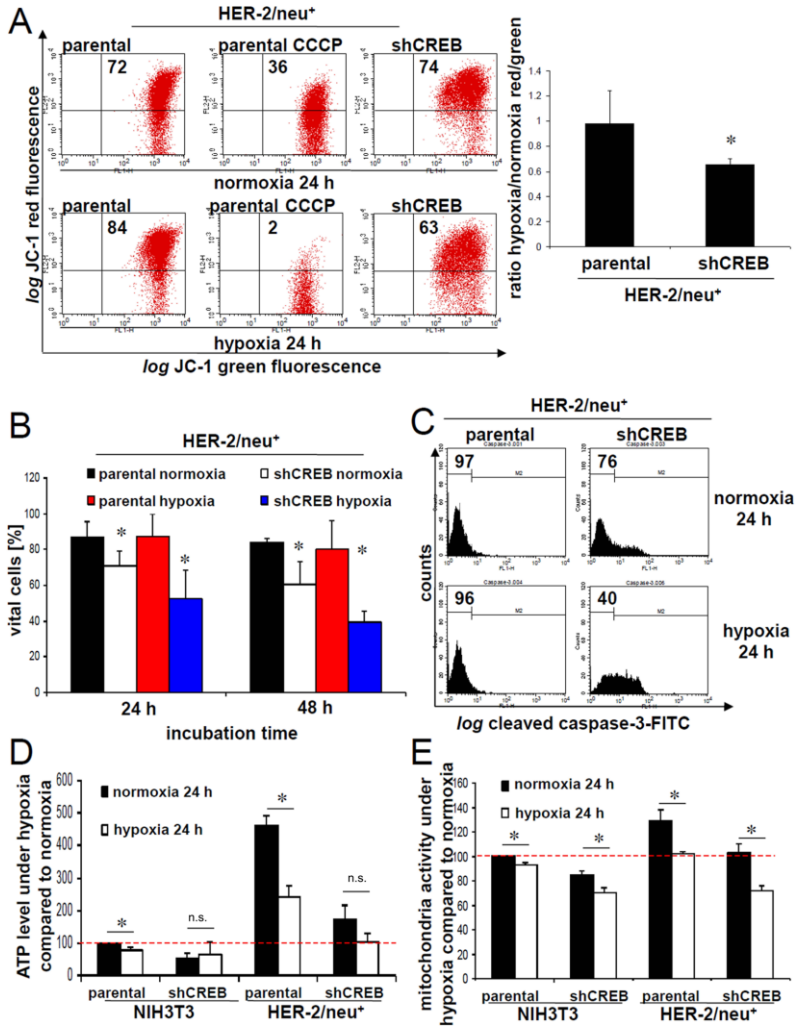


**Figure 7: Decreased mitochondrial membrane potential and cell vitality upon CREB silencing. A.** The mitochondrial membrane potential was determined in normoxic or hypoxic cultivated cells by using JC-1 fluorescence analysis. The fluorescence of $5x10^3$ stained cells was analysed with a FACsCalibur (BD) and CCCP-treated cells (2 µM) served as a control. The number of cells with an intact mitochondrial membrane potential is given in the upper right region (left). The ratio of cells with an intact mitochondrial membrane potential under normoxia/hypoxia is given for three independent experiments (right). **B.** The amount of apoptotic and necrotic cells was determined by annexin V/propidium iodide staining as recently described [35]. $1x10^4$ stained cells were analysed with a FACS Calibur (BD). The amount of vital cells after 24 h and 48 h cultivation is shown in the bar charts. Data represent the mean of three independent experiments. **C.** Cleaved caspase-3 activity was measured as recently described by Stehle and co-authors [35]. Both parental or CREB-deficient HER-2/neu$^-$ cells were cultured under normoxic and hypoxic conditions before cleaved caspase-3 was determined as described in Materials and Methods using flow cytometry. **D.** ATP levels were measured with a luciferase specific substrate as described in Materials and Methods. Data show mean values from three independent experiments. **E.** Mitochondrial activity was analysed with the colorimetrical XTT substrate assay as described in Materials and Methods. Data show mean values from three independent experiments.

This was confirmed by high levels of CREB expression and activation in tumors of distinct origin, which often correlated with disease progression and poor patients' survival [24, 29, 30], as well as in *in vitro* models of ras and HER-2/neu transformation [35, 39]. Furthermore, recent studies suggest that CREB activation is also involved in prolonged/late hypoxic responses [20]. Since the cellular localization and kinetic of phosphorylation as well as other PTMs of CREB are important features for its pathophysiologic function in tumors it is essential to analyse the changes of the CREB status under normal and hypoxic conditions.

*In vitro* analysis demonstrated a hypoxia-induced time-dependent CREB phosphorylation at position $Ser^{133}$, but not at position $Ser^{121}$. An altered CREB phosphorylation at $Ser^{133}$ was already detected one hour after hypoxia onset. During the acute phase of hypoxia CREB ubiquitination occurred in parental HER-2/$neu^+$ cells, which was transient and dependent on CREB phosphorylation and could be reverted by treatment with the proteasome inhibitor MG-132. Thus, ubiquitination of CREB might be responsible for signal transduction during early phase of hypoxia in parental HER-2/$neu^+$ cells, whereas CREB phosphorylation is responsible for both early and prolonged hypoxia. These results are in contrast to those reported by Nakayama [20] and might be explained by differences in the cell systems analysed. Furthermore, SUMOylation has been shown to regulate the activity and function of CREB under physiologic conditions [14-16]. These data were extended in this study to hypoxia-induced CREB SUMOylation, but its role during hypoxia requires further investigation.

The hypoxia-mediated enhanced CREB activation was directly associated with an upregulation of hypoxia-regulated molecules, like VEGF and ICAM-1. Furthermore, hypoxia caused a partly translocation of CREB from the nucleus to the mitochondrial matrix in parental HER-2/$neu^+$ cells, which was accompanied by an induction of pERK, but not of pAKT and increased levels of $pCREB^{Ser133}$. Although MMP expression and activity was induced by hypoxia in parental HER-2/$neu^+$ cells and an altered CREB-dependent migration and invasion

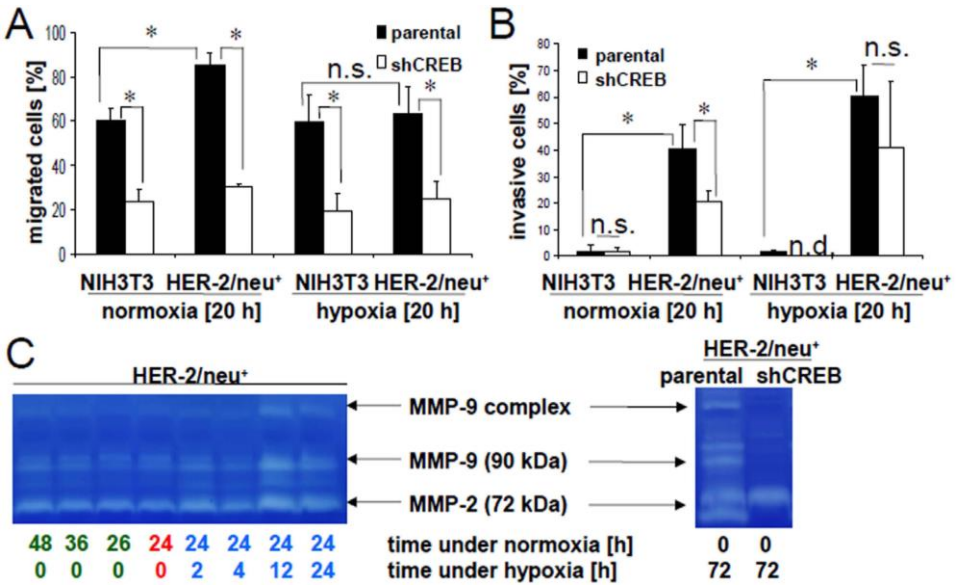


**Figure 8: Abrogation of hypoxia-induced invasion by CREB silencing.** The influence of 20 h hypoxia or normoxia on the migration **A.** and invasion **B.** of HER-2/$neu^-$ and HER-2/$neu^+$ cells was analysed using trans-well inserts as described in Material and Methods. The bar charts represent three independent experiments performed in duplicates. **C.** The MMP activity under normoxic and hypoxic conditions in the culture supernatant was determined by gelatin zymography (left). Cells were incubated for 24 h under normoxic conditions (red) and were then incubated for the indicated time under hypoxia (blue) or were left under normoxia (green). The increased activity of MMP-9 and MMP-2 after 12 h or 24 h hypoxia is visible in both right lanes compared to the normoxic controls (left lanes). Parental and CREB-deficient HER-2/$neu^+$ cells were incubated for 72 h under hypoxia and 20 µl supernatant was analysed on gelatin zymogram (right). A decreased activity of MMP-9 and of the cleaved MMP-2 was detected in CREB deficient cells, while the inactive MMP-2 (72 kDa) is not altered. The gels represent one of two independent experiments.

capacity of parental versus CREB-deficient HER-2/neu$^+$ exists, hypoxic conditions did not or only marginally alter their growth properties. These data suggest that the hypoxia-dependent induction of MMPs was not linked to enhanced invasion and migration, probably because of the morphological changes of the HER-2/neu$^+$ cells under hypoxia. However, these effects might alter the tumor microenvironment, which interfere with anti-tumoral immune responses by inhibiting T cell activation and cytotoxicity as well as by reducing antigen processing of dendritic cells [40].

A direct effect of CREB activation on angiogenesis was found, as determined by the increased number and density of blood vessels, CD31 staining of tumor lesions and enhanced expression of markers involved in angiogenesis. This could lead to a better oxygen and nutrient supply of parental HER-2/neu$^+$ tumor cells. Furthermore, hypoxia did not only alter expression pattern of genes and proteins involved in neoplastic transformation, but could also affect the cellular localization of CREB. Although CREB is a nuclear transcription factor known to regulate gene expression, there exists some evidence that CREB could be co-localized to other cellular compartments. A hypoxia-induced mitochondrial translocation was found in parental HER-2/neu$^+$ cells as determined by Western blot analysis of subcellular fractions, immunocytochemistry and analysis of mitochondrial gene expression (Figure 9). In the presence of hypoxia the pCREB$^{Ser133}$ expression was significantly higher in the mitochondria than in the nucleus demonstrating the importance of the localization of CREB for its activity (mitochondrion = nucleus > cytosol). This was in line with a decreased expression of a subset of mitochondrial genes including ND5, COXIII and ATP synthase 6 upon disruption of CREB activity demonstrating that CREB is transcriptionally active in

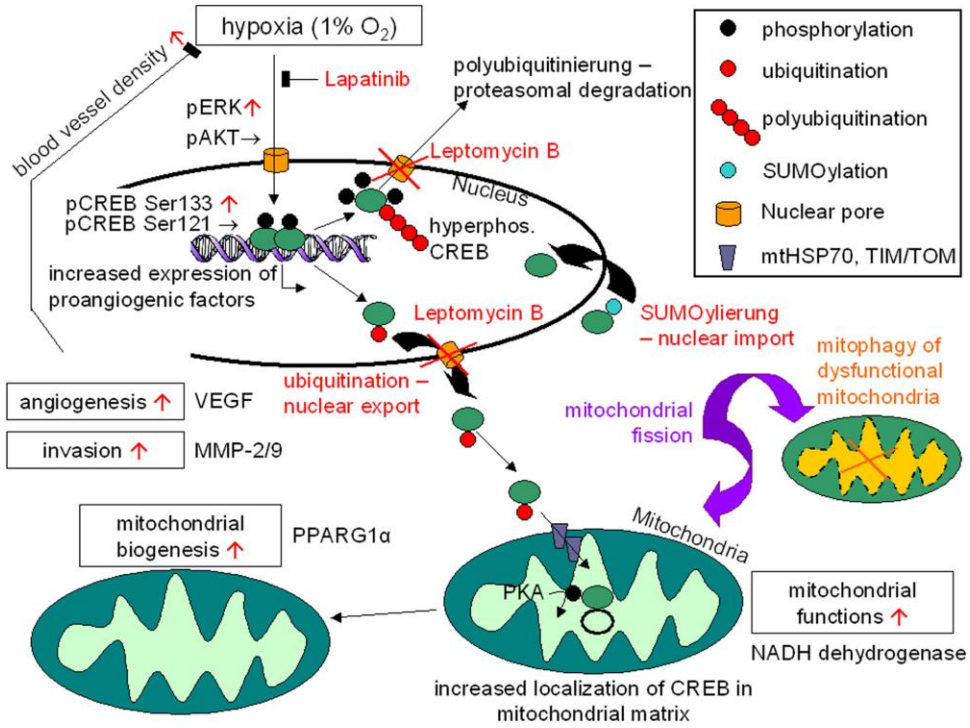


**Figure 9: Model for the regulation and functions of CREB activity under hypoxic conditions in nucleus and mitochondria.** Hypoxia increases the activity of CREB (phosphorylation at Ser133 but not Ser121) by the MEK-ERK pathway, leading to an increased expression of pro-angiogenic factors (VEGF). This mechanism can counteract hypoxia. Hyperphosphorylation of CREB under hypoxia causes protein degradation by ubiquitination, while CREB can be stabilizied by SUMOylation. Import of modified CREB into mitochondria is enhanced under decreased oxygen supply, which in return can promote mitochondrial biogenesis and mitochondrial functions by binding to the mitochondrial promoter (D-LOOP) as well as regulating the expression of Ppargc1a.

the mitochondria. Treatment of cells with leptomycin B caused an inhibition of mito-CREB. Since LY294002 had comparable effects, the AKT-mediated phosphorylation might be essential for the export of CREB into the mitochondria.

Mito-CREB has been shown to be involved in pathophysiologic processes of neurons and associated with altered apoptosis resistance [13]. This was correlated with changes in the mitochondrial membrane integrity and activation of caspases. The mitochondrial membrane potential provides a method for determination of early events of apoptosis. Indeed, hypoxic stress not only altered localization of CREB in parental HER-2/neu$^+$ cells, but also the sensitivity to apoptosis. Furthermore, mitochondrial dysfunction can be caused by defects in the energy metabolism and by stress including oxidative damage or hypoxia. This might be involved in the pathogenesis of neoplastic diseases. The localization of CREB in the mitochondrion after hypoxia suggests that CREB mediates survival by regulating mitochondrial function and biogenesis thereby altering the response to various stimuli. In parental HER-2/neu$^+$ cells the mitochondria were functional and increased respiratory rates correlated with the mitochondrial CREB levels. Increasing evidence suggests a close interrelationship between CREB overexpression and mitochondrial biogenesis in the presence of hypoxia. The adaption to hypoxia increased the biogenesis of novel and functional mitochondria. Similar results have been recently also demonstrated during the adaption to oxidative stress [41].

HER-2/neu signalling induced significant changes in the CREB status, in particular of CREB phosphorylation. While CREB activation occurs in response to pro-growth and pro-survival stimuli, it is also phosphorylated in response to harmful or stress stimuli, such as UV irradiation and hypoxia [42], due to an upregulation of the mitogen- and stress-activated protein kinase-1 [43]. Indeed, an increased activity of total and phosphorylated CREB along with a decreased localization of pCREB in the nucleus was demonstrated under hypoxia in parental HER-2/neu$^+$ cells. pCREB$^{Ser133}$, but not pCREB$^{Ser121}$ appears to play an important role in this process, which is in line with recent reports suggesting that despite the existence of several phosphorylation sites, phosphorylation of CREB at Ser$^{133}$ is the major modulator of CREB activity [44]. It cannot be ruled out, that the CREB-dependent gene expression may involve modifications of CREB at sites other than Ser$^{133}$.

In conclusion our data support a shuttling pathway of HER-2/neu-mediated CREB activation linking CREB signalling to mitochondrial and nuclear functions. Furthermore, a hypoxia-mediated induction of CREB expression and altered PTMs followed by enhanced angiogenesis was observed. Increased knowledge of the role of HER-2/neu-induced CREB expression and activity might lead to the development of treatment strategies including inhibition of angiogenesis and alteration of the cellular metabolism.

## MATERIALS AND METHODS

### Cell culture, hypoxia and drug treatment

The generation and culture conditions of HER-2/neu$^-$ NIH3T3 cells, their HER-2/neu$^+$ derivative and their respective CREB variants have been recently described [35]. HER-2/neu-overexpressing cells with high levels of pCREB were termed "parental HER-2/neu$^+$" cells, while HER-2/neu$^+$ cells with silenced CREB were "HER-2/neu$^+$ shCREB" cells. Human umbilical vein endothelial cells (HUVEC) purchased from the American Tissue Culture Collection (ATCC) were cultured in Ham's F-12K (ATCC) supplemented with 2% FBS, 1 ng/ml human epidermal growth factor (hEGF), 1 ng/ml human basic fibroblast growth factor (hbFGF), 1 µg/ml hydrocortison and 0.004 mg/ml ECGS (all supplements from PromoCell). The human mammary carcinoma cell lines HTB-122 (BT-549) and SKBR3, the lung cancer cell line H125 (NCI-H125) and the HER-2/neu-transformed cells have been previously described [45] and were cultivated in RPMI1640 supplemented with 10% FBS, 2 mM L-glutamine, 10 mM HEPES and penicillin/streptomycin. Cell lines were validated with their HER-2/neu$^+$ and CREB expression status (murine cells) or with DNA fingerprinting (human cells).

For hypoxia treatment cells were incubated in a 1% (v/v) $O_2$, 5% (v/v) $CO_2$ atmosphere by 37°C for the indicated time. Normoxic controls were exposed using standard conditions. For Western blot and qPCR cells were cultured under normoxic and hypoxic conditions for up to 5 days and cell pellets were frozen until use. The proteasome inhibitor MG-132 (Calbiochem), the ubiquitin inhibitor PYR-41 (Santa Cruz) and the nuclear export inhibitor Leptomycin B (Cayman) were used with the indicated concentrations for 4 h (MG-132, PYR-41) or 24 h (Leptomycin B), respectively.

### RNA isolation, cDNA synthesis, qPCR

Total cellular RNA from 5x10$^5$ cells/sample was extracted and subjected to qPCR analysis as recently described [35]. The specific primer sequences and PCR conditions used are given in Table 2A and 2B. Relative expression levels were calculated according to the ΔCt method and normalized against β-actin and/or GAPDH as internal control.

### Protein isolation, cell fractionation and western blot analysis

From 5x10$^6$ cells/sample protein was isolated and subjected to Western blot analysis as recently described

**Table 2: Primer used for real time quantitative PCR**

**A: Nuclear encoded genes**

| Primer | Sequence | Annealing temperature [°C] |
|---|---|---|
| GAPDH fwd | TTGTGCAGTGCCAGCCTCGT | 60 |
| GAPDH rev | TCGGCCTTGACTGTGCCGTT | 60 |
| CREB-1 fwd | CATTGCCCCTGGAGTTGTTATG | 60 |
| CREB-1 rev | TCTACGACATTCTCTTGCTGCCTC | 60 |
| Angiopoietin-1 fwd | TTGGGTCCAGAGAATGCCAC | 60 |
| Angiopoietin-1 rev | CCAGGTCACCTCCACAATCC | 60 |
| Angiopoietin-2 fwd | TTCTCCTCTGCCACGTTCAC | 60 |
| Angiopoietin-2 rev | TGTTGGCCCTGTCGACATTT | 60 |
| Beta-actin fwd | CTGTCGAGTCGCGTCCACCC | 60 |
| Beta-actin rev | TGCTCTGGGCCTCGTCACCC | 60 |
| ICAM-1 fwd | TGTCAGCCACCATGCCTTAG | 60 |
| ICAM-1 rev | CAGCTTGCACGACCCTTCTA | 60 |
| PECAM-1 fwd | CCAAGGCCAAACAGAAACCC | 60 |
| PECAM-1 rev | GTTCTTAGGGTCGACCTTCCG | 60 |
| VCAM-1 fwd | GTACAGTCTGGTGGAGGCAC | 60 |
| VCAM-1 rev | GCATGGCTTGGTTTGTGGAG | 60 |
| VEGF A fwd | AACCATGAACTTTCTGCTGTCTTGG | 60 |
| VEGF A rev | ATCAGGGTACTCCTGGAAGATGTCC | 60 |
| PPARGC1a fwd | CAAAGCAGCAGAGAGGGAAC | 60 |
| PPARGC1a rev | CTTCGTACAGCCATCAAAAAGGG | 60 |
| 18S rDNA fwd | TAGAGGGACAAGTGGCGTTC | 60 |
| 18S rDNA rev | CGCTGAGCCAGTCAGTGT | 60 |

**B: Mitochondrial encoded genes**

| Primer | Sequence | Annealing temperature [°C] |
|---|---|---|
| mATPSyn6 fwd | CCAATGGCATTAGCAGTCCG | 60 |
| mATPSyn6 rev | TGCATGAGTTTGGTGGGTCA | 60 |
| mATPSyn8 fwd | CAAACATTCCCACTGGCACC | 60 |
| mATPSyn8 rev | TTGTTGGGGTAATGAATGAGGC | 60 |
| mCOX I fwd | GACTTGCAACCCTACACGGA | 60 |
| mCOX I rev | GATGGCGAAGTGGGCTTTTG | 60 |
| mCOX II fwd | AACCGAGTCGTTCTGCCAAT | 60 |
| mCOX II rev | CTAGGGAGGGGACTGCTCAT | 60 |
| mCOX III fwd | CCAATGGCATTAGCAGTCCG | 60 |
| mCOX III rev | TGCATGAGTTTGGTGGGTCA | 60 |
| mND1 fwd | TCCGAGCATCTTATCCACGC | 60 |

(*Continued*)

| Primer | Sequence | Annealing temperature [°C] |
|---|---|---|
| mND1 rev | GTATGGTGGTACTCCCGCTG | 60 |
| mND2 fwd | CAAGGGATCCCACTGCACAT | 60 |
| mND2 rev | AAGTCCTCCTCATGCCCCTA | 60 |
| mND3 fwd | GTTGCATTCTGACTCCCCCA | 60 |
| mND3 rev | GGTAGACGTGCAGAGCTTGT | 60 |
| mND4 fwd | AGCTCCAATTGCTGGGTCAA | 60 |
| mND4 rev | GGCTAACTGAGGAGTAGGCG | 60 |
| mND4L fwd | ACCTCACCATAGCCTTCTCAC | 60 |
| mND4L rev | TAGTCCTACAGCTGCTTCGC | 60 |
| mND5 fwd | ACCCAATCAAACGCCTAGCA | 60 |
| mND5 rev | AGGACTGGAATGCTGGTTGG | 60 |
| mND6 fwd | GAAGGAGGGATTGGGGTAGC | 60 |
| mND6 rev | CCGCAAACAAAGATCACCCAG | 60 |
| COXI fwd | GCCCCAGATATAGCATTCCC | 60 |
| COXI rev | GTTCATCCTGTTCCTGCTCC | 60 |

**C: Primer used for real time quantitative PCR after mito DNA IP**

| Primer | Sequence | Annealing temperature [°C] |
|---|---|---|
| Mito D-LOOP 1 | GTGGTGTCATGCATTTGGTATCT | 60 |
| Mito D-LOOP 2 | ATCAACATAGCCGTCAAGGCATG | 60 |
| Mito D-LOOP 3 | TCACCGTAGGTGCGTCTAGACTGT | 60 |

[35] using following monoclonal antibodies (mAb): anti-phospho-CREB ($Ser^{133}$), anti-phospho-CREB ($Ser^{121}$) (Novus), anti-GAPDH, β-actin (Sigma), anti-phospho-ERK, anti-ERK, anti-phospho-AKT, anti-AKT and anti-histone-3. More detailed information regarding the antibodies used in this study are given in Table 3.

Furthermore, cells were fractionated into cytosolic, mitochondrial and nuclear compartments using a cell fractionation kit (Cell Signaling) according to the manufacturer's instructions. The isolation of subcellular compartments allows the analysis of the distribution of CREB in the cytosol, mitochondria and nucleus. The purity of the subcellular fractions was determined using histone H3 as nuclear, AIF as mitochondrial and MEK as cytosolic marker.

### Ubiquitin pull down assay, CREB immunoprecipitation and ubiquitin quantification

Cells were cultivated for 24 h under normoxia or hypoxia, harvested and lysed in 50 mM HEPES (pH 7.5), 5 mM EDTA, 50 mM NaCl, 1% Triton X-100, 10 mM N-ethylmaleimide and a protease inhibitor cocktail. After centrifugation, ubiquitin affinity beads (Ubiquitinated Protein Enrichment Kit, Calbiochem) were added to the supernatant with a protein concentration of ~1 mg/ml and pull down assays were performed according to the manufacturer´s protocol. The amount of ubiquitinated CREB protein was detected by Western blot using an anti-ubiquitin (Millipore) and anti-CREB-specific antibody (Cell Signaling).

For quantification, cell lysates were incubated with an anti-CREB antibody (Cell Signaling) overnight under agitation at 4°C, before 20 µl protein A agarose was added for 4 hrs. Beads were collected by centrifugation, washed four times with 200 µl wash buffer (50 mM HEPES pH 7.5, 5 mM EDTA, 50 mM NaCl) and heated in 50 µl Laemmli buffer. The supernatant was loaded onto a 12% SDS gel following Western Blot analysis with an ubiquitin-specific antibody.

### SUMO detection

Cell lysates were incubated over night by 4°C under slight agitation with a monoclonal SUMO-1 antibody (Cell Signaling #4930, 1:50 dilution). Protein A agarose slurry was added and was incubated for 2 h at 4°C (Sigma). After

**Table 3: Primary and labeled secondary antibodies used in this study**

| Antigen | Species | Manufacturer (#) | monoclonal | Application | Dilution | Dilution buffer |
|---|---|---|---|---|---|---|
| CREB-1 | Rabbit | Cell Signaling (#9197) | X (48H2) | Western Blot | 1:1000 | 5 % (w/v) BSA in TBS-T |
| | | | | ICC | 1:800 | HBSS + 0,1 % Triton X100 |
| | | | | IHC | 1:400 | Signal Stain Antibody Diluent (Cell Signaling) |
| | | | | ChIP | 1:100 | ChIP1 buffer |
| | | | | IP | 1:250 | IP buffer |
| CREB-1 | Mouse | Cell signaling (#9104) | X (86B10) | Western Blot (after IP) | 1:1000 | 5 % (w/v) BSA in TBS-T |
| phospho-CREB-1 (Ser133) | Rabbit | Cell Signaling (#9198) | X (87G3) | Western Blot | 1:1000 | 5 % (w/v) BSA in TBS-T |
| phospho-CREB-1 (Ser121) | Rabbit | Novus (#NB100-410) | polyclonal | Western Blot | 1:1000 | 5 % (w/v) BSA in TBS-T |
| anti-mouse IgG-HRP | Horse | Cell Signaling (#7076) | n/a | Western Blot | 1:5000 | 5 % (w/v) Skim milk in TBS-T |
| anti-rabbit IgG-HRP | Goat | Cell Signaling (#7074) | n/a | Western Blot | 1:5000 | 5 % (w/v) Skim milk in TBS-T |
| AIF1 | Rabbit | Cell Signaling (#5318) | X (D39D2) | Western Blot | 1:1000 | 5 % (w/v) BSA in TBS-T |
| AKT | Rabbit | Cell Signaling (#9272) | polyclonal | Western Blot | 1:2000 | 5 % (w/v) BSA in TBS-T |
| phospho-AKT (Ser473) | Rabbit | Cell Signaling (#9271) | polyclonal | Western Blot | 1:1000 | 5 % (w/v) BSA in TBS-T |
| $\beta$-Actin | Mouse | Sigma (#A2228) | X (AC74) | Western Blot | 1:5000 | 5 % (w/v) Skim milk in TBS-T |
| CD31 | Rabbit | Abbiotech (#250590) | n/a | IHC | 1:200 | PBS-T, 5 % goat serum |
| COX IV | Rabbit | Novus (#NB110-39115) | polyclonal | Western Blot | 1:2000 | 5 % (w/v) BSA in TBS-T |
| ERK-1/2 | Rabbit | Cell Signaling (#9102) | polyclonal | Western Blot | 1:2000 | 5 % (w/v) BSA in TBS-T |
| phospho-ERK1/2 (Thr202/204) | Rabbit | Cell Signaling (#4370) | X (D1314.4E) | Western Blot | 1:2000 | 5 % (w/v) BSA in TBS-T |
| GAPDH | Rabbit | Cell Signaling (#2118) | X (14C10) | Western Blot | 1:2000 | 5 % (w/v) BSA in TBS-T |
| HER-2/neu-PE (IgG1) | Mouse (IgG1) | BD (#340552) | X (neu 24.7) | Flow cytometry | 1:200 | PBS |
| HIF 1-α | Rabbit | Biorbyt (#orb223706) | X (n/a) | IHC | 1:200 | PBS-T, 5 % goat serum |
| Histone H3 | Mouse | Cell Signaling (#3638) | X (96C10) | Western Blot | 1:1000 | 5 % (w/v) BSA in TBS-T |
| IgG1-PE | Mouse | BC (#A07796) | X (679.1Mc7) | Flow cytometry | 1:200 | PBS |

(*Continued*)

| Antigen | Species | Manufacturer (#) | monoclonal | Application | Dilution | Dilution buffer |
|---|---|---|---|---|---|---|
| Ki-67 | Rabbit | Novus (#NB110-89717) | polyclonal | IHC | 1:250 | PBS-T, 5 % goat serum |
| MEK1 | Mouse | Cell Signaling (#2352) | X (61B12) | Western Blot | 1:2000 | 5 % (w/v) Skim milk in TBS-T |
| PDK4 | Rabbit | Biorbyt (#orb11259) | polyclonal | Western Blot | 1:1000 | 5 % (w/v) BSA in TBS-T |
| SUMO-1 | Rabbit | Cell Signaling (#4930) | polyclonal | Western Blot | 1:1000 | 5 % (w/v) BSA in TBS-T |
| | | | | IP | 1:50 | IP buffer |
| TOM20 | Rabbit | Biorbyt (#orb128858) | polyclonal | Western Blot | 1:1000 | 5 % (w/v) BSA in TBS-T |
| $\beta$-Tubulin | Mouse | Oncogene | X (Ab-1) | Western Blot | 1:2000 | 5 % (w/v) Skim milk in TBS-T |
| Ubiquitin | Mouse | Millipore (#MAB1510) | X (Ubi1) | Western Blot | 1:1000 | 5 % (w/v) BSA in TBS-T |

The mouse CREB-1 antibody was used for the Western-Blot after IP.

a centrifugation step (16.000 *g*, 30 s) the agarose beats were collected, washed four times with 200 µl wash buffer and were heated in laemmli buffer for 5 min. The protein extract was separated on a 10% SDS gel.

### Migration and invasion assays

For determination of cell migration $1x10^5$ cells cultured in medium supplemented with 1% FBS were seeded into the upper well of the chamber, whereas medium containing 10% FCS was added to the lower chamber of the trans-well chamber system (Corning). After incubation for 18 h at 37°C, non-migrated cells of the top insert were completely removed, whereas the cells migrated to the lower chamber were lysed with Cell Titer Glo (Promega) before the ATP content was determined according to the manufacturer's instructions using a luminometer (Berthold).

For invasion assays trans-well chambers were coated with 50 µl matrigel (Sigma) prior the experiments. Each experiment was performed in triplicates at least three times.

### Analysis of CREB binding to mtDNA

Proteins and mtDNA of hypoxic or normoxic conditioned cells were cross-linked by 1% formaldehyde for 5 min following the incubation with 1M glycine for 5 min. The cells were lysed and sonicated three times. After centrifugation, 10 µg of the shredded protein-DNA was incubated with the CREB antibody or a rabbit IgG control antibody over night for immunoprecipitation. Treatment with agarose A/G beads for 2 h and centrifugation collected the specific DNA, which was eluted by adding 1% SDS, 0.1 M $NaHCO_3$ pH 8.0 buffer. The crosslink was reverted by incubation for 4 h at 65°C and proteins were digested by protease K. The DNA was purified by phenol-chloroform extraction and ethanol cleaning. mtDNA was detected as described by Ryu and co-workers [13] using the primers in Table 2C.

### *In vivo* tumorigenicity

For all animal experiments mice were housed under standard conditions as described previously and the study was proofed by the ethical committee [35]. Briefly, $1x10^6$ cells/mouse were *subcutaneously* (s.c.) injected into the flank of DBA-1 mice (2 - 3 month old, male and female). The tumor growth and size were monitored overtime. Mice were killed 4 - 5 weeks after injection before tumors were isolated.

### *In vivo* angiogenesis assays

The *in vivo* angiogenesis assay was performed by injecting $1x10^6$ cells/mouse suspended in 250 or 500 µl growth factor reduced matrigel into the flank of DBA-1 mice. Seven days after injection the mice were sacrificed and plugs were removed. The plugs were divided and one half was embedded after formalin fixation into paraffin for histological staining, while the other part was used for hemoglobin measurement.

### Determination of the hemoglobin content

The matrigel plugs were homogenised with an ultra turrax homogenizer in 100 µl erythrocyte lysis buffer and the hemoglobin concentration was measured in the supernatant after centrifugation using the cyanomethemoglobin method. Briefly, 100 µl sample or blank were mixed with 25 µl Drabkin's reagent and after 10 min the absorption was measured at 540 nm. Control blood was used as a standard.

### *In vitro* angiogenesis assays

For determination of *in vitro* angiogenesis $5x10^3$ HUVEC/well were seeded into flat bottom 96 well plates onto polymerized matrigel and 100 µl conditioned cell culture supernatant obtained from parental or CREB-deficient HER-2/$neu^+$ cells was added. The cells were incubated for 16 h before the cell morphology and branches was analysed under a microscope.

### Histology, immunohistochemistry (IHC) and immunocytochemistry (ICC)

Tumors or matrigel plugs were fixed in 5% (v/v) formaldehyde overnight and then embedded in paraffin. Tumor samples were cut into 5 µm slices and then incubated with primary mAb directed against CD31 (Abbiotec) or HIF-1α (Novus) for 24 h. A compatible secondary antibody linked with HRP SignalStain® Boost IHC Detection Reagent (Cell Signaling) was used for the detection with the substrate DAB. Blood vessels of anti-CD31-stained slides were counted and their mean number calculated to determine the blood vessel density.

Matrigel plug slides were stained with hematoxyline-eosine, Giemsa or Masson-Goldner [46].

Immunocytochemical analysis was performed with $5x10^3$ cells/well seeded into clear bottom black 96 well plates (BD) and incubated in DMEM without phenol red for 24 h by 37°C. Cells were washed with PBS and fixed with 4% paraformaldehyde for 20 min. After washing with HBSS and 0.5% Triton X-100 (HBSS-T) cells were permeabilized in HBSS-T for 20 min, then incubated over night at 4°C with the primary antibody (CREB in HBSS-T) followed by washing with HBSS-T three times. After incubation for 1 h with a secondary Alexa488-linked anti-rabbit polyclonal antibody (Cell Signaling) at 4°C, the cells were washed with HBSS-T following HBSS. DAPI was employed for the nuclear staining and fluorescence was analysed with a fluorescence microscope (Leica).

For evaluation of localization of CREB in human breast cancer tissue, formalin-fixed paraffin embedded tissue samples that contained necrotic areas indicative of localized hypoxia were stained with the phospho-CREB (Ser133) (87G3) Rabbit mAb (Cell Signaling) in the indicated concentration using the Ventana Discovery Autostainer (Ventana).

### Determination of the MMP activity by zymography

Gelatin degradation activity of MMP-2 and 9 in the culture supernatant was determined with the gelatin zymography as recently described [35].

### Immunofluorescence microscopy of mitochondria

Mitochondria were visualized using the MitoTracker Red CMXROS (Life Technologies) and DAPI (Calbiochem) was added for nuclear staining. Cells were immediately analysed using a fluorescence microscope at a 20-fold magnification.

### Flow cytometry

Cells were harvested after 24 h under normoxia or hypoxia and stained with an anti-HER-2/neu-PE (BD) antibody or with the IgG1-PE isotype control (BD), respectively, for 20 min as recently described [47]. Fluorescence intensity was determined by flow cytometry (FACSCalibur, BD). The results were expressed as mean specific fluorescence intensity (MFI). Three independent experiments were performed.

### Apoptosis assays and determination of the mitochondrial membrane potential

Apoptosis was determined as previously described using annexin V and caspase-3 staining, respectively [35]. For determination of the mitochondrial membrane potential as an indicator for apoptosis cells were treated for 24 h under normoxia or hypoxia, before harvesting by trypsination. After centrifugation cells were stained with 2 µM JC-1 (Invitrogen) for 30 min at 37°C and fluorescence was measured with a FACSCalibur.

### Determination of the mitochondrial activity and ATP content

$5x10^3$ cells per 96 well were incubated for 24 h and mitochondrial activity was determined by using the XTT viability assay kit (Roche) according to the manufacturer's instructions. ATP levels of normoxic and hypoxic cells were analysed with the CellTiterGlo reagent (Promega). Values were normalized to cells cultured under normoxic condition.

### Analysis of cAMP concentrations

The concentration of cAMP in the cells was determined with the cAMP-Glo Assay kit (Promega). Briefly, $5x10^3$ cells/well were seeded into a white clear-bottom plate (BD) and then cultivated for 24 h under normoxia or hypoxia. The measurement of the cAMP was

performed as described in the manufacturer's instructions. Luminescence in the plates were analysed with a luminometer. The experiments were performed trice.

### Extracellular flux assays

Bioenergetics of parental and CREB-deficient HER-2/neu$^+$ and in HER-2/neu$^-$ cells were determined using the XF96e Extracellular Flux analyser (Seahorse Biosience) as recently described [41]. Briefly, 2x10$^5$ cells/well were reseeded in specialized tissue culture plates (96FX micro well plate). One hour prior measurement, cells were incubated at 37°C in a $CO_2$-free atmosphere. First basal oxygen consumption rate (OCR), which is an indicator for mitochondrial respiration was detected. In the next step OCR responses toward the application of 1 µM oligomycin, 2.5 µM FCCP (carbonyl cyanide-p-trifluoromethyloxy-phenylhydrazane) and the combination of 3 µM antimycin and 3 µM rotenone (XF Cell Mito Stress Test Kit, Seahorse Bioscience) were evaluated. All experiments were performed in at least octaplicates.

### Determination of mitochondrial DNA copy number, mitochondrial mass and oxidative potential

Genomic and mitochondrial DNA (mtDNA) was isolated from normoxic and hypoxic HER-2/neu$^+$ cells using the QiaAMP DNA mini kit following the manufacturer's instructions. The copy number of mtDNA was determined by qPCR as described [48]. For determination of the mitochondrial mass and oxidative potential cells were stained with 100 nM of the mitochondrial-specific dye MitoTracker Green (Life Technologies) according to the manufacturer's instructions for staining the mitochondrial lipid membrane and with 100 nM MitoTracker Red for determination of oxidation for 20 min at 37°C followed by flow cytometry [41].

### Mitochondrial sub fractionation and determination of mitochondrial complex activities

Cells were harvested and washed with PBS two times. After resuspension in 225 mM sorbitol, 75 mM sucrose, 0.1 mM EGTA and 30 mM Tris HCl pH 7,4 cells were ultrasonified (3 x 5 strokes with 10% frequence intensity). Upon centrifugation of lysate (600 *g*, 5 min, 4°C, repeated two times) the supernatant was centrifuged by 7000 *g* for 10 min at 4°C. The mitochondrial crude pellet was dissolved in 200 µl 10 µM $KH_2PO_4$ and was incubated for 20 min on ice. 200 µl isotonic buffer (32% sucrose, 30% glycerol, 10 mM $MgCl_2$) were added prior to centrifugation at 10,000 *g* for 10 min at 4°C.

The supernatant representing the outer membrane and the protein of the inter membrane space of mitochondrial was centrifuged for 1 h at 4°C and 15,000 *g*, resulting in a pellet P2 with the inner membrane proteins, while the supernatant S2 contains the proteins of the inter membrane space. The pellet representing the inner membrane and the matrix was resuspended in 200 µl 10 µM $KH_2PO_4$ pH 8.0 and followed by incubation for 20 min on ice. 200 µl isotonic buffer (32% sucrose, 30% glycerol, 10 mM $MgCl_2$) were added and the mixture was centrifuged (15,000 *g*, 1 h, 4°C). Pellet P3 are the proteins in the inner membrane while the supernatant S3 contains the mitochondrial matrix proteins. The four fractions as well as the crude extract were separated on a 12% SDS PAGE and proteins were identified by Western Blot analysis.

For determination of mitochondrial complex activities, crude mitochondria extracts were solubilized by adding DDM reaching a concentration of 0.45%. After centrifugation the supernatant was used for the activity measurement.

Complex I activity was determined by adding 1 ml NADH buffer (100 µM NADH, 10 mM $KH_2PO_4$ pH 8.0) to 50 µg mitochondrial proteins following the absorption at 340 nm for 1 min. After addition of 5 µl 10 mM ubichinon-10 the absorption was measured for 2 min. The turn-over rate was calculated with ε NADH = 6.21 $mM^{-1}*cm^{-1}$.

Complex II activity was measured by adding 25 µg mitochondrial proteins to 1 ml reaction buffer (50 mM $KH_2PO_4$ (pH 7.5), 90 µM ubichinon-2, 55 µM dichlorophenolindophenol and 10 mM sodium succinate).

### Blue native gel electrophoresis and in gel activity staining

Mitochondria (~ 1 mg) were prepared in ACA buffer (500 mM 6-aminocaproic acid, 0.5 mM EDTA, 50 mM BisTris (pH 7.0)) and were solubilized by adding DDM (concentration: 0.45%). Samples were gentle mixed at 4°C for 30 min and were centrifuged for 30 min at 4°C and 16,000 *g*. 200 µg mitochondrial proteins in the supernatant were mixed with blue native loading buffer leading to an end concentration of 10% glycerol, 0.05% Serva Blue G250 and 500 mM 6-aminocaproic acid. The sample were loaded onto 4-16% native gradient gels and protein complexes were separated by 45 V for 19 - 24 h under 4°C cooling using 50 mM BisTris pH 7.0 as the anode buffer and 50 mM Tricine, 15 mM BisTris, 0.002% Serva Blue G250 as cathode buffer. All components were from the ServaGel Native Gel starter kit (Serva). In gel activity staining was performed as described by [49].

### Statistical analysis and Kaplan-Meier survival analysis

Differences between groups were analysed by Mann-Whitney test, Student's t test or ANOVA as appropriate. Data are expressed as mean ± SD and p

values reported are 2-sided. Significance were accepted if p values were ≤ 0.05, *, ≤ 0.01, **. For the Kaplan-Meier curve analysis the KMplot database was used with the Affymetrix ID 225572_at for CREB1 and 200989_at for HIF-1α (http://kmplot.com/analysis/index.php?p=service&cancer=breast). The chosen Affymetrix IDs had the best JetSet score [50]. The following settings were used for the data analysis: Split patients by: median, Follow up threshold: all, Censore at threshold: checked, Compute median over entire database: false. Cut-off values and the expression range of the samples were automatically adjusted by the database and are depicted in the survival curves.

### Abbreviations

AIF, Apoptosis-inducing factor; AKT, ATCC, American Tissue Culture Collection; CaMK, calcium activated calmodulin kinase; CBP, CREB binding protein; CCCP, carbonyl cyanide *m*-chlorophenyl hydrazone; CD, cluster of differentiation; COX, cytochrome c oxidase; CRE, cAMP-responsive element; CREB, cAMP-responsive element-binding protein; ERK, extracellular-signal regulated kinase; FCCP, Carbonyl cyanide-*4*-(trifluoromethoxy)phenylhydrazone; DAPI, 4',6-diamidino-2-phenylindole; DDM, n-Dodecyl β-D-maltoside; FGF, fibroblast growth factor; GAPDH, Glyceraldehyde 3-phosphate dehydrogenase; GLUT 1, glucose transporter 1; GSH, glutathione; HBSS, Hank's buffered salt solution; hbFGF, human basic fibroblast growth factor; hEGF, human epidermal growth factor; HER-2/neu, human epidermal growth factor receptor 2 / neuroblastoma; HIF, hypoxia inducible factor; HRE, hypoxia responsible element; HUVEC, human umbilical vein endothelial cells; hypo, hypoxia; JC-1, 5,5′,6,6′-tetrachloro-1,1′,3,3′-tetraethylbenzimidazolylca rbocyanine iodide; mAb, monoclonal antibody; MAPK, mitogen-activated protein kinase; MEK, MAP/ERK kinase; MFI, mean fluorescence intensity; mito-CREB, mitochondrial CREB; MMP, matrix metalloproteinase; mtHSP70, mitochondrial heat shock protein 70 family; NADH, nicotinamide adenine dinucleotide; NC, non-sense control; ND, NADH dehydrogenase; NF, nuclear factor; OCR, oxygen consumption rate; OM, mitochondrial outer membrane; PDK4, pyruvate dehydrogenase kinase isoform 4; PE, phycoerythin; PECAM, Platelet endothelial cell adhesion molecule; PPARGc1a, Peroxisome proliferator-activated receptor gamma coactivator 1-alpha; PKA, protein kinase A; ProtK, proteinase K; PTM, post-transcriptional modification; qPCR, quantitative PCR; SUMO, small ubiquitin-related modifier; TOM20, translocase of outer membrane; VCAM, vascular cellular adhesion molecule; VEGF, vascular endothelial growth factor.

## ACKNOWLEDGMENTS

We would like to thank Prof. Holzhausen for help in the immunohistochemical analysis and Sylvi Magdeburg for excellent secretarial assistance.

## CONFLICTS OF INTEREST

The authors declare to have no conflicts of interest.

## GRANT SUPPORT

This work was supported by a Roux grant of the Medical Faculty of the Martin Luther University in Halle, Germany and a grant from the Deutsche Krebshilfe 14102510 (B.S.).

## REFERENCES

1. Dodson GE, Tibbetts RS. DNA replication stress-induced phosphorylation of cyclic AMP response element-binding protein mediated by ATM. J Biol Chem. 2006; 281:1692-1697.
2. Johannessen M, Delghandi MP, Moens U. What turns CREB on? Cell Signal. 2004; 16:1211-1227.
3. Shi Y, Venkataraman SL, Dodson GE, Mabb AM, LeBlanc S, Tibbetts RS. Direct regulation of CREB transcriptional activity by ATM in response to genotoxic stress. Proc Natl Acad Sci U S A. 2004; 101:5898-5903.
4. Ishimoto T, Mano H, Ozawa T, Mori H. Measuring CREB activation using bioluminescent probes that detect KID-KIX interaction in living cells. Bioconjug Chem. 2012; 23:923-932.
5. Braeuer RR, Zigler M, Villares GJ, Dobroff AS, Bar-Eli M. Transcriptional control of melanoma metastasis: the importance of the tumor microenvironment. Semin Cancer Biol. 2011; 21:83-88.
6. Cho EC, Mitton B, Sakamoto KM. CREB and leukemogenesis. Crit Rev Oncog. 2011; 16:37-46.
7. De Rasmo D, Signorile A, Roca E, Papa S. cAMP response element-binding protein (CREB) is imported into mitochondria and promotes protein synthesis. FEBS J. 2009; 276:4325-4333.
8. Kotla S, Singh NK, Heckle MR, Tigyi GJ, Rao GN. The transcription factor CREB enhances interleukin-17A production and inflammation in a mouse model of atherosclerosis. Sci Signal. 2013; 6:ra83.
9. Persengiev SP, Green MR. The role of ATF/CREB family members in cell growth, survival and apoptosis. Apoptosis. 2003; 8:225-228.
10. Bevilaqua LR, Cammarota M, Paratcha G, de Stein ML, Izquierdo I, Medina JH. Experience-dependent increase in cAMP-responsive element binding protein in synaptic and

nonsynaptic mitochondria of the rat hippocampus. Eur J Neurosci. 1999; 11:3753-3756.

11. Lee J, Sharma S, Kim J, Ferrante RJ, Ryu H. Mitochondrial nuclear receptors and transcription factors: who's minding the cell? J Neurosci Res. 2008; 86:961-971.
12. Ryu BJ, Lee H, Kim SH, Heo JN, Choi SW, Yeon JT, Lee J, Lee J, Cho JY, Kim SH, Lee SY. PF-3758309, p21-activated kinase 4 inhibitor, suppresses migration and invasion of A549 human lung cancer cells via regulation of CREB, NF-kappaB, and beta-catenin signalings. Mol Cell Biochem. 2014; 389:69-77.
13. Ryu H, Lee J, Impey S, Ratan RR, Ferrante RJ. Antioxidants modulate mitochondrial PKA and increase CREB binding to D-loop DNA of the mitochondrial genome in neurons. Proc Natl Acad Sci U S A. 2005; 102:13915-13920.
14. Chen YC, Hsu WL, Ma YL, Tai DJ, Lee EH. CREB SUMOylation by the E3 Ligase PIAS1 Enhances Spatial Memory. J Neurosci. 2014; 34:9574-9589.
15. Comerford KM, Leonard MO, Karhausen J, Carey R, Colgan SP, Taylor CT. Small ubiquitin-related modifier-1 modification mediates resolution of CREB-dependent responses to hypoxia. Proc Natl Acad Sci U S A. 2003; 100:986-991.
16. Ryan CM, Kindle KB, Collins HM, Heery DM. SUMOylation regulates the nuclear mobility of CREB binding protein and its association with nuclear bodies in live cells. Biochem Biophys Res Commun. 2010; 391:1136-1141.
17. Seo SR, Chung KC. CREB activates proteasomal degradation of DSCR1/RCAN1. FEBS Lett. 2008 (a); 582:1889-1893.
18. Melchior F. SUMO—nonclassical ubiquitin. Annu Rev Cell Dev Biol. 2000; 16:591-626.
19. Taylor CT, Furuta GT, Synnestvedt K, Colgan SP. Phosphorylation-dependent targeting of cAMP response element binding protein to the ubiquitin/proteasome pathway in hypoxia. Proc Natl Acad Sci U S A. 2000; 97:12091-12096.
20. Nakayama K. cAMP-response element-binding protein (CREB) and NF-kappaB transcription factors are activated during prolonged hypoxia and cooperatively regulate the induction of matrix metalloproteinase MMP1. J Biol Chem. 2013; 288:22584-22595.
21. Cammarota M, Paratcha G, Bevilaqua LR, Levi de Stein M, Lopez M, Pellegrino de Iraldi A, Izquierdo I, Medina JH. Cyclic AMP-responsive element binding protein in brain mitochondria. J Neurochem. 1999; 72:2272-2277.
22. Mootha VK, Bunkenborg J, Olsen JV, Hjerrild M, Wisniewski JR, Stahl E, Bolouri MS, Ray HN, Sihag S, Kamal M, Patterson N, Lander ES, Mann M. Integrated analysis of protein composition, tissue diversity, and gene regulation in mouse mitochondria. Cell. 2003; 115:629-640.
23. Cheng JC, Esparza S, Sandoval S, Shankar D, Fu C, Sakamoto KM. Potential role of CREB as a prognostic marker in acute myeloid leukemia. Future Oncol. 2007; 3:475-480.
24. Seo HS, Liu DD, Bekele BN, Kim MK, Pisters K, Lippman SM, Wistuba, II, Koo JS. Cyclic AMP response element-binding protein overexpression: a feature associated with negative prognosis in never smokers with non-small cell lung cancer. Cancer Res. 2008; 68:6065-6073.
25. Shankar DB, Cheng JC, Sakamoto KM. Role of cyclic AMP response element binding protein in human leukemias. Cancer. 2005; 104:1819-1824.
26. Siu YT, Jin DY. CREB—a real culprit in oncogenesis. FEBS J. 2007; 274:3224-3232.
27. Park JK, Park SH, So K, Bae IH, Yoo YD, Um HD. ICAM-3 enhances the migratory and invasive potential of human non-small cell lung cancer cells by inducing MMP-2 and MMP-9 via Akt and CREB. Int J Oncol. 2010; 36:181-192.
28. Abramovitch R, Tavor E, Jacob-Hirsch J, Zeira E, Amariglio N, Pappo O, Rechavi G, Galun E, Honigman A. A pivotal role of cyclic AMP-responsive element binding protein in tumor progression. Cancer Res. 2004; 64:1338-1346.
29. Deng X, Liu H, Huang J, Cheng L, Keller ET, Parsons SJ, Hu CD. Ionizing radiation induces prostate cancer neuroendocrine differentiation through interplay of CREB and ATF2: implications for disease progression. Cancer Res. 2008; 68:9663-9670.
30. Pigazzi M, Manara E, Bresolin S, Tregnago C, Beghin A, Baron E, Giarin E, Cho EC, Masetti R, Rao DS, Sakamoto KM, Basso G. MicroRNA-34b promoter hypermethylation induces CREB overexpression and contributes to myeloid transformation. Haematologica. 2013; 98:602-610.
31. Wang Z, Zhang L, Ni Z, Sun J, Gao H, Cheng Z, Xu J, Yin P. Resveratrol induces AMPK-dependent MDR1 inhibition in colorectal cancer HCT116/L-OHP cells by preventing activation of NF-kappaB signaling and suppressing cAMP-responsive element transcriptional activity. Tumour Biol. 2015; 36:9499-9510.
32. Vaupel P, Mayer A, Briest S, Hockel M. Oxygenation gain factor: a novel parameter characterizing the association between hemoglobin level and the oxygenation status of breast cancers. Cancer Res. 2003; 63:7634-7637.
33. Li D, Jin L, Alesi GN, Kim YM, Fan J, Seo JH, Wang D, Tucker M, Gu TL, Lee BH, Taunton J, Magliocca KR, Chen ZG, Shin DM, Khuri FR, Kang S. The prometastatic ribosomal S6 kinase 2-cAMP response element-binding protein (RSK2-CREB) signaling pathway up-regulates the actin-binding protein fascin-1 to promote tumor metastasis. J Biol Chem. 2013; 288:32528-32538.
34. Wang H, Huang M, Zhang DY, Zhang F. Global profiling of signaling networks: study of breast cancer stem cells and potential regulation. Oncologist. 2011; 16:966-979.
35. Steven A, Leisz S, Massa C, Iezzi M, Lattanzio R, Lamolinara A, Bukur J, Muller A, Hiebl B, Holzhausen HJ, Seliger B. HER-2/neu mediates oncogenic transformation

via altered CREB expression and function. Mol Cancer Res. 2013; 11:1462-1477.

36. Martinez-Outschoorn U, Sotgia F, Lisanti MP. Tumor microenvironment and metabolic synergy in breast cancers: critical importance of mitochondrial fuels and function. Semin Oncol. 2014; 41:195-216.
37. Lee J, Kim CH, Simon DK, Aminova LR, Andreyev AY, Kushnareva YE, Murphy AN, Lonze BE, Kim KS, Ginty DD, Ferrante RJ, Ryu H, Ratan RR. Mitochondrial cyclic AMP response element-binding protein (CREB) mediates mitochondrial gene expression and neuronal survival. J Biol Chem. 2005; 280:40398-40401.
38. Szczepanek K, Lesnefsky EJ, Larner AC. Multi-tasking: nuclear transcription factors with novel roles in the mitochondria. Trends Cell Biol. 2012; 22:429-437.
39. Steven A, Heiduk M, Recktenwald CV, Hiebl B, Wickenhauser C, Massa C, Seliger B. Colorectal Carcinogenesis: Connecting K-RAS-Induced Transformation and CREB Activity In Vitro and In Vivo. Mol Cancer Res. 2015; 13:1248-1262.
40. Singer K, Kastenberger M, Gottfried E, Hammerschmied CG, Buttner M, Aigner M, Seliger B, Walter B, Schlosser H, Hartmann A, Andreesen R, Mackensen A, Kreutz M. Warburg phenotype in renal cell carcinoma: high expression of glucose-transporter 1 (GLUT-1) correlates with low CD8(+) T-cell infiltration in the tumor. Int J Cancer. 2011; 128:2085-2095.
41. Jitschin R, Hofmann AD, Bruns H, Giessl A, Bricks J, Berger J, Saul D, Eckart MJ, Mackensen A, Mougiakakos D. Mitochondrial metabolism contributes to oxidative stress and reveals therapeutic targets in chronic lymphocytic leukemia. Blood. 2014; 123:2663-2672.
42. Yao K, Chen H, Liu K, Langfald A, Yang G, Zhang Y, Yu DH, Kim MO, Lee MH, Li H, Bae KB, Kim HG, Ma WY, Bode AM, Dong Z, Dong Z. Kaempferol targets RSK2 and MSK1 to suppress UV radiation-induced skin cancer. Cancer prevention research. 2014; 7:958-967.
43. Deak M, Clifton AD, Lucocq LM, Alessi DR. Mitogen- and stress-activated protein kinase-1 (MSK1) is directly activated by MAPK and SAPK2/p38, and may mediate activation of CREB. The EMBO journal. 1998; 17:4426-4441.
44. Ahmed BY, Husnain O, Stafford R, Howard M, Gujar AS, Moradiya V, Patel KK, Sihotra S. Hyperphosphorylation of CREB in human dopaminergic neurons: a kinetic study of cellular distribution of total CREB and phospho-CREB following oxidative stress. Neuroreport. 2013; 24:757-762.
45. Mimura K, Ando T, Poschke I, Mougiakakos D, Johansson CC, Ichikawa J, Okita R, Nishimura MI, Handke D, Krug N, Choudhury A, Seliger B, Kiessling R. T cell recognition of HLA-A2 restricted tumor antigens is impaired by the oncogene HER2. Int J Cancer. 2011; 128:390-401.
46. Straino S, Germani A, Di Carlo A, Porcelli D, De Mori R, Mangoni A, Napolitano M, Martelli F, Biglioli P, Capogrossi MC. Enhanced arteriogenesis and wound repair in dystrophin-deficient mdx mice. Circulation. 2004; 110:3341-3348.
47. Bukur J, Herrmann F, Handke D, Recktenwald C, Seliger B. Identification of E2F1 as an important transcription factor for the regulation of tapasin expression. J Biol Chem. 2010; 285:30419-30426.
48. Tal MC, Sasai M, Lee HK, Yordy B, Shadel GS, Iwasaki A. Absence of autophagy results in reactive oxygen species-dependent amplification of RLR signaling. Proc Natl Acad Sci U S A. 2009; 106:2770-2775.
49. Robles-Martinez L, Guerra-Sanchez MG, Flores-Herrera O, Hernandez-Lauzardo AN, Velazquez-Del Valle MG, Pardo JP. The mitochondrial respiratory chain of Rhizopus stolonifer (Ehrenb.:Fr.) Vuill. Arch Microbiol. 2013; 195:51-61.
50. Li Q, Birkbak NJ, Gyorffy B, Szallasi Z, Eklund AC. Jetset: selecting the optimal microarray probe set to represent a gene. BMC Bioinformatics. 2011 Dec 15;12:474.
51. Zhang J, Ye J, Ma D, Liu N, Wu H, Yu S, Sun X, Tse W, Ji C. Cross-talk between leukemic and endothelial cells promotes angiogenesis by VEGF activation of the Notch/Dll4 pathway. Carcinogenesis. 2013; 34:667-677.



„*Supplementary tables and figures*“ siehe Anhang auf CD

## 4.4 „Linking CREB function with altered metabolism in murine fibroblast-based model cell lines"

www.impactjournals.com/oncotarget/ Oncotarget, 2017, Vol. 8, (No. 57), pp: 97439-97463

Research Paper

# Linking CREB function with altered metabolism in murine fibroblast-based model cell lines

**André Steven[1], Sandra Leisz[1], Claudia Wickenhauser[2], Kristin Schulz[1], Dimitrios Mougiakakos[3], Rolf Kiessling[4], Carsten Denkert[5] and Barbara Seliger[1]**

[1]Institute of Medical Immunology, Martin Luther University Halle-Wittenberg, Halle, Germany

[2]Institute of Pathology, Martin Luther University Halle-Wittenberg, Halle, Germany

[3]Department of Internal Medicine 5, Hematology and Oncology, University of Erlangen-Nuremberg, Erlangen, Germany

[4]Karolinska Institute, CCK, Stockholm, Sweden

[5]Charité Berlin, Institute of Pathology, Berlin, Germany

***Correspondence to:*** *Barbara Seliger,* ***email:*** *Barbara.Seliger@uk-halle.de*

***Keywords:*** *CREB; HER-2/neu; metabolism; mitochondria; ROS*

***Received:*** *February 23, 2017* ***Accepted:*** *August 26, 2017* ***Published:*** *October 27, 2017*

**Copyright:** Steven et al. This is an open-access article distributed under the terms of the Creative Commons Attribution License 3.0 (CC BY 3.0), which permits unrestricted use, distribution, and reproduction in any medium, provided the original author and source are credited.

## ABSTRACT

**The cAMP-responsive element binding protein CREB is frequently overexpressed and activated in tumors of distinct histology, leading to enhanced proliferation, migration, invasion and angiogenesis as well as reduced apoptosis. The de-regulated expression of CREB might be linked with transcriptional as well as post-transcriptional regulation mechanisms. We show here that altered CREB expression levels and function are associated with changes in the cellular metabolism. Using comparative proteome-based analysis an altered expression pattern of proteins involved in the cellular metabolism in particular in glycolysis was found upon CREB down-regulation in HER-2/neu-transfected cell lines. This was associated with diminished expression levels of the glucose transporter 1, reduced glucose uptake and reduced glycolytic activity in HER-2/neu-transfected cells with down-regulated CREB when compared to HER-2/neu$^+$ cells. Furthermore, hypoxia-induced CREB activity resulted in changes of the metabolism in HER-2/neu transfected cells. Low pH values in the supernatant of HER-2/neu transformants were restored by CREB down-regulation, but further decreased by hypoxia. The altered intracellular pH values were associated with a distinct expression of lactate dehydrogenase, and its substrate lactate. Moreover, enhanced phosphorylation of CREB on residue Ser133 was accompanied by a down-regulation of pERK and an up-regulation of pAKT. CREB promotes the detoxification of ROS by catalase, therefore protecting the mitochondrial activity under oxidative stress. These data suggest that there might exists a link between CREB function and the altered metabolism in HER-2/neu-transformed cells. Thus, targeting these altered metabolic pathways might represent an attractive therapeutic approach at least for the treatment of patients with HER-2/neu overexpressing tumors.**

## INTRODUCTION

The 43 kDa cyclic AMP (cAMP)-responsive element binding protein (CREB) is a member of the large family of basic leucine zipper (bZIP)-containing transcription factors (TF) and plays a key role in many physiologic as well as pathophysiologic processes including cell growth, differentiation, apoptosis, cell cycle progression and immune response amongst others [1]. CREB exerts distinct activities in context and time-dependent manners [2–4], which depend on its phosphorylation status mediated by various kinases. Phosphorylated CREB

interacts with the CREB-binding protein CBP/p300 via its kinase inducible domain (KID) and the KID-interacting domain (KIX) in CBP/p300 [5]. The CREB/CBP complex induces a transcriptional machinery leading to activation of cAMP-responsive element (CRE) containing gene promoters. CREB mediates transcriptional responses to different stimuli including hormones, growth factors and neurotransmitters thereby acting as mediator between signaling pathways and their downstream activation target [3, 6].

However, based on its frequent overexpression and persistent activation CREB is also involved in the malignant transformation process [7]. This is mediated by aberrant activation of cAMP signal transduction-dependent pathways such as G-coupled receptors, receptor tyrosine kinase (RTK) like human epidermal growth factor receptor 2 (HER-2/neu) and the cytokine/JAK/STAT signaling cascades, as well as signaling events downstream of CREB.

HER-2/neu is a member of the transmembrane epidermal growth factor receptor (EGF-R) family and is physiological expressed in many epithelial cells. However, it is overexpressed and/or amplified in human tumor of distinct origin including mammary carcinoma [8] and colorectal cancer [9]. HER-2/neu transformation is associated with an increased cell proliferation, migration, enhanced cell cycle progression as well as a survival of patients [10]. Recently, we could demonstrate in the murine model system used also in this study, that HER-2/neu can increase the phosphorylation rate of CREB and that HER-2/neu overexpressing cells had more detectable CREB protein than the parental NIH3T3 cells [11].

As recently reviewed CREB overexpression and its constitutive activation was found in many solid tumors, including non-small cell lung carcinoma, glioblastoma, melanoma, mammary carcinoma, renal cell carcinoma and mesothelioma as well as in different hematopoietic malignancies [4, 12–18], leading to enhanced cell proliferation, reduced apoptosis, increased angiogenesis and migration rates. Downregulation of CREB expression inhibits proliferation, migration and/or invasion, which was accompanied by suppression of matrix metallopeptidases and proteins of the epithelial mesenchymal transition [18]. Furthermore, CREB overexpression can be correlated with clinico-pathological parameters, in particular with tumor grade, stage, metastasis formation, poor prognosis and reduced patients' survival [14, 19–22]. In addition, CREB overexpression is often caused by an up-regulation of downstream target genes involved in neoplastic transformation as demonstrated by different high throughput analysis [23].

The expression level and activity of CREB is dynamically regulated by different mechanisms [24] and critical for maintaining a homeostatic cellular environment [25]. CREB transcriptionally controls a large number of putative target genes, which are involved in numerous cellular processes, such as signal transduction, cell structure, differentiation, cell survival as well as proliferation [17]. So far, amplifications and/or deletions in CREB have only been rarely detected suggesting that rather deregulation mechanisms of CREB appear to be responsible for its overexpression in tumors [26, 27]. Recently, a post-transcriptional control mechanism for CREB has been described, which seems to be mediated by microRNAs (miRs) known to for their binding to the 3' untranslated region (UTR) of CREB thereby contributing to tumorigenesis in different tumor models as demonstrated both *in vitro* and *in vivo* [28–31]. In addition, there is increasing evidence that different extra-cellular signals have an impact on the tumor microenvironment (TME), like hypoxia, pH variation and oxidative stress [32]. Furthermore, post-translational modifications (PTM) of CREB, which can be quite diverse including phosphorylation, ubiquitination, methylation, glycosylation and SUMOylation, might have an impact on CREB function(s) [3, 17, 33]. So far, a link between CREB expression levels/function(s) and tumor metabolism has not been identified. Therefore, this study analyzed the effects of CREB on the metabolism using a murine model of HER-2/neu transformation with distinct CREB expression and activation levels, which has been previously well characterized and was able to induce tumors in immunocompetend DBA mice [11, 17, 34].

## RESULTS

### CREB-mediated changes in the protein expression pattern

Since the level of CREB and HER-2/neu expression has been correlated with growth characteristics and altered signaling cascades [32], the protein expression pattern of HER-2/neu$^+$ versus CREB-diminished HER-2/neu$^+$ (shCREB) cells (Supplementary Figure 1A), with a knock down of up to 80% on the protein level (Supplementary Figure 1B, 1C) were determined by using two-dimensional gel electrophoresis (2-DE)-based proteome analysis and differentially expressed protein spots, defined by a 2-fold regulation, were identified by mass spectrometry. Overall 23 differentially expressed protein spots have been identified from three biological replicates (merged gels of all three experiments can be found in Supplementary Figure 2A), from which 13 proteins were down-regulated including four different forms of alpha-tubulin and 10 up-regulated upon CREB down-regulation. The differentially expressed proteins were mainly involved in metabolic processes (Table 1, Figure 1A, Supplementary Figure 2B), in particular in glycolysis (Figure 1B). Based on their distinct expression pattern the following candidate CREB-regulated proteins were selected and their expression validated by qPCR and/or Western blot analyses: The panel of potential targets includes the phosphoglycerate

**Table 1: CREB-regulated proteins identified by 2-DE-based proteomics**

| Protein | Acc no. | Molecular weight estimated | found | IP | Ratio (range) | Sequence coverage | Score (range) | Localization | Function |
|---|---|---|---|---|---|---|---|---|---|
| pyruvate kinase isozymes M1/ M2 | P52480 | 58.3 | 55 | 7.18 | 0.09 - 0.201 | 19 | 78 - 212 | cytoplasm and nucleus | glycolysis, degradation of carbohydrates |
| heat shock protein HSP 90-alpha | P07901 | 83.5 | 38 | 4.93 | 0.145 - 0.192 | 14 | 56 - 62 | cytoplasm and melanosome | chaperon, cell cycle control, signal transduction |
| tubulin alpha-1A chain | P68369 | 50.7 | 45 | 4.94 | 0.179 - 0.45 | 25 | 83 - 102 | cytoplasm and cytoskeleton | microtubules |
| tubulin alpha-1B chain | P05213 | 50.8 | | 4.94 | | 25 | 83 - 102 | | |
| tubulin alpha-1C chain | P68373 | 50.5 | | 4.96 | | 26 | 83 - 102 | | |
| tubulin alpha-3 chain | P68373 | 50.6 | | 4.97 | | 20 | 53 - 74 | | |
| phosphoglycerate kinase 1 | P09411 | 44.9 | 41 | 8.02 | 0.228 - 0.457 | 38 | 66 - 116 | cytoplasm | glycolysis, degradation of carbohydrates, angiogenesis |
| catalase | P24270 | 59.7 | 57 | 7.72 | 0.248 - 0.324 | 29 | 76 - 90 | peroxisome | detoxification of hydrogen peroxide |
| alpha-enolase | P17182 | 47.5 | 41 | 6.37 | 0.125 - 0.448 | 35 | 116 - 128 | cytoplasm and cell membrane | glycolysis, growth, regulation of hypoxic events |
| phosphoglycerate mutase 1 | Q9DBJ1 | 28.9 | 30 | 6.67 | 0.077 - 0.392 | 31 | 101 - 135 | cytoplasm and membrane | glycolysis |
| vimentin | P20152 | 53.7 | 60 | 5.06 | 0.244 - 0.33 | 29 | 62 - 81 | cytoplasm | structural protein |
| protein disulfide-isomerase A6 | P09103 | 48.5 | 42 | 5.00 | 0.273 - 0.46 | 21 | 78 - 80 | ER lumen | yield of disulfide bridges, chaperone |
| triosephosphate isomerase | P17751 | 32.6 | 29 | 5.56 | 0.246 - 0.483 | 33 | 92 - 191 | nucleus | glycolysis, gluconeogenesis |
| prolyl endopeptidase | Q8C167 | 81.6 | 77 | 5.44 | 2.144 - 3.569 | 20 | 136 - 202 | cytoplasm | serine protease, synthesis and degradation of peptide hormones |
| spliceosome RNA helicase Ddx39b | Q9Z1N5 | 49.4 | 50 | 5.44 | 2.01 - 4.405 | 35 | 61 - 95 | nucleus | splicing |

(*Continued*)

| Protein | Acc no. | Molecular weight estimated | found | IP | Ratio (range) | Sequence coverage | Score (range) | Localization | Function |
|---|---|---|---|---|---|---|---|---|---|
| 26S proteasome non-ATPase regulatory subunit 13 | Q9WVJ2 | 43.1 | 39 | 5.46 | 2.352 - 2.725 | 57 | 65 - 245 | cytoplasm | protein degradation, regulation of proteasomal activity |
| superoxide dismutase [Cu-Zn] | P08228 | 16.1 | **23** | 6.02 | 2.574 - 3.33 | 38 | 80 - 91 | cytoplasm | radical detoxification |
| flavin reductase (NADPH) | Q923D2 | 22.2 | 24 | 6.49 | 2.696 - 3.244 | 38 | 84 - 104 | cytoplasm | oxidoreductase |
| peroxiredoxin-4 | O08807 | 31.2 | 28 | 6.67 | 2.704 - 5.096 | 40 | 59 - 98 | cytoplasm and extracellular | redox regulation, regulation of NF-k-B activity |
| ATP-dependent RNA helicase DDX39A | Q8VDW0 | 49.5 | **60** | 5.46 | 3.473 - 4.461 | 43 | 167 - 188 | cytoplasm and nucleus | splicing |
| leukocyte elastase inhibitor A | Q9D154 | 42.7 | 40 | 5.85 | 7.577 - 9.137 | 33 | 138 - 183 | cytoplasm | regulation of protease activity |
| cofilin-1 | P18760 | 18.7 | 21 | 8.22 | 21.579 - 24.771 | 46 | 92 - 107 | cytoplasm and nucleus | cell morphology and cytoskeleton, mitosis |
| alpha-crystallin B chain | P23927 | 20.0 | 22 | 6.76 | 20.082 - 86.972 | 58 | 108 - 173 | cytoplasm and nucleus | stress induced chaperone, protection against protein aggregation |

Functions, localization, IP, estimated molecular weigth and accession number of the proteins were added according to the MASCOT and SwissProt database.
Up-regulated proteins after CREB knock down are marked in red, down-regulated proteins in green. The red bold value in the row "molecular weight found" indicates samples with an alteration of the molecular weight by 15 or more percent compared to the estimated molecular weight. For the ratio and the score value the range of the three experiments is given.

kinase (PKG)1, prolyl endopeptidase, peroxiredoxin (PRX)4, enolase (ENO), triose phosphate isomerase (TPI), pyruvate kinase M (PKM) and citrate synthase. In line with the proteomic profiling data reduced transcription levels of PKM, citrate synthase and TPI were found in CREB down-regulated HER-2/neu$^+$ cells (Table 2), while the mRNA expression level of PGK1 remained unchanged and that of the prolyl endopeptidase (PEP) induced. In addition, a CREB-mediated transcriptional control was detected for cofilin and α-crystalline (Table 2). The decreased mRNA levels were associated with decreased protein expression levels of ENO, PRX4, PGK1, PGAM1, PKM and TPI in HER-2/neu$^+$ shCREB versus HER-2/neu$^+$ cells (Figure 1C), which was further confirmed by a down-regulated PKM, TPI, and PGK1 enzyme activity (Table 3). Other differentially expressed proteins were enzymes important for detoxification mechanisms (catalase, PRX4, superoxide dismutase [Cu-Zn]) or linked to the protein degradation process (26S proteasome non-ATPase regulatory subunit 13, PEP, leukocyte elastase inhibitor A) (Table 1).

*In silico* analysis of gene promoters from differentially expressed proteins upon CREB down-regulation revealed that most of the identified proteins were controlled by half CRE sites (TGACG or CGTCA), whereas full CRE sites (TGACGTCA) were merely found in promoters of up-regulated proteins (Tables 4 and 5). Since the promoter of the oncogene HER-2/neu contains

no CRE elements, its expression was not affected by CREB down-regulation [11].

### Association of CREB and hypoxia-induced changes on the cell metabolism of HER-2/neu$^+$ cells

The comparative proteomics profiling of HER-2/neu$^+$ cells and its shCREB derivatives suggests a link between the CREB expression levels/activation status and metabolic changes. In order to determine the functional relevance of this altered expression pattern, intracellular pH values were determined in the model system. Reduced intracellular pH values were detected in HER-2/neu$^+$ cells when compared to NIH3T3 cells, while the intracellular pH values were restored to that of NIH3T3 cells by CREB down-regulation in HER-2/neu$^+$ cells (Figure 2A). As expected treatment of the cells with the proton pump

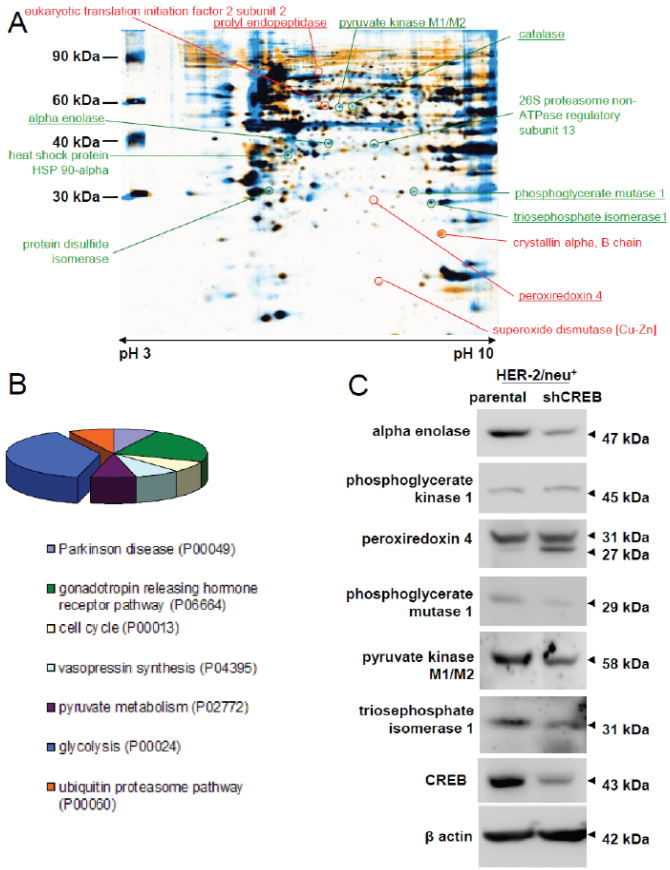


**Figure 1: Influence of CREB knock down on metabolism and glycolytic enzymes. (A)** HER-2/neu$^-$ and CREB-downregulated HER-2/neu$^+$ (shCREB) cells were lysed and the protein pattern was analyzed by 2-DE gel electrophoresis following staining of the gels with colloidal Coomassie Blue. Differentially regulated protein spots of interest were digested with trypsin and the fragments were identified by MS/MS-TOF analysis. The picture represents a representative overlay of merged profiles (four technical replicates for both cell lines) in sum of three independent experiments. Some identified proteins are marked and listed. Red marked spots were up-regulated in CREB knock down cells, whereas green marked spots were down-regulated. The underlined proteins were further validated by measuring the mRNA expression status. **(B)** The graph shows the distribution pattern of the identified targets in (A) based on their classification into various pathways, functional roles or diseases and was performed by using the PANTHER database (pantherdb.org). **(C)** Validation of the differentially expressed proteins in (A). The representative protein expression pattern in one HER-2/neu overexpressing cell line (HER-2/neu$^-$, left lane) and one shCREB HER-2/neu$^+$ (right lane) is shown for metabolic enzymes. The blot represents one of three experiments.

**Table 2: mRNA expression level of metabolic and stress related genes as identified to be differentially expressed in 2D gel electrophoresis of CREB down-regulated vs. HER-2/neu$^+$ and NIH3T3 cells**

| | NIH3T3 | NIH3T3 shCREB | HER-2/neu$^+$ | HER-2/neu$^+$ shCREB |
|---|---|---|---|---|
| citrate synthase | 1 | 0.87 +/- 0.28 | 1.09 +/- 0.13 | 0.34 +/- 0.05 * |
| cofilin 1 | 1 | 0.68 +/- 0.12 * | 0.41 +/- 0.16 * | 0.93 +/- 0.22 * |
| α-crystalline B | 1 | 0.61 +/- 0.17 * | 0.45 +/- 0.12 * | 0.2 +/- 0.04 * |
| peroxiredoxin 4 | 1 | 1.23 +/- 0.42 | 0.81 +/- 0.17 | 1.76 +/- 0.18 * |
| PGAM1 | 1 | 0.89 +/- 0.17 | 1.87 +/- 0.12 * | 1.21 +/- 0.2 * |
| PGK1 | 1 | 0.68 +/- 0.18 * | 1.76 +/- 0.45 * | 0.78 +/- 0.02 * |
| prolyl endopeptidase | 1 | 0.42 +/- 0.12 * | 0.3 +/- 0.08 * | 0.57 +/- 0.08 * |
| pyruvate kinase M1/2 | 1 | 0.62 +/- 0.05 * | 1.68 +/- 0.14 * | 0.12 +/- 0.03 * |
| triose phosphate isomerase | 1 | 0.7 +/- 0.12 * | 4.97 +/- 1.11 * | 4.82 +/- 1.23 |

Expression levels of the parental NIH3T3 were normalized to 1. For the significance of the row HER-2/neu$^+$ the values were compared to that of the parental NIH3T3.
The expression of the genes analysed was compared to parental NIH3T3 cells (normalizied to 1). * statistical significant ($p < 0.05$).

**Table 3: Modulation of enzymatic activities by CREB down-regulation in HER-2/neu$^+$ cells**

| Activity [U/mg total protein] | HER-2/neu$^+$ | HER-2/neu$^+$ shCREB |
|---|---|---|
| PKM | 12.64 + 0.52 | 3.01 +/- 0.7 * |
| TPI | 38.64 +/- 0.31 | 6.81 +/- 0.47 * |
| PGAM1 | 5.24 +/- 0.61 | 2.28 +/- 0.24 * |
| PGK | 5.45 +/- 0.62 | 2.56 +/- 0.21 * |
| prolyl endopeptidase | 0.63 +/- 0.45 | 1.57 +/- 0.54 |
| peroxiredoxin 4 | 1.48 +/- 0.79 | 3.44 +/- 0.35 * |

The enzyme activity was calculated to the protein concentration.

inhibitor Esomeprazole (ESOM), which served as control, strongly decreased the intracellular pH value in CREB down-regulated HER-2/neu$^+$ cells (Figure 2A).

Although a correlation between hypoxic conditions and metabolic reprogramming as well as the survival of tumor cells has been demonstrated [35–37], the role of CREB in this process has not yet been analyzed in detail. Therefore, the effect(s) of hypoxia on the energy metabolism of HER-2/neu$^+$ and HER-2/neu$^+$ shCREB as well as HER-2/neu$^-$ (NIH3T3) cells was compared by determining the intracellular and extracellular pH values, lactate and lactate dehydrogenase (LDH) concentrations. Under hypoxic conditions the intracellular pH was even further reduced in HER-2/neu$^+$ cells, but also reduced in CREB down-regulated HER-2/neu$^+$ cells (Figure 2A). The hypoxia-mediated decline of the intracellular pH values in HER-2/neu$^+$ cells could be restored over time by culturing these cells under normoxia suggesting that this is a rather reversible process (Figure 2B).

Altered extracellular pH conditions also affected both CREB activity and CREB-relevant signaling pathways as determined by Western blot analysis of HER-2/neu$^+$ cells cultured at pH 6.3 and pH 7.3, respectively (Figure 2C). A shift from slightly acidic towards neutral pH conditions resulted in a decreased pCREB$^{Ser133}$ phosphorylation rate in HER-2/neu$^+$ cells, which was accompanied by a down-regulation of pERK and an up-regulation of pAkt as well as of total CREB.

The modulation of the intracellular pH values was linked to changes of the LDH expression levels and of lactate concentrations as determined in the supernatants of normoxic and hypoxic HER-2/neu$^+$ and CREB down-regulated HER-2/neu$^+$ cells: The lactate concentrations were increased in HER-2/neu$^+$ vs. HER-2/neu$^+$ shCREB and NIH3T3 cells, while hypoxia enhanced lactate concentrations in all cell supernatants tested with the highest increase in supernatants of NIH3T3 cells (Figure 2D). Total LDH concentrations were comparable across all

**Table 4: CRE elements in gene promoter of differential regulated proteins identified after CREB knock down by 2-DE and MS**

| Symbol | Gene name | Accession | CRE prediction | CRE flag | Full site | Half site | Conserved CRE | CRE cluster | pHMM+Pos | Chrom. localization | Strand | Pos |
|---|---|---|---|---|---|---|---|---|---|---|---|---|
| Pkm2 | "pyruvate kinase, muscle" | NM_011099 | Others | ht h | | ht_-1433<br>h_-2 | | | | chr9 | + | 59830243 |
| Pkm2 | "pyruvate kinase, muscle" | NM_011099 | Others | none | | h_506<br>h_630 | | | | chr9 | + | 59830243 |
| Hspca | "heat shock protein 1, alpha" | NM_010480 | Others | h | | ht_-4769<br>ht_-3435<br>h_0 ht_830<br>h_893 | | | | chr12 | - | 104744737 |
| Tuba1 | "tubulin, alpha 1" | NM_011653 | Others | ht | | ht_-2171 | | | | chr15 | - | 99318440 |
| Tuba2 | "tubulin, alpha 2" | NM_011654 | Others | none | | | | | | chr15 | - | 99299381 |
| Tuba6 | "tubulin, alpha 6" | NM_009448 | Others | h | | ht_-3468<br>h_-497<br>h_18<br>ht_575 | | | | chr15 | + | 99396317 |
| Tuba7 | "tubulin, alpha 7" | NM_009449 | Others | ht | | ht_95 | | | | chrUn_<br>random | + | 117747169 |
| Pgk1 | phosphoglycerate kinase 1 | NM_008828 | Others | ht | | ht_-1021<br>ht_-707<br>ht_512 | | | | chrX | + | 91115110 |
| Cat | catalase | NM_009804 | Others | ht | | h_-4839<br>ht_-2392<br>h_910 | | | | chr2 | - | 104935582 |
| Eno1 | "enolase 1, alpha non-neuron" | NM_023119 | Others | none | | h_527 | | | | chr4 | + | 146873883 |
| Pgam1 | phosphoglycerate mutase 1 | NM_023418 | Others | none | | ht_-4353<br>ht_-3676 | | | | chr19 | + | 41498057 |
| Vim | vimentin | NM_011701 | others | ht h | | ht_-580<br>h_-226 | | | | chr2 | + | 13567777 |
| Tpi | triose phosphate isomerase | NM_009415 | others | none | | h_-3599 | | | | chr6 | - | 125622026 |
| Prep | prolyl endopeptidase | NM_011156 | others | ht | | ht_-4229<br>ht_-918<br>ht_613 | | | | chr10 | + | 44917660 |
| Bat1a | HLA-B-associated transcript 1A | NM_019693 | CRE_<br>TATA | none | | ht_-4510<br>ht_-3773<br>ht_-3526<br>h_886 | | | FF_<br>human_1.0_-4904_<br>mouse_1.3_-5083 | chr17 | + | 33858338 |
| Psmd13 | "proteasome (prosome, macropain) 26S subunit, non-ATPase, 13" | NM_011875 | others | ht h | | h_-4162<br>ht_-1835<br>h_-65<br>ht_866 | | | | chr7 | + | 129902896 |
| Blvrb | biliverdin reductase B (flavin reductase (NADPH)) | NM_144923 | CRE_<br>NoTATA | H h | | ht_-4463<br>H_-1237<br>h_-1191 | H_-<br>1237_635 | \|H_-<br>1237_h_-1191_0 | | chr7 | + | 19020950 |
| Prdx4 | peroxiredoxin 4 | NM_016764 | CRE_<br>TATA | HT<br>FH<br>h | FH_-<br>1215 | HT_-2035<br>h_-101 | FH_-<br>1215_378<br>HT_-<br>2035_177 | | | chrX | - | 135097408 |
| Ddx39 | DEAD (Asp-Glu-Ala-Asp) box polypeptide 39 | NM_197982 | CRE_<br>TATA | ht | | ht_-4185<br>ht_-669<br>ht_702 | | | FH_<br>human_2.2_-3409_<br>mouse_1.7_-3491 | chr8 | + | 82993770 |
| NE | neutrophil elastase | NM_015779 | others | none | | h_-4246<br>h_505 | | | | chr10 | + | 79703208 |
| Cfl1 | "cofilin 1, non-muscle" | NM_007687 | CRE_<br>TATA | none | | ht_-3170<br>ht_558 | | | FF_<br>human_1.2_-8876_<br>mouse_1.2_-8835 | chr19 | - | 5190328 |
| Cfl1 | "cofilin 1, non-muscle" | NM_007687 | CRE_<br>TATA | none | | | | | FF_<br>human_1.2_-8876_<br>mouse_1.2_-8835 | chr8 | + | 41275610 |
| Cryab | "crystallin, alpha B" | NM_009964 | others | ht h | | ht_-4617<br>ht_-3003<br>ht_-1195<br>h_-716 | | | | chr9 | + | 50875865 |

Chr: chromosome.

**Table 5: CRE elements in gene promoter of differential regulated proteins identified after CREB knock down by qPCR**

| Symbol | Gene name | Accession | CRE prediction | CRE flag | full site | Half site | Conserved CRE | CRE cluster | pHMM+Pos | Chrom localization | Strand | Pos |
|---|---|---|---|---|---|---|---|---|---|---|---|---|
| ERBB2 * (HER-2;HER2;NEU; NGL;TKR1) | "v-erb-b2 erythroblastic leukemia viral oncogene homolog 2, neuro/ glioblastoma derived oncogene homolog (avian)" | NM_004448 | others | none | | | | | | chr17 | + | 38231358 |
| Cs | citrate synthase | NM_026444 | others | ht | | ht_-2966 ht_-2751 | | | | chr10 | + | 128362478 |
| Es10 | esterase 10 | NM_016903 | others | ht h | | h_-2215 ht_151 ht_481 | | | | chr14 | + | 65179735 |
| Slc2a1 (Glut-1) | "solute carrier family 2 (facilitated glucose transporter), member 1" | NM_011400 | CRE_ NoTATA | ht h | | ht_-3367 ht_-1283 h_62 h_91 h_560 | | \|h_62_h_91_0 | | chr4 | + | 117243469 |
| Gss | glutathione synthetase | NM_008180 | others | ht h | | ht_-2831 h_-2156 h_119 h_732 | | | | chr2 | - | 157439425 |

* - Erbb2 expression is unregulated after CREB knock down.
Chr: chromosome.

cells under normoxic conditions. Furthermore, culturing the cells under hypoxic conditions caused an up-regulation of total LDH activity in all cell lines to a similar extent (Figure 2E), while CREB knock down had no significant influence.

### HIF-1α inhibitor blocks CREB activity and regulates metabolism

Since hypoxia (1% $O_2$) can increase the phosphorylation of CREB at serine residue 133 [32], it was analyzed whether hypoxia-related TFs, like HIF-1α, can influence the CREB activity. Therefore, HER-2/neu$^+$ cells were incubated with the HIF-1α inhibitor 2-methoxyestradiol (2-ME) for 24 h resulting in a decreased HIF-1α protein expression (Figure 3A), which was linked with a down-regulation of CREB phosphorylation at serine 133 in HER-2/neu$^+$ cells. This effect was already visible upon treatment of HER-2/neu$^+$ cells with 1 μM 2-ME and was not further enhanced in the presence of higher 2-ME concentrations (Figure 3B). In contrast, NIH3T3 cells exhibited the highest CREB phosphorylation at 1 μM 2-ME, which was strongly reduced with higher concentrations of this substance. Furthermore, electromobility shift assays (EMSA) revealed that 2-ME inhibited the formation of CREB-CRE complexes by decreasing the phosphorylation of CREB (Figure 3C).

In addition, blocking HIF-1α changed the morphology of NIH3T3 from a fibroblast-like to a foci-like grown pattern, while HER-2/neu$^+$ cells lost their ability to form bigger foci (Figure 3D). It is noteworthy that the treatment of both cell lines with 10 μM 2-ME did not altered the cell vitality significantly (data not show), but decreased concentration-dependent the proliferation (Figure 3E) and the metabolic / glycolytic activity (Figure 3F).

### CREB-mediated control of apoptosis in HER-2/neu$^+$ cells

In order to determine whether HER-2/neu$^+$ cells are more resistant to apoptosis compared to shCREB cells, cells were cultured in medium supplemented with different FCS and glucose concentrations. CREB down-regulated HER-2/neu$^+$ cells, but not the parental HER-2/neu$^+$ cells cultured in 0.1 % FCS showed a reduced cell vitality as determined by flow cytometry upon annexin V / PI stainings (Figure 4A). Cultivation of HER-2/neu$^+$ cells with increasing FCS concentrations correlated with higher CREB and pCREB levels, which were further correlated with the higher frequency rates of vital cells (Figure 4B).

In addition, glucose deprivation resulted in reduced cell vitalities in particular in CREB down-regulated HER-2/neu$^+$ cells. The increased apoptosis rates were linked to reduced pCREB levels (Figure 4C) suggesting that growth properties, in particular the neoplastic features of HER-2/neu$^+$ cells, are tightly linked with cell vitality. Moreover, supplementation of

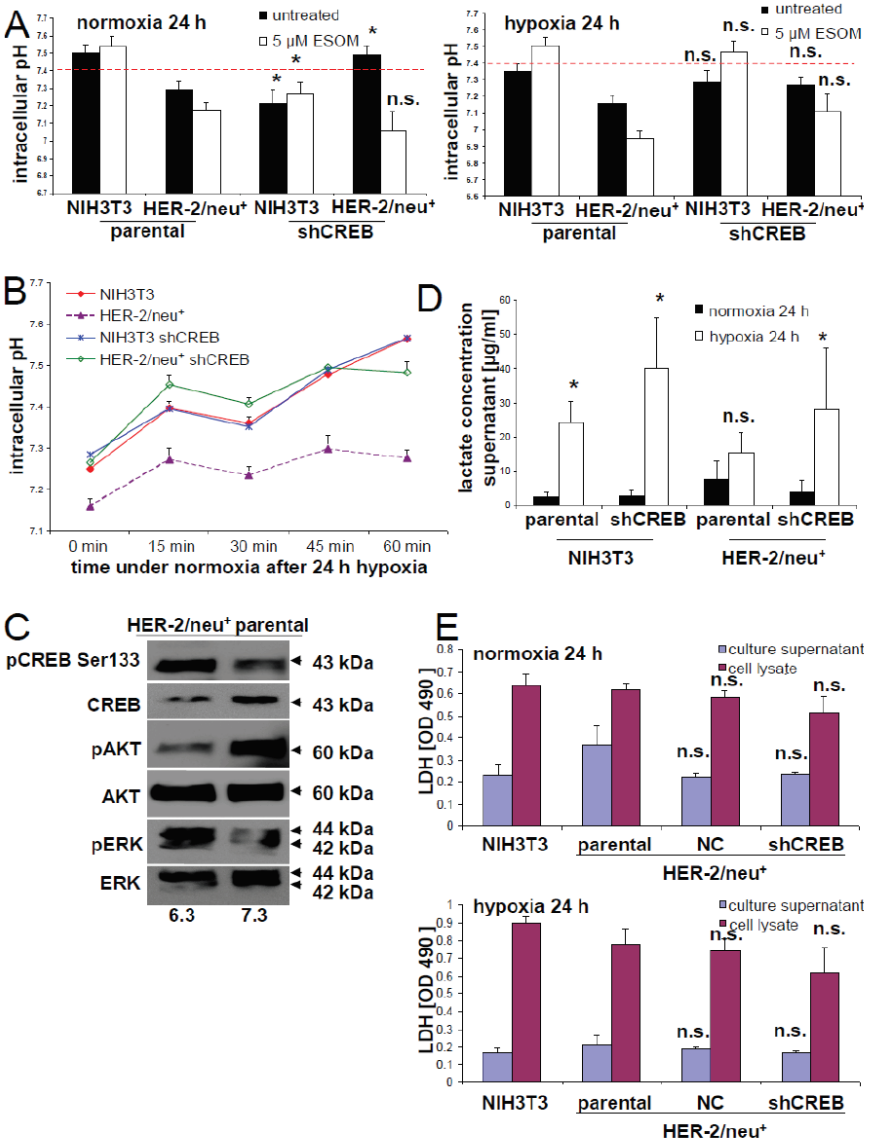


**Figure 2: Induction of an altered microenvironment in CREB-reduced cells under hypoxia.** **(A)** Intracellular pH was determined by staining with BCECF-AM under the conditions given in Material and Methods. As a control, cells were treated with the inhibitor ESOM (5 µM/24 h) was used blocking the $H^+/K^+$ pump. **(B)** The intracellular pH was followed during the re-oxygenation phase after cultivation under hypoxic conditions for 24 h. The data represents one of two independently performed experiments. **(C)** The effects of distinct pH conditions in the culture medium on the phosphorylation of CREB, AKT and ERK was determined by Western blot. The blot represents one of two experiments. **(D)** Lactate levels in the culture supernatants of NIH3T3 (HER-2/neu$^-$) vs. HER-2/neu$^+$ cells were determined using a commercial kit. Data in the columns represent the average of three different experiments along with the error bars. **(E)** LDH activity in the supernatant and in the cells was measured with a cytotoxicity assay as described in Materials and Methods. The columns and bars represent the data from three experiments.

high glucose concentrations caused a significant induction of the corresponding pCREB levels (Figure 4D).

### Influence of altered CREB expression levels on the cellular metabolism

Based on the results of the proteomics profiling and glucose deprivation experiments alterations within the glycolytic pathway in HER-2/neu$^+$ cells vs. CREB down-regulated HER-2/neu$^+$ cells are expected. Therefore, modulations of glycolysis pathways were determined by the extracellular acidification rates (ECAR). CREB down-regulation in HER-2/neu$^+$ cells led to a marked decrease of the ECAR under baseline conditions as well as induction of glycolysis by adding glucose (Figure 5A). The glycolytic capacity of the cells, meaning the highest glycolytic activity under inhibition of the mitochondrial ATPase with oligomycin was lower in CREB knock down cells. This was accompanied with a diminished glycolytic activity observed in these cells (Figure 5B).

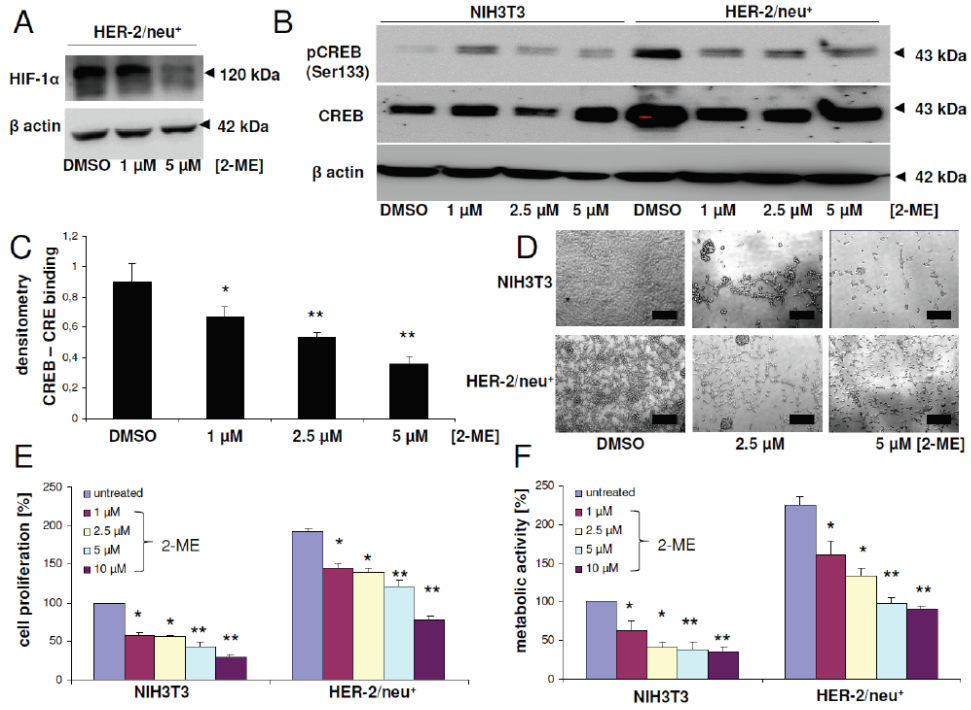


**Figure 3: Modulation of CREB activity, proliferation and metabolic activity upon treatment with the HIF-1α inhibitor 2-methoxyestradiol.** **(A)** HER-2/neu$^+$ cells were treated with 2-ME or with DMSO as the solvent control for 24 h with the indicated concentrations and HIF-1α expression was analyzed by Western blot. β actin served as a loading control. The bands represent one of three independent experiments. **(B)** NIH3T3 cells and HER-2/neu$^+$ cells were cultivated for 24 h with 2-ME or with DMSO before CREB phosphorylation and CREB protein expression was determined by Western blot. 50 µg total protein per lane were used. The blot represents one of two independent experiments. **(C)** Binding of CREB to the CRE element was determined by EMSA analysis. Nuclear extracts of HER-2/neu$^+$ cells were treated with DMSO or the indicated concentration of 2-ME prior to an EMSA reaction by incubating a biotinylated CRE oligonucleotide with the nuclear extract in reaction buffer. Following gel electrophoresis, the complexes were blotted onto a nylon membrane and DNA was detected with streptavidin-HRP. The diagram represents the densitometry of the shifted CREB-CRE complex obtained from two independent experiments. **(D)** The morphology of the 2-ME-treated cells was documented. The bar represents 50 µm. **(E)** Cell proliferation was measured by a BrdU ELISA in 96 well plate formats. Cells were incubated with BrdU and 2-ME or DMSO as the untreated control, respectively, for 24 h and the integrated BrdU was detected with a specific antibody after cell fixation. Columns represent the mean of three independent experiments with two technical replicates. The data were normalized to the DMSO-treated NIH3T3 control, which was set to 100%. **(F)** Metabolic or mitochondrial activity of the cells was measured by adding XTT reagent for 4 h to the cells after 24 h incubation period with the inhibitors. The absorption was determined with an ELISA reader. Columns represent mean values of three independent experiments with three technical replicates each. The data of all columns were normalized to the DMSO-treated NIH3T3 control, which was set to 100%.

In line with this observation, a reduced glucose uptake rate was recorded in CREB down-regulated HER-2/neu$^+$ cells (Figure 5C), which was further associated with significantly decreased expression levels of the glucose transporter GLUT1 (Figure 5D) as well as with diminished pyruvate and citrate concentrations (Figure 5E, 5F). Interestingly, the concentrations of both glycolytic metabolites were reduced in the oncogenic HER-2/neu$^+$ cell line after CREB knock down, but not in the parental NIH3T3 after diminishing of CREB by shRNA (Figure 5E, 5F). Under hypoxia the loss of pyruvate was even more pronounced in HER-2/neu$^+$ shCREB cells, while it was unchanged in NIH3T3 shCREB cells.

To validate if the loss of CREB binding activity has an effect on the cellular metabolism, two CREB inhibitors were used: 666-15, a potent inhibitor of CREB-regulated gene transcription [38], which disturbs the interaction of CREB and the CREB binding protein (CBP) resulting also in *in vivo* anticancer effects, and surfen, affecting the CREB-CRE complex [17, 39]. As determined by EMSA surfen prevented the formation of the CREB-CRE complex, while 666-15 had no effect on this interaction (Supplementary Figure 3A). Furthermore, surfen cannot displace ethidium bromide from the CRE oligonucleotide in a cell-free assay system (Supplementary Figure 3B) indicating that surfen did not bind to the CRE DNA element, but could interact with the basic leucine zipper of CREB. Both inhibitors diminished the proliferation by slowing down the cell cycle transition from the G1 to the S phase (Supplementary Figure 3C). This effect was more pronounced upon treatment with 666-15 than with surfen. Both 666-15 and surfen lowered the metabolic activity of HER-2/neu$^+$ cells, while 666-15 but not surfen diminished the metabolic activity of NIH3T3 cells (Figure 6A).

Using specific fluorescence dyes we could show that 666-15 treatment resulted in an accumulation of

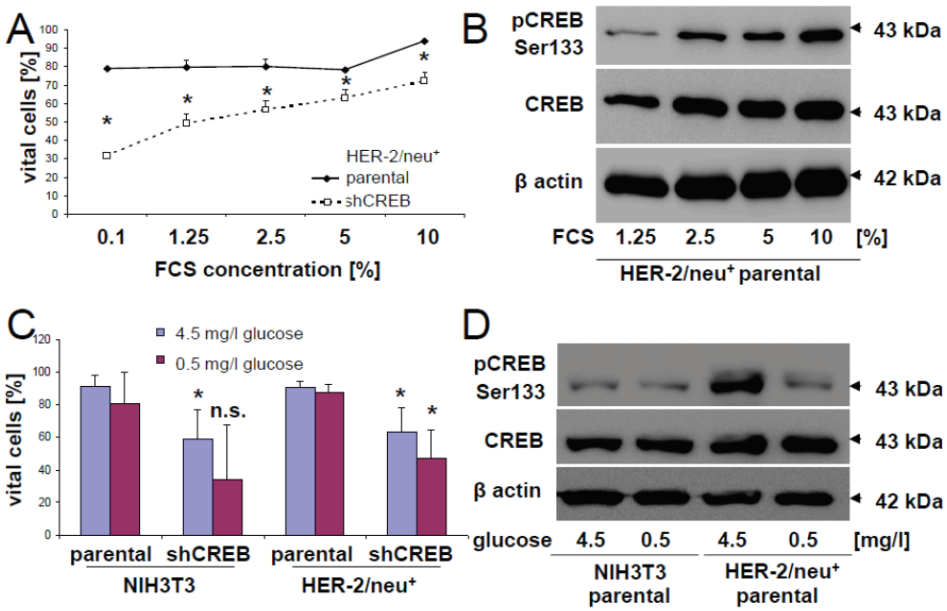


**Figure 4: Regulation of the phosphorylation rate of CREB by glucose and FCS.** **(A)** HER-2/neu$^+$ and shCREB derivatives were cultivated in EMEM supplemented with different FCS concentrations, before apoptosis was measured by flow cytometry after annexin V/PI staining as described in Materials and Methods. 5000 cells were measured per histogram and the experiment was independently repeated two additional times. **(B)** HER-2/neu$^+$ cells were incubated with the indicated concentrations of FCS and the corresponding phosphorylation rate of CREB (upper panel) and of total CREB (middle panel) were determined by immune blotting whereas the detection of β-actin served as loading control. The blot represents one of two experiments. **(C)** HER-2/neu$^+$ and shCREB derivatives were cultivated in RPMI with high (4.5 g/l) or low (0.5 g/l) glucose concentrations. The glucose content after addition of 10 % FCS was verified by DNSA measurement. The apoptosis rate of the cells after 24 h cultivation was quantified as described in (A). Data are the mean value and error bars from three experiments. **(D)** NIH3T3 and HER-2/neu$^+$ cells were cultivated under low and high concentrations of glucose, before the corresponding phosphorylation rate of CREB was analyzed by Western blot as described in Materials and Methods. The blot represents one of two experiments.

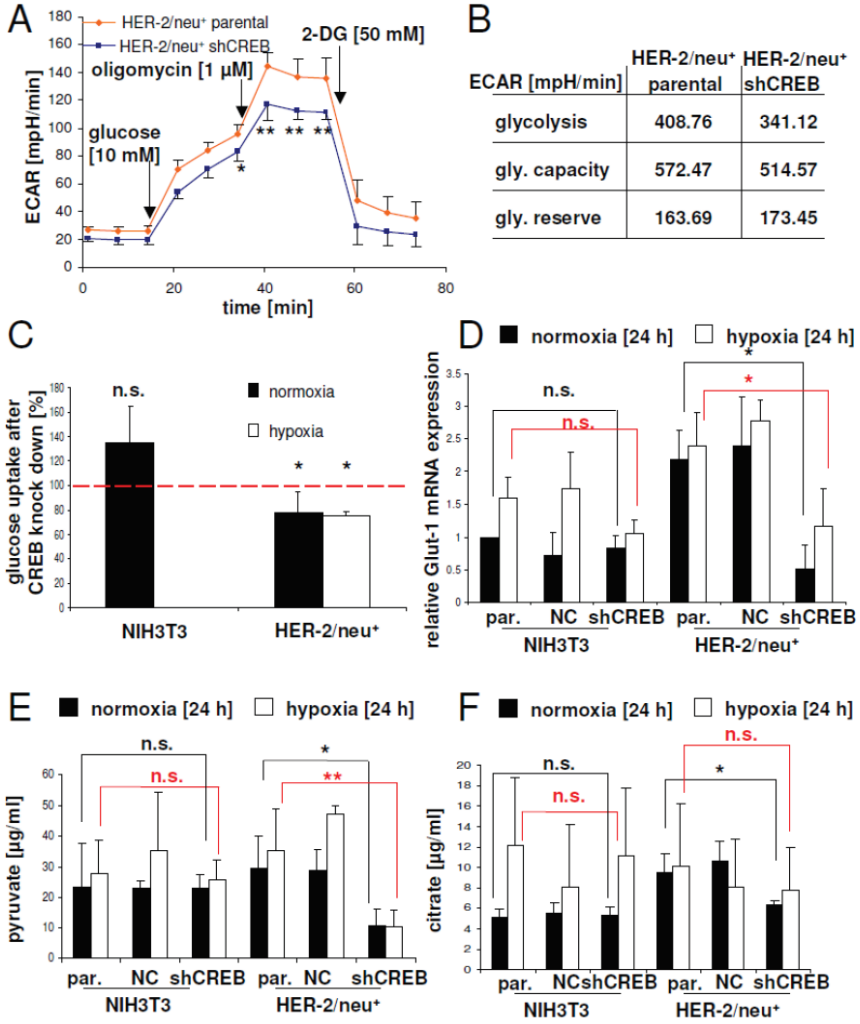


**Figure 5: CREB-mediated regulation of glucose uptake by Glut-1 expression and glycolysis.** **(A)** Glycolytic activity was measured by the extracellular acidification rate. At the indicated time points glucose, oligomycin or 2-desoxyglucose (2-DG) was added. Data represents four independent experiments with eight replicates. **(B)** Glycolytic capacity and reserve were calculated with the data from (A). **(C)** Glucose uptake in NIH3T3 and HER-2/neu$^+$ cells as well as their shCREB derivatives was analysed under normoxic and hypoxic conditions as described in Materials and Methods. Cells were seeded into 96 well plates with black walls in EMEM and were cultivated for 20 h under normoxic or hypoxic conditions. The cells were washed twice with PBS and 0.1 mM 2-NBDG was added. After 20 min. the cells were washed again with PBS and the plate was measured in a fluorescence ELISA at 485/525 nm. The experiment was repeated two more times. **(D)** The Glut-1 expression in shCREB transfectants and parental cell lines was determined by qPCR. The results are expressed as bar charts with mean and standard error from three independent experiments. The statistical analysis (between parental and shCREB cell lines) in black is from the normoxic dataset, while the red symbols are from the hypoxic dataset. Expression data were normalized to the cell line NIH3T3, which was set to "1". **(E, F)** The concentrations of pyruvate (E) and citrate (F) in cell lysates under normoxia and hypoxia were measured with colorimetrical tests. The results are expressed as bar charts with mean and standard error from four independent experiments with two wells each. The statistical analysis (between parental and shCREB cell lines) in black is from the normoxic dataset, while the red symbols are from the hypoxic dataset.

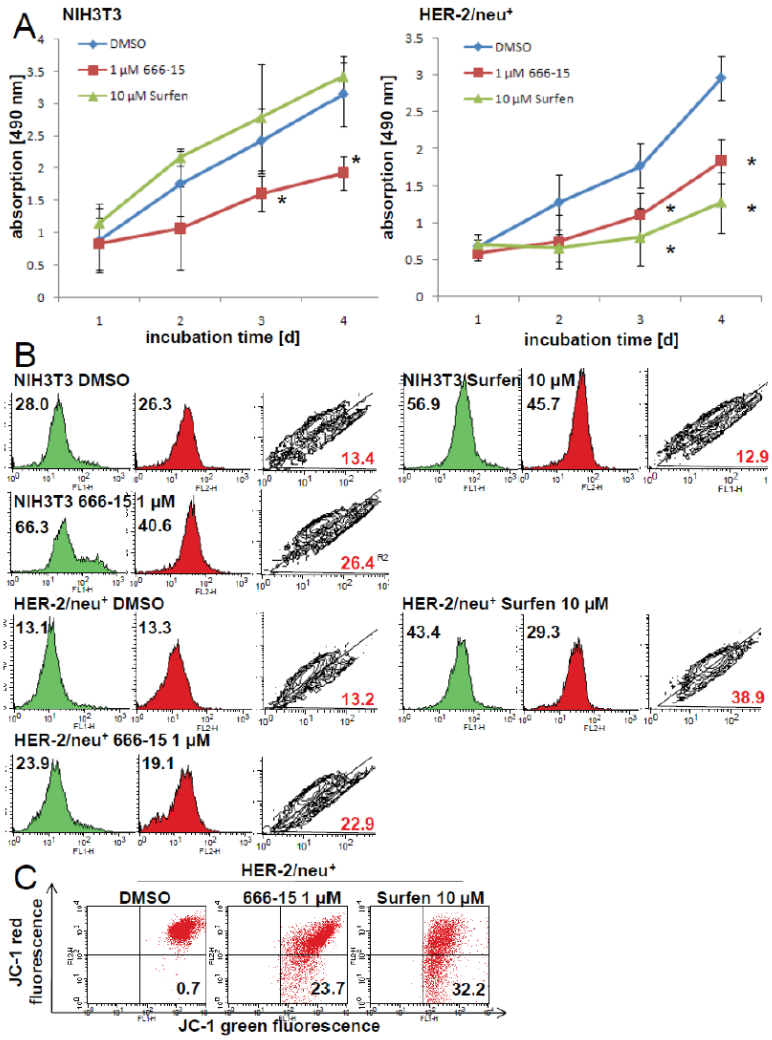


**Figure 6: Inhibition of the mitochondrial activity and increased amount of dysfunctional mitochondria by CREB inhibitors 666-15 and surfen.** **(A)** NIH3T3 and HER-2/neu$^+$ cells were incubated with 1 µM 666-15, 10 µM surfen or DMSO up to four days. For each time point XTT reagent was added for four h to the cell culture medium and cells were incubated at 37°C. Absorption was determined in 96 well plates with an ELISA reader. Data represents three independent experiments with three wells each. **(B)** The effect of the CREB inhibitors on "mitochondrial mass" and the mitochondrial activity was measured by staining the cultivated cells (24 h incubation period with the inhibitors) with 100 nM MitoTracker green and 100 nM MitoTracker red for 30 min following flow cytometrical analysis. 5000 events are displayed in every histogram and the mean fluorescence value is given in the histogram. Green areas are the MitoTracker green signals and the red filled histograms are the MitoTracker red signals. The contour plot shows the cells with dysfunctional mitochondria (R2) and the red number is the percentage of these cells with more mitochondrial "mass" (x axis) than mitochondrial activity (y axis). One out of three independent dataset is shown. **(C)** HER-2/neu$^+$ cells treated with 666-15 or surfen for 24 h were stained with the dye JC-1 for 20 min at 37°C and the complex formation was analyzed by flow cytometry. CCCP was used as a positive control to set the quadrants. The number in the lower right quadrant is the amount of cells with a decreased mitochondrial potential. Histograms are from one of two independent experiments.

dysfunctional mitochondria in HER-2/neu$^+$ and NIH3T3 cells, while for surfen treatment this effect was only detectable in the HER-2/neu-transformed cell line (Figure 6B). This accumulation of dysfunctional mitochondria can be explained by the CREB-regulated "master switch for mitochondrial biogenesis" peroxisome proliferator-activated receptor gamma coactivator 1α [32] or by the loss of autophagy-related proteins ATG5 and ATG7 (Supplementary Figure 4A), a mechanism that can prevent mitochondrial dysfunctions in several cell lines [40, 41]. Furthermore, under normoxia and hypoxia an increased intracellular lactate level was determined in HER-2/neu$^+$ shCREB cells (Supplementary Figure 4B). This can be caused by dysfunctional mitochondria and leading to an acidosis. Since pyruvate and citrate levels were decreased upon CREB knock down, we analyzed the levels of the metabolite acetyl-CoA. In both tested cell lines the concentration of acetyl-CoA was was increased when compared to the parental and to the vector control (Supplementary Figure 4C).

Since a loss of mitochondrial membrane potential was detected under treatment with both inhibitors (Figure 6C), the release of cytochrome c and ROS into the cytoplasm is suggested.

### Detoxification mechanisms regulated by CREB

One of the CREB-regulated proteins identified to be differentially expressed upon CREB down-regulation was catalase, an enzyme involved in the detoxification of hydrogen peroxide. Since oxidative stress can increase CREB phosphorylation and activity, the effect of

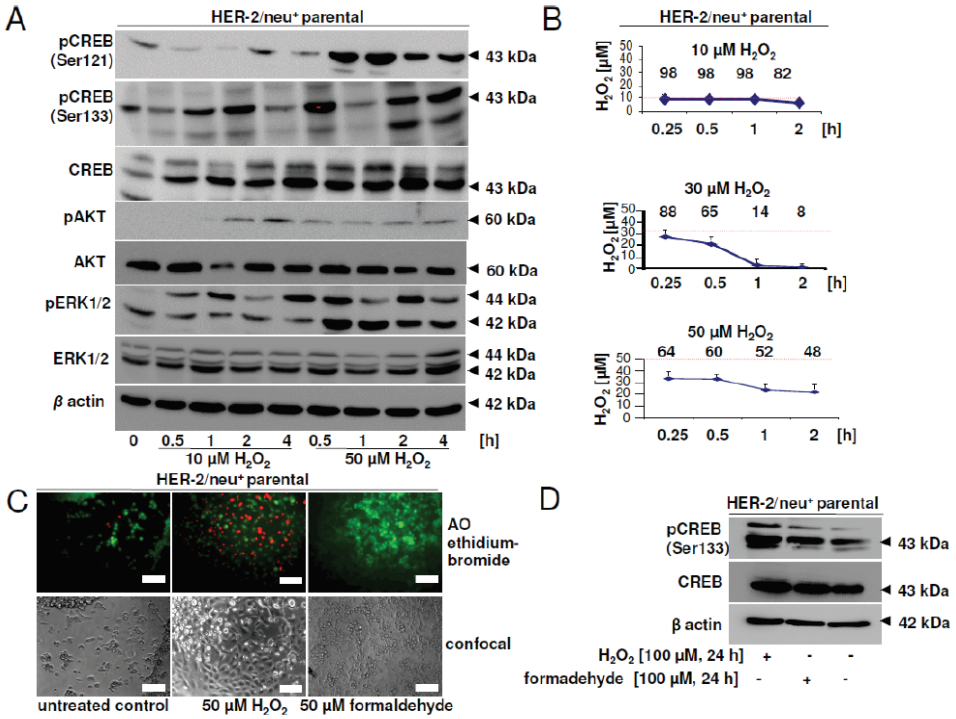


**Figure 7: Effect of hydrogen peroxide and formaldehyde on CREB activity and viability. (A)** HER-2/neu$^+$ cells were incubated with 10 or 50 μM $H_2O_2$ for the indicated time and phosphorylation of CREB, AKT and ERK was detected by Western blotting. Staining with an anti-β-actin mAb served as a loading control. The picture shows one of two independent Western blots. **(B)** Hydrogen peroxide in the cell culture supernatant was measured with the xylenol orange method and was compared to a standard curve. The red line indicates the starting concentration of $H_2O_2$ and the numbers are the remaining % of $H_2O_2$ at each time point. Data are the mean values from two independent experiments. **(C)** 80 % confluent cells were incubated with $H_2O_2$ or formaldehyde for 24 h and the dead cells were stained by adding 10 μM acridin orange and 10 μM ethidium bromide after treatment. Cells were visualized with a fluorescence microscope. The bar represents 50 μm. **(D)** Phosphorylation of CREB protein after long-term incubation with $H_2O_2$ or formaldehyde (24 h) was detected by specific antibodies as described in Materials and Methods. The experiment was performed three times and the blot is one representative picture.

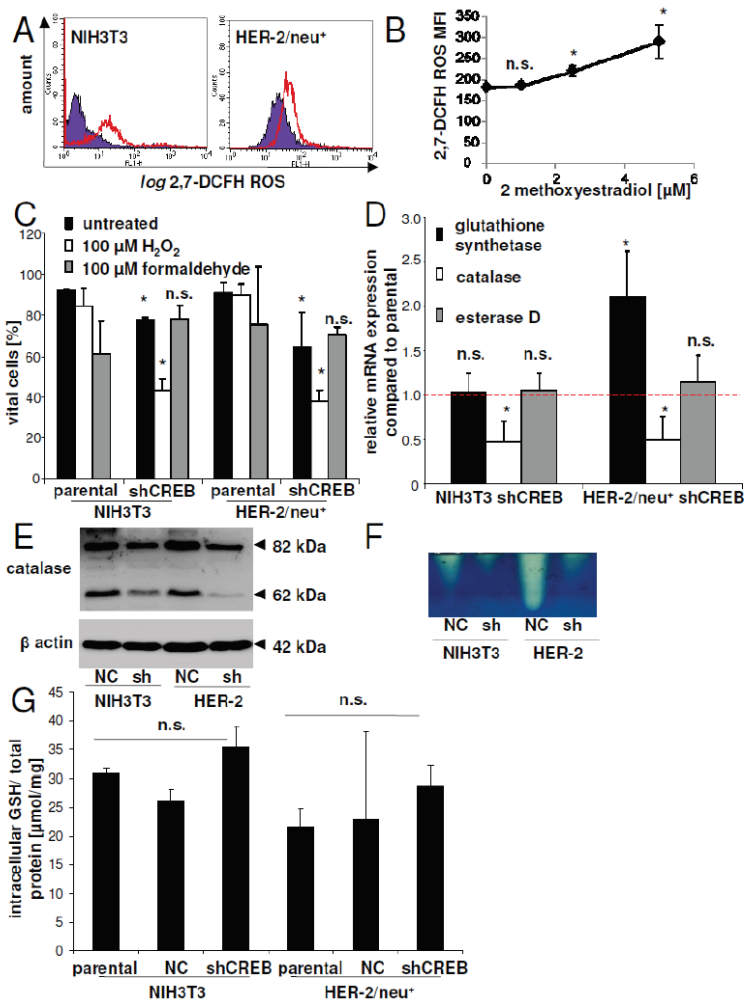


**Figure 8: Regulation of detoxification enzymes by CREB. (A)** The ROS status/cell was determined by flow cytometry after staining with the ROS sensitive dye 2,7-DCFH. 10,000 cells were measured for one replicate. shCREB cells are within the red bordered area, while parental cells (NIH3T3 or HER-2/neu$^+$ cells) can be found in the violet area. Representative histograms from one of three experiments are shown. **(B)** The mean 2,7-DCFH fluorescence intensity values of 2-ME treated cells was measured as in (A). The data points represents three independent experiments. **(C)** Viability of NIH3T3, HER-2/neu$^+$ and their CREB down-regulated counterparts treated with high concentrations of $H_2O_2$ or formaldehyde for 2 h was measured with annexin V and PI staining. After staining 10,000 cells were analyzed by flow cytometry and cell viability was compared to that of untreated cells. Columns represens mean values of three independent experiments. **(D)** mRNA expression of catalase, esterase D and glutathione synthetase was determined in the cell lines. The red dashed line indicates the mRNA expression in the parental cell lines (NIH3T3 or HER-2/neu$^+$), while the columns represent the mRNA expression in the CREB down-regulated cells. **(E)** Protein expression in NIH3T3 control cells (NC) and CREB down-regulated cells (shCREB) as well as in HER-2/neu$^+$ cells was determined by Western blot using catalase specific antibodies. The Western blot is representative from one out of three experiments. **(F)** Cell lysates were separated on native gels and catalase activity was visualized by a catalase specific staining. The picture shows one experiment and was repeated thrice. **(G)** GSH concentrations in the cell lysates were determined using the glutathione assay kit as described in Materials and Methods. The concentration was normalized to the protein concentration. Data represents mean values of three independent experiments with two replicates.

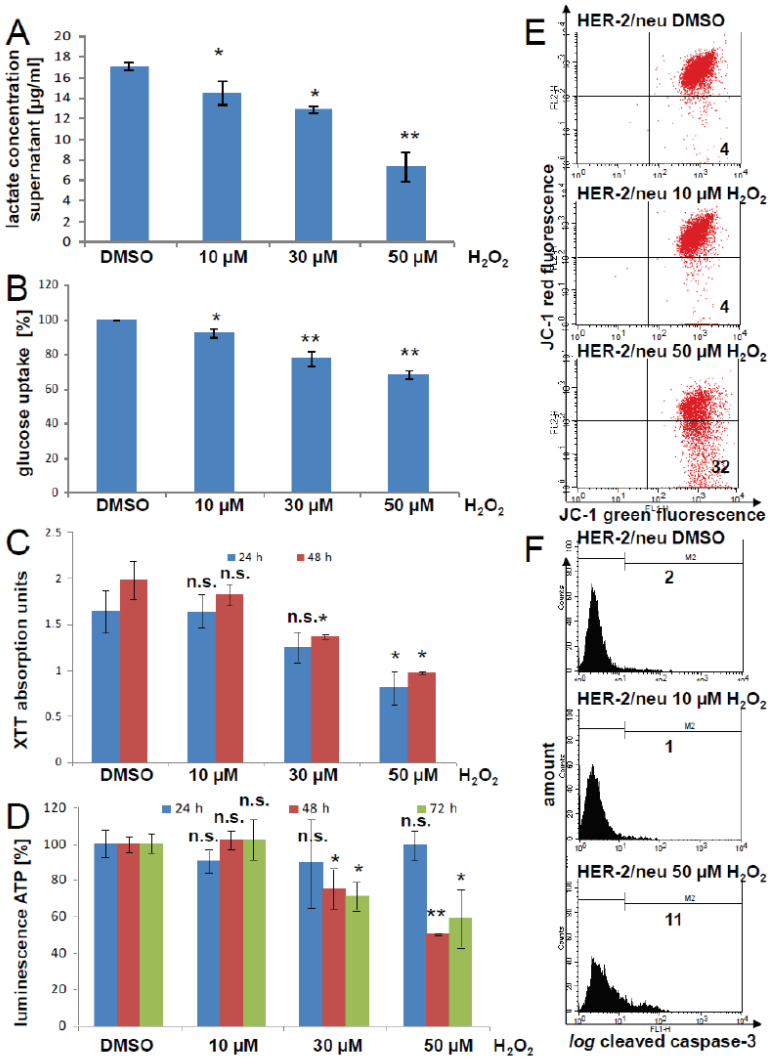


**Figure 9: Inhibition of the metabolic and mitochondrial activities by hydrogen peroxide in HER-2/neu$^+$ cells. (A)** The lactate concentration in the cell culture supernatant of HER-2/neu$^+$ cells incubated for 24 h with the indicated $H_2O_2$ concentration was measured with an enzyme assay kit. A lactate standard was used for the calibration. Data represents two independent experiments with three replicates per run. **(B)** Glucose uptake was determined fluorimetrically by cultivation of $H_2O_2$-treated cells for 15 min with 1 mg/ml 2-NDBG. Fluorescence units were normalized to the DMSO control. Columns represent three replicates with three wells each. **(C)** HER-2/neu$^+$ cells were incubated with the indicated concentration of $H_2O_2$ for 24 or 48 h and the mitochondrial activity was measured with XTT. Data represents two experiments with three replicates. **(D)** HER-2/neu$^+$ cells were incubated with the indicated concentration of $H_2O_2$ for 24, 48 or 72 h and ATP concentrations was analyzed by using the "CellTiter glo" system. Data represents two experiments with three replicates. **(E)** The effect of 10 and 50 M $H_2O_2$ for a 24 h cultivation period on the mitochondrial potential was determined by JC-1 staining and fluorescence analysis. The number in the lower right quadrant is the amount of cells with damaged mitochondrial membranes. 5,000 cells were measured for every dot plot. The histograms show one of three independent experiments. **(F)** Cleavage of the effector caspase-3 was monitored by flow cytometry by using a cleavage specific antibody. 5,000 cells / sample were determined. The histogram is representative and the experiment was repeated twice. M2 represents the cells with an activated caspase-3 and the percentage is given.

different concentrations of $H_2O_2$ on HER-2/neu$^+$ cells was determined. While low concentrations (10 µM) increased the CREB phosphorylation rate at Ser133, but not at Ser121 during 4 h, high concentrations of 50 µM $H_2O_2$ significantly increased CREB phosphorylation after 30 min. to 4 h (Figure 7A). The phosphorylation rate of AKT was strongly increased in response to exposure to 50 µM $H_2O_2$, while the phosphorylation level of ERK reached the maximal signal after a 4 h incubation period.

The most efficient detoxification of $H_2O_2$ was determined in the presence of 30 µM $H_2O_2$. Under these conditions almost 90 % of $H_2O_2$ was degraded after 2 h, while at higher or lower concentrations more than 50 % of the starting $H_2O_2$ levels remained still detectable in the given culture supernatants (Figure 7B). Exposure to 50 µM $H_2O_2$ significantly induced necrosis after 24 h (Figure 7C), which was absent at lower $H_2O_2$ concentrations (data not shown). Furthermore, incubation with formaldehyde over the same time had no effect on the vitality of the cells. However, long-term intervals (24 h) exposure resulted in increased phosphorylation rates of CREB (Figure 7D) regardless of the type of toxic compound ($H_2O_2$, formaldehyde).

Using the ROS sensitive dye 2,7-DCFH an accumulation of ROS in CREB down-regulated cells and in HER-2/neu$^+$ transformants was detected, which was higher than that of parental NIH3T3 cells (Figure 8A). In the presence of the HIF-1α inhibitor 2-ME an accumulation of ROS was also found in HER-2/neu$^+$ cells (Figure 8B). CREB knock down decreased the cell viability in the presence of $H_2O_2$ but not of formaldehyde-treated cells up to 60 % when compared to untreated cells (Figure 8C). We therefore analyzed the mRNA expression of three "detoxifying" enzymes important in cellular homeostasis: catalase, esterase D, an enzyme an enzyme involved in the detoxification of formaldehyde and glutathione synthetase, which is an important antioxidant. Only catalase mRNA expression levels were decreased in response to CREB

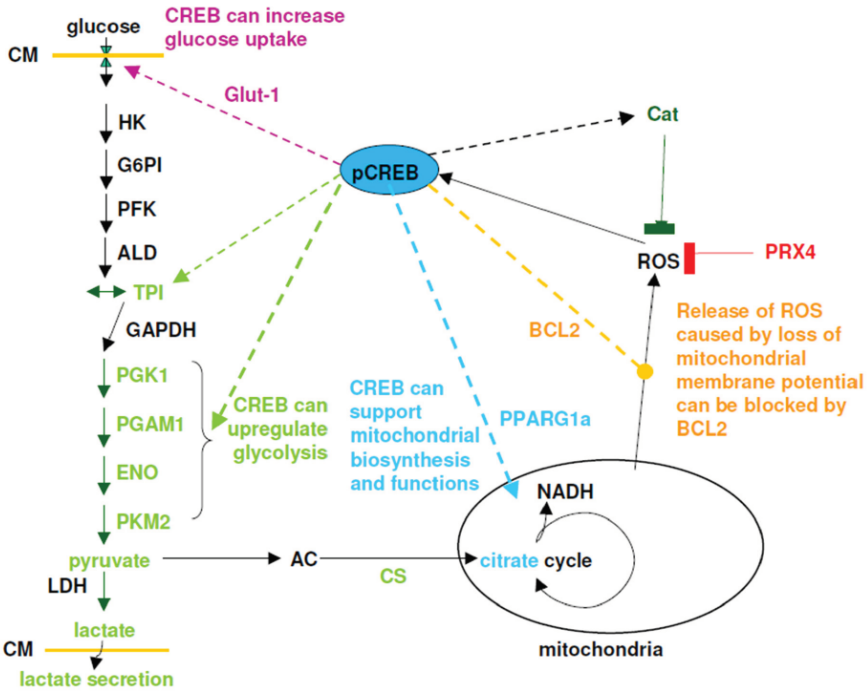


**Figure 10: Model for effect of CREB on glycolysis, mitochondrial activity and detoxification mechanisms.** Solid lines are reactions or reaction pathways, while dashed lines indicates mechanisms regulated by CREB.
Abbreviation used: CM = cytoplasma membrane, Glut1 = glucose transporter, HK = hexokinase, G6PI = glucose-6-phosphate isomerase, PFK = phospho-fructokinase, ALD = aldolase, TPI = triosephosphate isomerase, GAPDH = glycerin-3-phosphate dehydrogenase, PGK1 = phospho glycerate kinase, PGAM1 = phosphoglycerate mutase, ENO = enolase, PKM2 = pyruvate dehydrogenase, LDH = lactate dehydrogenase, AC = acetyl-CoA, CS = citrate synthase, PPARG1a = peroxisome proliferator activated receptor gamma, cat = catalase, PRX4 = peroxiredoxin 4, bcl2 = B-cell lymphoma 2.

down-regulation, while the mRNA expression levels of esterase D was not altered (Figure 8D). The decreased mRNA expression levels of catalase was accompanied by diminished catalase protein expression (Figure 8E) and consequently by a lower catalase activity (Figure 8F). In addition, glutathione synthetase was 2.1-fold up-regulated in CREB down-regulated HER-2/neu$^+$ cells, but not in the parental NIH3T3 cells. However, free glutathione remained unaltered in all cell lines analyzed (Figure 8G).

### Disturbation of glycolysis and mitochondrial functions by ROS

Next, we tested the effect of $H_2O_2$ as a ROS on the glycolysis and the mitochondrial activity. In the culture supernatant of $H_2O_2$-treated cells lower concentrations of lactate was detectable than in the DMSO control (Figure 9A). Furthermore, $H_2O_2$ reduced the uptake of glucose as determined using the glucose analogue 2-NBDG (Figure 9B). Both mechanisms were concentration dependent. This led to lower metabolic activity (Figure 9C) and reduced ATP production (Figure 9D), which was not only due to a decreased cell proliferation (Supplementary Figure 5). However, higher concentrations of $H_2O_2$ decreased mitochondrial membrane potential (Figure 9E), as well as induced the cleavage of caspase-3 (Figure 9F).

## DISCUSSION

Major advances have been made in our understanding of the molecular mechanism of CREB function in malignant transformation and its association with hypoxia [17], but so far there exists only little information about the role of CREB in modulation of the cellular metabolism. Therefore, the aim of this study was to determine the effects of CREB and/or hypoxia-induced pathways on the cellular metabolism. Using 2-DE-based proteomic profiling of HER-2/neu$^+$ versus HER-2/neu$^+$ shCREB cells differentially expressed proteins were identified mainly involved in cell metabolism and localized in the cytoplasm. In particular, the expression of proteins associated with the glycolysis was altered. Validation of the CREB-regulated genes revealed in some cases a coordinated down-regulation of the respective mRNA and protein expression levels, while e.g. PGK 1 transcription remained unchanged upon CREB modulation, but altered at the protein level suggesting a posttranscriptional control. Thus, metabolic changes mediated by CREB seem to occur at both the transcriptional as well as at the posttranscriptional level. In this context it is also noteworthy that hypoxia could lead to posttranslational modifications of CREB [32]. The increased glycolysis of HER-2/neu$^+$ cells was in accordance with the neoplastic properties of these cells. Different phosphorylation of CREB serine residues can affect metabolic enzymes, like PEPCK [42].

The altered metabolism due to HER-2/neu-controlled CREB overexpression modulates the TME. High lactate concentrations and low pH values were found in the supernatant of HER-2/neu$^+$ cells, which might affect the anti-tumoral immune response. Indeed, acidic pH values could negatively interfere with the activity and function of effector T cells, dendritic cells as well as NK cells [43]. Furthermore, the direct influence of CREB on the cellular metabolism was strengthened by altered intra-cellular LDH levels. LDH representing the key enzyme of the glycolytic cascade and converting pyruvate to lactate is a CREB target [44]. Up-regulation of LDH levels led to an increased aerobic glycolysis, while CREB knock down not only reduced LDH levels in our HER-2/neu model system, but also in breast cancer [45]. The activation of the MEK/ERK pathway by HER-2/neu increased the CREB binding to the CREB-binding site (CRE) in the LDH promoter leading to its transcriptional up-regulation [46]. Furthermore, loss or reduced LDH expression abrogated cell proliferation *in vitro* and tumor formation *in vivo* in particular in triple negative mammary carcinoma [47], while high levels of LDH expression could be associated with poor patients' outcome and inhibition of immune surveillance [48].

Comparative analysis of HER-2/neu$^+$ and HER-2/neu$^+$ shCREB cells demonstrated that CREB suppression correlated with an increased respiration and respiratory reserve. Thus, CREB-controlled altered metabolism was also associated with a reduced sensitivity to undergo apoptosis since HER-2/neu$^+$ cells were able to grow under limited serum and glucose concentrations. This could be even further altered under hypoxic conditions leading to pronounced changes of the intracellular lactate dehydrogenase levels, extracellular lactate concentrations as well as extracellular pH values. *In silico* analysis of the transcriptional profile of chronic myeloid leukemia cells, in which CREB was knocked out demonstrated an upregulation of genes involved in tumor initiation and progression as well as in hypoxic signaling [49]. Since tumors with a higher glycolytic rate were associated with a worse prognosis accompanied by a poor clinical outcome of patients [48, 50], targeting of metabolic pathways might become an attractive therapeutic approach to treat cancer patients.

Increased ROS accumulation could be caused by mitochondrial dysfunction through the endoplasmic reticulum [51]. Furthermore, decreased mitochondrial activity implemented by mitochondrial dysfunction could activate CREB [52], which could in turn promote mitochondrial biogenesis [32]. Therefore, we tested whether oxidative stress like hydrogen peroxide could induce CREB activity *in vitro*. By upregulation of the AKT pathway the phosphorylation of CREB at Ser 133 was increased. Similar results were reported in a PKA-independent pathway by Pregni and co-authors [53] in neuronal cells, while treatment of melanoma cells with $H_2O_2$ increased CREB

expression by the cAMP/PKA pathway [54]. Furthermore, $H_2O_2$ could stimulate phosphorylation of CREB by AKT thereby promoting mitochondrial respiration and biosynthesis [55], while the expression levels of esterase D (formyl glutathione hydrolase), an enzyme important for formaldehyde detoxification and upregulated by K-Ras mutations in murine fibroblasts [56], were not altered under these conditions.

CREB supports metabolism in several ways: First it can up-regulate the expression of Glut-1, therefore increasing uptake potential of glucose and intracellular glucose levels. Second, it can positive regulates some glycolytic enzymes (PKM2, TPI, alpha-enolase). Third it can enable mitochondrial respiration and biogenesis under stress conditions like hypoxia and ROS, therefore allowing a better survival of tumor and tumor cell (Figure 10).

However, further research is required for better understand the role of TFs, like CREB, in the mitochondria and their effect on the regulation of the cellular metabolism and oxidative stress under physiologic, but also pathophysiologic conditions [57].

## MATERIALS AND METHODS

### Cell culture, hypoxia, drug treatment and glucose uptake

The generation and culture conditions of HER-2/neu$^-$ NIH3T3 cells, their HER-2/neu$^+$ derivative and their respective CREB variants have been recently described [11, 34]. HER-2/neu-overexpressing cells with high levels of pCREB were termed HER-2/neu$^+$ cells, HER-2/neu$^+$ cells, in which CREB was down-regulated by shCREB were termed HER-2/neu$^+$ shCREB cells.

For determination of the impact of FCS and glucose concentrations on the cell growth, cells were cultivated in 1 – 10 % FCS and 0.5 – 4.5 g/l glucose, respectively.

For hypoxia induction, cells were incubated in a 1 % (v/v) $O_2$, 5% (v/v) $CO_2$ atmosphere at 37°C for the indicated time spans [32]. Normoxic controls were cultured using standard conditions.

Cells were treated for 24 – 48 h with different inhibitors (HIF-1α inhibitor 2-methoxyestradiol, CREB-CBP inhibitor 666-15 (Tocris), CREB-CRE inhibitor surfen (Sigma), proton pump inhibitor Esomeprazole) and toxic components ($H_2O_2$, formaldehyde). Cytotoxicity of the substances was analyzed by treatment of cells with increasing concentrations of these inhibitors to determine the $IC_{50}$ value by using the cytoto assay kit (Promega). Glucose uptake was determined as recently described in detail [58].

### RNA isolation, cDNA synthesis, qPCR

Total cellular RNA from 5 x $10^5$ cells/sample was extracted and subjected to qPCR analysis as recently described [11]. The specific primer sequences and PCR conditions used were provided in Supplementary Table 1. Relative expression levels were calculated according to the ΔCt method and normalized against β-actin and/or GAPDH as internal controls. Three independent experiments were performed.

### Protein isolation, western blot analysis and CREB ELISA

Total protein was isolated from 5 x $10^6$ cells/sample and the resulting lysates subjected to Western blot analysis as recently described [11] using the panel of antibodies listed in Supplementary Table 2. Blot membranes were stripped with 2.5 M glycine (pH 2) for 15 min. and were then re-probed with a new antibody after re-blocking with skim milk. For data analysis, three independent experiments were used.

The loss of CREB phosphorylation and protein was further quantified with a CREB specific ELISA system (Cayman). 10 µg total protein were incubated with the antibody coated plates for 1 h at 25°C before CREB phosphorylation and CREB protein expression were determined by adding the primary antibody. After three washing steps the samples were incubated with the HRP-linked secondary antibody for 30 min., washed three times and reaction was started by adding TNB substrate. After 30 min. the reaction was stopped with 1 mM acetic acid and absorption was measured af 490 nm. Three biological samples with three reactions were measured with each cell line.

### Flow cytometry

Cells were harvested after cultivation for 24 h under normoxia or hypoxia, respectively, and then stained for 20 min. with an anti-HER-2/neu-PE-conjugated (Becton Dickinson) antibody or with the IgG1-PE conjugated isotype control (BD), respectively, as recently described [59]. Fluorescence intensity was determined by flow cytometry on a FACSCalibur (BD). The results were expressed as mean specific fluorescence intensity (MFI) of three independent experiments.

For measuring the mitochondrial mass and the mitochondrial activity per single cell, the fluorescent dyes MitoTracker green (Cell signaling) staining the mitochondrial membrane, and MitoTracker red CFXRos (Invitrogen), which changed to a fluorescent dye under mitochondrial activity, were used. Cell pellets were resuspended in PBS supplemented with 100 nM of both dyes and then stained for 30 min. at 37°C in the dark. Cells were washed with PBS and directly analyzed by flow cytometry. Three biological replicates were used for every condition.

### Determination of apoptosis and caspase-3 activation

Annexin V - propidium iodide staining was used for the detection of apoptotic and necrotic cells as previously

described [11]. For fluorescence analysis, 10 µM acridine orange and 10 µM ethidium bromide were added to the given cell culture. After a 10 min incubation period the samples were analyzed by fluorescence microscopy using both green / red filter settings. Three biological replicates with three biological replicated each were photographed.

To determine the caspase-3 activation through cleavage, the FITC Active Caspase-3 Apoptosis Kit (BD) was used following the manufacturer's instruction. Briefly, 2.5 x $10^6$ cells were fixed in 500 µl cytofix/cytoperm at 4°C for 30 min., and then washed once with 1 ml cytowash, before they were stained in 100 µl cytowash and 10 µl anti-active-caspase-3-FITC for 30 min. After one additional washing step, 1x$10^5$ cells/sample were analyzed on a FacsCalibur (BD). The experiment was independently repeated twice.

### Determination of $H_2O_2$ concentrations and enzyme activities

The concentration of $H_2O_2$ in the culture media was determined by the xylenol orange-$Fe^{2+}$ method described by Gay and co-authors [60]. The enzymatic activity of PKM in cell lysates was measured by the method of Tietz and Ochoa [61]. 100 µl cell lysate were incubated with reaction puffer (50 mM Tris HCl pH 7.5, 4 mM $MgCl_2$, 75 mM KCl, 0.2 mM ADP, 1.5 mM PEP, 0.2 mM NADH, 12 U/ml LDH) for 5 min. at room temperature. The reaction was started by addition of pyruvate kinase (end concentration 0.3 U/ml) and the absorbance change at 340 nm was recorded for 5 minutes.

Activity of prolyl endopeptidase was determined fluorometrically by the cleavage of the substrate Z-glycyl-prolyl-4-methylcoumarinyl-7-amide as described by Goossens and co-workers [62] with the following modifications: 100 µl of cell lysate were diluted with 100 µl incubation buffer (100 mM $KH_2PO_4$ pH 7.4, 100 µM $NaN_3$, 1 mM DTT, 1 mM EDTA). Next the samples were incubated for 15 min. at 37°C and 10 µl of substrate was added (5 mM in DMSO). After incubation for 2 h in the dark at 37°C 500 µl 1.5 mM acetic acid were added and mixed. Fluorescence was analyzed with an ELISA reader (Tecan) with $\lambda_{ex}$ 370 nm and $\lambda_{em}$ 440 nm.

PGAM1 activity was measured following the protocol published by Hallows and co-authors [63].

TPI enzyme activity in cell lysate was analyzed by adding 2 ml reaction buffer (220 mM triethanolamine HCl, pH 7.6, 3 µM DL-glyceraldehyde-3-phosphate, 0.26 µM NADH, 50 mU glycerol-3-phosphate dehydrogenase, 0.2 U/ml triose phosphate isomerase) to 100 µl of cell lysate. The decrease in absorbance at 240 nm was recorded by a spectrometer.

PGK activity was determined by ATP formation: 100 µl cell lysate were mixed with 50 mM potassium phosphate, 5 mM 1,3-bisphosphoglycerate, 1 mM ADP, 5 mM $CaCl_2$. The formation of $Ca_3(PO_4)_2$ was measured by 340 nm after incubation by 25°C for 15 min.

For determination of the PRX 4 activity the protocol from Nelson and Parsonage [64] was used.

The enzymatic activity was normalizied to the total protein concentration in the cell lysate. All experiments were performed with three cell preparations.

### Extracellular flux assays

Bioenergetics of CREB down-regulated and CREB expressing HER-2/$neu^+$ and HER-2/$neu^-$ control cells were determined using the XF96e Extracellular Flux analyzer (Seahorse Bioscience) as recently described [65]. Briefly, 2x$10^5$ cells/well were reseeded in specialized tissue culture plates (96FX micro well plate) and subsequently immobilized using CELL-TAK (BD Biosciences). One hour prior measurement, cells were incubated at 37°C in a $CO_2$-free atmosphere. First, the basal extracellular acidification rate (ECAR), as an indicator for lactic acid production or glycolysis, was recorded. In the next step ECAR in response to the application of 1 µM oligomycin (XF Cell Mito Glyco Test Kit, Seahorse Bioscience) as well as 10 mM glucose was evaluated. All experiments were performed in four independent experiments with at least hexaplicates.

### Determination of lactate, pyruvate, citrate levels, acetyl-CoA and glucose concentrations in cell culture supernatants and cell lysats

The amount of lactate in 100 µl cell culture supernatants was analyzed with a lactate detection kit (Sigma) according to the manufacturer's instructions in a 96 well plate format. The deproteinated samples were measured at 570 nm in an ELISA reader (Tecan) after enzymatic reaction. Three independent experiments were performed using three technical replicates in each run and the results were expressed as mean ± SD using bar charts.

For the detection of pyruvate and citrate in cell lysates commercial kits (Biovision) were used following the manufacturer's protocol. Samples and standards were measured with an ELISA reader as described above.

Acetyl-CoA was measured fluorimetrically with an acetyl-CoA assay kit following the manufacturer's instructions (Sigma).

The amount of glucose in the culture medium was controlled with the DNSA method as described by Miller [66].

### Proliferation and cell cycle analysis

Proliferation of treated cells was determined by measuring the DNA synthesis with the cell proliferation ELISA, BrdU (colorimetric) kit (Roche). 5 x $10^4$ cells were seeded per 96/well and were treated with or without

$H_2O_2$. The inclusion of BrdU was analyzed following the manufacturer's instructions. Three biological replicates with three biological sample each were analyzed at an ELISA reader (Tecan).

For cell cycle analysis the DNA content per cell was measured as described previously [11]. Briefly, after synchronization of the cells by serum deprivation (0.5% FCS) for 48 h, cells were incubated with media containing inhibitors and 10% FCS for the indicated time span. The cells were fixed after harvesting in 70% ethanol for at least 24 h by 4°C, following the isolation of nucleus by washing once with PBS, 0.5% tween 20 and then PBS, 0,5% tween 20 and 100 mM citrate. RNA was digested with RNase A treatment and DNA was stained with 0.1 mg/ml PI. DNA content was measured with a FacsAria III (BD) with three biological replicates for each condition.

### CREB – DNA binding analysis

Binding of CREB to the CRE DNA element was analyzed by an EMSA. Nuclear extracts of HER-2/neu$^+$ cells were incubated with a biotinylated oligonucleotide (TGACGTCA) and the testing substances as described by Bukur and co-authors [59].

Furthermore, the ethidium bromide displacement assay was used to determine whether surfen interacts with the CRE element and therefore prevents binding of CREB or whether surfen binds to the CREB protein. The assay was conducted as published in Rishi and co-workers [67] for three times independently. The following hairpin oligonucleotids were used: TGACGTCAAAAAATGACGTCA (CREB), TGACTCAAAAAATGACTCA (AP1), TTAATTAAAAAA ATTAATTAA (AT rich), GGCCGGCCAAAAAGGCC GGCC (GC rich).

### Detection of reactive oxygen species (ROS)

Cells were incubated in 10 µM 2',7'-dichlorodihyd rofluorescein diacetate (2,7-DCFH) for 15 min. at room temperature and then were washed twice with PBS. Fluorescence intensity was analysed by flow cytometry (BD) as recently described [68].

### Determination of glutathione levels

The glutathione levels were determined using the GSH/oxidized GSH ratio kit (Calbiochem) as previously described [56]. Briefly, 1 x $10^6$ cells were incubated for 48 h, washed twice with PBS, scratched of the plates and resuspended in 100 µl PBS. After cell lysis obtained by 6 cycles of freezing and thawing 900 µl 5 % (w/v) meta phosphoric acid/sample was added. 50 µl of the cell supernatant was analyzed according to the manufacturer's instructions at 412 nm in a spectrometer (Merck). The amount of glutathione was correlated to the protein concentration determined with the bicinchoninic acid kit (Thermo).

### Catalase activity staining

Catalase staining was performed according to Weydert and Cullen [69]. 150 µg non-denaturated total protein lysate was separated with a native 8 % PAGE gel in a cold room (6°C) at ~40 mA for 6 to 8 h. After electrophoresis the gel was washed with aqua dest. and incubated for 10 min by RT in 0.03 % $H_2O_2$. After washing twice with aqua dest. the gel was stained in 2 % (w/v) $FeCl_3$ and 2 % (w/v) $K_3[Fe(CN)_6]$) until clear bands appeared. Finally, the gels were extensively washed with water and documented with a gel scanner. Four single protein lysates were used for every condition.

### Intracellular pH measurement

1 x $10^6$ cells were stained with 0.1 µM BCECF-AM for 30 min. at 4°C and washed twice with culture medium. 1 x $10^4$ cells/well were seeded into a black 96 well plate with a clear bottom and incubated at 37 °C for 24 h under normoxic or hypoxic conditions. The fluorescence intensity/ well was determined in a fluorescence reader (Tecan, excitation wavelength 480 nm, emission wavelength 535 nm). For the analysis of pH stability and the regeneration time under normoxia, the fluorescence intensity was monitored for one h. For the standard curve the cells were incubated in buffer with known pH whereas nigericin-KCl (25 µM and 125 mM) was used for permeabilization.

### 2D gel electrophoresis, spot digestion and mass spectrometry

For determination of the differential protein expression pattern upon CREB down-regulation, 2-DE-based proteome analysis followed by mass spectrometry was performed as recently described [58]. Three biological replicates with four to six technical replicates (gels) were used for proteome analysis. Coomassie stained gels were documented with a gel scanner and gel pictures were compared with the Delta2D software (Decodon). The cut-off for up and down-regulation of protein spot was $< 0.5$ and $> 2.5$. Putative CREB-regulated proteins were cut-out with an automatic spot picker (Spothunter, Herolab) and prepared for MALDI TOF/TOF-MS with a α-cyano-hydroxycinnamic acid matrix. MS data were identified with the Mascot database. Protein spots with a score value higher than 55 and found in all three biological replicates were used for further validation processes.

### Statistical analysis

Differences between groups were analyzed by Mann-Whitney test, Student's t test or ANOVA as appropriate. Data are expressed as mean ± SD and the corresponding $p$ values reported are 2-sided. Significance was accepted if $p$ values were $\leq 0.05$ ($^*$). The statistical

analysis of the graphs and tables compares the CREB diminished cells with their parental cell lines (NIH3T3 or HER-2/neu$^+$) if nothing else is stated in the figure legend. For the analysis of putative CRE regions in the listed gene promoter sequence the CREB target gene database (natural.salk.edu/CREB/) was used [70].

### Abbreviations

2-ME, 2-methoxyestradiol; 2-NBDG, 2-[N-(7-nitrobenz-2-oxa-1,3-diazol-4-yl)amino]-2-deoxy-D-glucose; 2-DE, two-dimensional gel electrophoresis; 2,7-DCFH, 2',7'-dichlorodihydrofluorescein diacetate; ATCC, American Tissue Culture Collection; CaMK, calcium activated calmodulin kinase; CBP, CREB binding protein; CRE, cAMP-responsive element; CREB, cAMP-responsive element binding protein; ECAR, extracellular acidification rate; EMSA, electromobility shift assays; ENO, enolase; ERK, extracellular-signal regulated kinase; ESOM, Esomeprazole; FGF, fibroblast growth factor; GLUT, glucose transporter; GSH, glutathione; KID, kinase-inducible domain; KIX, KID-interacting domain; LDH, lactate dehydrogenase; mAb, monoclonal antibody; MALDI-TOF, matrix-assisted laser desorption/ionization time-of-flight; MAPK, mitogen-activated protein kinase; MCT, monocarboxylate transporter; MEK, MAP/ERK kinase; MFI, mean fluorescence intensity; NF, nuclear factor; OCR, oxygen consumption rate; p, *p*-value; PBS, phosphate-buffered saline; pCREB, phosphorylated CREB; PEP, prolyl endopeptidase; PGK, phosphoglycerate kinase; PGAM, phosphoglycerate mutase; PKA, protein kinase A; PKM, pyruvate kinase; PRX, peroxiredoxin; PTM, post-transcriptional modification; qPCR, quantitative PCR; ROS, reactive oxygen species; RTK, receptor tyrosine kinase; TF, transcription factor; TME, tumor microenvironment; TPI, triose phosphate isomerase; UTR, untranslated region.

## ACKNOWLEDGMENTS AND FUNDING

We would like to thank Sylvi Magdeburg for excellent secretarial work.

This work was supported by the Mildred Scheel Foundation (BS).

## CONFLICTS OF INTEREST

The authors declare that they have no conflicts of interest.

## REFERENCES

1. Johannessen M, Moens U. Multisite phosphorylation of the cAMP response element-binding protein (CREB) by a diversity of protein kinases. Front Biosci. 2007; 12:1814-32.
2. Finkbeiner S. New roles for introns: sites of combinatorial regulation of Ca2+- and cyclic AMP-dependent gene transcription. Sci STKE. 2001; 2001(94):pe1.
3. Mayr B, Montminy M. Transcriptional regulation by the phosphorylation-dependent factor CREB. Nat Rev Mol Cell Biol. 2001; 2:599-609.
4. Melnikova VO, Dobroff AS, Zigler M, Villares GJ, Braeuer RR, Wang H, Huang L, Bar-Eli M. CREB inhibits AP-2alpha expression to regulate the malignant phenotype of melanoma. PLoS One. 2010; 5:e12452.
5. Radhakrishnan I, Pérez-Alvarado GC, Parker D, Dyson HJ, Montminy MR, Wright PE. Solution structure of the KIX domain of CBP bound to the transactivation domain of CREB: a model for activator:coactivator interactions. Cell. 1997; 91:741-52.
6. Rudolph D, Tafuri A, Gass P, Hämmerling GJ, Arnold B, Schütz G. Impaired fetal T cell development and perinatal lethality in mice lacking the cAMP response element binding protein. Proc Natl Acad Sci U S A. 1998; 95:4481-6.
7. Cho EC, Mitton B, Sakamoto KM. CREB and leukemogenesis. Crit Rev Oncog. 2011; 16:37-46.
8. De Giovanni C, Nicoletti G, Quaglino E, Landuzzi L, Palladini A, Ianzano ML, Dall'Ora M, Grosso V, Ranieri D, Laranga R, Croci S, Amici A, Penichet ML, et al. Vaccines against human HER2 prevent mammary carcinoma in mice transgenic for human HER2. Breast Cancer Res. 2014; 16:R10.
9. Stahler A, Heinemann V, Neumann J, Crispin A, Schalhorn A, Stintzing S, Giessen-Jung C, Fischer von Weikersthal L, Vehling-Kaiser U, Stauch M, Quietzsch D, Holch JW, Kruger S, et al. Prevalence and influence on outcome of HER2/neu, HER3 and NRG1 expression in patients with metastatic colorectal cancer. Anticancer Drugs. 2017; 28:717-22.
10. Gutierrez C, Schiff R. HER2: biology, detection, and clinical implications. Arch Pathol Lab Med. 2010; 135:55-62.
11. Steven A, Leisz S, Massa C, Iezzi M, Lattanzio R, Lamolinara A, Bukur J, Müller A, Hiebl B, Holzhausen HJ, Seliger B. HER-2/neu mediates oncogenic transformation via altered CREB expression and function. Mol Cancer Res. 2013; 11:1462-77.
12. Abramovitch R, Tavor E, Jacob-Hirsch J, Zeira E, Amariglio N, Pappo O, Rechavi G, Galun E, Honigman A. A pivotal role of cyclic AMP-responsive element binding protein in tumor progression. Cancer Res. 2004; 64:1338-46.
13. Braeuer RR, Zigler M, Villares GJ, Dobroff AS, Bar-Eli M. Transcriptional control of melanoma metastasis: the importance of the tumor microenvironment. Semin Cancer Biol. 2011; 21:83-8.
14. Chhabra A, Fernando H, Watkins G, Mansel RE, Jiang WG. Expression of transcription factor CREB1 in human breast

cancer and its correlation with prognosis. Oncol Rep. 2007; 18:953-8.

15. Fan CF, Mao XY, Wang EH. Elevated p-CREB-2 (ser 245) expression is potentially associated with carcinogenesis and development of breast carcinoma. Mol Med Rep. 2012; 5:357-62.
16. Pigazzi M, Manara E, Bresolin S, Tregnago C, Beghin A, Baron E, Giarin E, Cho EC, Masetti R, Rao DS, Sakamoto KM, Basso G. MicroRNA-34b promoter hypermethylation induces CREB overexpression and contributes to myeloid transformation. Haematologica. 2013; 98:602-10.
17. Steven A, Seliger B. Control of CREB expression in tumors: from molecular mechanisms and signal transduction pathways to therapeutic target. Oncotarget. 2016; 7:35454-65. https://doi.org/10.18632/oncotarget.7721.
18. Wang X, Cui H, Lou Z, Huang S, Ren Y, Wang P, Weng G. Cyclic AMP responsive element-binding protein induces metastatic renal cell carcinoma by mediating the expression of matrix metallopeptidase-2/9 and proteins associated with epithelial-mesenchymal transition. Mol Med Rep. 2017;15:4191-8.
19. Deng X, Liu H, Huang J, Cheng L, Keller ET, Parsons SJ, Hu CD. Ionizing radiation induces prostate cancer neuroendocrine differentiation through interplay of CREB and ATF2: implications for disease progression. Cancer Res. 2008; 68:9663-70.
20. Johannessen CM, Johnson LA, Piccioni F, Townes A, Frederick DT, Donahue MK, Narayan R, Flaherty KT, Wargo JA, Root DE, Garraway LA. A melanocyte lineage program confers resistance to MAP kinase pathway inhibition. Nature. 2013; 504:138-42.
21. Sakamoto KM, Frank DA. CREB in the pathophysiology of cancer: implications for targeting transcription factors for cancer therapy. Clin Cancer Res. 2009; 15:2583-7.
22. Seo HS, Liu DD, Bekele BN, Kim MK, Pisters K, Lippman SM, Wistuba II, Koo JS. Cyclic AMP response element-binding protein overexpression: a feature associated with negative prognosis in never smokers with non-small cell lung cancer. Cancer Res. 2008; 68:6065-73.
23. Hartzell DD, Trinklein ND, Mendez J, Murphy N, Aldred SF, Wood K, Urh M. A functional analysis of the CREB signaling pathway using HaloCHIP-chip and high throughput reporter assays. BMC Genomics. 2009; 10:497.
24. Johannessen M, Delghandi MP, Moens U. What turns CREB on? Cell Signal. 2004; 16:1211-27.
25. Shi Y, Venkataraman SL, Dodson GE, Mabb AM, LeBlanc S, Tibbetts RS. Direct regulation of CREB transcriptional activity by ATM in response to genotoxic stress. Proc Natl Acad Sci U S A. 2004; 101:5898-903.
26. Tan X, Wang S, Yang B, Zhu L, Yin B, Chao T, Zhao J, Yuan J, Qiang B, Peng X. The CREB-miR-9 negative feedback minicircuitry coordinates the migration and proliferation of glioma cells. PLoS One. 2012; 7:e49570.
27. Tan X, Wang S, Zhu L, Wu C, Yin B, Zhao J, Yuan J, Qiang B, Peng X. cAMP response element-binding protein promotes gliomagenesis by modulating the expression of oncogenic microRNA-23a. Proc Natl Acad Sci U S A. 2012; 109:15805-10.
28. Liu YL, Lensing SY, Yan Y, Cooper TM, Loh ML, Emanuel PD. Deficiency of CREB and over expression of miR-183 in juvenile myelomonocytic leukemia. Leukemia. 2010; 27:1585-8.
29. Yang SF, Lee WJ, Tan P, Tang CH, Hsiao M, Hsieh FK, Chien MH. Upregulation of miR-328 and inhibition of CREB-DNA-binding activity are critical for resveratrol-mediated suppression of matrix metalloproteinase-2 and subsequent metastatic ability in human osteosarcomas. Oncotarget. 2015; 6:2736-53. https://doi.org/10.18632/oncotarget.3088.
30. Zhang JQ, Yao QH, Kuang YQ, Ma Y, Yang LB, Huang HD, Cheng JM, Yang T, Liu EY, Liang L, Fan KX, Zhao K, Xia X, Gu JW. Prognostic value of coexistence of abnormal expression of micro-RNA-200b and cyclic adenosine monophosphate-responsive element-binding protein 1 in human astrocytoma. Hum Pathol. 2014; 45:2154-61.
31. Zhang Y, Yang J, Cui X, Chen Y, Zhu VF, Hagan JP, Wang H, Yu X, Hodges SE, Fang J, Chiao PJ, Logsdon CD, Fisher WE, et al. A novel epigenetic CREB-miR-373 axis mediates ZIP4-induced pancreatic cancer growth. EMBO Mol Med. 2013; 5:1322-34.
32. Steven A, Leisz S, Sychra K, Hiebl B, Wickenhauser C, Mougiakakos D, Kiessling R, Denkert C, Seliger B. Hypoxia-mediated alterations and their role in the HER-2/neu-regulated CREB status and localization. Oncotarget. 2016; 7:52061-84. https://doi.org/10.18632/oncotarget.10474.
33. Knutson TP, Daniel AR, Fan D, Silverstein KA, Covington KR, Fuqua SA, Lange CA. Phosphorylated and sumoylation-deficient progesterone receptors drive proliferative gene signatures during breast cancer progression. Breast Cancer Res. 2012; 14:R95.
34. Herrmann F, Lehr HA, Drexler I, Sutter G, Hengstler J, Wollscheid U, Seliger B. HER-2/neu-mediated regulation of components of the MHC class I antigen-processing pathway. Cancer Res. 2004; 64:215-20.
35. Morin A, Letouzé E, Gimenez-Roqueplo AP, Favier J. Oncometabolites-driven tumorigenesis: from genetics to targeted therapy. Int J Cancer. 2014; 135:2237-48.
36. Semenza GL. HIF-1 mediates metabolic responses to intratumoral hypoxia and oncogenic mutations. J Clin Invest. 2013; 123:3664-71.
37. Yang C, Jiang L, Zhang H, Shimoda LA, DeBerardinis RJ, Semenza GL. Analysis of hypoxia-induced metabolic reprogramming. Methods Enzymol. 2014; 542:425-55.
38. Xie F, Li BX, Kassenbrock A, Xue C, Wang X, Qian DZ, Sears RC, Xiao X. Identification of a potent inhibitor of

CREB-mediated gene transcription with efficacious *in vivo* anticancer activity. J Med Chem. 2015; 58:5075-87.

39. Xiao X, Li BX, Mitton B, Ikeda A, Sakamoto KM. Targeting CREB for cancer therapy: friend or foe. Curr Cancer Drug Targets. 2010; 10:384-91.
40. Garcia-Prat L, Martínez-Vicente M, Perdiguero E, Ortet L, Rodríguez-Ubreva J, Rebollo E, Ruiz-Bonilla V, Gutarra S, Ballestar E, Serrano AL, Sandri M, Muñoz-Cánoves P. Autophagy maintains stemness by preventing senescence. Nature. 2016; 529:37-42.
41. Lopez de Figueroa P, Lotz MK, Blanco FJ, Caramés B. Autophagy activation and protection from mitochondrial dysfunction in human chondrocytes. Arthritis Rheumatol. 2015; 67:966-76.
42. Kim SH, Trinh AT, Larsen MC, Mastrocola AS, Jefcoate CR, Bushel PR, Tibbetts RS. Tunable regulation of CREB DNA binding activity couples genotoxic stress response and metabolism. Nucleic Acids Res. 2016; 44:9667-80.
43. Singer K, Kastenberger M, Gottfried E, Hammerschmied CG, Büttner M, Aigner M, Seliger B, Walter B, Schlösser H, Hartmann A, Andreesen R, Mackensen A, Kreutz M. Warburg phenotype in renal cell carcinoma: high expression of glucose-transporter 1 (GLUT-1) correlates with low CD8(+) T-cell infiltration in the tumor. Int J Cancer. 2011; 128:2085-95.
44. Conkright MD, Guzmán E, Flechner L, Su AI, Hogenesch JB, Montminy M. Genome-wide analysis of CREB target genes reveals a core promoter requirement for cAMP responsiveness. Mol Cell. 2003; 11:1101-8.
45. Chang CC, Zhang C, Zhang Q, Sahin O, Wang H, Xu J, Xiao Y, Zhang J, Rehman SK, Li P, Hung MC, Behbod F, Yu D. Upregulation of lactate dehydrogenase a by 14-3-3zeta leads to increased glycolysis critical for breast cancer initiation and progression. Oncotarget. 2016; 7:35270-83. https://doi.org/10.18632/oncotarget.9136.
46. Tang H, Goldberg E. Homo sapiens lactate dehydrogenase c (Ldhc) gene expression in cancer cells is regulated by transcription factor Sp1, CREB, and CpG island methylation. J Androl. 2009; 30:157-67.
47. McCleland ML, Adler AS, Shang Y, Hunsaker T, Truong T, Peterson D, Torres E, Li L, Haley B, Stephan JP, Belvin M, Hatzivassiliou G, Blackwood EM, et al. An integrated genomic screen identifies LDHB as an essential gene for triple-negative breast cancer. Cancer Res. 2012; 72:5812-23.
48. Brand A, Singer K, Koehl GE, Kolitzus M, Schoenhammer G, Thiel A, Matos C, Bruss C, Klobuch S, Peter K, Kastenberger M, Bogdan C, Schleicher U, et al. LDHA-associated lactic acid production blunts tumor immunosurveillance by T and NK cells. Cell Metab. 2016; 24:657-71.
49. Xia H, Gong Z, Lian Y, Zhou J, Wang X. Gene expression profile regulated by CREB in K562 cell line. Transplant Proc. 2016; 48:2221-34.
50. Walenta S, Wetterling M, Lehrke M, Schwickert G, Sundfør K, Rofstad EK, Mueller-Klieser W. High lactate levels predict likelihood of metastases, tumor recurrence, and restricted patient survival in human cervical cancers. Cancer Res. 2000; 60:916-21.
51. Murphy MP. Mitochondrial dysfunction indirectly elevates ROS production by the endoplasmic reticulum. Cell Metab. 2013; 18:145-6.
52. Arnould T, Vankoningsloo S, Renard P, Houbion A, Ninane N, Demazy C, Remacle J, Raes M. CREB activation induced by mitochondrial dysfunction is a new signaling pathway that impairs cell proliferation. EMBO J. 2002; 21:53-63.
53. Pregi N, Belluscio LM, Berardino BG, Castillo DS, Cánepa ET. Oxidative stress-induced CREB upregulation promotes DNA damage repair prior to neuronal cell death protection. Mol Cell Biochem. 2017; 425:9-24.
54. Kim HE, Lee SG. Induction of ATP synthase β by H2O2 induces melanogenesis by activating PAH and cAMP/CREB/MITF signaling in melanoma cells. Int J Biochem Cell Biol. 2013; 45:1217-22.
55. Barbosa MR, Sampaio IH, Teodoro BG, Sousa TA, Zoppi CC, Queiroz AL, Passos MA, Alberici LC, Teixeira FR, Manfiolli AO, Batista TM, Cappelli AP, Reis RI, et al. Hydrogen peroxide production regulates the mitochondrial function in insulin resistant muscle cells: effect of catalase overexpression. Biochim Biophys Acta. 2013; 1832:1591-604.
56. Recktenwald CV, Kellner R, Lichtenfels R, Seliger B. Altered detoxification status and increased resistance to oxidative stress by K-ras transformation. Cancer Res. 2008; 68:10086-93.
57. Sepuri NB, Tammineni P, Mohammed F, Paripati A. Nuclear transcription factors in the mitochondria: a new paradigm in fine-tuning mitochondrial metabolism. Handb Exp Pharmacol. 2017; 240:3-20.
58. Leisz S, Schulz K, Erb S, Oefner P, Dettmer K, Mougiakakos D, Wang E, Marincola FM, Stehle F, Seliger B. Distinct von Hippel-Lindau gene and hypoxia-regulated alterations in gene and protein expression patterns of renal cell carcinoma and their effects on metabolism. Oncotarget. 2015; 6:11395-406. https://doi.org/10.18632/oncotarget.3456.
59. Bukur J, Herrmann F, Handke D, Recktenwald C, Seliger B. Identification of E2F1 as an important transcription factor for the regulation of tapasin expression. J Biol Chem. 2010; 285:30419-26.
60. Gay C, Collins J, Gebicki JM. Hydroperoxide assay with the ferric-xylenol orange complex. Anal Biochem. 1999; 273:149-55.
61. Tietz A, Ochoa S. Fluorokinase and pyruvic kinase. Arch Biochem Biophys. 1958; 78:477-93.
62. Goossens F, De Meester I, Vanhoof G, Scharpé S. A sensitive method for the assay of serum prolyl

endopeptidase. Eur J Clin Chem Clin Biochem. 1992; 30:235-8.

63. Hallows WC, Yu W, Denu JM. Regulation of glycolytic enzyme phosphoglycerate mutase-1 by Sirt1 protein-mediated deacetylation. J Biol Chem. 2012; 287:3850-8.
64. Nelson KJ, Parsonage D. Measurement of peroxiredoxin activity. Curr Protoc Toxicol. 2011; Chapter 7:Unit7.10.
65. Jitschin R, Hofmann AD, Bruns H, Giessl A, Bricks J, Berger J, Saul D, Eckart MJ, Mackensen A, Mougiakakos D. Mitochondrial metabolism contributes to oxidative stress and reveals therapeutic targets in chronic lymphocytic leukemia. Blood. 2014; 123:2663-72.
66. Miller GL. Use of dinitrosalicylic acid reagent for determination of reducing augar. Anal Chem. 1959; 31:426-28.
67. Rishi V, Potter T, Laudeman J, Reinhart R, Silvers T, Selby M, Stevenson T, Krosky P, Stephen AG, Acharya A, Moll J, Oh WJ, Scudiero D, et al. A high-throughput fluorescence-anisotropy screen that identifies small molecule inhibitors of the DNA binding of B-ZIP transcription factors. Anal Biochem. 2005; 340:259-71.
68. Chen X, Zhong Z, Xu Z, Chen L, Wang Y. 2',7'-Dichlor odihydrofluorescein as a fluorescent probe for reactive oxygen species measurement: forty years of application and controversy. Free Radic Res. 2010; 44:587-604.
69. Weydert C, Cullen J. Measurement of superoxide dismutase, catalase and glutathione peroxidase in cultured cells and tissue. Nat Protoc. 2010; 5:51-66.
70. Zhang X, Odom DT, Koo SH, Conkright MD, Canettieri G, Best J, Chen H, Jenner R, Herbolsheimer E, Jacobsen E, Kadam S, Ecker JR, Emerson B, et al. Genome-wide analysis of cAMP-response element binding protein occupancy, phosphorylation, and target gene activation in human tissues. Proc Natl Acad Sci U S A. 2004; 102:4459-64.



„*Supplementary materials*“ siehe Anhang auf CD

# 5 Diskussion

Das Institut für Medizinische Immunologie der Martin-Luther-Universität Halle-Wittenberg beschäftigt sich seit vielen Jahren mit dem Vergleich des Proteoms von NZK-Zelllinien mit Zelllinien von korrespondierendem Nierenepithel dieser Patienten[121,122,172-177]. Etwa 80 % der kzNZK weisen dabei einen Funktionsverlust des Tumorsuppressors VHL durch Promotormethylierung, *Missense*-Mutationen oder Deletionen in der Chromosom 3p-Region auf, was mit einem verminderten Abbau des sauerstoffabhängigen Transkriptionsfaktors HIF und der verstärkten Aktivierung des Transkriptionsfaktors CREB einhergeht. Die vorangegangen 2D-Gel-Analysen des Instituts und anderer Arbeitsgruppen zeigten bereits, dass im NZK häufig Proteine des Zellmetabolismus dereguliert vorliegen[121,122,173,176,178,179]. Die angefertigte Dissertation sollte deshalb den Einfluss der VHL-Funktion und Hypoxie sowie der Transkriptionsfaktoren HIF und CREB auf die Veränderungen im Zellmetabolismus in verschiedenen *in vitro*-Modellsystemen untersuchen. In **Abbildung 5** sind die wesentlichen Untersuchungen der zusammengefassten Manuskripte schematisch dargestellt. In den folgenden Abschnitten werden die publizierten Ergebnisse mit der aktuellen Literatur diskutiert.

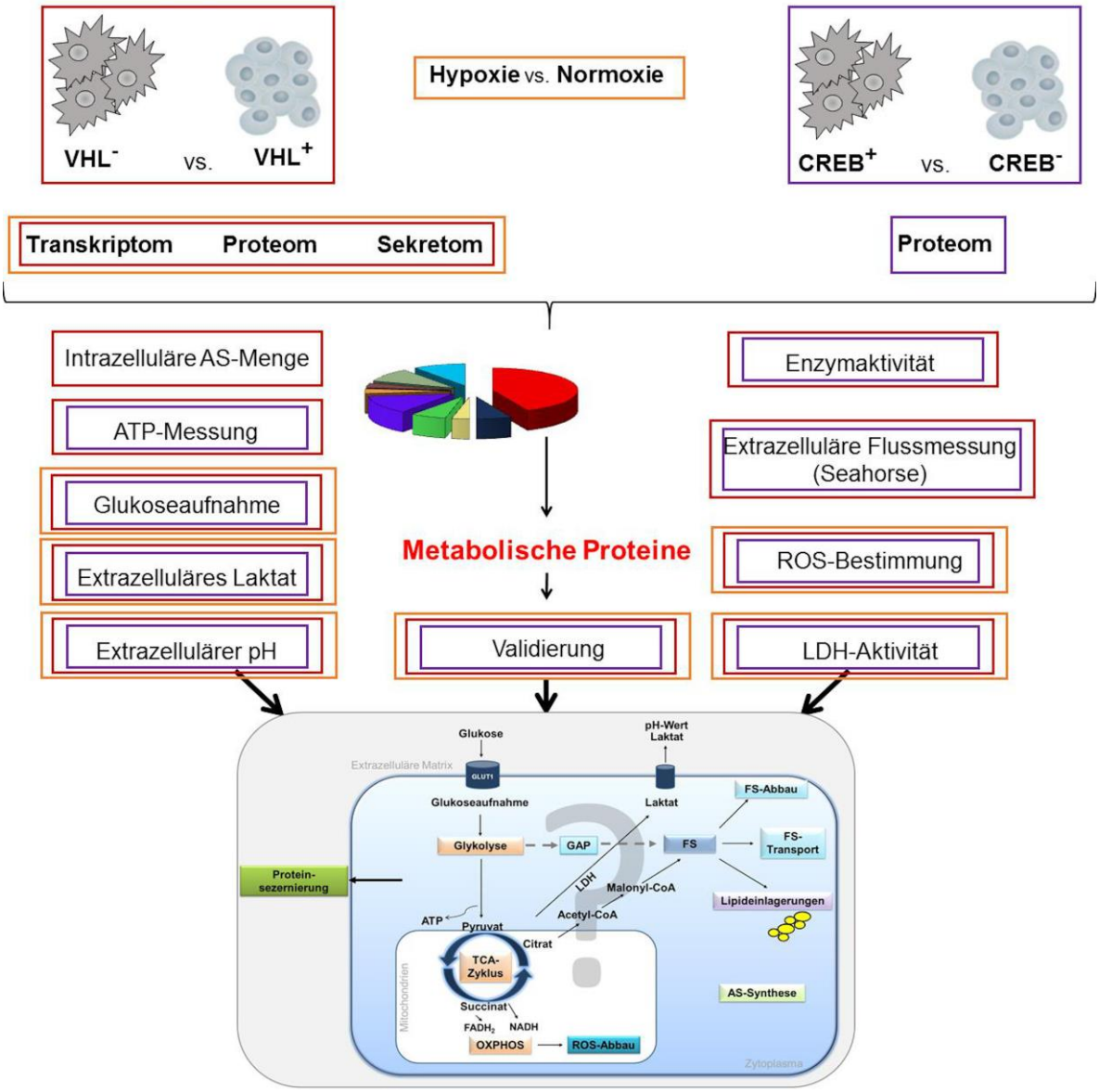


**Abbildung 5: Schematische Übersicht der publizierten Untersuchungen zu den VHL-, Hypoxie-, und CREB-abhängigen Veränderungen im Zellmetabolismus.**
AS, Aminosäure; ATP, Adenosintriphosphat; CREB, *Cyclic adenosin monophosphate response element-binding protein* 1; GAP, Glycerinaldehyd-3-phosphat; FS, Fettsäure; ROS, *reactive oxygen species*; TCA, *tricarbonic acid*; VHL, Von Hippel-Lindau-Protein. Die durchgeführten Analysen zur Untersuchung der ☐ VHL-Defizienz, ☐ Hypoxie oder ☐ CREB-Überexpression wurden jeweils farbig markiert.

## 5.1 Diskrepanz und Konvergenz des VHL-, CREB-, und Sauerstoff-gesteuerten Expressionsmusters

In vorangegangenen Studien der VHL-abhängigen Expressionsveränderungen im NZK wurde hauptsächlich die Destabilisierung des Transkriptionsfaktors HIF, welche als Hauptfunktion von VHL beschrieben ist, untersucht. Häufig wird dabei der Verlust des funktionellen VHL-Proteins mit einem „pseudohypoxischen“ Zustand gleichgesetzt[67]. Die Ergebnisse der Manuskripte 1 und 2 zeigen jedoch, dass der Verlust des funktionellen VHL-Proteins nicht mit hypoxischen Verhältnissen gleichzusetzen ist. Unter den verwendeten Bedingungen wurden

662 Transkripte identifiziert, welche sauerstoffunabhängig durch VHL reguliert vorlagen (Manuskript 1). Dabei waren das Transkript Nidogen 2 (NID2) mit einer 60-fachen Reduktion und die *Rat sarcoma* (RAS)-assoziierte GTPase (RAB)31 mit einer 25-fach gesteigerten Expression am stärksten VHL-abhängig reguliert. RAB31-Überexpression ist bisher als prognostischer Marker für Brust-[180,181], Magen-[182], Pankreas[183]- und Leberzellkrebs[184] bekannt und mit einem reduzierten metastasenfreien Überleben sowie mit einem kürzeren Gesamtüberleben der Patienten assoziiert. Somit könnte RAB31 ein wichtiges HIF-unabhängig reguliertes Zielprotein in der Therapie des NZK darstellen.

Das Glykoprotein NID2 bildet eine der ubiquitären Hauptkomponenten der Basallamina und fungiert als Verbindungsprotein zwischen dem Laminin- und dem Kollagennetzwerk[185]. Dabei zeigen Nidogen-*Knock out*-Mäuse keine Veränderungen in der Nierenbasallamina[186]. Weitere Arbeiten haben den Promotor des *NID2*-Gens bei Magenkrebs bis zu 95 % methyliert nachgewiesen, was zu einer stark verminderten Expression im Tumor führt[187]. Eine mittels *TCGA*-Daten erstellte Kaplan-Meier Überlebenskurve[188] (**Anhang Abbildung 1A**) zeigt, dass eine niedrige NID2-Expression mit einem kürzeren Patientenüberleben im kzNZK assoziiert ist (p=0,009). Da NID2 in das humane Serum sezerniert wird, stellt dieses Protein einen zukunftsweisenden Marker für die Prognostik und Diagnostik des VHL-defizienten kzNZK dar. Dieses Ergebnis wird zusätzlich durch die Tatsache unterstützt, dass NID2 bereits als diagnostischer Marker für Leberzellkrebs dient[189].

Weiterhin wurden 194 VHL-unabhängige Hypoxie-regulierte Zielgene identifiziert, was darauf hinweist, dass die Inkubation unter Hypoxie zusätzlich HIF-unabhängig gesteuerte Funktionen aufweist, die in die Betrachtungen der Krankheits- bzw. Tumorentwicklung einbezogen werden sollten. Manuskript 3 zeigt unter Hypoxie eine verstärkte Phosphorylierung des Transkriptionsfaktors CREB am Serinrest 133, aber nicht am Serinrest 121. Das dieser Zustand HIF-bedingt ist, wurde mittels eines HIF1$\alpha$-Inhibitors untersucht. Diese Daten beweisen, dass die Hypoxie-Induktion mittels HIF-Stabilisierung zusätzlich indirekt weitere für die Tumorentwicklung essentielle Transkriptionsfaktoren wie CREB aktiviert. CREB spielt unter anderem eine Rolle in der Progression zahlreicher Tumorentitäten[100,101,103-105,107,190] wie auch des kzNZK[111,191]. Zusätzlich wurde bereits in anderen Arbeiten gezeigt, dass eine HIF1$\alpha$-Stabilisierung die CREB-Aktivierung verstärkt[93,192-194]. Außerdem interagiert HIF direkt mit dem CREB-bindenden Protein (**Abbildung 2**). Die Ergebnisse des Manuskriptes 3 zeigen, dass neben der erhöhten CREB-Aktivierung durch Phosphorylierung am Serinrest 133 ebenfalls die Lokalisation, Ubiquitinierung und SUMOylierung des Proteins unter hypoxischen Bedingungen verändert ist. Weiterhin ist die Hyperphosphorylierung von CREB unter Hypoxie beschrieben, welche zum proteasomalen Abbau des Transkriptionsfaktors führt[195]. Unter Sauerstoffmangel ist CREB bis zu 30 % außerhalb des Zellkerns lokalisiert, wobei dies mit einer gesteigerten mitochondrialen Lokalisation und einer verstärkten Bindung zum D-Loop der mitochondrialen

DNA einhergeht (Manuskript 3). Zusätzlich wurde bereits gezeigt, dass CREB unter Hypoxie die zelluläre Invasivität steuert[194]. Zusammenfassend lassen diese Daten darauf schließen, dass es eine große Konvergenz im VHL-Defizienz-, Hypoxie– und CREB-gesteuerten Expressionsmuster gibt. Ebenfalls existieren unabhängig voneinander regulierte Prozesse, welche in den folgenden Abschnitten detailierter betrachtet werden sollen.

Mittels 2D-Gel-Analysen wurde die VHL-, CREB-, und Hypoxie-gesteuerte Proteinsignatur in verschiedenen Zellsystemen untersucht (Manuskript 1, Manuskript 2, Manuskript 4). Dabei zeigte sich, dass die prominenteste Gruppe der beeinflussten Proteine funktionell am Zellmetabolismus beteiligt ist (VHL 30 %, Hypoxie 38 %, CREB 35 %).

Nur wenige der differentiell exprimierten metabolischen Enzyme konnten als HIF2α-Zielgene identifiziert werden. Im NZK ist häufig HIF1α nicht exprimiert, während HIF2α die tumorigene Entwicklung der Zellen vorantreibt. Die verwendete kzNZK-Zelllinie besitzt ebenfalls keine HIF1α-Expression. Da die HIF-Ubiquitinierung und der damit verbundene proteasomale Abbau des HIF-Proteins gleichermaßen durch VHL-Defizienz oder Hypoxie gehemmt wird, wurden die HIF2α-Zielgene durch die konträre Expression nach VHL-Transfektion *versus* Hypoxie-Inkubation nachgewiesen. Eines dieser identifizierten HIF2α-Zielgene, welches am Zellmetabolismus beteiligt ist, stellt die Transglutaminase (TGM) 2 dar (Manuskript 1, *Supplementary table 6*). Diese Protein-Glutamin-γ-Glutamyltransferase wurde bereits von Wykoff *et al.* als Hypoxie- und VHL-abhängig differentiell exprimiert beschrieben[196]. Die Transglutaminasefunktion der TGM2 katalysiert den Transfer eines Acylrestes von proteingebundenen Glutaminresten auf primäre Amine. Wenn an dieser Reaktion neben der γ-Glutamylgruppe der Aminosäure Glutamin auch die ε-Aminofunktion eines proteingebundenen Lysinrestes beteiligt ist, kommt es zu einer intra- oder intermolekularen Vernetzung von Proteinen durch Ausbildung einer Isopeptidbindung[197]. Die TGM stellt damit stabile Querverbindungen innerhalb oder zwischen Proteinen her, welche nicht durch Proteasen gespalten werden können[198]. Die Gewebsglutaminase TGM2 hat außerdem nicht nur die Funktion der posttranslationalen Proteinmodifikation, sondern ebenfalls zahlreiche weitere intra- und extrazelluläre Funktionen[199,200] (**Abbildung 6**). Dabei liegt das calciumabhängige Enzym normalerweise inaktiv im Zytoplasma vor und wird durch Stress, Trauma oder Entzündungsprozesse aktiviert[201]. TGM2 kann zusätzlich im Zellkern, in der Plasmamembran oder im extrazellulären Raum lokalisiert sein[198,202]. Entzündungsprozesse spielen häufig in der Tumorentwicklung, Invasion und Metastasierung eine progressive Rolle[203,204]. Dabei geht eine gesteigerte TGM2-Expression in Tumorzellen mit erhöhter Metastasierung, Therapieresistenz und kürzerem Patientenüberleben einher, was bereits für verschiedene Tumorentitäten, wie das Pankreaskarzinom[205], Brust-[206], Ovarial-[207] und nicht-kleinzelligem Lungenkrebs[208] sowie das maligne Melanom[209], Glioblastom[210] und NZK[211,212], beschrieben wurde. Die Auswertung von *TCGA*-Daten weisen auf ein verringertes Überleben

von kzNZK-Patienten mit hoher TGM2-Expression hin (Kaplan-Meier Überlebenskurve, **Anhang Abbildung 1B**). TGM2 steuert außerdem die epithelial-mesenchymale Transition (EMT)[213-215]. Ku *et al.* zeigten, dass die Induktion der TGM2-Expression den Tumormetabolismus mittels Reduktion der Aconitase-Expression im NZK beeinflusst[216]. Die mitochondriale Aconitase katalysiert im TCA-Zyklus die Umwandlung von Citrat zu Aconitat. Citrat dient ebenfalls der Fettsäure- bzw. Cholesterol-Biosynthese (Kapitel 5.5). Weiterführend wird die TGM2 in seiner geschlossenen GTP-gebundenen Form bereits als Tumorstammzellmarker beschrieben[217].

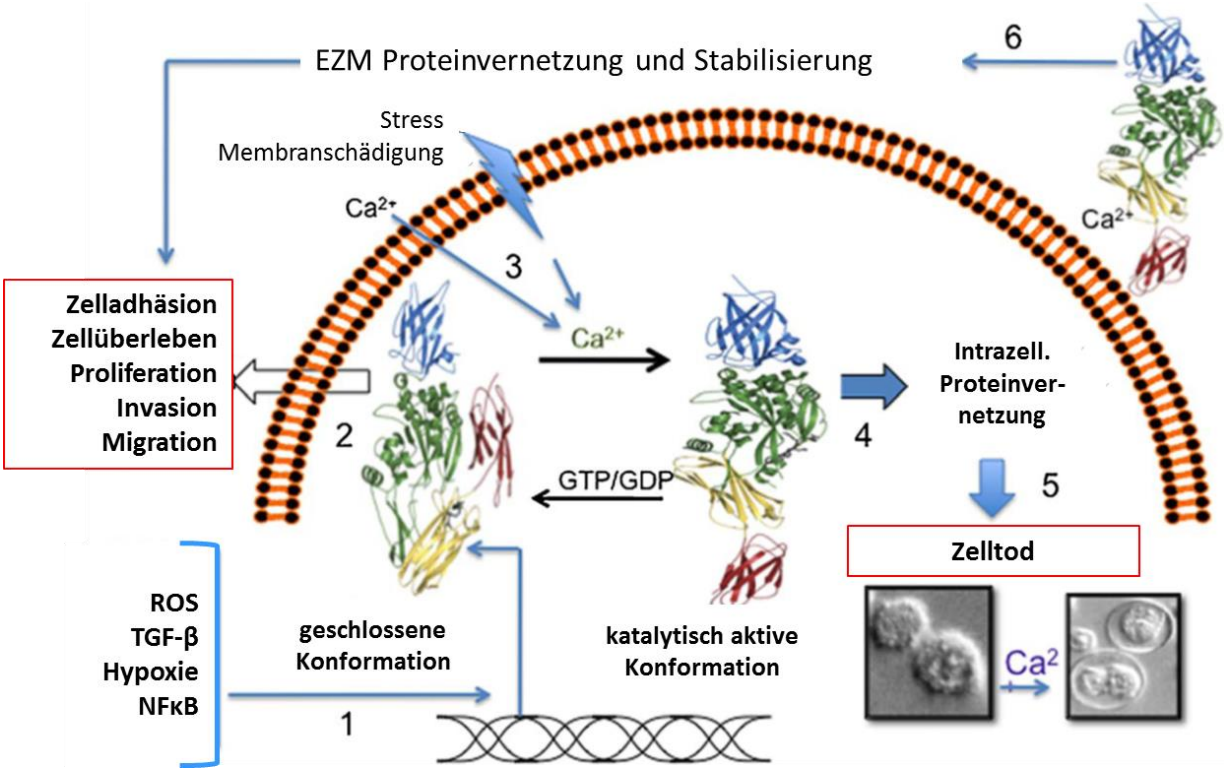


**Abbildung 6: Funktionen der TGM2.**
TGM2 fördert oder hemmt verschiedene zelluläre oder extrazelluläre Funktionen abhängig von seiner Lokalisation und den Stressbedingungen. Verschiedene Entzündungs- oder Stresssignale erhöhen die TGM2-Expression (**1**). Unter Normalbedingungen (niedrige intrazelluläre Calciumkonzentration) liegt TGM2 in einer kompakten, katalytisch inaktiven Form vor. In dieser Form werden die katalytisch unabhängigen Funktionen der TGM2 direkt durch die Bindung von GTP und der damit assoziierten Aktivitäts-, Stabilitäts- und Funktionsänderung oder indirekt über die Induktion der Genexpression gesteuert (**2**). Extreme Stress- oder Traumabedingungen erhöhen die intrazelluläre Calciumkonzentration (**3**), was zur katalytischen Aktivierung von TGM2 führt (**4**). Katalytisch aktives TGM2 induziert die Vernetzung von zellulären Proteinen und begünstigt den Zelltod (**5**). In den extrazellulären Raum sezerniert, vernetzt katalytisch aktives TGM2 die Proteine der extrazellulären Matrix (EZM), was zu einer Stabilisierung und damit zur verstärkten Zelladhäsion bzw. –motilität führt (**6**). ROS, reaktive Sauerstoffspezies; TGF-β, *Transforming growth factor β*; NFκB, *nuclear factor k-light-chain-enhancer of activated B cells*; GTP/GDP, Guanosintriphosphat /Guanosindiphosphat. Verändert nach Mehta *et* al., 2010[218]

Konträre TGM2-Level wurden sowohl auf mRNA- als auch auf Proteinebene in der NZK-Zelllinie 786-0 validiert (**Abbildung 7**). In weiteren Analysen zeigte sich eine Induktion der TGM2-mRNA in 7 NZK-Zelllinien nach Inkubation unter einer verminderten

Sauerstoffkonzentration (1 % $O_2$, 24 h). Die verstärkte TGM2-Expression korrelierte mit der HIF2α-Proteinmenge bzw. der Fähigkeit zur Hypoxie-Induktion der Zellen (**Abbildung 8**). Zusätzlich konnte eine TGF-β-induzierbare Hochregulation sowie eine verstärkte Expression in Sunitinib-adaptierten Kolonkarzinomzelllinien und einer Melanomzelllinie (Daten nicht gezeigt) im Vergleich zu den Sunitinib-sensitiven Zellen nachgewiesen werden. Sunitinib ist ein TKI, welcher hauptsächlich gegen die Aktivität des VEGF- und PDGF-Rezeptors gerichtet und in der Therapie des metastasierenden NZK zugelassen ist. Interessanterweise zeigten Huang *et al*., dass Sorafinib, ein TKI mit ähnlichem Wirkspektrum, die Proliferation, Migration und Invasion von NZK-Zellen über die Reduktion der CREB-Phosphorylierung inhibiert[219]. Grundsätzlich steigert TGM2-Expression die HIF1α-Expression[220] und die Phosphorylierung von CREB am Serinrest 133 über den Abbau der Serin-Threonin-Phosphatase PP2A-α, was zum Anschalten CREB-gesteuerter EMT-Gene wie der Matrixmetalloproteinase (MMP) 2 führt[221]. Diese zusätzlichen Ergebnisse und die funktionelle Komplexität dieses Enzyms in der Tumorentstehung beweisen seine Eignung als zukünftiges therapeutisches Ziel im kzNKZ.

A) B)

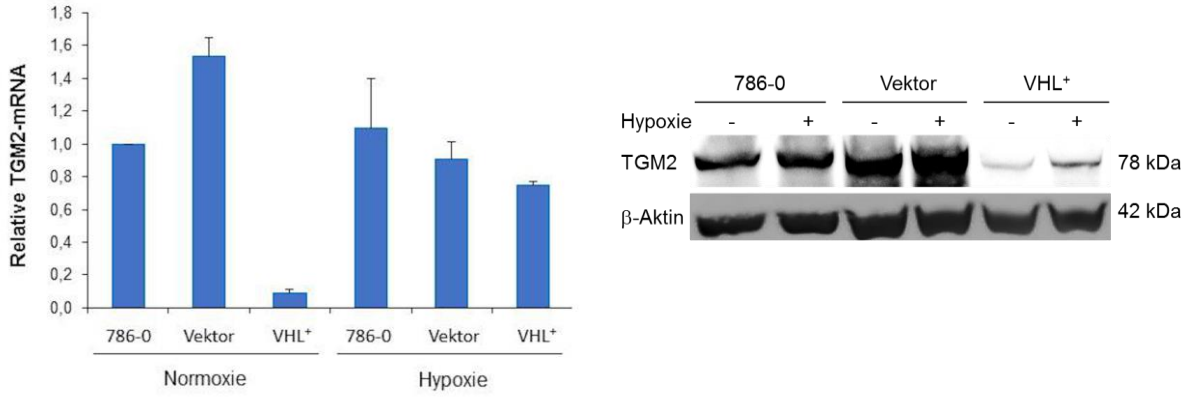


**Abbildung 7: Validierung der TGM2-Transkript- und Proteinmenge unter Normoxie und Hypoxie.** Mittels 2D-Gel Analysen wurde eine VHL-abhängig herunterregulierte TGM2-Proteinmenge detektiert (Manuskript 1). Zur Validierung der Ergebnisse wurde die TGM2-mRNA-Expression mittels quantitativer Echtzeit-PCR (qPCR) (**A**) sowie die Proteinmenge mittels Immunoblotanalysen (**B**) bestimmt. Dabei wurde die VHL-defiziente NZK-Zelllinie 786-0 mit einem Leervektor (Vektor) und einem VHL-Überexpressionskonstrukt ($VHL^+$) stabil transfiziert. Die VHL-negativen (786-0, Vektor) und VHL-positiven ($VHL^+$) NZK-Zellen wurden für 24 h unter Normoxie (21 % $O_2$) oder Hypoxie (1 % $O_2$) inkubiert und anschließend, wie im Material und Methodenteil des Manuskriptes 1 beschrieben, die mRNA-Expression und das Protein detektiert. Die qPCR erfolgte mit spezifischen Primern (TGM2fwd, ATGGTCAACTGCAACGATGA; TGM2rev, GTCATGGGCCGAGTTGTAGT). Das Diagramm zeigt die Mittelwerte und Standardabweichungen aus drei unabhängigen Experimenten (**A**). Die Immunoblotanalysen erfolgten mit einem TGM2-spezifischen Antikörper (Cell Signaling, Frankfurt am Main, Deutschland). Die Abbildung zeigt ein repräsentatives Replikat aus drei unabhängigen Experimenten (**B**).

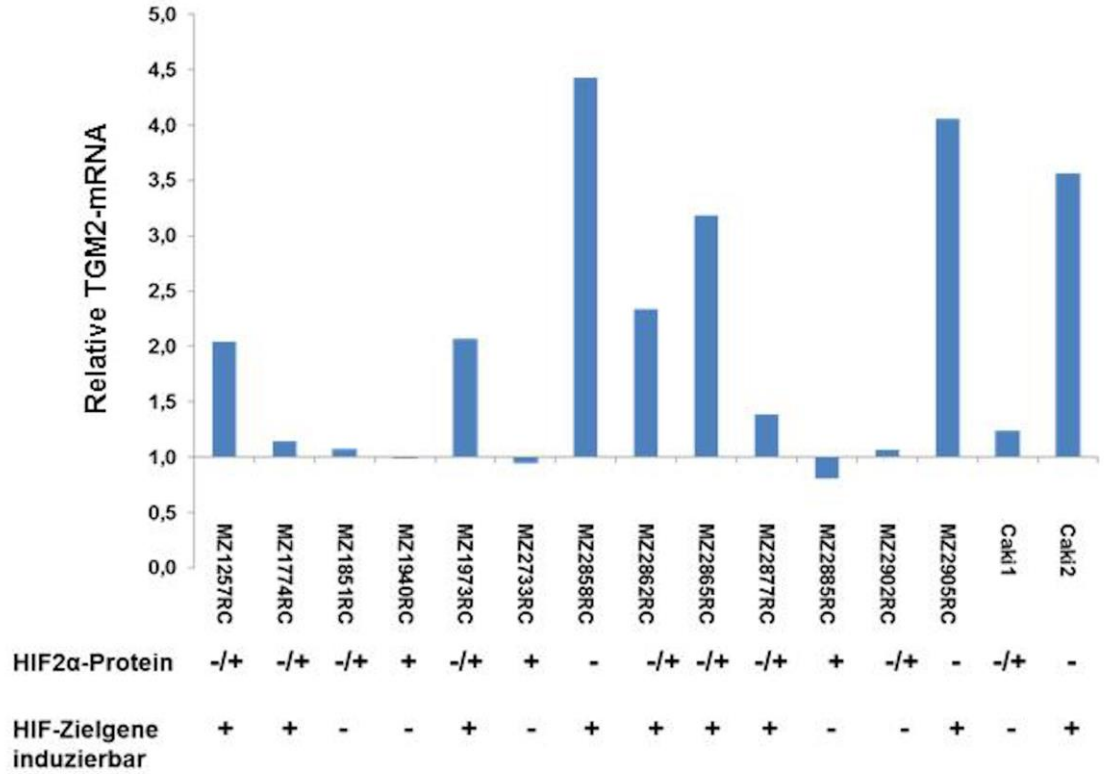


**Abbildung 8: Einfluss von Hypoxie und HIF2α-Proteinmenge auf die TGM2-mRNA-Expression.** 15 NZK-Zelllinien wurden für 24 h unter Normoxie und Hypoxie (1 % $O_2$) inkubiert, die RNA der Zellen extrahiert und das TGM2-Transkriptlevel, wie in Abbildung 6 beschrieben, detektiert. Die Induzierbarkeit der HIF-Zielgene GLUT1 und VEGF wurde anhand der mindestens 1,5-fachen Induktion der Transkriptmengen unter Hypoxie bestimmt (HIF-Zielgene induzierbar: **+**, Induktion von GLUT1 und VEGF >1,5; **-**, keine Induktion oder ≤1,5). Die HIF2α-Proteinmenge wurde unter Normoxie mittels Immunoblotanalysen unter Verwendung eines HIF2α-spezifischen Antikörpers (Novus Biologicals, Bio-Techne, Wiesbaden, Deutschland) analysiert (Daten nicht gezeigt; **-**, kein HIF2α-Protein detektierbar; ***-/+***; wenig Protein detektierbar; **+**, verstärkt HIF2α-Protein detektierbar). Dabei weist eine stabile HIF2α-Proteinmenge und die fehlende Induktion der HIF2α -Zielgene (GLUT1, VEGF) unter Hypoxie auf eine defiziente VHL-Proteinfunktion hin. Eine Hochregulation der TGM2-Expression unter Hypoxie zeigen 7 von 9 Hypoxie-induzierbare NZK-Zelllinien. Bei den Zelllinien, welche eine fehlende Induktion der HIF2α-Zielgene (GLUT1, VEGF) aufwiesen, war keine Hochregulation der TGM2-Expression detektierbar. Die Darstellung zeigt ein biologisches Replikat.

Bis heute gibt es keinen therapeutisch zugelassenen TGM2-Inhibitor. Die Firma Zedira testet derzeit den reversiblen Inhibitor ZD1227 gegen Zöliakie in klinischen Studien[222]. In experimentellen Arbeiten mit verschiedenen TGM2-Inhibitoren wurde bereits ein antitumoraler Effekt nachgewiesen[223]. Dabei führte die Behandlung mit dem Inhibitor GK921 im *Xenograft*-Modell zu einem reduzierten NZK-Wachstum, zur Stabilisierung von TP53 und zu einem synergistischem antitumoralen Effekt bei zusätzlicher Doxorubicin-Behandlung[224]. Der klinische Einsatz dieser TGM2-Inhibitoren ist aufgrund seiner unspezifischen Hemmung anderer Transglutaminasen kritisch[222]. Ebenfalls wurden bereits HIF-Inhibitoren in *in vitro*- und *in vivo*-Experimenten getestet. So wirkte der HIF-Inhibitor 2-Methoxyestradiol, welcher ebenfalls in Manuskript 4 verwendet wurde, synergistisch mit Sorafenib progressionshemmend auf Leberzellkarzinome im Tiermodell[225]. Zusätzlich wurden

Inhibitoren, welche die Dimerisierung von HIF2α mit HIFβ im Zellkern verhindern, gegen NZK-Zellen getestet[226,227]. Der Inhibitor PT2385 befindet sich zurzeit in der klinischen Studie Phase I (NCT02293980) gegen das fortgeschrittene kzNZK. Eine weitere Möglichkeit der Hochregulation von TGM2 oder auch der HIF-Stabilisierung direkt entgegen zu wirken, wäre der Einsatz von siRNA oder miR. In siRNA-Studien sowohl gegen HIF2α als auch gegen TGM2 wurde eine verminderte Proliferation und erhöhte Apoptose von NZK-Zellen detektiert[228,229]. Die Transfektion von NZK-Zellen mit der miR-1285 führte zum Abbau von TGM2, was mit der Hemmung der Proliferation einherging[230]. Zusätzliche eigene Analysen weisen auf eine VHL-abhängige Regulation der miR-1285 hin (Daten nicht gezeigt). In den letzten Jahren wurden miR identifiziert, welche die posttranskriptionelle Regulation von VHL (miR-210, miR-224), HIF2α (miR-182-5p), HIF-Zielgene, wie VEGF (miR-17-5p) oder CA9 (miR-155), oder CREB (miR-22-3p, miR-26a-5p, miR-27a-3p, miR-221-3p) im NZK steuern[231,232]. Die Arbeitsgruppe von Carsten Müller-Tidow entwickelt seit einigen Jahren zunächst an der Martin-Luther-Universität Halle-Wittenberg und später an der Ruprecht-Karls-Universität Heidelberg si- oder miR-gekoppelte therapeutische Antikörper, um Therapieresistenzen zu überwinden und zielgerichtete Tumortherapien zu entwickeln[233,234]. Zukunftsweisend wäre es ebenfalls für das kzNZK denkbar, siRNA/miR gegen HIF, CREB oder TGM2, wie z. B. die miR-1285, an einen Antikörper wie WX-G250 (Rencarex, Wilex), zu koppeln, um zielgerichtete Therapien zu verbessern und Therapieresistenzen zu überwinden. WX-G250 ist gegen das Protein CA9 gerichtet, welches zu 95 % auf der Oberfläche von NZK-Zellen vorkommt[235] und ebenfalls ein HIF-Zielgen darstellt[81]. Die Zulassung des Antikörpers scheiterte 2017 in der Phase III der klinischen Zulassungsstudien, weil der Antikörper singulär zu keiner Verlängerung des rezidivfreien Überlebens führte[236].

### 5.2 Der Einfluss von VHL, CREB und Hypoxie auf die Glykolyse

Der zelluläre schrittweise Abbau von Monosacchariden (Glukose) wird als Glykolyse bezeichnet. In Manuskript 1 und 4 wurde einerseits gezeigt, dass der intrazelluläre Glukosetransport (2-fach) VHL-abhängig sowie durch CREB-Minderexpression erniedrigt wird. Dies geht mit der verringerten Expression des Glukosetransporters GLUT1 einher, welcher im NZK mit dem Tumorgrad, einer verminderten Infiltration von CD8-positiven T-Zellen und dem Patientenüberleben korreliert[146,237]. In der vorliegenden Arbeit wurden VHL-abhängig reduzierte Proteinmenge zahlreicher Glykolyseenzyme wie Aldolase (ALDOA), Triosephosphatisomerase (TPI) 1, Enolase (ENO) und Pyruvatkinase (PKM) nachgewiesen, während durch Hypoxie keine Hochregulation der Phosphoglyceratmutase (PGAM) 1 und PKM beobachtet wurde (Manuskript 1). Zusätzlich wurden durch verminderte CREB-Expression die Glykolyseenzyme TPI1, ENO1, PGAM1, PKM und die Phosphoglyceratkinase (PKG)1 herunterreguliert detektiert (Manuskript 4). Umgekehrt kommt es daher in VHL-

defizienten und CREB-aktiven Tumorzellen nicht ausschließlich zu einer erhöhten Glukoseaufnahme, sondern zur gesteigerten glykolytischen Aktivität, welche mittels extrazellulärer Flussmessung (Fluxanalyzer, Seahorse) detektiert wurde (Manuskript 1 und 4). Craven *et* al. zeigte in NZK-Primärzelllinien bereits 2006 eine vermehrte ALDOA-Expression[238]. Weiterhin konnte eine gesteigerte Konzentration im Serum von NZK-Patienten nachgewiesen werden[239]. Die gesteigerte ALDOA-Expression ist mit einem kürzeren Gesamtüberleben[157] und einem kürzeren rezidivfreien Überleben (**Anhang Abbildung 1C**) assoziert und geht *in vitro* mit einer gesteigerter Proliferation, Migration und Invasion von NZK-Zellen einher[240]. ALDOA repräsentiert damit einen potentiellen Biomarker, welcher einerseits für die Detektion hypoxischer Tumorbereiche und anderseits bei Tumoren, welche mit einem Funktionsverlust des VHL-Proteins einhergehen, verwendet werden könnte. Für die Glykolyseenzyme ENO1 und TPI1 wurden zusätzlich erhöhte Proteinmengen im Sekretom der VHL-defizienten NZK-Zellen gefunden, was darauf schließen lässt, dass beide Enzyme in der Zusammensetzung des Tumormikromilieus (TME) eine Rolle spielen oder als prognostische Serummarker zur Erkennung des NZK dienen könnten (Manuskript 2). Die Expression von ALDOA und ENO1 wird von mehreren HRE im Promotorbereich gesteuert[125]. ENO1 wurde bereits als prognostischer und diagnostischer Faktor in verschiedenen Tumoren wie z. B. Magen-, Prostata-, Dickdarm- oder Brustkrebs identifiziert[241], wobei das Enzym den Abbau der extrazellulären Matrix und damit die Migrationsfähigkeit der Tumorzellen steigert. Weiterhin stellt ENO1 eine potentielle Zielstruktur für gerichtete Immuntherapien dar. Für TPI1 ist bisher keine extrazelluläre Funktion bekannt. Allerdings wurde das Enzym als Tumorstammzellmarker sowie als prognostischer Faktor für Magenkrebs beschrieben[242].

In Manuskript 4 wurde gezeigt, dass das die verminderte Expression von CREB durch „Small hairpin“ RNA (shRNA) in einem Zellmodell der onkogenen Transformation zu einer verminderten glykolytischen Aktivität und zur verminderten Expression von Glykolyseenzymen wie TPI1, PGAM, ENO1 und PKM2 führt. Zusätzlich wurde auch eine reduzierte Enzymaktivität nachgewiesen. Dabei weisen die Promotorregionen jedes dieser Enzyme regulatorische CRE-Elemente auf. Von daher kann angenommen werden, dass die erhöhte Aktivierung des Transkriptionsfaktors CREB durch die Stabilisierung von HIF bei Hypoxie oder VHL-Funktionsverlust zum metabolischen Umschalten der Tumorzellen zur verstärkten Glykolyse beiträgt. Das HIF-Stabilisierung zur verstärkten CREB-Phosphorylierung führt, wurde bereits für andere Tumorentitäten nachgewiesen[93,192-194] und zusätzlich in Manuskript 3 gezeigt sowie in Manuskript 4 durch den Einsatz des HIF1$\alpha$-Inhibitors 2-Methoxyestradiol bestätigt.

In den letzten Jahren wurde der Einfluss des Tumormetabolismus insbesondere der Glykolyse auf Immunzellen untersucht, da immer wieder neue Mechanismen bekannt werden, wie Tumorzellen der Erkennung des Immunsystems entgehen (*immune escape*-Mechanismen) und in Folge dessen ungehindert wachsen können[243-246] oder nicht auf Therapien

ansprechen[247,248]. Cascone *et. al* zeigte beispielweise 2018, dass die Überexpression von Glykolysegenen, wie z. B. ALDOA und PGAM, im Tumor die T-Zellaktivität verringert, während die Hemmung der Glykolyse zur T-Zell-mediierten Erkennung des Tumors durch das Immunsystem führte[112]. Diese Ergebnisse weisen darauf hin, dass ein Umschalten des Metabolismus (durch VHL-Defizienz, Hypoxie oder CREB-Aktivierung) zur Glykolyse dem Entgehen der Tumorzellen vor der Erkennung des Immunsystems beiträgt, wie im Abschnitt 5.7 diskutiert wird. Weiterhin wurde bereits ein therapeutischer Einsatz des Glykolyseinhibitors Dichloroacetat untersucht[249-253]. Dabei hat sich die Behandlung mit Dichloroacetat allerdings als immunzellhemmend erwiesen[254-256]. Zusätzlich zeigten Analysen mit Inhibitoren der Glukoseaufnahme (GLUT1-Hemmer) wie Resveratrol oder Apigenin (Flavon) antitumorale Effekte[257,258]. In **Abbildung 9** sind die einzelnen Reaktionsschritte der Glykolyse schematisch dargestellt, wobei die durch VHL-Defizienz, Hypoxie und CREB-Überexpression regulierten Enzyme jeweils farbig hervorgehoben sind.

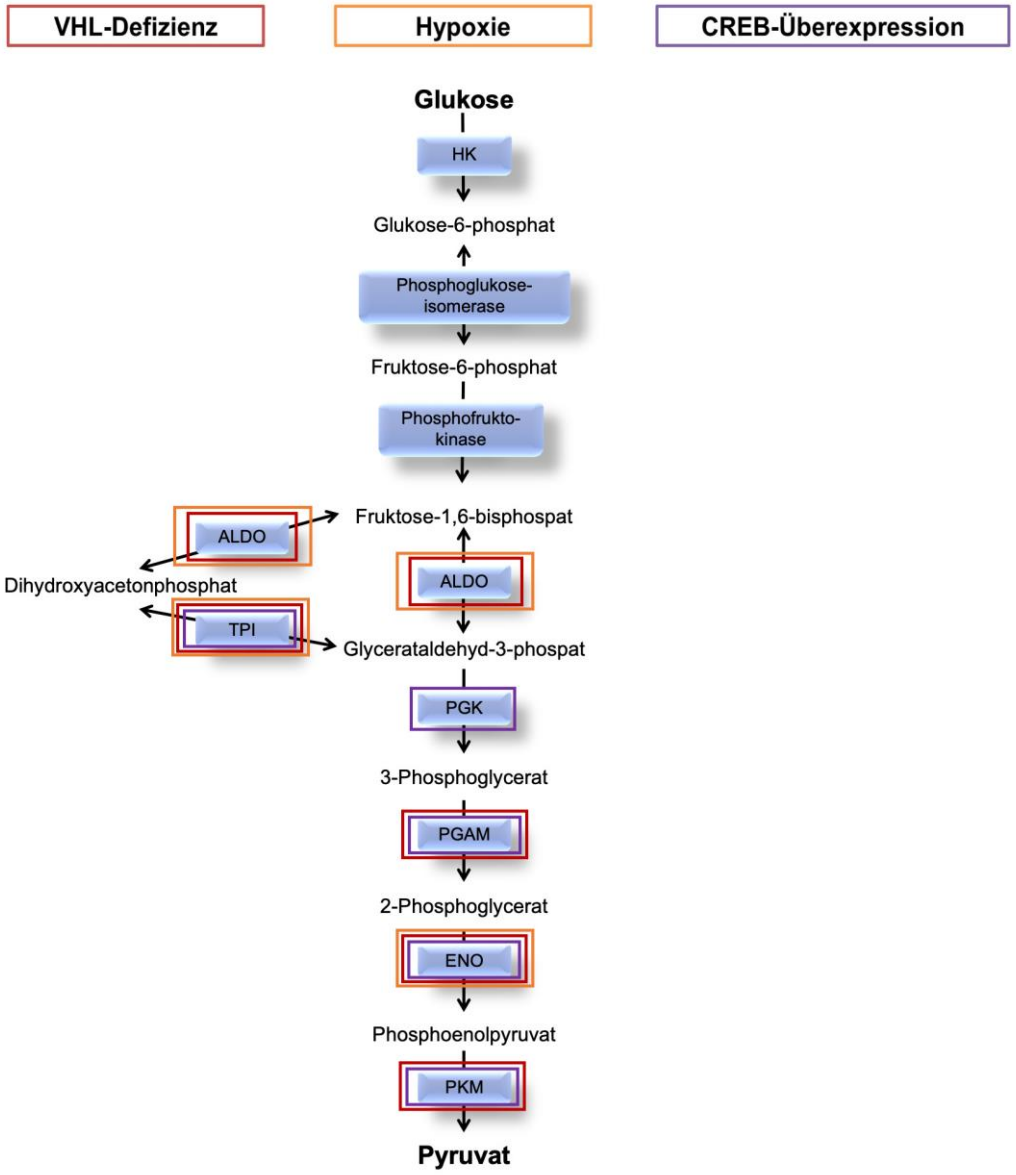


**Abbildung 9: VHL-, CREB- und Hypoxie-abhängige differenziell exprimierte Enzyme der Glykolyse.**
Die Abbildung zeigt schematisch die Reaktionsschritte der Glykolyse, dabei wurden die regulierten Enzyme farbig markiert ( VHL-Defizienz, Hypoxie, CREB-Überexpression).
ALDOA, Aldolase; ENO, Enolase; HK, Hexokinase; PGAM, Phosphoglyceratmutase; PGK, Phosphoglyceratkinase; PKM, Pyruvatkinase M; TPI, Triosephosphatisomerase.

## 5.3 Differentieller Einfluss von VHL, CREB und Hypoxie auf die Atmungskette und die mitochondriale Aktivität

Die Untersuchungen des VHL-, CREB-, und Hypoxie-regulierten Proteinmusters zeigten nicht nur Änderungen in der Glykolyse, sondern ebenfalls im TCA-Zyklus, der oxidativen Phosphorylierung (OXPHOS) und der mitochondrialen Aktivität. Die OXPHOS ist ein effizienter Mechanismus zur Synthese von ATP aus ADP. Dabei erfolgt die Elektronentransportkette über vier Redoxkomplexe in der mitochondrialen Matrix. Komplex I (NADH-Dehydrogenase) reduziert mittels Elektronen aus NADH, während Komplex II (Succinatdehydrogenase) Succinat zu Fumarat mittels der Reduktion von Flavin-Adenin-

Dinukleotid (FAD) zu $FADH_2$ oxidiert[259]. Beides führt letztendlich zur Reduktion von Ubichinon zum Ubihydrochinon. Die Detektion der Succinatdehydrogenase (SDH)A-Proteinmenge zeigte eine zweifache VHL-abhängige Hochregulation (Manuskript 1). In Krebszellen kommt es häufig zu *loss of function*-Mutationen von SDHA, welche zur Ansammlung von Succinat (Onkometabolit) führen, sowie epigenetische Veränderungen induzieren, die zum malignen Phänotyp beitragen[260-263]. Dies weist darauf hin, dass die verminderte SDHA-Proteinmenge zur Malignität von VHL-defizienten Tumoren beitragen könnte, was weiterführend in funktionellen Untersuchungen überprüft werden sollte. Ebenfalls wurden VHL-abhängig höhere Proteinmengen des Komplex III (Ubiquinol-Cytochrom-c-Reduktase) der OXPHOS nachgewiesen. Dieses Enzym katalysiert die Reduktion von Cytochrome-c und trägt entscheidend zur Erzeugung des Protonenkonzentrationsunterschieds zwischen der inneren und äußeren Mitochondrienmembran bei. Weiterhin wurde eine VHL-abhängige Hochregulation der Aconitase (ACO)1 nachgewiesen, welche unter Hypoxie reversibel war (Manuskript 1). Für die Reduktion der ACO1 durch VHL-Defizienz oder Hypoxie könnte die verstärkte Expression der TGM2 ursächlich sein (Kapitel 5.1). ACO1 katalysiert die Umwandlung von Citrat zu Aconitat im TCA-Zyklus. Die verminderte Expression der ACO1 könnte zu einer Citratanreicherung führen, welche wiederum die Fettsäuresynthese induziert, wobei es zu den für das NZK typischen Lipidablagerungen kommt (Kapitel 5.5).

Aufgrund dieser Ergebnisse scheint es nicht verwunderlich, dass VHL-defiziente Zellen eine verminderte respiratorische und mitochondriale (Dehydrogenase-) Aktivität zeigen (Manuskript 1). Währenddessen führt die CREB-Minderexpression zu einer niedrigeren respiratorischen Reserve, zur verminderten Aktivität der OXPHOS (Manuskript 3) und zu einer verminderten Citratsynthaseproteinmenge (Manuskript 4), was darauf hinweist, dass Tumore mit einer erhöhten CREB-Expression/-Aktivität ebenfalls eine erhöhte mitochondriale Aktivität aufweisen.

Verminderte mitochondriale Aktivität, wie sie bei VHL-Defizienz oder Sauerstoffreduktion nachgewiesen wurde (Manuskript 1), führt zu einer Aktivierung von CREB[264] sowie zur verstärkten ROS-Freisetzung[265] (Kapitel 5.6). Andererseits kam es zu einer stärkeren mitochondrialen Lokalisation von CREB unter Hypoxie (Manuskript 3). Um diese teilweise widersprüchlichen Daten aufzuklären, bedarf es weiterer Untersuchungen.

### 5.4 VHL-abhängige Reduktion des Aminosäuremetabolismus

Die Bestimmung des intrazellulären Aminosäurelevels zeigte eine Reduktion von bis zu 25 % durch Reversion der VHL-Funktionalität (Manuskript 1). Dabei war die Aminosäure (AS) Serin, welche eine funktionelle Rolle bei der Aktivierung von Kinasen durch die Phosphorylierung von Serinresten besitzt, 2,5-fach reduziert. In früheren Studien wurde gezeigt, dass Tumorzellen in der Lage sind exogenes Serin aufzunehmen[266]. Zusätzlich wurde eine signifikante Reduktion der Aminosäuremenge von Glycin, Methionin, Tryptophan, Alanin und Glutamin

detektiert (Manuskript 1). Ein Zusammenhang der Tumorzellproliferation mit dem intrazellulären Serin-, Glutamin- und Glycinlevel wurde bereits in anderen Arbeiten nachgewiesen[267]. Glutamin ist die am stärksten vertretene freie AS im Zellstoffwechsel und spielt neben der aeroben Glykolyse eine Schlüsselrolle im Vorantreiben des Tumorwachstums[138]. Glutamin wird auf vielen verschiedenen Wegen metabolisiert, um in proliferierenden Zellen Energie und Biomasse zur Membran- sowie DNA-Synthese zu erzeugen[268,269]. Weiterhin ist Glutamin an der NADPH-Regeneration und Erhaltung des Glutathionlevels und damit an der Neutralisierung von reaktiven Sauerstoffspezies (ROS) beteiligt (Kapitel 5.6). Dementsprechend kann der Glutaminstoffwechsel bei aerober Glykolyse die Glukoseoxidation ersetzen[270]. Dieser Effekt wurde mittels isotopisch markiertem $^{13}$C-Glutamin nachgewiesen[271-273]. Da sich die Glutaminolyse mit einem Teil des TCA-Zyklus überschneidet, verwenden stark proliferierende Zellen Glutamin (über die Metabolisierung zu Glutamat und anschließend $\alpha$-Ketoglutarat) als Energie- und Ammoniumquelle[274]. Dabei spielen die verstärkte Aufnahme, aber auch eine erhöhte Glutaminaseaktivität eine treibende Rolle[275]. Durch diese metabolische Flexibilität, welche die Glutaminolyse für den TCA-Zyklus ermöglicht, schaffen es Tumorzellen, während der Tumorprogression auf die sich ändernde Mikroumgebung zu reagieren[131]. Kappler *et* al. zeigte in verschiedenen Tumorzelllinien (Brustkrebs, Osteosarkom, Plattenepithelkarzinom), dass die HIF1-Aktivität durch den Glutaminmetabolismus (Glutaminolyse) und die damit verbundene zelluläre Ammoniumanreicherung unter normoxischen Bedingungen verstärkt wird, was mit einer gesteigerten Expression von HIF-Zielgenen wie CA9, erhöhter Proliferation und verringerter Alaninproduktion der Zellen einherging[276,277]. Außerdem wurde eine Reversion der HIF-Stabilisierung durch die Behandlung der Zellen mit Acetylsalicylsäure, Ascorbat oder Ibuprofen unter Normoxie erreicht[277]. Ascorbat ist als Kofaktor der Prolinhydroxylasen bekannt[278]. Für das papilläre NZK und kzNZK ohne funktionellen VHL-Verlust wurde eine negative Korrelation der Ascorbatspiegel mit der Expression von HIF-Zielgenen nachgewiesen. Bei VHL-defizienten kzNZK konnte keine Modulation der HIF-Aktivität gezeigt werden, da der HIF-Abbau unabhängig von der Hydroxylierung gehemmt wird[279].

Weiterhin ist Glutamin am Nukleotidaufbau beteiligt und fungiert als Elektronendonor in der anaplerotischen Synthese von Aspartat[275,280]. Zusätzlich weist die verstärkte Expression der Guanosinmonophosphat (GMP)-Synthase durch VHL-Defizienz auf eine verstärkte Synthese von GMP mittels ATP-abhängiger Glutaminhydrolyse hin, welches zum Aufbau zum Nukleotid Guanosintriphosphat (GTP) oder der Base Guanosin beiträgt. GTP fungiert ähnlich wie ATP als Energieträger. Wobei eine erhöhte GTP-Konzentration eine funktionelle Bedeutung für die TGM2-Aktivität haben könnte (**Abbildung 5**, GTP-abhängige Funktion). Eine Aktivierung der Transkriptionsfaktoren MYC und mTOR, wie im NZK bereits gezeigt, führen zur verstärkten Glutamin- und Tryptophanaufnahme in Tumorzellen[281-283]. Folglich könnte die Reduktion des

intrazellulären Glutaminlevels in der Therapie des NZK einen hemmenden Effekt auf das Tumorzellwachstum haben. Dazu konnte Shroff *et al.* bereits zeigen, dass Glutaminaseinhibitoren, dass Tumorwachstum des kzNZK reduzieren[284]. Anderseits sind Glutamin und Tryptophan essentielle AS für die T-Zellfunktion[285,286], was zur Immunsuppression führen könnte.

### 5.5 Die Rolle von VHL und Hypoxie im Abbau und Transport von Fettsäuren

Das kzNZK ist histologisch häufig durch lipid- und glykogenreiche Einlagerungen im Zytoplasma gekennzeichnet. Dabei wird die Fettsäuresynthese durch einen Citratüberschuss induziert[287]. Citrat wird einerseits über die Metabolisierung von Pyruvat über Acetyl-CoA im TCA-Zyklus angereichert, andererseits kann Citrat auch mittels Glutaminolyse (Kaptiel 5.4) produziert werden. Überschüssiges Citrat wird ins Zytosol transportiert und dort in zytosolisches Acetyl-CoA umgewandelt und anschließend zu Malonyl-CoA carboxyliert[288]. Fettsäuren dienen als Substrate für die Membransynthese, Energiespeicher und zur Produktion von Signalmolekülen. Du *et al.* beschreibt HIF-induzierte Lipidablagerungen, welche mit dem verminderten Fettsäureabbau und verminderten mitochondrialen Fettsäuretransport einhergehen[289]. Dabei inhibiert HIF die Expression der Carnitin-Palmitoyltransferase 1A. Interessanterweise sind die beschriebenen zellulären Lipidablagerungen glukose-, aber nicht glutaminabhängig.

Die Enoyl-CoA-Hydratase (ECHS1), welche am Fettsäureabbau beteiligt ist, wurde in der vorliegenden Arbeit als VHL-abhängig hochreguliert identifiziert (Manuskript 1). Der Abbau von Fettsäuren (β-Oxidation) in den Mitochondrien erzeugt Acetyl-CoA und die Reduktionsäquivalente NADH und $FADH_2$, die mittels OXPHOS zur Herstellung von mitochondrialem ATP verwendet werden. In einer erst kürzlich erschienenen Studie wurde nachgewiesen, dass ECHS1 die Progression des NZK durch die verminderte Aktivierung des mTOR-Signalweges inhibiert[290]. Dabei führte ECHS1-Überexpression zur verminderten Proliferation und Migration der NZK-Zellen. Außerdem wurde mittels *TCGA-Kidney Renal Clear Cell Carcinoma*-Datenanalyse eine statistisch signifikante ECHS1-Minderexpression im NZK gezeigt. Folglich eignet sich ECHS1 sowohl als prognostischer Marker als auch als neues therapeutisches Zielprotein gegen das VHL-defiziente NZK.

Im Gegensatz dazu ist eine differentielle Expression der fettsäurebindenden Proteine (FABP) im NZK seit vielen Jahren bekannt. In eigenen Arbeiten des Instituts für Medizinische Immunologie wurde bereits 2005 und 2009 die Hochregulation von FABP7 sowie verminderte Proteinmengen von FABP1 im NZK nachgewiesen[122,175].

FABP wirken als solubilisierende Moleküle und ermöglichen den Fettsäuretransport in verschiedene zelluläre Kompartimente. Damit steuern FABP zahlreiche zelluläre Prozesse wie z. B. die Proliferation oder die Inflammation. FABP7-Überexpression ist beim kzNZK mit einer

schlechteren Prognose assoziiert und erhöht die Proliferation von NZK-Zellen über die Aktivierung von STAT3 und ERK[291]. In der vorliegenden Arbeit wurde die FABP5-Proteinmenge VHL-abhängig ca. 3-fach reduziert detektiert (Manuskript 1). FABP5 wurde bisher in Brust-, Prostata-, Leber- und Kolonkarzinomen hochreguliert beschrieben und steuert dabei den Transport von langkettigen Fettsäuren, welche als Liganden der Peroxisom-Proliferator-aktivierten Rezeptoren (PPAR) fungieren[292,293]. In Manuskript 3 wurde die CREB-abhängige Hochregulation des PPARγ-Coaktivator 1α nachgewiesen, was ebenfalls zu einer Aktivierung des PPARγ-Signalweges beitragen könnte. Über die Aktivierung des PPAR-Signalweges beeinflusst FABP5 die Proliferation und das Zellüberleben[294,295]. Außerdem führte die PPARβ/δ-Aktivierung zur Induktion der VEGF-Expression und somit zur verstärkten Angiogenese im Prostatakarzinom[296]. In Kolonkarzinomzellen war eine erhöhte FABP5-Expression mit reduzierter p21-Aktivität, erhöhter MYC-Expression und verstärkter Invasionskapazität der Zellen assoziiert[297]. Weitere Untersuchungen müssen klären, ob sich FABP5, als prognostischer Faktor für das NZK eignet. Aufgrund der funktionellen Daten, die bereits für das Prostata- und Kolonkarzinom existieren, ist es wahrscheinlich, dass FABP5 ebenfalls eine funktionelle Rolle in der Entwicklung des NZK hat und damit als neues therapeutisches Zielprotein in Frage kommt. Erst kürzlich zeigten Wu *et* al. mittels der Auswertung der zur Verfügung stehenden *TGCA*-Datenbank eine FABP5-Hochregulation im kzNZK und beschreiben FABP5 als ein wichtiges Onkogen, welches die Proliferation, Invasion und Migration im kzNZK fördert[298,299]. Weiterhin wurde die Aktivierung des PI3K/Akt-Signalweges als ursächlich für die FABP5-mediierte gesteigerte Proliferation von kzNZK-Zellen identifiziert[298,300]. Die Behandlung von Prostatakarzinomzellen mit spezifischen FABP5-Inhibitoren (SBFI-102, SBFI-103) und Docetaxel oder Cabazitaxel zeigten stärkere zytotoxische Effekte und eine stärkere Reduktion des Tumorwachstums in Balb/c-Nacktmäusen im Vergleich zur singulären Behandlung mit den jeweiligen Chemotherapeutika[301]. Ebenfalls zeigte der FABP5-Inhibitor SBFI-26 antitumorigene Eigenschaften bei Prostatakarzinomzellen *in vitro* und *in vivo*[302]. Aufgrund dessen wäre es denkbar, dass die Hemmung des zellulären Fettsäuretransports einen positiven synergistischen Effekt bei der Behandlung des NZK haben könnte. Jedoch müsste dies zunächst in weiteren *in vitro* Experimenten überprüft werden. Insgesamt scheint das Umschalten der Tumorzellen vom Katabolismus zum Anabolismus die tumorigenen Eigenschaften wie z. B. verstärkte Zellteilung über den Aufbau von Nukleotiden und die verstärkte Membransynthese zu fördern.

### 5.6 VHL-, CREB- und Hypoxie-abhängiger Abbau reaktiver Sauerstoffspezies

Bereits 2003 konnte in einer Veröffentlichung des Instituts für Medizinische Immunologie erhöhte Proteinmengen von ROS-abbauenden detoxifizierenden Enzymen wie

Superoxiddismutase (SOD) und Thioredoxin (Trx) in NZK-Zelllinien nachgewiesen werden[173]. Weiterhin ist bereits beschrieben, dass die OXPHOS im NZK herunterreguliert wird, wobei NZK-Zellen bei geringen ROS-Konzentrationen bereits eine Apoptoseinduktion zeigten[303]. ROS sind chemische Sauerstoffradikale wie Superoxide ($O_2^-$), Hydroxylradikale (OH·), Peroxylradikale (ROO·) und Alkoxylradikale (RO·) oder stabilere molekulare Oxidantien wie Wasserstoffperoxid ($H_2O_2$), Hydroperoxide (ROOH), Ozon und Hypochlorit-Anionen sowie angeregte Sauerstoffmoleküle[304]. Mitochondrien und zytosolische NADPH-Oxidasen produzieren $O_2^-$ aus der Elektronenreduktion des Sauerstoffs[305]. In den Mitochondrien geht dabei ein geringer Teil der Elektronen aus der Elektrontransportkette der OXPHOS direkt auf den Sauerstoff über. Vorwiegend sind der Komplex I und III der Atmungskette an der ROS-Bildung beteiligt[259], aber es ist ebenfalls die Entstehung mittels des Komplex II beschrieben[306]. $O_2^-$ reagiert durch die enzymatische Aktivität der SOD im Zytosol bzw. in der Mitochondrienmatrix zu $H_2O_2$, welches anschließend mittels Peroxiredoxinen (PRDX) zu Wasser umgewandelt wird. Dabei kommt es zu einer Oxidation der Cysteine im aktiven Zentrum der PRDX[307]. Danach erfolgt die Reduktion der Cysteine durch Trx, Thioredoxinreduktase (TXNR) und NADPH, um den Ausgangszustand der PRDX wieder herzustellen[308]. Glutathionperoxidasen (GPX) können ebenfalls $H_2O_2$ mittels Oxidation von reduziertem Glutathion (GSH) in Wasser umwandeln. Wobei oxidiertes Glutathion (GSSG) anschließend via Glutathionreduktase (GR) und NADPH wieder zu GSH reduziert wird[309]. Der dritte Weg, um die Zelle von $H_2O_2$ zu entgiften, ist die Katalaseaktivität in den Peroxisomen (**Abbildung 10**). Zur verstärkten Bildung von mitochondrialen ROS kommt es vor allem unter Hypoxie, Ischämie, der Gabe von Medikamenten und durch verschiedene pathophysiologische Zustände[310]. Grundsätzlich sind ROS ein Abfallprodukt, welches in höheren Konzentrationen zu Schäden an DNA, Proteinen und Lipiden und damit zum Zelltod führt. Geringe Mengen ROS widerum aktivieren intrazelluläre proliferative Signalwege und stabilisieren HIF[303]. In Tumorzellen induziert die Aktivierung von Onkogenen oder die Sauerstoffreduktion die Produktion von ROS, was die Tumorgenese fördert[311,312].

Die Ergebnisse der vorliegenden Arbeit zeigten eine Hochregulation der SOD sowohl durch VHL-Defizienz (Manuskript 1) als auch durch CREB-Stilllegung (Manuskript 4). Weiterhin wurde bei VHL-Defizienz eine vermehrte extrazelluläre Sekretion der SOD2 beobachtet, welche mit einer Inhibition der T-Zellaktivierung und IL-2-Sekretion der T-Zellen einherging. Die Auswirkung der SOD2-Sekretion auf das TME wird in Abschnitt 5.7 diskutiert.

Die intrazellulär erhöhten SOD2-Level führen nicht nur zu einem verstärkten Abbau von $O_2^-$ zu $H_2O_2$, sondern ebenfalls zu vermehrter Invasionskapazität, Proliferation und Apoptoseresistenz von Tumorzellen[313]. Von daher wird vermutet, dass die vermehrte Expression der SOD2 vorteilhaft für die Tumorprogression ist. Einerseits begünstigt der verstärkte Abbau der toxischen, reaktiven $O_2^-$ die Zellviabilität. Andererseits scheint die lokal

erhöhte ROS-Konzentration proliferative und invasive Signalwege der Tumorzellen zu aktivieren und immunsuppressiv (Kapitel 5.7) zu wirken. Eine hohe SOD2-Expression geht ebenfalls einher mit einem kürzeren rezidivfreien Patientenüberleben im kzNKZ (*TCGA*-Daten, **Anhang Abbildung 1D**) sowie einer erhöhten Expression in allen NZK-Subtypen und -Metastasen im Vergleich zum Normalgewebe (*NCBI-GEO*-Daten, **Anhang Abbildung 2**). Weiterhin wurden VHL-abhängig die Peroxiredoxine PRDX1, PRDX2 und PRDX3 3- bis 4-fach sowie Trx 6-fach hochreguliert (Manuskript 1) identifiziert. Eine höhere PRDX2-Expression im NZK ist assoziiert mit einem niedrigeren Tumorgrad, weniger Metastasen und einer längeren Überlebenszeit der Patienten[314]. Durch CREB-Minderexpression ist das PRDX4-Proteinlevel etwa 4-fach erhöht, währenddessen das Katalase Proteinlevel ca. 3-fach und zusätzlich die Katalaseaktivität (Manuskript 4) reduziert ist. Folglich bauen VHL-defiziente oder CREB-überexprimierende Tumorzellen erhöhte $H_2O_2$-Konzentrationen nicht über die Peroxiredoxine ab, sondern vermutlich über den Katalase- oder den GPX-Weg (**Abbildung 10**). Zusätzlich führte die Behandlung mit $H_2O_2$ zu einer transient verstärkten CREB-Phosphorylierung, während die onkogentransformierten Zellen mit höherer CREB-Aktivität auch resistenter gegenüber der Zelltodinduktion bei höheren $H_2O_2$-Konzentrationen waren (Manuskript 3). Durch Behandlung mit einem HIF-Inhibitor sowie bei CREB-Minderexpression waren intrazellulär höhere ROS-Konzentrationen detektierbar (Manuskript 4).

GSH führt mittels des Enzyms GPX zum Abbau von $H_2O_2$, wobei die GSH-Mengen im NZK im Vergleich zum gesunden Gewebe vermindert sind[315]. Eigene Studien zeigten einen erhöhten GSH-Spiegel durch VHL-Überexpression (Daten nicht gezeigt) oder CREB-Minderexpression (Manuskript 4). Die Ursachen dafür sind bisher ungeklärt. In der vorliegenden Arbeit wurde lediglich eine VHL-abhängige Hochregulation der Glutathion-S-Transferase P1 (GSTP1, Manuskript 1) und eine Hochregulation der Glutathionsynthetase (GSS) nach CREB-Minderexpression in onkogentransformierten Zellen (Manuskript 4) bzw. eine VHL-abhängige Herunterregulation der GSS im Zellkulturüberstand (Manuskript 2) nachgewiesen. Hypothetisch könnte der verminderte Abbau von Glutamat zu GSH in Tumorzellen dazu dienen, Glutamat als Energiequelle für den TCA-Zyklus zu nutzen (Kapitel 5.4), was durch weitere Untersuchungen belegt werden müsste. Aus therapeutischer Sicht wird häufig angenommen, dass Antioxidantien durch den Abbau von ROS gegen Krebs schützen. Jedoch zeigen verschiedene Studien diskrepante Ergebnisse. Einige internationale Studien belegen sogar ein höheres Tumorrisiko durch antioxidative Substanzen[243,316-318]. Erst kürzlich untersuchte eine Studie mit 95 kzNZK-Patienten den Status antioxidativer Enzyme (SOD, Katalase, GPX, GST, GR, GSH und Malondialdehyd) nach einer Nephrektomie, wobei keine Korrelation mit dem 5-Jahres-Gesamtüberleben nachgewiesen werden konnte[319].

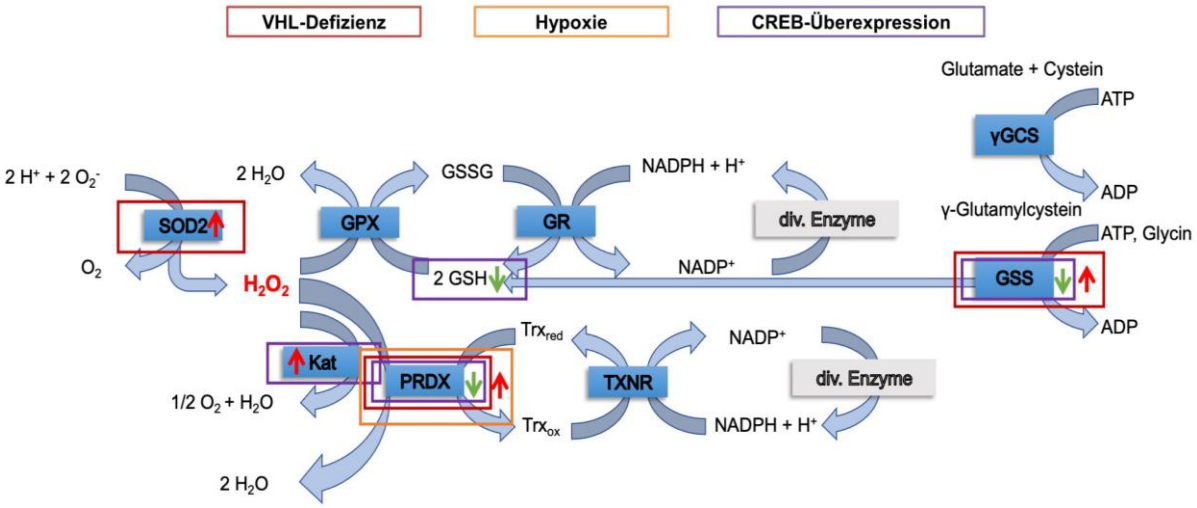


**Abbildung 10: VHL-, Hypoxie- und CREB-mediierter ROS-Abbau.**
Die Abbildung stellt schematisch den enzymatischen Abbau von Superoxiden ($O_2^-$) und Wasserstoffperoxid ($H_2O_2$) dar. Die differentiell regulierten Enzyme und Metabolite sind farbig markiert (VHL-Defizienz, Hypoxie, CREB-Überexpression). Eine Hochregulation der Superoxiddismutase (SOD) 2-Proteinmenge wurde in den VHL-defizienten NZK-Zelllinie 786-0 detektiert. Zusätzlich wiesen die Überstände dieser Zellen eine höhere SOD2-Menge und Glutathionsyntethase (GSS) auf. VHL-Defizienz führte zu weniger Peroxiredoxin (PRDX) 2- und 3-Protein. Im Gegensatz dazu wurde unter Hypoxie PRDX1 hochreguliert nachgewiesen. CREB-Überexpression zeigte in Onkogen-transformierten Zellen erhöhte Katalase (Kat)- sowie verringerte (PRDX) 4-, GSS- und Glutathion (GSH)-Level. ↑, erhöht; ↓, reduziert; ADP/ATP, Adenosindiphosphat/Adenosintriphosphat; GCS, Glutamyl-Cystein-Synthetase, GPX, Glutathionperoxidase; GSSG, Glutathiondisulfid; $NADP^+/H$,. Nicotinamidadenindinukleotidphosphat (oxidiert/reduziert); Trx, Thioredoxin; TXNR Thioredoxinreduktase.

## 5.7 Die Auswirkung von VHL-Defizienz, verstärkte CREB-Aktivität oder Hypoxie auf das TME und die Zellen des Immunsystems

Eine Konsequenz des „Warburg-Effektes“ ist eine Protonen- und Laktatanreicherung im TME[320]. Ein saures Mikromilieu des Tumors hat Einfluss auf eine Reihe von Immunzellen[321]. So werden T-Zellen, NK-Zellen und Makrophagen in Proliferation und Aktivität gehemmt (**Tabelle 4**), was dem Tumor einen selektiven Vorteil verschafft, der Erkennung des Immunsystems zu entgehen. Weiterhin geht ein niedriger pH-Wert des TME mit der Resistenz der Tumore gegen Chemo- und Radiotherapie[322-326] sowie mit einer schlechteren Prognose[327,328] und reduzierter Überlebenszeit nach Tumorresektion einher[329,330]. Zusätzlich sprechen Tumore mit saurem TME weniger auf Therapien mit *Checkpoint*-Inhibitoren, wie z. B. Ipilimumab, an[331,332].

**Tabelle 4: Auswirkung der Ansäuerung des TME auf Immunzellen.**

| Immunzellen | Effekt durch Ansäuerung des TME |
|---|---|
| Effektor-T-Zellen | Proliferation ↓[151]<br>Zytokinproduktion ↓[151]<br>Induktion von $T_{reg}$ ↓[254,255] |
| $T_{reg}$ | Immunsuppression ↑[254,255] |
| NK-Zellen | Zytokinproduktion IFNy, ↓[333,334]<br>Granzym B ↓[151]<br>Apoptose ↑[151] |
| Makrophagen | ICER ↑[243]<br>Polarisation zu M2 TAMs↑[243]<br>Produktion inflammatorischer Zytokine ↓[335]<br>T-Zell-Aktivierung ↓[256]<br>VEGF ↑[149] |
| Dendritische Zellen | T-Zell-Aktivierung ↓[147,336]<br>IL-10 ↑[337] |

↑, erhöht; ↓ reduziert; ICER, *Inducible cyclic adenosine monophosphate early repressor*; IFN, Interferon; IL, Interleukin; NK-Zellen, natürliche Killerzellen; TAM, Tumor-assoziierte Makrophagen; $T_{reg}$, regulatorische T-Zellen; VEGF, vaskulärer endothelialer Wachstumsfaktor; verändert nach Lacroix *et* al., 2018[126]

Die *in vitro*-Untersuchungen in Manuskript 1 zeigten eine bis zu 55 % erniedrigte Laktatkonzentration und einen gesteigerten pH-Wert im Zellkulturüberstand nach Überexpression des funktionellen VHL-Proteins in drei verschiedenen kzNZK-Zelllinien. Die Reversion dieses Effektes war durch Inkubation der Zellen unter hypoxischen Bedingungen detektierbar. Intrazellulär zeigte sich eine verringerte LDH-Aktivität (bis 66 %) durch VHL-Überexpression (Manuskript 1) oder verminderte CREB-Expression in Onkogen-transformierten Zellen (Manuskript 4). Ebenfalls führte die shRNA-vermittelte CREB-Reduktion zu einer verminderten extrazellulären Laktatkonzentration bzw. zu einem erhöhten pH-Wert (Manuskript 4). *In vivo* können intratumorale Laktatwerte bereits mit verschiedenen Methoden (PET, CEST-MRT, $1^{H}$-MRT) bestimmt werden[338-343]. Dabei erreichen Tumorzellen intrazelluläre Laktatlevel von bis zu 40 nmol/l[151]. Weiterhin können sich intratumoral mehrere Subpopulationen verschiedener glykolytisch aktiver Zellen bilden[168]. Dabei sezernieren (z. B. VHL-defiziente, hypoxische oder CREB-überexprimierende) anabole Tumorzellen verstärkt Laktat, während umliegende oxidative katabole Tumorzellen dieses als Energiequelle nutzen und in den TCA-Zyklus einbringen[344](**Abbildung 4**). Folglich kommt es zu einer Kooperation heterogener Tumorzelltypen und damit zum stärkeren Vorantreiben der Tumorprogression (**Abbildung 11**), trotz der partiell schlechten Versorgung des Tumors mit Sauerstoff und der ungeordneten tumorassoziierten Neovaskularisierung. Hypothetisch könnte die Versorgung

von anabolen Tumorzellen mit Laktat zusätzlich das Auswachsen von Tumorstammzellen (TSZ) begünstigen. Die Entstehung von TSZ, welche ebenfalls als tumorinitiierende Zellen bezeichnet werden, ist bisher nicht vollständig geklärt. Bei TSZ handelt es sich um eine Tumorzellsubpopulation, die eine hohe Proliferation und Tumorigenität aufweisen und vermutlich eine entscheidende Rolle bei der Entstehung, Progression, Chemotherapieresistenz, Rezidiv und Metastasierung des NZK spielen[161]. NZK-TSZ exprimieren Stammzellmarker wie CXCR4, CD105, CD133 und CD44 auf der Zelloberfläche[345]. Ob TSZ von einem glykolytischen Metabolismus profitieren ist bisher unklar[346,347]. Allerdings wurde bereits gezeigt, dass sowohl ruhende als auch proliferierende TSZ eine gesteigerte OXPHOS besitzen und den mitochondrialen oxidativen Metabolismus präferieren[346]. Folglich ist es denkbar, dass Tumorzellen mit anabolem Stoffwechsel die Versorgung von TSZ in hypoxischen Nischen des Tumor unterstützen.

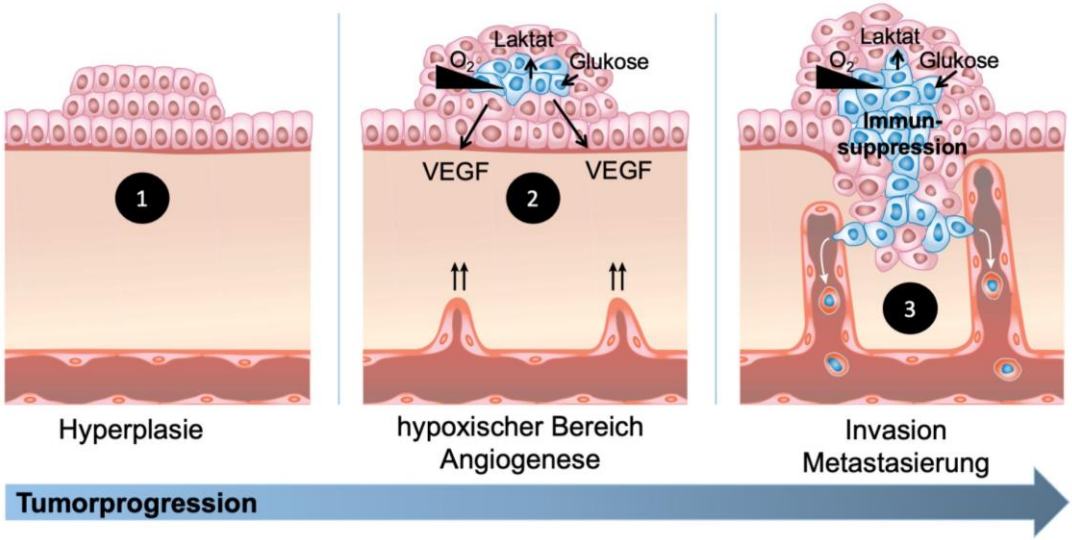


**Abbildung 11: Interaktion zwischen heterogenen Tumorbereichen mit unterschiedlichem glykolytischen Phänotyp.**
Durch Aktivierung von Onkogenen bzw. Inaktivierung von Tumorsuppressorgenen kommt es zur unkontrollierten Zellteilung (Hyperplasie) (**1**). Aufgrund der Volumenzunahme des Tumors sinkt einerseits die Versorgung mit Sauerstoff ($O_2$) im Inneren. Andererseits können sich durch die genetische Instabilität der stark proliferierenden Tumorzellen weitere Tumorzellsubpopulationen ausbilden, die ein Umschalten des Metabolismus zur aeroben Glykolyse (Warburg Effekt) aufweisen. Durch die verstärkte Laktatsezernierung und die Ausschüttung des vaskulären epithelialen Wachstumsfaktors (VEGF) dieser anabolen Tumorzellen wird das umliegende oxigenierte katabole Gewebe mit Laktat als Energieträger versorgt und die Vaskularisierung des Tumors angeregt (**2**).Folglich können verschiedene Tumorregionen mit unterschiedlichen metabolischen Phänotypen miteinander interagieren und somit die Tumorprogression, Invasion und Metastasierung vorantreiben. Zusätzlich führt die Ansäuerung des Tumormikromilieus zur Inaktivierung von Immunzellen (Tabelle 4), was die Ausbreitung und Invasion des Tumors begünstigt (**3**). Verändert nach DeBerardinis und Chandel, 2016[348].

Die LDH-Aktivität *in vivo* kann im Serum sowie im Tumor bestimmt werden und dient beim Melanom als ein prognostischer Überlebensfaktor[349]. Dabei korreliert eine hohe LDH-Aktivität mit einer negativen Prognose (Gesamtüberleben, progressionsfreies Überleben, Therapieansprechen) bei Immuntherapien mit dem *Cytotoxic T-lymphocyte-associated* (CTLA)-4 Antikörper Ipilimumab und/oder dem *Programmed cell death* (PD)-1 Antikörper

Pembrolizumab[350]. Weiterhin gehen erhöhte LDH-Mengen ebenfalls bei anderen Tumorentitäten mit einer schlechteren Prognose einher[351-353]. siRNA-vermittelte LDHA-Reduktion führte interessanterweise zur verminderten Expression des CREB-Zielgens MMP2 und zur verminderten Migrations- und Invasionskapazität von Gliomzellen[354]. Zurzeit gibt es eine Reihe klinischer Studien, die die Kombination aus der Behandlung mit *Checkpoint*-Inhibitoren und der Reduktion der Ansäuerung des TME untersuchen (NCT02968303, NCT02631447, NCT02902029)[355]. Es wurde bereits gezeigt, dass LDHA-defiziente Tumore langsamer in immunkompetenten Mäusen wachsen. Dieser Effekt konnte in T- und NK-Zell-depletierten Mäusen revertiert werden[151].

Ebenfalls werden weitere Therapieoptionen, wie die Blockierung der Laktattransporter (NCT01791595, Phase I klinische Studie)[356-358], der Protonenpumpen (z. B. durch Pantoprazol)[359-361] oder der Carboanhydrasen[362,363] untersucht, um eine pH-Wert-Reduktion des TME zu verhindern und damit eine Immunzellhemmung zu vermeiden. Für den Wirkstoff Diclofenac wurde gezeigt, dass dieser die Laktatproduktion der Tumorzellen reduziert. Dabei führte die Behandlung mit Diclofenac aber ebenfalls zur Hemmung der T-Zell-Aktivität[254,255,336]. Zusätzlich könnten Puffertherapien wie z. B. die Bicarbonattherapie zur pH-Wert-Stabilisierung im TME in Erwägung gezogen werden[364,365]. Folglich zeigen die Ergebnisse der vorliegenden Manuskripte, dass diese verschiedenen neuartigen Behandlungsoptionen gegen die Ansäuerung des TME zukünftig die Therapieeffizienz des VHL-defizienten, hypoxischen und CREB-überexprimierenden NZK entscheidend steigern und zur Überwindung von immuntherapeutischen Resistenzen beitragen könnten.

Weiterhin wurde beschrieben, dass Hypoxie über die Stabilisierung von HIF zur Herunterregulation der MHC Klasse I-Antigenpräsentation und damit zur verminderten T-Zellantwort führt[366]. Neben der pH-Wert-Reduktion und der verminderten Antigenpräsentation wird die Erkennung der Tumorzellen durch das Immunsystem durch tumorspezifische Proteinsezernierung in das TME beeinflusst. In Manuskript 2 wurde die VHL- und Hypoxie-mediierte Proteinsezernierung mittels 2D-Gelelektrophorese untersucht. Dabei zeigte sich die differentielle Regulation einiger immunmodulatorischer Proteine, wie die VHL-abhängige Herunterregulation des antioxidativen Enzyms SOD2 und die verstärkte Sezernierung von Beta-2-Mikroglobulin (β2M), welches funktionell an der MHC Klasse I-Antigenpräsentation beteiligt ist. Zusätzlich wurde nachgewiesen, dass die Inkubation mit SOD2 zu einer verringerten Aktivität, Proliferation und IL-2-Sekretion von T-Zellen (PBMC) führt (Manuskript 2). Folglich wäre SOD2 für VHL-defiziente NZK sowohl als prognostischer Marker sowie auch als Zielprotein für therapeutische Ansätze, z. B. mittels Entwicklung eines spezifischen Inhibitors, geeignet.

# 6 Zusammenfassung

Während des letzten Jahrzehnts hat das Wissen über die molekularen Mechanismen der zellulären Anpassung an Hypoxie, über die Funktion des VHL-Proteins und der Transkriptionsfaktoren HIF und CREB im Metabolismus des NZK stark zugenommen. Trotzdem gab es zum Zeitpunkt der Erstellung, der in der Arbeit verwendeten Manuskripte, wenige Informationen über die Konvergenz und Diskrepanz in der Genexpression und Proteinsekretion dieser Prozesse. Ziel dieser Arbeit war es daher, VHL-, CREB- und Hypoxie-regulierte Veränderungen im Tumormetabolismus mittels Transkriptom- und Proteom-basierenden Strategien (**Abbildung 5**) zu untersuchen. Weiterhin wurde der Einfluss von VHL, CREB und Hypoxie auf den Zellstoffwechsel durch die Bestimmung der Glukoseaufnahme, der Laktatsekretion, des extrazellulären pH-Werts, der intrazellulären LDH-Aktivität, des AS-Gehalts und der ATP-Mengen analysiert. Zusätzlich wurde das Sekretom einer VHL-negativen NZK-Zelllinie und der korrespondierenden VHL-positiven Überexpressionsvariante unter sauerstoffarmen und sauerstoffreichen Bedingungen verglichen.
Zusammenfassend lassen sich folgende Erkenntnisse aus der vorliegenden Dissertation gewinnen:

**i)** Sowohl VHL-Defizienz und Hypoxie als auch CREB-Überexpression führen zur Überexpression der Glykolyseenzyme, zu einer verstärkten zellulären glykolytischen Aktivität, erhöhter LDH-Aktivität und zu verstärkter Laktat- sowie Protonensekretion in den extrazellulären Raum („Warburg Effekt“). Somit wäre eine antiglykolytische Therapie oder eine Therapie, die die Laktatsekretion bzw. das Ansäuern des TME unterbindet in VHL-defizienten, hypoxischen oder CREB-überexprimierenden NZK vermutlich gleichermaßen wirksam. Zusätzlich wurde eine ausschließlich CREB-abhängige Expression der PKG sowie die Expression von Enzymen, die zwar VHL-abhängig, aber nicht Hypoxie-abhängig reguliert vorlagen (PGAM, PKM), nachgewiesen. Im Gegensatz dazu wären TPI1 und ENO einerseits als therapeutische antiglykolytische Zielproteine besonders geeignet, weil beide Enzyme HIF-abhängig (divergent exprimiert durch Hypoxie und VHL-Funktionalität) und CREB-abhängig reguliert werden. Andererseits stellen beide Enzyme neue prognostische Marker dar, da sie ebenfalls in höherer Menge im Sekretom der NZK-Zellen nachgewiesen wurden.

**ii)** Im Gegensatz zur Glykolyse zeigen die Analysen der VHL-, CREB- und Hypoxie-abhängigen mitochondrialen Aktivität Unterschiede: CREB-Überexpression führt zu einer erhöhten mitochondrialen Aktivität und zur verstärkten Expression der Citratsynthase, während es bei VHL-Verlust zu einer reduzierten mitochondrialen Aktivität und zur verminderten ACO1-Expression kommt. Zusätzlich waren bei VHL-Defizienz die Enzyme der Komplexe II und III der Atmungskette auf Proteinebene herunterreguliert. Unklar bleibt hier

inwiefern eine therapeutische Intervention der mitochondrialen Aktivität im NZK die Tumorprogression beeinflussen würde. Zwar scheint die Ansammlung von Succinat durch die reduzierte SDHA tumorigen zu wirken, jedoch wird den Tumorzellen durch die verminderte OXPHOS weniger ATP zur Verfügung gestellt.

**iii)** Durch VHL-Defizienz und Hypoxie wird ACO1 vermindert exprimiert, was zu einer erhöhten Citratansammlung führt. Ebenfalls könnte die CREB-abhängige Hochregulation der Citratsynthase zur vermehrten Citratansammlung beitragen. Beide Vorgänge könnten ursächlich für die vermehrte Lipidansammlung im NZK sein, welche nachweislich zum malignen Phänotyp beiträgt. Zusätzlich wurde eine reduzierter Fettsäureabbau und erhöhter Fettsäuretransport in den VHL-defizienten NZK-Zellen nachgewiesen.

**iv)** Sowohl VHL-Verlust als auch verstärkte CREB-Expression führen zu erhöhtem Abbau von ROS. Allerdings sind verschiedene Abbauwege ursächlich.

**v)** Die VHL-Defizienz- und Hypoxie-bedingte SOD2-Hochregulation führt nicht ausschließlich zum intrazellulären ROS-Abbau, sondern gleichermaßen zur verstärkten Sekretion des Proteins. Sekretiertes SOD2 vermindert die T-Zell-Aktivierung, -Proliferation und -IL-2-Sekretion. Aufgrund dessen ist SOD2 eine geeignete Zielstruktur für Therapieansätze, die zur gesteigerten tumoralen Immunantwort gegen das NZK führen könnten.

**vi)** Aufgrund der funktionellen Bedeutung des Proteins TGM2 in der Tumorentwicklung und seiner Abhängigkeit von der HIF2α-Proteinmenge, stellt TGM2 sowohl einen neuen prognostischen Faktor als auch ein wichtiges putatives therapeutisches Ziel für das kzNZK dar.

Ein schematischer Überblick über die Ergebnisse der VHL-, Hypoxie- und CREB-gesteuerten Änderungen im Zellmetabolismus ist in **Abbildung 12** dargestellt.

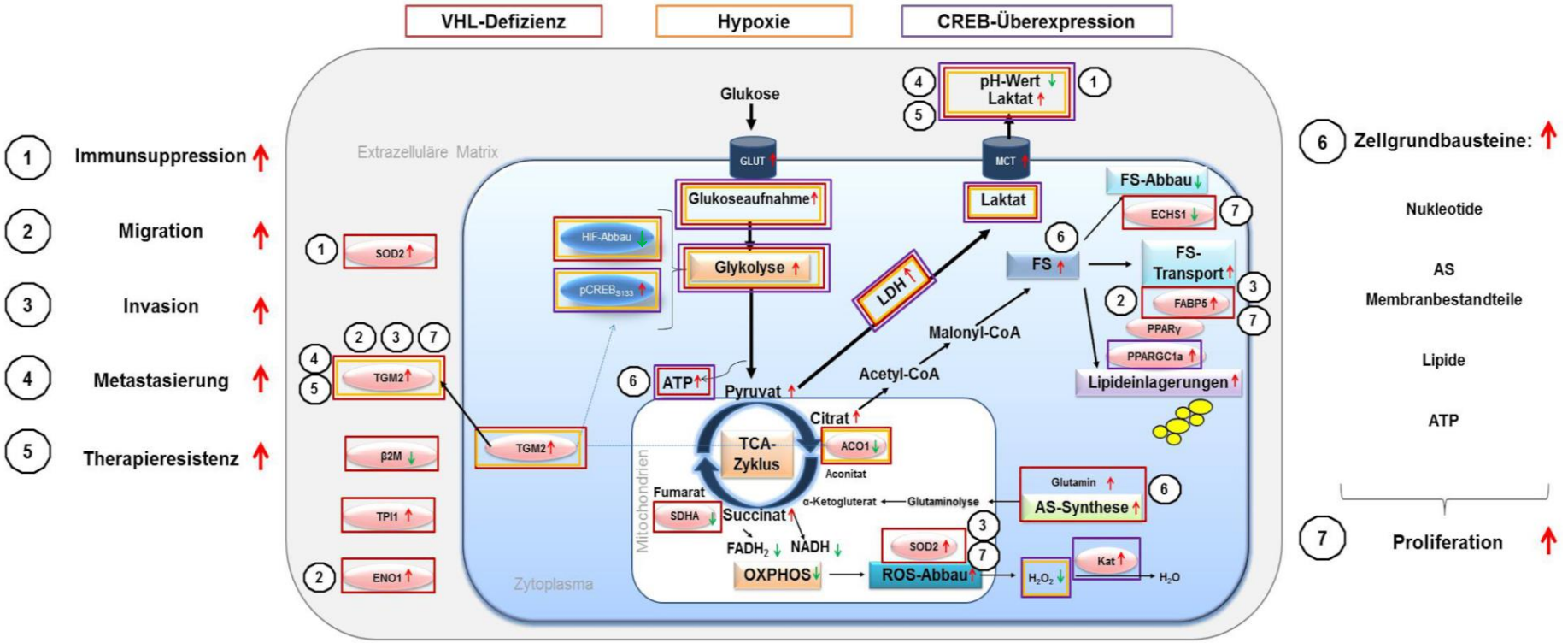


**Abbildung 12: Schematische Zusammenfassung der VHL-, Hypoxie-, und CREB-gesteuerten Deregulation des Zellmetabolismus.**
Die differentiell regulierten und am Metabolismus beteiligten Enzyme oder Metabolite sind farbig markiert ( VHL-Defizienz, Hypoxie, CREB-Überexpression). ↑, erhöht; ↓, reduziert; ACO, Aconitase; ATP, Adenosintriphosphat; AS, Aminosäure; β2M, Beta-2-Mikroglobulin; Kat, Katalase; CREB, *Cyclic adenosin monophosphate response element-binding protein* 1; ECHS, *Enoyl-CoA hydratase, short chain*; ENO, Enolase; FABP, *Fatty-acid binding protein*; FAD; Flavinadenindinukleotid; FS, Fettsäure; HIF, *Hypoxia-inducible factor*; LDH, Laktatdehydrogenase; NAD, Nicotinamidadenindinukleotid; OXPHOS, Oxidative Phosphorylierung; PPAR, Peroxisom-Proliferator-aktivierter Rezeptor; PPARGC1a, PPAR Gamma Coaktivator 1 alpha; ROS, *Reactive oxygen species*, SDH, Succinatdehydrogenase; SOD, Superoxiddismutase; TCA, *Tricarbonic acid*; TGM, Transglutaminase; TPI, Triosephosphatisomerase; VHL, Von Hippel-Lindau-Protein.

# 7 Ausblick

Trotz der Fortschritte der letzten Jahre in der Behandlung des metastasierenden NZK mit Zytokinen, Antikörpertherapien, Tumorvakzinierungen oder TKI liegt die 5-Jahres-Überlebensrate fortgeschrittener Stadien bei unter 20 %. Dies zeigt die Unerlässlichkeit der Etablierung neuer Ansätze in der Therapie des NZK. Dazu ist es u. a. notwendig, die tumoralen Stoffwechselvorgänge und die Veränderungen der Genexpression durch den Verlust von Tumorsuppressoren wie VHL oder des Anschaltens von Transkriptionsfaktoren wie HIF und CREB oder auch Tumorstammzellmarkern wie TGM2 zu analysieren. Die vorliegende Dissertation trägt diesbezüglich zur Aufklärung bei und schafft Ansatzpunkte für die Entwicklung und Einsatzmöglichkeiten neuer oder bereits existierender Inhibitoren/Antikörper. Erst in den letzten Jahren (teilweise nach dem Erscheinen der Manuskripte) wurden zahlreiche klinische Studien zur Untersuchung der Wirksamkeit von Substanzen, welche gegen die metabolischen Veränderungen in Tumoren gerichtet sind, initiiert (siehe Diskussion). Für die Therapie des kzNZK wären vor allem Substanzen, die entweder direkt gegen das glykolytische Umschalten der Tumorzellen oder zumindest das Ansäuern des TME unterbinden von Vorteil, um die Wirkung von Immuntherapien zu verbessern und Therapieresistenzen zu vermeiden. Ebenfalls sollten TGM2-, TPI1- und SOD2-Inhibitoren gegen das kzNZK zur Unterstützung der konventionellen Therapie getestet werden. Zukünftig wäre auch eine personalisierte Therapie denkbar, welche auf der Bestimmung von prognostischen Markern wie ENO, TPI1, ALDOA oder SOD2 aus dem Patientenserum basiert. Allerdings müssten der Etablierung solcher Therapien eine Reihe weiterer klinischer Studien vorangehen, um die Sicherheit der Patienten zu gewährleisten.

# 8 Literaturverzeichnis


1 Lopez-Beltran, A., Scarpelli, M., Montironi, R. & Kirkali, Z. 2004 WHO classification of the renal tumors of the adults. *Eur Urol* **49**, 798-805, doi:10.1016/j.eururo.2005.11.035 (2006).

2 Bray, F. *et al.* Global cancer statistics 2018: GLOBOCAN estimates of incidence and mortality worldwide for 36 cancers in 185 countries. *CA Cancer J Clin* **68**, 394-424, doi:10.3322/caac.21492 (2018).

3 Hsieh, J. J. *et al.* Renal cell carcinoma. *Nat Rev Dis Primers* **3**, 17009, doi:10.1038/nrdp.2017.9 (2017).

4 Frew, I. J. & Moch, H. A clearer view of the molecular complexity of clear cell renal cell carcinoma. *Annu Rev Pathol* **10**, 263-289, doi:10.1146/annurev-pathol-012414-040306 (2015).

5 Linehan, W. M. *et al.* Comprehensive Molecular Characterization of Papillary Renal-Cell Carcinoma. *N Engl J Med* **374**, 135-145, doi:10.1056/NEJMoa1505917 (2016).

6 Davis, C. F. *et al.* The somatic genomic landscape of chromophobe renal cell carcinoma. *Cancer Cell* **26**, 319-330, doi:10.1016/j.ccr.2014.07.014 (2014).

7 Chen, F. *et al.* Multilevel Genomics-Based Taxonomy of Renal Cell Carcinoma. *Cell Rep* **14**, 2476-2489, doi:10.1016/j.celrep.2016.02.024 (2016).

8 Kovacs, G. *et al.* The Heidelberg classification of renal cell tumours. *J Pathol* **183**, 131-133, doi:10.1002/(SICI)1096-9896(199710)183:2<131::AID-PATH931>3.0.CO;2-G (1997).

9 Srigley, J. R. *et al.* The International Society of Urological Pathology (ISUP) Vancouver Classification of Renal Neoplasia. *Am J Surg Pathol* **37**, 1469-1489, doi:10.1097/PAS.0b013e318299f2d1 (2013).

10 Delahunt, B., Eble, J. N., Egevad, L. & Samaratunga, H. Grading of renal cell carcinoma. *Histopathology* **74**, 4-17, doi:10.1111/his.13735 (2019).

11 Swami, U., Nussenzveig, R. H., Haaland, B. & Agarwal, N. in *Ann Transl Med* Vol. 7 S18 (2019).

12 Rini, B. I., Campbell, S. C. & Escudier, B. Renal cell carcinoma. *Lancet* **373**, 1119-1132, doi:10.1016/S0140-6736(09)60229-4 (2009).

13 Kroeger, N. *et al.* Metastatic non-clear cell renal cell carcinoma treated with targeted therapy agents: characterization of survival outcome and application of the International mRCC Database Consortium criteria. *Cancer* **119**, 2999-3006, doi:10.1002/cncr.28151 (2013).

14 Gerlinger, M. *et al.* Intratumor heterogeneity and branched evolution revealed by multiregion sequencing. *N Engl J Med* **366**, 883-892, doi:10.1056/NEJMoa1113205 (2012).

15 Gerlinger, M. *et al.* Genomic architecture and evolution of clear cell renal cell carcinomas defined by multiregion sequencing. *Nat Genet* **46**, 225-233, doi:10.1038/ng.2891 (2014).

16 Sankin, A. *et al.* The impact of genetic heterogeneity on biomarker development in kidney cancer assessed by multiregional sampling. *Cancer Med* **3**, 1485-1492, doi:10.1002/cam4.293 (2014).

17 Network, C. G. A. R. Comprehensive molecular characterization of clear cell renal cell carcinoma. *Nature* **499**, 43-49, doi:10.1038/nature12222 (2013).

18 Hsieh, J. J. *et al.* Overcome tumor heterogeneity-imposed therapeutic barriers through convergent genomic biomarker discovery: A braided cancer river model of kidney cancer. *Semin Cell Dev Biol* **64**, 98-106, doi:10.1016/j.semcdb.2016.09.002 (2017).

19 Ljungberg, B. *et al.* EAU guidelines on renal cell carcinoma: 2014 update. *Eur Urol* **67**, 913-924, doi:10.1016/j.eururo.2015.01.005 (2015).

20 El Dib, R., Touma, N. J. & Kapoor, A. Cryoablation vs radiofrequency ablation for the treatment of renal cell carcinoma: a meta-analysis of case series studies. *BJU Int* **110**, 510-516, doi:10.1111/j.1464-410X.2011.10885.x (2012).

21 Kuijpers, Y. A. *et al.* Potentially curable recurrent disease after surgically managed non-metastatic renal cell carcinoma in low-, intermediate- and high-risk patients. *World J Urol* **34**, 1073-1079, doi:10.1007/s00345-016-1822-6 (2016).

22 Frank, I. *et al.* An outcome prediction model for patients with clear cell renal cell carcinoma treated with radical nephrectomy based on tumor stage, size, grade and necrosis: the SSIGN score. *J Urol* **168**, 2395-2400, doi:10.1097/01.ju.0000035885.91935.d5 (2002).

23 Wolff, I. *et al.* Do we need new high-risk criteria for surgically treated renal cancer patients to improve the outcome of future clinical trials in the adjuvant setting? Results of a comprehensive analysis based on the multicenter CORONA database. *Eur J Surg Oncol* **42**, 744-750, doi:10.1016/j.ejso.2016.01.009 (2016).

24 Shuch, B. *et al.* Defining early-onset kidney cancer: implications for germline and somatic mutation testing and clinical management. *J Clin Oncol* **32**, 431-437, doi:10.1200/JCO.2013.50.8192 (2014).

25 McLaughlin, J. K., Lipworth, L. & Tarone, R. E. Epidemiologic aspects of renal cell carcinoma. *Semin Oncol* **33**, 527-533, doi:10.1053/j.seminoncol.2006.06.010 (2006).

26 Lee, J. E. *et al.* Fat, protein, and meat consumption and renal cell cancer risk: a pooled analysis of 13 prospective studies. *J Natl Cancer Inst* **100**, 1695-1706, doi:10.1093/jnci/djn386 (2008).

27 Setiawan, V. W., Stram, D. O., Nomura, A. M., Kolonel, L. N. & Henderson, B. E. Risk factors for renal cell cancer: the multiethnic cohort. *Am J Epidemiol* **166**, 932-940, doi:10.1093/aje/kwm170 (2007).

28 Lipworth, L., Tarone, R. E., Lund, L. & McLaughlin, J. K. Epidemiologic characteristics and risk factors for renal cell cancer. *Clin Epidemiol* **1**, 33-43 (2009).

29 Chow, W. H., Dong, L. M. & Devesa, S. S. Epidemiology and risk factors for kidney cancer. *Nat Rev Urol* **7**, 245-257, doi:10.1038/nrurol.2010.46 (2010).

30 McDermott, D. F. *et al.* Randomized phase III trial of high-dose interleukin-2 versus subcutaneous interleukin-2 and interferon in patients with metastatic renal cell carcinoma. *J Clin Oncol* **23**, 133-141, doi:10.1200/JCO.2005.03.206 (2005).

31 Rini, B. I. *et al.* Society for Immunotherapy of Cancer consensus statement on immunotherapy for the treatment of renal cell carcinoma. *J Immunother Cancer* **4**, 81, doi:10.1186/s40425-016-0180-7 (2016).

32 Rini, B. I. *et al.* The society for immunotherapy of cancer consensus statement on immunotherapy for the treatment of advanced renal cell carcinoma (RCC). *J Immunother Cancer* **7**, 354, doi:10.1186/s40425-019-0813-8 (2019).

33 Ahrens, M., Hartmann, A. & Bergmann, L. Was ist neu bei der Diagnostik und Therapie des Nierenzellkarzinoms? *Dtsch Med Wochenschr* **145**, 734-739 (2020).

34 Miller, K. *et al.* Interdisziplinäre Empfehlungen zur Behandlung des fortgeschrittenen Nierenzellkarzinoms. *Aktuelle Urol* **51**, 572-581 (2020).

35 Moch, H., Cubilla, A. L., Humphrey, P. A., Reuter, V. E. & Ulbright, T. M. The 2016 WHO Classification of Tumours of the Urinary System and Male Genital Organs-Part A: Renal, Penile, and Testicular Tumours. *Eur Urol* **70**, 93-105, doi:10.1016/j.eururo.2016.02.029 (2016).

36 Sato, Y. *et al.* Integrated molecular analysis of clear-cell renal cell carcinoma. *Nat Genet* **45**, 860-867, doi:10.1038/ng.2699 (2013).

37 Hakimi, A. A. *et al.* Adverse outcomes in clear cell renal cell carcinoma with mutations of 3p21 epigenetic regulators BAP1 and SETD2: a report by MSKCC and the KIRC TCGA research network. *Clin Cancer Res* **19**, 3259-3267, doi:10.1158/1078-0432.CCR-12-3886 (2013).

38 Hakimi, A. A. *et al.* Clinical and pathologic impact of select chromatin-modulating tumor suppressors in clear cell renal cell carcinoma. *Eur Urol* **63**, 848-854, doi:10.1016/j.eururo.2012.09.005 (2013).

39 Peña-Llopis, S. *et al.* BAP1 loss defines a new class of renal cell carcinoma. *Nat Genet* **44**, 751-759, doi:10.1038/ng.2323 (2012).

40 Haas, N. B. & Nathanson, K. L. Hereditary kidney cancer syndromes. *Adv Chronic Kidney Dis* **21**, 81-90, doi:10.1053/j.ackd.2013.10.001 (2014).

41 Gnarra, J. R. *et al.* Mutations of the VHL tumour suppressor gene in renal carcinoma. *Nat Genet* **7**, 85-90, doi:10.1038/ng0594-85 (1994).

42 Linehan, W. M., Gnarra, J. R., Lerman, M. I., Latif, F. & Zbar, B. Genetic basis of renal cell cancer. *Important Adv Oncol*, 47-70 (1993).

43 Audenet, F., Yates, D. R., Cancel-Tassin, G., Cussenot, O. & Rouprêt, M. Genetic pathways involved in carcinogenesis of clear cell renal cell carcinoma: genomics towards personalized medicine. *BJU Int* **109**, 1864-1870, doi:10.1111/j.1464-410X.2011.10661.x (2012).

44 Young, A. C. *et al.* Analysis of VHL Gene Alterations and their Relationship to Clinical Parameters in Sporadic Conventional Renal Cell Carcinoma. *Clin Cancer Res* **15**, 7582-7592, doi:10.1158/1078-0432.CCR-09-2131 (2009).

45 Gattolliat, C. H. *et al.* Integrative analysis of dysregulated microRNAs and mRNAs in multiple recurrent synchronized renal tumors from patients with von Hippel-Lindau disease. *Int J Oncol* **53**, 1455-1468, doi:10.3892/ijo.2018.4490 (2018).

46 Maher, E. R., Neumann, H. P. & Richard, S. von Hippel-Lindau disease: a clinical and scientific review. *Eur J Hum Genet* **19**, 617-623, doi:10.1038/ejhg.2010.175 (2011).

47 Cowey, C. L. & Rathmell, W. K. VHL gene mutations in renal cell carcinoma: role as a biomarker of disease outcome and drug efficacy. *Curr Oncol Rep* **11**, 94-101 (2009).

48 Schoenfeld, A., Davidowitz, E. J. & Burk, R. D. A second major native von Hippel-Lindau gene product, initiated from an internal translation start site, functions as a tumor suppressor. *Proc Natl Acad Sci U S A* **95**, 8817-8822, doi:10.1073/pnas.95.15.8817 (1998).

49 Iliopoulos, O., Ohh, M. & Kaelin, W. G. pVHL19 is a biologically active product of the von Hippel-Lindau gene arising from internal translation initiation. *Proc Natl Acad Sci U S A* **95**, 11661-11666, doi:10.1073/pnas.95.20.11661 (1998).

50 Blankenship, C., Naglich, J. G., Whaley, J. M., Seizinger, B. & Kley, N. Alternate choice of initiation codon produces a biologically active product of the von Hippel Lindau gene with tumor suppressor activity. *Oncogene* **18**, 1529-1535, doi:10.1038/sj.onc.1202473 (1999).

51 Kibel, A., Iliopoulos, O., DeCaprio, J. A. & Kaelin, W. G. Binding of the von Hippel-Lindau tumor suppressor protein to Elongin B and C. *Science* **269**, 1444-1446, doi:10.1126/science.7660130 (1995).

52 Lonergan, K. M. *et al.* Regulation of hypoxia-inducible mRNAs by the von Hippel-Lindau tumor suppressor protein requires binding to complexes containing elongins B/C and Cul2. *Mol Cell Biol* **18**, 732-741, doi:10.1128/mcb.18.2.732 (1998).

53 Stebbins, C. E., Kaelin, W. G. & Pavletich, N. P. Structure of the VHL-ElonginC-ElonginB complex: implications for VHL tumor suppressor function. *Science* **284**, 455-461, doi:10.1126/science.284.5413.455 (1999).

54 Kishida, T., Stackhouse, T. M., Chen, F., Lerman, M. I. & Zbar, B. Cellular proteins that bind the von Hippel-Lindau disease gene product: mapping of binding domains and the effect of missense mutations. *Cancer Res* **55**, 4544-4548 (1995).

55 Schoenfeld, A. R., Davidowitz, E. J. & Burk, R. D. Elongin BC complex prevents degradation of von Hippel-Lindau tumor suppressor gene products. *Proc Natl Acad Sci U S A* **97**, 8507-8512, doi:10.1073/pnas.97.15.8507 (2000).

56 Maxwell, P. H. *et al.* The tumour suppressor protein VHL targets hypoxia-inducible factors for oxygen-dependent proteolysis. *Nature* **399**, 271-275, doi:10.1038/20459 (1999).

57 Xia, X. *et al.* Integrative analysis of HIF binding and transactivation reveals its role in maintaining histone methylation homeostasis. *Proc Natl Acad Sci U S A* **106**, 4260-4265, doi:10.1073/pnas.0810067106 (2009).

58 Schödel, J. *et al.* High-resolution genome-wide mapping of HIF-binding sites by ChIP-seq. *Blood* **117**, e207-217, doi:10.1182/blood-2010-10-314427 (2011).

59 Hon, W. C. *et al.* Structural basis for the recognition of hydroxyproline in HIF-1 alpha by pVHL. *Nature* **417**, 975-978, doi:10.1038/nature00767 (2002).

60 Min, J. H. *et al.* Structure of an HIF-1alpha -pVHL complex: hydroxyproline recognition in signaling. *Science* **296**, 1886-1889, doi:10.1126/science.1073440 (2002).

61 Bruick, R. K. & McKnight, S. L. A conserved family of prolyl-4-hydroxylases that modify HIF. *Science* **294**, 1337-1340, doi:10.1126/science.1066373 (2001).

62 Ivan, M. *et al.* HIFalpha targeted for VHL-mediated destruction by proline hydroxylation: implications for O2 sensing. *Science* **292**, 464-468, doi:10.1126/science.1059817 (2001).

63 Jaakkola, P. *et al.* Targeting of HIF-alpha to the von Hippel-Lindau ubiquitylation complex by O2-regulated prolyl hydroxylation. *Science* **292**, 468-472, doi:10.1126/science.1059796 (2001).

64 Yu, F., White, S. B., Zhao, Q. & Lee, F. S. HIF-1alpha binding to VHL is regulated by stimulus-sensitive proline hydroxylation. *Proc Natl Acad Sci U S A* **98**, 9630-9635, doi:10.1073/pnas.181341498 (2001).

65 Löfstedt, T. *et al.* Hypoxia inducible factor-2alpha in cancer. *Cell Cycle* **6**, 919-926, doi:10.4161/cc.6.8.4133 (2007).

66 Befani, C. & Liakos, P. The role of hypoxia-inducible factor-2 alpha in angiogenesis. *J Cell Physiol* **233**, 9087-9098, doi:10.1002/jcp.26805 (2018).

67 Akhtar, M., Al-Bozom, I. A. & Al Hussain, T. Molecular and Metabolic Basis of Clear Cell Carcinoma of the Kidney. *Adv Anat Pathol* **25**, 189-196, doi:10.1097/PAP.0000000000000185 (2018).

68 Gossage, L., Eisen, T. & Maher, E. R. VHL, the story of a tumour suppressor gene. *Nat Rev Cancer* **15**, 55-64, doi:10.1038/nrc3844 (2015).

69 Knudson, A. G. Genetics of human cancer. *Annu Rev Genet* **20**, 231-251, doi:10.1146/annurev.ge.20.120186.001311 (1986).

70 Knudson, A. G. Cancer genetics. *Am J Med Genet* **111**, 96-102, doi:10.1002/ajmg.10320 (2002).

71 Ricketts, C. J. *et al.* The Cancer Genome Atlas Comprehensive Molecular Characterization of Renal Cell Carcinoma. *Cell Rep* **23**, 313-326.e315, doi:10.1016/j.celrep.2018.03.075 (2018).

72 Nargund, A. M. *et al.* The SWI/SNF Protein PBRM1 Restrains VHL-Loss-Driven Clear Cell Renal Cell Carcinoma. *Cell Rep* **18**, 2893-2906, doi:10.1016/j.celrep.2017.02.074 (2017).

73 Gu, Y. F. *et al.* Modeling Renal Cell Carcinoma in Mice: Bap1 and Pbrm1 Inactivation Drive Tumor Grade. *Cancer Discov* **7**, 900-917, doi:10.1158/2159-8290.cd-17-0292 (2017).

74 Clark, D. J. *et al.* Integrated Proteogenomic Characterization of Clear Cell Renal Cell Carcinoma. *Cell* **179**, 964-983.e931, doi:10.1016/j.cell.2019.10.007 (2019).

75 Chakraborty, A. A. Coalescing lessons from oxygen sensing, tumor metabolism, and epigenetics to target VHL loss in kidney cancer. *Semin Cancer Biol* **67**, 34-42, doi:10.1016/j.semcancer.2020.03.012 (2020).

76 Liu, X. *et al.* Genome-wide Screening Identifies SFMBT1 as an Oncogenic Driver in Cancer with VHL Loss. *Mol Cell* **77**, 1294-1306.e1295, doi:10.1016/j.molcel.2020.01.009 (2020).

77 Roberts, A. M. *et al.* Suppression of hypoxia-inducible factor 2alpha restores p53 activity via Hdm2 and reverses chemoresistance of renal carcinoma cells. *Cancer Res* **69**, 9056-9064, doi:10.1158/0008-5472.CAN-09-1770 (2009).

78 An, W. G., Chuman, Y., Fojo, T. & Blagosklonny, M. V. Inhibitors of transcription, proteasome inhibitors, and DNA-damaging drugs differentially affect feedback of p53 degradation. *Exp Cell Res* **244**, 54-60, doi:10.1006/excr.1998.4193 (1998).

79 Sánchez-Puig, N., Veprintsev, D. B. & Fersht, A. R. Binding of natively unfolded HIF-1alpha ODD domain to p53. *Mol Cell* **17**, 11-21, doi:10.1016/j.molcel.2004.11.019 (2005).

80 Sendoel, A., Kohler, I., Fellmann, C., Lowe, S. W. & Hengartner, M. O. HIF-1 antagonizes p53-mediated apoptosis through a secreted neuronal tyrosinase. *Nature* **465**, 577-583, doi:10.1038/nature09141 (2010).

81 Semenza, G. L. Targeting HIF-1 for cancer therapy. *Nat Rev Cancer* **3**, 721-732, doi:10.1038/nrc1187 (2003).

82 Schödel, J. *et al.* Hypoxia, Hypoxia-inducible Transcription Factors, and Renal Cancer. *Eur Urol* **69**, 646-657, doi:10.1016/j.eururo.2015.08.007 (2016).

83 Talks, K. L. *et al.* The expression and distribution of the hypoxia-inducible factors HIF-1alpha and HIF-2alpha in normal human tissues, cancers, and tumor-associated macrophages. *Am J Pathol* **157**, 411-421, doi:10.1016/s0002-9440(10)64554-3 (2000).

84 Keith, B., Johnson, R. S. & Simon, M. C. HIF1α and HIF2α: sibling rivalry in hypoxic tumour growth and progression. *Nat Rev Cancer* **12**, 9-22, doi:10.1038/nrc3183 (2011).

85 Nanus, D. M. & Gudas, L. J. The Tale of Two Hypoxia-Inducible Factors in Renal Cell Carcinoma. *Eur Urol* **69**, 658-659, doi:10.1016/j.eururo.2015.09.020 (2016).

86 Giatromanolaki, A. *et al.* Relation of hypoxia inducible factor 1 alpha and 2 alpha in operable non-small cell lung cancer to angiogenic/molecular profile of tumours and survival. *Br J Cancer* **85**, 881-890, doi:10.1054/bjoc.2001.2018 (2001).

87 Sivridis, E., Giatromanolaki, A., Gatter, K. C., Harris, A. L. & Koukourakis, M. I. Association of hypoxia-inducible factors 1alpha and 2alpha with activated angiogenic pathways and prognosis in patients with endometrial carcinoma. *Cancer* **95**, 1055-1063, doi:10.1002/cncr.10774 (2002).

88 Koukourakis, M. I. *et al.* Hypoxia-inducible factor (HIF1A and HIF2A), angiogenesis, and chemoradiotherapy outcome of squamous cell head-and-neck cancer. *Int J Radiat Oncol Biol Phys* **53**, 1192-1202, doi:10.1016/s0360-3016(02)02848-1 (2002).

89 Khatua, S. *et al.* Overexpression of the EGFR/FKBP12/HIF-2alpha pathway identified in childhood astrocytomas by angiogenesis gene profiling. *Cancer Res* **63**, 1865-1870 (2003).

90 Yoshimura, H. *et al.* Prognostic impact of hypoxia-inducible factors 1alpha and 2alpha in colorectal cancer patients: correlation with tumor angiogenesis and cyclooxygenase-2 expression. *Clin Cancer Res* **10**, 8554-8560, doi:10.1158/1078-0432.ccr-0946-03 (2004).

91 Giatromanolaki, A. *et al.* Hypoxia inducible factors 1alpha and 2alpha are associated with VEGF expression and angiogenesis in gallbladder carcinomas. *J Surg Oncol* **94**, 242-247, doi:10.1002/jso.20443 (2006).

92 Johannessen, M., Delghandi, M. P., Seternes, O. M., Johansen, B. & Moens, U. Synergistic activation of CREB-mediated transcription by forskolin and phorbol ester requires PKC and depends on the glutamine-rich Q2 transactivation domain. *Cell Signal* **16**, 1187-1199, doi:10.1016/j.cellsig.2004.03.009 (2004).

93 Johannessen, M., Delghandi, M. P. & Moens, U. What turns CREB on? *Cell Signal* **16**, 1211-1227, doi:10.1016/j.cellsig.2004.05.001 (2004).

94 Herdegen, T. & Leah, J. D. Inducible and constitutive transcription factors in the mammalian nervous system: control of gene expression by Jun, Fos and Krox, and CREB/ATF proteins. *Brain Res Brain Res Rev* **28**, 370-490 (1998).

95 Montminy, M. R. & Bilezikjian, L. M. Binding of a nuclear protein to the cyclic-AMP response element of the somatostatin gene. *Nature* **328**, 175-178, doi:10.1038/328175a0 (1987).

96 Nichols, M. *et al.* Phosphorylation of CREB affects its binding to high and low affinity sites: implications for cAMP induced gene transcription. *EMBO J* **11**, 3337-3346 (1992).

97 Mayr, B. M., Canettieri, G. & Montminy, M. R. Distinct effects of cAMP and mitogenic signals on CREB-binding protein recruitment impart specificity to target gene activation via CREB. *Proc Natl Acad Sci U S A* **98**, 10936-10941, doi:10.1073/pnas.191152098 (2001).

98 Mayr, B. & Montminy, M. Transcriptional regulation by the phosphorylation-dependent factor CREB. *Nat Rev Mol Cell Biol* **2**, 599-609, doi:10.1038/35085068 (2001).

99 Finkbeiner, S. CREB couples neurotrophin signals to survival messages. *Neuron* **25**, 11-14, doi:10.1016/s0896-6273(00)80866-1 (2000).

100 Melnikova, V. O. *et al.* CREB inhibits AP-2alpha expression to regulate the malignant phenotype of melanoma. *PLoS One* **5**, e12452, doi:10.1371/journal.pone.0012452 (2010).

101 Cho, E. C., Mitton, B. & Sakamoto, K. M. CREB and leukemogenesis. *Crit Rev Oncog* **16**, 37-46, doi:10.1615/critrevoncog.v16.i1-2.50 (2011).

102 van der Sligte, N. E. *et al.* Essential role for cyclic-AMP responsive element binding protein 1 (CREB) in the survival of acute lymphoblastic leukemia. *Oncotarget* **6**, 14970-14981, doi:10.18632/oncotarget.3911 (2015).

103 Peng, B., Lei, N., Chai, Y., Chan, E. K. & Zhang, J. Y. CIP2A regulates cancer metabolism and CREB phosphorylation in non-small cell lung cancer. *Mol Biosyst* **11**, 105-114, doi:10.1039/c4mb00513a (2015).

104 Seo, H. S. *et al.* Cyclic AMP response element-binding protein overexpression: a feature associated with negative prognosis in never smokers with non-small cell lung cancer. *Cancer Res* **68**, 6065-6073, doi:10.1158/0008-5472.CAN-07-5376 (2008).

105 Kovach, S. J., Price, J. A., Shaw, C. M., Theodorakis, N. G. & McKillop, I. H. Role of cyclic-AMP responsive element binding (CREB) proteins in cell proliferation in a rat model of hepatocellular carcinoma. *J Cell Physiol* **206**, 411-419, doi:10.1002/jcp.20474 (2006).

106 Singh, R., Shankar, B. S. & Sainis, K. B. TGF-β1-ROS-ATM-CREB signaling axis in macrophage mediated migration of human breast cancer MCF7 cells. *Cell Signal* **26**, 1604-1615, doi:10.1016/j.cellsig.2014.03.028 (2014).

107 Liu, Y. L. *et al.* Noxa upregulation by oncogenic activation of MEK/ERK through CREB promotes autophagy in human melanoma cells. *Oncotarget* **5**, 11237-11251, doi:10.18632/oncotarget.2616 (2014).

108 Shneor, D., Folberg, R., Pe'er, J., Honigman, A. & Frenkel, S. Stable knockdown of CREB, HIF-1 and HIF-2 by replication-competent retroviruses abrogates the responses to hypoxia in hepatocellular carcinoma. *Cancer Gene Ther* **24**, 64-74, doi:10.1038/cgt.2016.68 (2017).

109 Wang, X. *et al.* Decrease of phosphorylated proto-oncogene CREB at Ser 133 site inhibits growth and metastatic activity of renal cell cancer. *Expert Opin Ther Targets* **19**, 985-995, doi:10.1517/14728222.2015.1053208 (2015).

110 Zhuang, H. *et al.* Cyclic AMP responsive element-binding protein promotes renal cell carcinoma proliferation probably via the expression of spindle and kinetochore-associated protein 2. *Oncotarget* **7**, 16325-16337, doi:10.18632/oncotarget.7017 (2016).

111 Wang, X. *et al.* Cyclic AMP responsive element-binding protein induces metastatic renal cell carcinoma by mediating the expression of matrix metallopeptidase-2/9 and proteins associated with epithelial-mesenchymal transition. *Mol Med Rep* **15**, 4191-4198, doi:10.3892/mmr.2017.6519 (2017).

112 Cascone, T. *et al.* Increased Tumor Glycolysis Characterizes Immune Resistance to Adoptive T Cell Therapy. *Cell Metab* **27**, 977-987.e974, doi:10.1016/j.cmet.2018.02.024 (2018).

113 John, A. & Tuszynski, G. The role of matrix metalloproteinases in tumor angiogenesis and tumor metastasis. *Pathol Oncol Res* **7**, 14-23, doi:10.1007/BF03032599 (2001).

114 Friedrich, M. *et al.* Characterization of the expression and immunological impact of the transcriptional activator CREB in renal cell carcinoma. *J Transl Med* **18**, 371, doi:10.1186/s12967-020-02544-0 (2020).

115 Morrot, A. *et al.* Metabolic Symbiosis and Immunomodulation: How Tumor Cell-Derived Lactate May Disturb Innate and Adaptive Immune Responses. *Front Oncol* **8**, 81, doi:10.3389/fonc.2018.00081 (2018).

116 Koppenol, W. H., Bounds, P. L. & Dang, C. V. Otto Warburg's contributions to current concepts of cancer metabolism. *Nat Rev Cancer* **11**, 325-337, doi:10.1038/nrc3038 (2011).

117 Warburg, O., Wind, F. & Negelein, E. THE METABOLISM OF TUMORS IN THE BODY. *J Gen Physiol* **8**, 519-530 (1927).

118 Warburg, O. On respiratory impairment in cancer cells. *Science* **124**, 269-270 (1956).

119 Mankoff, D. A. *et al.* Tumor-specific positron emission tomography imaging in patients: [18F] fluorodeoxyglucose and beyond. *Clin Cancer Res* **13**, 3460-3469, doi:10.1158/1078-0432.CCR-07-0074 (2007).

120 Vander Heiden, M. G., Cantley, L. C. & Thompson, C. B. Understanding the Warburg effect: the metabolic requirements of cell proliferation. *Science* **324**, 1029-1033, doi:10.1126/science.1160809 (2009).

121 Seliger, B., Lichtenfels, R. & Kellner, R. Detection of renal cell carcinoma-associated markers via proteome- and other 'ome'-based analyses. *Brief Funct Genomic Proteomic* **2**, 194-212, doi:10.1093/bfgp/2.3.194 (2003).

122 Seliger, B. *et al.* Combined analysis of transcriptome and proteome data as a tool for the identification of candidate biomarkers in renal cell carcinoma. *Proteomics* **9**, 1567-1581, doi:10.1002/pmic.200700288 (2009).

123 Robey, R. B. & Hay, N. Is Akt the "Warburg kinase"?-Akt-energy metabolism interactions and oncogenesis. *Semin Cancer Biol* **19**, 25-31, doi:10.1016/j.semcancer.2008.11.010 (2009).

124 Luo, Y. *et al.* UQCRH downregulation promotes Warburg effect in renal cell carcinoma cells. *Sci Rep* **10**, 15021, doi:10.1038/s41598-020-72107-2 (2020).

125 Semenza, G. L. *et al.* Hypoxia response elements in the aldolase A, enolase 1, and lactate dehydrogenase A gene promoters contain essential binding sites for hypoxia-inducible factor 1. *J Biol Chem* **271**, 32529-32537, doi:10.1074/jbc.271.51.32529 (1996).

126 Lacroix, R., Rozeman, E. A., Kreutz, M., Renner, K. & Blank, C. U. Targeting tumor-associated acidity in cancer immunotherapy. *Cancer Immunol Immunother* **67**, 1331-1348, doi:10.1007/s00262-018-2195-z (2018).

127 Deberardinis, R. J., Lum, J. J. & Thompson, C. B. Phosphatidylinositol 3-kinase-dependent modulation of carnitine palmitoyltransferase 1A expression regulates lipid metabolism during hematopoietic cell growth. *J Biol Chem* **281**, 37372-37380, doi:10.1074/jbc.M608372200 (2006).

128 Wang, H. Q. *et al.* Positive feedback regulation between AKT activation and fatty acid synthase expression in ovarian carcinoma cells. *Oncogene* **24**, 3574-3582, doi:10.1038/sj.onc.1208463 (2005).

129 Yoon, S. *et al.* Up-regulation of acetyl-CoA carboxylase alpha and fatty acid synthase by human epidermal growth factor receptor 2 at the translational level in breast cancer cells. *J Biol Chem* **282**, 26122-26131, doi:10.1074/jbc.M702854200 (2007).

130 Christofk, H. R., Vander Heiden, M. G., Wu, N., Asara, J. M. & Cantley, L. C. Pyruvate kinase M2 is a phosphotyrosine-binding protein. *Nature* **452**, 181-186, doi:10.1038/nature06667 (2008).

131 Boroughs, L. K. & DeBerardinis, R. J. Metabolic pathways promoting cancer cell survival and growth. *Nat Cell Biol* **17**, 351-359, doi:10.1038/ncb3124 (2015).

132 Mucaj, V., Shay, J. E. & Simon, M. C. Effects of hypoxia and HIFs on cancer metabolism. *Int J Hematol* **95**, 464-470, doi:10.1007/s12185-012-1070-5 (2012).

133 Shaw, R. J. & Cantley, L. C. Ras, PI(3)K and mTOR signalling controls tumour cell growth. *Nature* **441**, 424-430, doi:10.1038/nature04869 (2006).

134 Matoba, S. *et al.* p53 regulates mitochondrial respiration. *Science* **312**, 1650-1653, doi:10.1126/science.1126863 (2006).

135 Bensaad, K. *et al.* TIGAR, a p53-inducible regulator of glycolysis and apoptosis. *Cell* **126**, 107-120, doi:10.1016/j.cell.2006.05.036 (2006).

136 Kondoh, H. *et al.* Glycolytic enzymes can modulate cellular life span. *Cancer Res* **65**, 177-185 (2005).

137 Gottlieb, E. & Tomlinson, I. P. Mitochondrial tumour suppressors: a genetic and biochemical update. *Nat Rev Cancer* **5**, 857-866, doi:10.1038/nrc1737 (2005).

138 Danhier, P. *et al.* Cancer metabolism in space and time: Beyond the Warburg effect. *Biochim Biophys Acta Bioenerg* **1858**, 556-572, doi:10.1016/j.bbabio.2017.02.001 (2017).

139 Renner, K. *et al.* Metabolic plasticity of human T cells: Preserved cytokine production under glucose deprivation or mitochondrial restriction, but 2-deoxy-glucose affects effector functions. *Eur J Immunol* **45**, 2504-2516, doi:10.1002/eji.201545473 (2015).

140 Renner, K. *et al.* Metabolic Hallmarks of Tumor and Immune Cells in the Tumor Microenvironment. *Front Immunol* **8**, 248, doi:10.3389/fimmu.2017.00248 (2017).

141 Seliger, B. Different regulation of MHC class I antigen processing components in human tumors. *J Immunotoxicol* **5**, 361-367, doi:10.1080/15476910802482870 (2008).

142 Seliger, B. Molecular mechanisms of MHC class I abnormalities and APM components in human tumors. *Cancer Immunol Immunother* **57**, 1719-1726, doi:10.1007/s00262-008-0515-4 (2008).

143 Jasinski-Bergner, S. *et al.* Clinical relevance of miR-mediated HLA-G regulation and the associated immune cell infiltration in renal cell carcinoma. *Oncoimmunology* **4**, e1008805, doi:10.1080/2162402X.2015.1008805 (2015).

144 Seliger, B. & Schlaf, G. Structure, expression and function of HLA-G in renal cell carcinoma. *Semin Cancer Biol* **17**, 444-450, doi:10.1016/j.semcancer.2007.07.001 (2007).

145 Fischer, K. *et al.* Inhibitory effect of tumor cell-derived lactic acid on human T cells. *Blood* **109**, 3812-3819, doi:blood-2006-07-035972 [pii]
10.1182/blood-2006-07-035972 (2007).

146 Singer, K. *et al.* Warburg phenotype in renal cell carcinoma: high expression of glucose-transporter 1 (GLUT-1) correlates with low CD8(+) T-cell infiltration in the tumor. I*nt J Cancer* 1**28,** 2085-2095, doi:10.1002/ijc.25543 (2011).

147 Gottfried, E. *et al.* Tumor-derived lactic acid modulates dendritic cell activation and antigen expression. B*lood* 1**07,** 2013-2021, doi:10.1182/blood-2005-05-1795 (2006).

148 Dietl, K. *et al.* Lactic acid and acidification inhibit TNF secretion and glycolysis of human monocytes. J *Immunol* 1**84,** 1200-1209, doi:10.4049/jimmunol.0902584 (2010).

149 Colegio, O. R. *et al.* Functional polarization of tumour-associated macrophages by tumour-derived lactic acid. N*ature* 5**13,** 559-563, doi:10.1038/nature13490 (2014).

150 Shime, H. *et al.* Tumor-secreted lactic acid promotes IL-23/IL-17 proinflammatory pathway. J *Immunol* 1**80,** 7175-7183, doi:10.4049/jimmunol.180.11.7175 (2008).

151 Brand, A. *et al.* LDHA-Associated Lactic Acid Production Blunts Tumor Immunosurveillance by T and NK Cells. C*ell Metab* 2**4,** 657-671, doi:10.1016/j.cmet.2016.08.011 (2016).

152 Junker, K. *et al.* Potential role of genetic markers in the management of kidney cancer. E*ur Urol* 6**3,** 333-340, doi:10.1016/j.eururo.2012.09.040 (2013).

153 Hu, Q. *et al.* The prognostic value of C-reactive protein in renal cell carcinoma: a systematic review and meta-analysis. U*rol Oncol* 3**2,** 50.e51-58, doi:10.1016/j.urolonc.2013.07.016 (2014).

154 Tan, P. H. *et al.* Renal tumors: diagnostic and prognostic biomarkers. A*m J Surg Pathol* 3**7,** 1518-1531, doi:10.1097/PAS.0b013e318299f12e (2013).

155 Peña, C., Lathia, C., Shan, M., Escudier, B. & Bukowski, R. M. Biomarkers predicting outcome in patients with advanced renal cell carcinoma: Results from sorafenib phase III Treatment Approaches in Renal Cancer Global Evaluation Trial. C*lin Cancer Res* 1**6,** 4853-4863, doi:10.1158/1078-0432.ccr-09-3343 (2010).

156 Tran, H. T. *et al.* Prognostic or predictive plasma cytokines and angiogenic factors for patients treated with pazopanib for metastatic renal-cell cancer: a retrospective analysis of phase 2 and phase 3 trials. L*ancet Oncol* 1**3,** 827-837, doi:10.1016/s1470-2045(12)70241-3 (2012).

157 Na, N. *et al.* High expression of Aldolase A predicts poor survival in patients with clear-cell renal cell carcinoma. T*her Clin Risk Manag* 1**3,** 279-285, doi:10.2147/tcrm.s123199 (2017).

158 Konishi, S. *et al.* C-reactive protein/albumin ratio is a predictive factor for prognosis in patients with metastatic renal cell carcinoma. I*nt J Urol* 2**6,** 992-998, doi:10.1111/iju.14078 (2019).

159 Suzuki, K. *et al.* C-reactive protein and the neutrophil-to-lymphocyte ratio are prognostic biomarkers in metastatic renal cell carcinoma patients treated with nivolumab. I*nt J Clin Oncol* 2**5,** 135-144, doi:10.1007/s10147-019-01528-5 (2020).

160 Ball, M. W. *et al.* Circulating Tumor DNA as a Marker of Therapeutic Response in Patients With Renal Cell Carcinoma: A Pilot Study. C*lin Genitourin Cancer* 1**4,** e515-e520, doi:10.1016/j.clgc.2016.03.019 (2016).

161 Fang, P. *et al.* Targeting Strategies for Renal Cancer Stem Cell Therapy. C*urr Pharm Des* 2**6,** 1964-1978, doi:10.2174/1381612826666200318153106 (2020).

162 Grange, C., Brossa, A. & Bussolati, B. Extracellular Vesicles and Carried miRNAs in the Progression of Renal Cell Carcinoma. I*nt J Mol Sci* 2**0,** doi:10.3390/ijms20081832 (2019).

163 Théry, C., Ostrowski, M. & Segura, E. Membrane vesicles as conveyors of immune responses. N*at Rev Immunol* 9**,** 581-593, doi:10.1038/nri2567 (2009).

164 Peinado, H. *et al.* Melanoma exosomes educate bone marrow progenitor cells toward a pro-metastatic phenotype through MET. N*at Med* 1**8,** 883-891, doi:10.1038/nm.2753 (2012).

165 Raimondo, F. *et al.* Differential protein profiling of renal cell carcinoma urinary exosomes. M*ol Biosyst* 9**,** 1220-1233, doi:10.1039/c3mb25582d (2013).

166 Miranda, K. C. *et al.* Nucleic acids within urinary exosomes/microvesicles are potential biomarkers for renal disease. K*idney Int* 7**8,** 191-199, doi:10.1038/ki.2010.106 (2010).

167 Gai, C., Pomatto, M. A. C., Grange, C., Deregibus, M. C. & Camussi, G. Extracellular vesicles in onco-nephrology. E*xp Mol Med* 5**1,** 1-8, doi:10.1038/s12276-019-0213-7 (2019).

168 Hanahan, D. & Weinberg, R. A. Hallmarks of cancer: the next generation. C*ell* 1**44,** 646-674, doi:10.1016/j.cell.2011.02.013 (2011).

169 Schaeffeler, E. *et al.* Metabolic and Lipidomic Reprogramming in Renal Cell Carcinoma Subtypes Reflects Regions of Tumor Origin. E*ur Urol Focus* 5**,** 608-618, doi:10.1016/j.euf.2018.01.016 (2019).

170 Sun, M. *et al.* Prognostic factors and predictive models in renal cell carcinoma: a contemporary review. E*ur Urol* 6**0,** 644-661, doi:10.1016/j.eururo.2011.06.041 (2011).

171 Parker, A. S. *et al.* Development and evaluation of BioScore: a biomarker panel to enhance prognostic algorithms for clear cell renal cell carcinoma. C*ancer* 1**15,** 2092-2103, doi:10.1002/cncr.24263 (2009).

172 Lichtenfels, R. *et al.* Heat shock protein expression and anti-heat shock protein reactivity in renal cell carcinoma. P*roteomics* 2**,** 561-570, doi:10.1002/1615-9861(200205)2:5<561::AID-PROT561>3.0.CO;2-K (2002).

173 Lichtenfels, R. *et al.* Identification of metabolic enzymes in renal cell carcinoma utilizing PROTEOMEX analyses. B*iochim Biophys Acta* 1**646,** 21-31, doi:10.1016/s1570-9639(02)00547-2 (2003).

174 Lichtenfels, R. *et al.* Systematic comparative protein expression profiling of clear cell renal cell carcinoma: a pilot study based on the separation of tissue specimens by two-dimensional gel electrophoresis. M*ol Cell Proteomics* 8**,** 2827-2842, doi:10.1074/mcp.M900168-MCP200 (2009).

175 Seliger, B. *et al.* Identification of fatty acid binding proteins as markers associated with the initiation and/or progression of renal cell carcinoma. P*roteomics* 5**,** 2631-2640, doi:10.1002/pmic.200401264 (2005).

176 Seliger, B., Dressler, S. P., Lichtenfels, R. & Kellner, R. Candidate biomarkers in renal cell carcinoma. P*roteomics* 7**,** 4601-4612, doi:10.1002/pmic.200700415 (2007).

177 Seliger, B. *et al.* Ubiquitin COOH-terminal hydrolase 1: a biomarker of renal cell carcinoma associated with enhanced tumor cell proliferation and migration. C*lin Cancer Res* 1**3,** 27-37, doi:10.1158/1078-0432.CCR-06-0824 (2007).

178 Balabanov, S. *et al.* Tumour-related enzyme alterations in the clear cell type of human renal cell carcinoma identified by two-dimensional gel electrophoresis. E*ur J Biochem* 2**68,** 5977-5980, doi:10.1046/j.0014-2956.2001.02546.x (2001).

179 Raimondo, F. *et al.* Proteomic analysis in clear cell renal cell carcinoma: identification of differentially expressed protein by 2-D DIGE. M*ol Biosyst* 8**,** 1040-1051, doi:10.1039/c2mb05390j (2012).

180 Kotzsch, M. *et al.* Urokinase receptor splice variant uPAR-del4/5-associated gene expression in breast cancer: identification of rab31 as an independent prognostic factor. B*reast Cancer Res Treat* 1**11,** 229-240, doi:10.1007/s10549-007-9782-6 (2008).

181 Grismayer, B. *et al.* Rab31 expression levels modulate tumor-relevant characteristics of breast cancer cells. M*ol Cancer* 1**1,** 62, doi:10.1186/1476-4598-11-62 (2012).

182 Tang, C. T. *et al.* RAB31 Targeted by MiR-30c-2-3p Regulates the GLI1 Signaling Pathway, Affecting Gastric Cancer Cell Proliferation and Apoptosis. F*ront Oncol* 8**,** 554, doi:10.3389/fonc.2018.00554 (2018).

183 Li, H. *et al.* SRPX2 and RAB31 are effective prognostic biomarkers in pancreatic cancer. J *Cancer* 1**0,** 2670-2678, doi:10.7150/jca.32072 (2019).

184 Sui, Y., Zheng, X. & Zhao, D. Rab31 promoted hepatocellular carcinoma (HCC) progression via inhibition of cell apoptosis induced by PI3K/AKT/Bcl-2/BAX pathway. T*umour Biol* 3**6,** 8661-8670, doi:10.1007/s13277-015-3626-5 (2015).

185 Kohfeldt, E., Sasaki, T., Göhring, W. & Timpl, R. Nidogen-2: a new basement membrane protein with diverse binding properties. J *Mol Biol* 2**82,** 99-109, doi:10.1006/jmbi.1998.2004 (1998).

186 Gersdorff, N., Otto, S., Roediger, M., Kruegel, J. & Miosge, N. The absence of one or both nidogens does not alter basement membrane composition in adult murine kidney. H*istol Histopathol* 2**2,** 1077-1084, doi:10.14670/HH-22.1077 (2007).

187 Ulazzi, L. *et al.* Nidogen 1 and 2 gene promoters are aberrantly methylated in human gastrointestinal cancer. M*ol Cancer* 6**,** 17, doi:10.1186/1476-4598-6-17 (2007).

188 Nagy, Á., Lánczky, A., Menyhárt, O. & Győrffy, B. Validation of miRNA prognostic power in hepatocellular carcinoma using expression data of independent datasets. S*ci Rep* 8**,** 9227, doi:10.1038/s41598-018-27521-y (2018).

189 Cheng, Z. X. *et al.* Clinical significance of decreased nidogen-2 expression in the tumor tissue and serum of patients with hepatocellular carcinoma. J *Surg Oncol* 1**05,** 71-80, doi:10.1002/jso.22047 (2012).

190 Steven, A. & Seliger, B. Control of CREB expression in tumors: from molecular mechanisms and signal transduction pathways to therapeutic target. O*ncotarget* 7**,** 35454-35465, doi:10.18632/oncotarget.7721 (2016).

191 Antonescu, C. R., Nafa, K., Segal, N. H., Dal Cin, P. & Ladanyi, M. EWS-CREB1: a recurrent variant fusion in clear cell sarcoma--association with gastrointestinal location and absence of melanocytic differentiation. C*lin Cancer Res* 1**2,** 5356-5362, doi:10.1158/1078-0432.CCR-05-2811 (2006).

192 Arany, Z. *et al.* An essential role for p300/CBP in the cellular response to hypoxia. P*roc Natl Acad Sci U S A* 9**3,** 12969-12973, doi:10.1073/pnas.93.23.12969 (1996).

193 Beitner-Johnson, D. & Millhorn, D. E. Hypoxia induces phosphorylation of the cyclic AMP response element-binding protein by a novel signaling mechanism. J *Biol Chem* 2**73,** 19834-19839, doi:10.1074/jbc.273.31.19834 (1998).

194 Nakayama, K. cAMP-response element-binding protein (CREB) and NF-κB transcription factors are activated during prolonged hypoxia and cooperatively regulate the induction of matrix metalloproteinase MMP1. J *Biol Chem* 2**88,** 22584-22595, doi:10.1074/jbc.M112.421636 (2013).

195 Taylor, C. T., Furuta, G. T., Synnestvedt, K. & Colgan, S. P. Phosphorylation-dependent targeting of cAMP response element binding protein to the ubiquitin/proteasome pathway in hypoxia. P*roc Natl Acad Sci U S A* 9**7,** 12091-12096, doi:10.1073/pnas.220211797 (2000).

196 Wykoff, C. C., Pugh, C. W., Maxwell, P. H., Harris, A. L. & Ratcliffe, P. J. Identification of novel hypoxia dependent and independent target genes of the von Hippel-Lindau (VHL) tumour suppressor by mRNA differential expression profiling. O*ncogene* 1**9,** 6297-6305, doi:10.1038/sj.onc.1204012 (2000).

197 Eckert, R. L. *et al.* Transglutaminase regulation of cell function. P*hysiol Rev* 9**4,** 383-417, doi:10.1152/physrev.00019.2013 (2014).

198 Lorand, L. & Graham, R. M. Transglutaminases: crosslinking enzymes with pleiotropic functions. N*at Rev Mol Cell Biol* 4**,** 140-156, doi:10.1038/nrm1014 (2003).

199 Mehta, K. Mammalian transglutaminases: a family portrait. P*rog Exp Tumor Res* 3**8,** 1-18, doi:10.1159/000084229 (2005).

200 Nakaoka, H. *et al.* Gh: a GTP-binding protein with transglutaminase activity and receptor signaling function. S*cience* 2**64,** 1593-1596, doi:10.1126/science.7911253 (1994).

201 Fesus, L., Madi, A., Balajthy, Z., Nemes, Z. & Szondy, Z. Transglutaminase induction by various cell death and apoptosis pathways. E*xperientia* 5**2,** 942-949, doi:10.1007/BF01920102 (1996).

202 Lentini, A., Abbruzzese, A., Provenzano, B., Tabolacci, C. & Beninati, S. Transglutaminases: key regulators of cancer metastasis. A*mino Acids* 4**4,** 25-32, doi:10.1007/s00726-012-1229-7 (2013).

203 Mantovani, A., Allavena, P., Sica, A. & Balkwill, F. Cancer-related inflammation. N*ature* 4**54,** 436-444, doi:10.1038/nature07205 (2008).

204 Grivennikov, S. I., Greten, F. R. & Karin, M. Immunity, inflammation, and cancer. C*ell* 1**40,** 883-899, doi:10.1016/j.cell.2010.01.025 (2010).

205 Verma, A. *et al.* Increased expression of tissue transglutaminase in pancreatic ductal adenocarcinoma and its implications in drug resistance and metastasis. C*ancer Res* 6**6,** 10525-10533, doi:10.1158/0008-5472.CAN-06-2387 (2006).

206 Mangala, L. S., Fok, J. Y., Zorrilla-Calancha, I. R., Verma, A. & Mehta, K. Tissue transglutaminase expression promotes cell attachment, invasion and survival in breast cancer cells. O*ncogene* 2**6,** 2459-2470, doi:10.1038/sj.onc.1210035 (2007).

207 Hwang, J. Y. *et al.* Clinical and biological significance of tissue transglutaminase in ovarian carcinoma. C*ancer Res* 6**8,** 5849-5858, doi:10.1158/0008-5472.CAN-07-6130 (2008).

208 Park, K. S. *et al.* Transglutaminase 2 as a cisplatin resistance marker in non-small cell lung cancer. J *Cancer Res Clin Oncol* 1**36,** 493-502, doi:10.1007/s00432-009-0681-6 (2010).

209 Fok, J. Y., Ekmekcioglu, S. & Mehta, K. Implications of tissue transglutaminase expression in malignant melanoma. M*ol Cancer Ther* 5**,** 1493-1503, doi:10.1158/1535-7163.MCT-06-0083 (2006).

210 Yuan, L. *et al.* Transglutaminase 2 inhibitor, KCC009, disrupts fibronectin assembly in the extracellular matrix and sensitizes orthotopic glioblastomas to chemotherapy. O*ncogene* 2**6,** 2563-2573, doi:10.1038/sj.onc.1210048 (2007).

211 Park, M. J. *et al.* Transglutaminase 2 expression and its prognostic significance in clear cell renal cell carcinoma. J *Pathol Transl Med* 4**9,** 37-43, doi:10.4132/jptm.2014.10.25 (2015).

212 Erdem, S. *et al.* The increased transglutaminase 2 expression levels during initial tumorigenesis predict increased risk of metastasis and decreased disease-free and cancer-specific survivals in renal cell carcinoma. W*orld J Urol* 3**3,** 1553-1560, doi:10.1007/s00345-014-1462-7 (2015).

213 Kumar, A. *et al.* Evidence that GTP-binding domain but not catalytic domain of transglutaminase 2 is essential for epithelial-to-mesenchymal transition in mammary epithelial cells. B*reast Cancer Res* 1**4,** R4, doi:10.1186/bcr3085 (2012).

214 Nezir, A. E., Ulukan, B. & Telci, D. Transglutaminase 2: The Maestro of the Oncogenic Mediators in Renal Cell Carcinoma. M*ed Sci (Basel)* 7**,** doi:10.3390/medsci7020024 (2019).

215 Shao, M. *et al.* Epithelial-to-mesenchymal transition and ovarian tumor progression induced by tissue transglutaminase. C*ancer Res* 6**9,** 9192-9201, doi:10.1158/0008-5472.CAN-09-1257 (2009).

216 Ku, B. M., Lee, C. H., Lee, S. H. & Kim, S. Y. Increased expression of transglutaminase 2 drives glycolytic metabolism in renal carcinoma cells. A*mino Acids* 4**6,** 1527-1536, doi:10.1007/s00726-014-1714-2 (2014).

217 Eckert, R. L. *et al.* Transglutaminase is a tumor cell and cancer stem cell survival factor. M*ol Carcinog* 5**4,** 947-958, doi:10.1002/mc.22375 (2015).

218 Mehta, K., Kumar, A. & Kim, H. I. Transglutaminase 2: a multi-tasking protein in the complex circuitry of inflammation and cancer. B*iochem Pharmacol* 8**0,** 1921-1929, doi:10.1016/j.bcp.2010.06.029 (2010).

219 Huang, S. *et al.* The Transcription Factor Creb is Involved in Sorafenib-Inhibited Renal Cancer Cell Proliferation, Migration and Invasion. A*cta Pharm* 6**8,** 497-506, doi:10.2478/acph-2018-0033 (2018).

220 Kumar, S. & Mehta, K. Tissue transglutaminase constitutively activates HIF-1α promoter and nuclear factor-κB via a non-canonical pathway. P*LoS One* 7**,** e49321, doi:10.1371/journal.pone.0049321 (2012).

221 Satpathy, M., Shao, M., Emerson, R., Donner, D. B. & Matei, D. Tissue transglutaminase regulates matrix metalloproteinase-2 in ovarian cancer by modulating cAMP-response element-binding protein activity. J *Biol Chem* 2**84,** 15390-15399, doi:10.1074/jbc.M808331200 (2009).

222 Song, M., Hwang, H., Im, C. Y. & Kim, S. Y. Recent Progress in the Development of Transglutaminase 2 (TGase2) Inhibitors. J *Med Chem* 6**0,** 554-567, doi:10.1021/acs.jmedchem.6b01036 (2017).

223 Eckert, R. L. Transglutaminase 2 takes center stage as a cancer cell survival factor and therapy target. M*ol Carcinog* 5**8,** 837-853, doi:10.1002/mc.22986 (2019).

224 Ku, B. M. *et al.* Transglutaminase 2 inhibitor abrogates renal cell carcinoma in xenograft models. J *Cancer Res Clin Oncol* 1**40,** 757-767, doi:10.1007/s00432-014-1623-5 (2014).

225 Ma, L. *et al.* 2-Methoxyestradiol synergizes with sorafenib to suppress hepatocellular carcinoma by simultaneously dysregulating hypoxia-inducible factor-1 and -2. C*ancer Lett* 3**55,** 96-105, doi:10.1016/j.canlet.2014.09.011 (2014).

226 Chen, W. *et al.* Targeting renal cell carcinoma with a HIF-2 antagonist. N*ature* 5**39,** 112-117, doi:10.1038/nature19796 (2016).

227 Wallace, E. M. *et al.* A Small-Molecule Antagonist of HIF2α Is Efficacious in Preclinical Models of Renal Cell Carcinoma. C*ancer Res* 7**6,** 5491-5500, doi:10.1158/0008-5472.CAN-16-0473 (2016).

228 Ku, B. M. *et al.* Transglutaminase 2 inhibition found to induce p53 mediated apoptosis in renal cell carcinoma. F*aseb j* 2**7,** 3487-3495, doi:10.1096/fj.12-224220 (2013).

229 Raval, R. R. *et al.* Contrasting properties of hypoxia-inducible factor 1 (HIF-1) and HIF-2 in von Hippel-Lindau-associated renal cell carcinoma. M*ol Cell Biol* 2**5,** 5675-5686, doi:10.1128/mcb.25.13.5675-5686.2005 (2005).

230 Hidaka, H. *et al.* Tumor suppressive microRNA-1285 regulates novel molecular targets: aberrant expression and functional significance in renal cell carcinoma. O*ncotarget* 3**,** 44-57, doi:10.18632/oncotarget.417 (2012).

231 Schanza, L. M. *et al.* MicroRNAs Associated with Von Hippel-Lindau Pathway in Renal Cell Carcinoma: A Comprehensive Review. I*nt J Mol Sci* 1**8,** doi:10.3390/ijms18112495 (2017).

232 Friedrich, M. *et al.* CREB1 is affected by the microRNAs miR-22-3p, miR-26a-5p, miR-27a-3p, and miR-221-3p and correlates with adverse clinicopathological features in renal cell carcinoma. S*ci Rep* 1**0,** 6499, doi:10.1038/s41598-020-63403-y (2020).

233 Bäumer, S. *et al.* Antibody-mediated delivery of anti-KRAS-siRNA in vivo overcomes therapy resistance in colon cancer. C*lin Cancer Res* 2**1,** 1383-1394, doi:10.1158/1078-0432.ccr-13-2017 (2015).

234 Bäumer, N. *et al.* Downregulation of PIK3CA via antibody-esiRNA-complexes suppresses human xenograft tumor growth. P*LoS One* 1**3,** e0200163, doi:10.1371/journal.pone.0200163 (2018).

235 Bleumer, I. *et al.* A clinical trial with chimeric monoclonal antibody WX-G250 and low dose interleukin-2 pulsing scheme for advanced renal cell carcinoma. J *Urol* 1**75,** 57-62, doi:10.1016/s0022-5347(05)00040-6 (2006).

236 Chamie, K. *et al.* Adjuvant Weekly Girentuximab Following Nephrectomy for High-Risk Renal Cell Carcinoma: The ARISER Randomized Clinical Trial. J*AMA Oncol* 3**,** 913-920, doi:10.1001/jamaoncol.2016.4419 (2017).

237 Ambrosetti, D. *et al.* The two glycolytic markers GLUT1 and MCT1 correlate with tumor grade and survival in clear-cell renal cell carcinoma. P*LoS One* 1**3,** e0193477, doi:10.1371/journal.pone.0193477 (2018).

238 Craven, R. A. *et al.* Proteomic analysis of primary cell lines identifies protein changes present in renal cell carcinoma. P*roteomics* 6**,** 2853-2864, doi:10.1002/pmic.200500549 (2006).

239 Takashi, M., Zhu, Y., Nakano, Y., Miyake, K. & Kato, K. Elevated levels of serum aldolase A in patients with renal cell carcinoma. U*rol Res* 2**0,** 307-311, doi:10.1007/bf00300265 (1992).

240 Huang, Z. *et al.* High expression of fructose-bisphosphate aldolase A induces progression of renal cell carcinoma. O*ncol Rep* 3**9,** 2996-3006, doi:10.3892/or.2018.6378 (2018).

241 Capello, M., Ferri-Borgogno, S., Cappello, P. & Novelli, F. α-Enolase: a promising therapeutic and diagnostic tumor target. F*EBS J* 2**78,** 1064-1074, doi:10.1111/j.1742-4658.2011.08025.x (2011).

242 Chen, T. *et al.* Role of triosephosphate isomerase and downstream functional genes on gastric cancer. O*ncol Rep* 3**8,** 1822-1832, doi:10.3892/or.2017.5846 (2017).

243 Bohn, T. *et al.* Tumor immunoevasion via acidosis-dependent induction of regulatory tumor-associated macrophages. N*at Immunol* 1**9,** 1319-1329, doi:10.1038/s41590-018-0226-8 (2018).

244 Gottfried, E., Kreutz, M. & Mackensen, A. Tumor metabolism as modulator of immune response and tumor progression. S*emin Cancer Biol* 2**2,** 335-341, doi:10.1016/j.semcancer.2012.02.009 (2012).

245 Singer, K., Gottfried, E., Kreutz, M. & Mackensen, A. Suppression of T-cell responses by tumor metabolites. C*ancer Immunol Immunother* 6**0,** 425-431, doi:10.1007/s00262-010-0967-1 (2011).

246 Singer, K., Cheng, W. C., Kreutz, M., Ho, P. C. & Siska, P. J. Immunometabolism in cancer at a glance. D*is Model Mech* 1**1,** doi:10.1242/dmm.034272 (2018).

247 Friedrich, M. *et al.* Tumor-induced escape mechanisms and their association with resistance to checkpoint inhibitor therapy. C*ancer Immunol Immunother* 6**8,** 1689-1700, doi:10.1007/s00262-019-02373-1 (2019).

248 Seliger, B. The Role of the Lymphocyte Functional Crosstalk and Regulation in the Context of Checkpoint Inhibitor Treatment-Review. F*ront Immunol* 1**0,** 2043, doi:10.3389/fimmu.2019.02043 (2019).

249 Dunbar, E. M. *et al.* Phase 1 trial of dichloroacetate (DCA) in adults with recurrent malignant brain tumors. I*nvest New Drugs* 3**2,** 452-464, doi:10.1007/s10637-013-0047-4 (2014).

250 Lin, G. *et al.* Dichloroacetate induces autophagy in colorectal cancer cells and tumours. B*r J Cancer* 1**11,** 375-385, doi:10.1038/bjc.2014.281 (2014).

251 Madhok, B. M., Yeluri, S., Perry, S. L., Hughes, T. A. & Jayne, D. G. Dichloroacetate induces apoptosis and cell-cycle arrest in colorectal cancer cells. B*r J Cancer* 1**02,** 1746-1752, doi:10.1038/sj.bjc.6605701 (2010).

252 Park, J. M. *et al.* Metabolic response of glioma to dichloroacetate measured in vivo by hyperpolarized (13)C magnetic resonance spectroscopic imaging. N*euro Oncol* 1**5,** 433-441, doi:10.1093/neuonc/nos319 (2013).

253 Sun, R. C. *et al.* Reversal of the glycolytic phenotype by dichloroacetate inhibits metastatic breast cancer cell growth in vitro and in vivo. B*reast Cancer Res Treat* 1**20,** 253-260, doi:10.1007/s10549-009-0435-9 (2010).

254 Eleftheriadis, T. *et al.* Dichloroacetate at therapeutic concentration alters glucose metabolism and induces regulatory T-cell differentiation in alloreactive human lymphocytes. J *Basic Clin Physiol Pharmacol* 2**4,** 271-276, doi:10.1515/jbcpp-2013-0001 (2013).

255 Eleftheriadis, T. *et al.* In human alloreactive $CD4^+$ T-cells, dichloroacetate inhibits aerobic glycolysis, induces apoptosis and favors differentiation towards the regulatory T-cell subset instead of effector T-cell subsets. M*ol Med Rep* 1**3,** 3370-3376, doi:10.3892/mmr.2016.4912 (2016).

256 Ohashi, T. *et al.* Dichloroacetate improves immune dysfunction caused by tumor-secreted lactic acid and increases antitumor immunoreactivity. I*nt J Cancer* 1**33,** 1107-1118, doi:10.1002/ijc.28114 (2013).

257 Zambrano, A., Molt, M., Uribe, E. & Salas, M. Glut 1 in Cancer Cells and the Inhibitory Action of Resveratrol as A Potential Therapeutic Strategy. I*nt J Mol Sci* 2**0,** doi:10.3390/ijms20133374 (2019).

258 Chunhua, L. *et al.* Apigenin up-regulates transgelin and inhibits invasion and migration of colorectal cancer through decreased phosphorylation of AKT. J *Nutr Biochem* 2**4,** 1766-1775, doi:10.1016/j.jnutbio.2013.03.006 (2013).

259 Venditti, P., Di Stefano, L. & Di Meo, S. Mitochondrial metabolism of reactive oxygen species. M*itochondrion* 1**3,** 71-82, doi:10.1016/j.mito.2013.01.008 (2013).

260 Baysal, B. E. *et al.* Mutations in SDHD, a mitochondrial complex II gene, in hereditary paraganglioma. S*cience* 2**87,** 848-851, doi:10.1126/science.287.5454.848 (2000).

261 Xiao, M. *et al.* Inhibition of α-KG-dependent histone and DNA demethylases by fumarate and succinate that are accumulated in mutations of FH and SDH tumor suppressors. G*enes Dev* 2**6,** 1326-1338, doi:10.1101/gad.191056.112 (2012).

262 Yang, M., Soga, T. & Pollard, P. J. Oncometabolites: linking altered metabolism with cancer. J *Clin Invest* 1**23,** 3652-3658, doi:10.1172/JCI67228 (2013).

263 Wong, K. S., Bhandari, V., Janga, S. C. & Houry, W. A. The RavA-ViaA Chaperone-Like System Interacts with and Modulates the Activity of the Fumarate Reductase Respiratory Complex. J *Mol Biol* 4**29,** 324-344, doi:10.1016/j.jmb.2016.12.008 (2017).

264 Arnould, T. *et al.* CREB activation induced by mitochondrial dysfunction is a new signaling pathway that impairs cell proliferation. E*MBO J* 2**1,** 53-63, doi:10.1093/emboj/21.1.53 (2002).

265 Murphy, M. P. Mitochondrial dysfunction indirectly elevates ROS production by the endoplasmic reticulum. C*ell Metab* 1**8,** 145-146, doi:10.1016/j.cmet.2013.07.006 (2013).

266 Maddocks, O. D. *et al.* Serine starvation induces stress and p53-dependent metabolic remodelling in cancer cells. N*ature* 4**93,** 542-546, doi:10.1038/nature11743 (2013).

267 Keibler, M. A. *et al.* Metabolic requirements for cancer cell proliferation. C*ancer Metab* 4**,** 16, doi:10.1186/s40170-016-0156-6 (2016).

268 EAGLE, H., OYAMA, V. I., LEVY, M., HORTON, C. L. & FLEISCHMAN, R. The growth response of mammalian cells in tissue culture to L-glutamine and L-glutamic acid. J *Biol Chem* 2**18,** 607-616 (1956).

269 Kovacevic, Z. & McGivan, J. D. Mitochondrial metabolism of glutamine and glutamate and its physiological significance. P*hysiol Rev* 6**3,** 547-605, doi:10.1152/physrev.1983.63.2.547 (1983).

270 Reitzer, L. J., Wice, B. M. & Kennell, D. Evidence that glutamine, not sugar, is the major energy source for cultured HeLa cells. J *Biol Chem* 2**54,** 2669-2676 (1979).

271 Mullen, A. R. *et al.* Reductive carboxylation supports growth in tumour cells with defective mitochondria. N*ature* 4**81,** 385-388, doi:10.1038/nature10642 (2011).

272 Metallo, C. M. *et al.* Reductive glutamine metabolism by IDH1 mediates lipogenesis under hypoxia. N*ature* 4**81,** 380-384, doi:10.1038/nature10602 (2011).

273 Al-Mufti, F. *et al.* Novel management strategies for medically-refractory vasospasm following aneurysmal subarachnoid hemorrhage. J *Neurol Sci* 3**90,** 44-51, doi:10.1016/j.jns.2018.02.039 (2018).

274 DeBerardinis, R. J., Lum, J. J., Hatzivassiliou, G. & Thompson, C. B. The biology of cancer: metabolic reprogramming fuels cell growth and proliferation. C*ell Metab* 7**,** 11-20, doi:10.1016/j.cmet.2007.10.002 (2008).

275 Hensley, C. T., Wasti, A. T. & DeBerardinis, R. J. Glutamine and cancer: cell biology, physiology, and clinical opportunities. J *Clin Invest* 1**23,** 3678-3684, doi:10.1172/JCI69600 (2013).

276 Kappler, M. *et al.* Normoxic accumulation of HIF1α is associated with glutaminolysis. C*lin Oral Investig* 2**1,** 211-224, doi:10.1007/s00784-016-1780-9 (2017).

277 Kappler, M. *et al.* Causes and Consequences of A Glutamine Induced Normoxic HIF1 Activity for the Tumor Metabolism. I*nt J Mol Sci* 2**0,** doi:10.3390/ijms20194742 (2019).

278 Masson, N. & Ratcliffe, P. J. Hypoxia signaling pathways in cancer metabolism: the importance of co-selecting interconnected physiological pathways. C*ancer Metab* 2**,** 3, doi:10.1186/2049-3002-2-3 (2014).

279 Wohlrab, C. *et al.* The Association Between Ascorbate and the Hypoxia-Inducible Factors in Human Renal Cell Carcinoma Requires a Functional Von Hippel-Lindau Protein. F*ront Oncol* 8**,** 574, doi:10.3389/fonc.2018.00574 (2018).

280 DeBerardinis, R. J. *et al.* Beyond aerobic glycolysis: transformed cells can engage in glutamine metabolism that exceeds the requirement for protein and nucleotide synthesis. P*roc Natl Acad Sci U S A* 1**04,** 19345-19350, doi:10.1073/pnas.0709747104 (2007).

281 Gao, P. *et al.* c-Myc suppression of miR-23a/b enhances mitochondrial glutaminase expression and glutamine metabolism. N*ature* 4**58,** 762-765, doi:10.1038/nature07823 (2009).

282 Venkateswaran, N. *et al.* MYC promotes tryptophan uptake and metabolism by the kynurenine pathway in colon cancer. G*enes Dev* 3**3,** 1236-1251, doi:10.1101/gad.327056.119 (2019).

283 Nicklin, P. *et al.* Bidirectional transport of amino acids regulates mTOR and autophagy. C*ell* 1**36,** 521-534, doi:10.1016/j.cell.2008.11.044 (2009).

284 Shroff, E. H. *et al.* MYC oncogene overexpression drives renal cell carcinoma in a mouse model through glutamine metabolism. P*roc Natl Acad Sci U S A* 1**12,** 6539-6544, doi:10.1073/pnas.1507228112 (2015).

285 Johnson, M. O., Siska, P. J., Contreras, D. C. & Rathmell, J. C. Nutrients and the microenvironment to feed a T cell army. S*emin Immunol* 2**8,** 505-513, doi:10.1016/j.smim.2016.09.003 (2016).

286 Munn, D. H. & Mellor, A. L. Indoleamine 2,3 dioxygenase and metabolic control of immune responses. T*rends Immunol* 3**4,** 137-143, doi:10.1016/j.it.2012.10.001 (2013).

287 Currie, E., Schulze, A., Zechner, R., Walther, T. C. & Farese, R. V., Jr. Cellular fatty acid metabolism and cancer. C*ell Metab* 1**8,** 153-161, doi:10.1016/j.cmet.2013.05.017 (2013).

288 Gameiro, P. A. *et al.* In vivo HIF-mediated reductive carboxylation is regulated by citrate levels and sensitizes VHL-deficient cells to glutamine deprivation. C*ell Metab* 1**7,** 372-385, doi:10.1016/j.cmet.2013.02.002 (2013).

289 Du, W. *et al.* HIF drives lipid deposition and cancer in ccRCC via repression of fatty acid metabolism. N*at Commun* 8**,** 1769, doi:10.1038/s41467-017-01965-8 (2017).

290 Wang, L. *et al.* ECHS1 suppresses renal cell carcinoma development through inhibiting mTOR signaling activation. B*iomed Pharmacother* 1**23,** 109750, doi:10.1016/j.biopha.2019.109750 (2020).

291 Zhou, J. *et al.* Overexpression of FABP7 promotes cell growth and predicts poor prognosis of clear cell renal cell carcinoma. U*rol Oncol* 3**3,** 113.e119-117, doi:10.1016/j.urolonc.2014.08.001 (2015).

292 Levi, L., Wang, Z., Doud, M. K., Hazen, S. L. & Noy, N. Saturated fatty acids regulate retinoic acid signalling and suppress tumorigenesis by targeting fatty acid-binding protein 5. N*at Commun* 6**,** 8794, doi:10.1038/ncomms9794 (2015).

293 Marion-Letellier, R., Savoye, G. & Ghosh, S. Fatty acids, eicosanoids and PPAR gamma. E*ur J Pharmacol* 7**85,** 44-49, doi:10.1016/j.ejphar.2015.11.004 (2016).

294 Morgan, E., Kannan-Thulasiraman, P. & Noy, N. Involvement of Fatty Acid Binding Protein 5 and PPARβ/δ in Prostate Cancer Cell Growth. P*PAR Res* 2**010,** doi:10.1155/2010/234629 (2010).

295 Carbonetti, G. *et al.* FABP5 coordinates lipid signaling that promotes prostate cancer metastasis. S*ci Rep* 9**,** 18944, doi:10.1038/s41598-019-55418-x (2019).

296 Forootan, F. S. *et al.* Fatty acid activated PPARγ promotes tumorigenicity of prostate cancer cells by up regulating VEGF via PPAR responsive elements of the promoter. O*ncotarget* 7**,** 9322-9339, doi:10.18632/oncotarget.6975 (2016).

297 Kawaguchi, K. *et al.* High expression of Fatty Acid-Binding Protein 5 promotes cell growth and metastatic potential of colorectal cancer cells. F*EBS Open Bio* 6**,** 190-199, doi:10.1002/2211-5463.12031 (2016).

298 Wu, G. *et al.* Study of FABP's interactome and detecting new molecular targets in clear cell renal cell carcinoma. J *Cell Physiol* 2**35,** 3776-3789, doi:10.1002/jcp.29272 (2020).

299 Wu, G. *et al.* FABP5 is correlated with poor prognosis and promotes tumour cell growth and metastasis in clear cell renal cell carcinoma. E*ur J Pharmacol* 8**62,** 172637, doi:10.1016/j.ejphar.2019.172637 (2019).

300 Lv, Q. *et al.* FABP5 regulates the proliferation of clear cell renal cell carcinoma cells via the PI3K/AKT signaling pathway. I*nt J Oncol* 5**4,** 1221-1232, doi:10.3892/ijo.2019.4721 (2019).

301 Carbonetti, G. *et al.* Docetaxel/cabazitaxel and fatty acid binding protein 5 inhibitors produce synergistic inhibition of prostate cancer growth. P*rostate* 8**0,** 88-98, doi:10.1002/pros.23921 (2020).

302 Al-Jameel, W. *et al.* Inhibitor SBFI26 suppresses the malignant progression of castration-resistant PC3-M cells by competitively binding to oncogenic FABP5. O*ncotarget* 8**,** 31041-31056, doi:10.18632/oncotarget.16055 (2017).

303 Hervouet, E. *et al.* HIF and reactive oxygen species regulate oxidative phosphorylation in cancer. C*arcinogenesis* 2**9,** 1528-1537, doi:10.1093/carcin/bgn125 (2008).

304 Murphy, M. P. How mitochondria produce reactive oxygen species. B*iochem J* 4**17,** 1-13, doi:10.1042/bj20081386 (2009).

305 Brand, M. D. The sites and topology of mitochondrial superoxide production. E*xp Gerontol* 4**5,** 466-472, doi:10.1016/j.exger.2010.01.003 (2010).

306 Quinlan, C. L. *et al.* Mitochondrial complex II can generate reactive oxygen species at high rates in both the forward and reverse reactions. J *Biol Chem* 2**87,** 27255-27264, doi:10.1074/jbc.M112.374629 (2012).

307 Rhee, S. G., Woo, H. A., Kil, I. S. & Bae, S. H. Peroxiredoxin functions as a peroxidase and a regulator and sensor of local peroxides. J *Biol Chem* 2**87,** 4403-4410, doi:10.1074/jbc.R111.283432 (2012).

308 Cox, A. G., Winterbourn, C. C. & Hampton, M. B. Mitochondrial peroxiredoxin involvement in antioxidant defence and redox signalling. B*iochem J* 4**25,** 313-325, doi:10.1042/bj20091541 (2009).

309 Murphy, M. P. Mitochondrial thiols in antioxidant protection and redox signaling: distinct roles for glutathionylation and other thiol modifications. A*ntioxid Redox Signal* 1**6,** 476-495, doi:10.1089/ars.2011.4289 (2012).

310 Srinivasan, S. & Avadhani, N. G. Cytochrome c oxidase dysfunction in oxidative stress. F*ree Radic Biol Med* 5**3,** 1252-1263, doi:10.1016/j.freeradbiomed.2012.07.021 (2012).

311 Irani, K. *et al.* Mitogenic signaling mediated by oxidants in Ras-transformed fibroblasts. S*cience* 2**75,** 1649-1652, doi:10.1126/science.275.5306.1649 (1997).

312 Chandel, N. S. *et al.* Mitochondrial reactive oxygen species trigger hypoxia-induced transcription. P*roc Natl Acad Sci U S A* 9**5,** 11715-11720, doi:10.1073/pnas.95.20.11715 (1998).

313 Connor, K. M. *et al.* Manganese superoxide dismutase enhances the invasive and migratory activity of tumor cells. C*ancer Res* 6**7,** 10260-10267, doi:10.1158/0008-5472.can-07-1204 (2007).

314 Soini, Y. *et al.* Oxidative/nitrosative stress and peroxiredoxin 2 are associated with grade and prognosis of human renal carcinoma. A*pmis* 1**14,** 329-337, doi:10.1111/j.1600-0463.2006.apm_315.x (2006).

315 Pljesa-Ercegovac, M. *et al.* Altered antioxidant capacity in human renal cell carcinoma: role of glutathione associated enzymes. U*rol Oncol* 2**6,** 175-181, doi:10.1016/j.urolonc.2007.02.007 (2008).

316 van Zandwijk, N., Dalesio, O., Pastorino, U., de Vries, N. & van Tinteren, H. EUROSCAN, a randomized trial of vitamin A and N-acetylcysteine in patients with head and neck cancer or lung cancer. For the EUropean Organization for Research and Treatment of Cancer Head and Neck and Lung Cancer Cooperative Groups. J *Natl Cancer Inst* 9**2,** 977-986, doi:10.1093/jnci/92.12.977 (2000).

317 Klein, E. A. *et al.* Vitamin E and the risk of prostate cancer: the Selenium and Vitamin E Cancer Prevention Trial (SELECT). J*ama* 3**06,** 1549-1556, doi:10.1001/jama.2011.1437 (2011).

318 Watson, J. Oxidants, antioxidants and the current incurability of metastatic cancers. O*pen Biol* 3**,** 120144, doi:10.1098/rsob.120144 (2013).

319 Pavlović, I. *et al.* The effect of antioxidant status on overall survival in renal cell carcinoma. A*rch Med Sci* 1**6,** 94-101, doi:10.5114/aoms.2019.86818 (2020).

320 Corbet, C. & Feron, O. Tumour acidosis: from the passenger to the driver's seat. N*at Rev Cancer* 1**7,** 577-593, doi:10.1038/nrc.2017.77 (2017).

321 Romero-Garcia, S., Moreno-Altamirano, M. M., Prado-Garcia, H. & Sánchez-García, F. J. Lactate Contribution to the Tumor Microenvironment: Mechanisms, Effects on Immune Cells and Therapeutic Relevance. F*ront Immunol* 7**,** 52, doi:10.3389/fimmu.2016.00052 (2016).

322 Sauvant, C. *et al.* Acidosis induces multi-drug resistance in rat prostate cancer cells (AT1) in vitro and in vivo by increasing the activity of the p-glycoprotein via activation of p38. I*nt J Cancer* 1**23,** 2532-2542, doi:10.1002/ijc.23818 (2008).

323 Wachsberger, P. R. *et al.* Mammalian cells adapted to growth at pH 6.7 have elevated HSP27 levels and are resistant to cisplatin. I*nt J Hyperthermia* 1**3,** 251-255; discussion 257-259, doi:10.3109/02656739709023533 (1997).

324 Lee, H. S. *et al.* Radiation-induced apoptosis in different pH environments in vitro. I*nt J Radiat Oncol Biol Phys* 3**8,** 1079-1087, doi:10.1016/s0360-3016(97)00073-4 (1997).

325 Park, H. J. *et al.* Influence of environmental pH on G2-phase arrest caused by ionizing radiation. R*adiat Res* 1**59,** 86-93, doi:10.1667/0033-7587(2003)159[0086:ioepog]2.0.co;2 (2003).

326 Phua, L. C. *et al.* Metabolomic prediction of treatment outcome in pancreatic ductal adenocarcinoma patients receiving gemcitabine. C*ancer Chemother Pharmacol* 8**1,** 277-289, doi:10.1007/s00280-017-3475-6 (2018).

327 Walenta, S. *et al.* High lactate levels predict likelihood of metastases, tumor recurrence, and restricted patient survival in human cervical cancers. C*ancer Res* 6**0,** 916-921 (2000).

328 Walenta, S., Schroeder, T. & Mueller-Klieser, W. Lactate in solid malignant tumors: potential basis of a metabolic classification in clinical oncology. C*urr Med Chem* 1**1,** 2195-2204, doi:10.2174/0929867043364711 (2004).

329 Shih, C. C. *et al.* Pretreatment serum lactate level as a prognostic biomarker in patients undergoing supratentorial primary brain tumor resection. O*ncotarget* 8**,** 63715-63723, doi:10.18632/oncotarget.18891 (2017).

330 Yuan, Z. Y. *et al.* Prognostic value of preoperative serum lactate dehydrogenase in thymic carcinoma. J *Thorac Dis* 8**,** 2464-2472, doi:10.21037/jtd.2016.08.56 (2016).

331 Martens, A. *et al.* Baseline Peripheral Blood Biomarkers Associated with Clinical Outcome of Advanced Melanoma Patients Treated with Ipilimumab. C*lin Cancer Res* 2**2,** 2908-2918, doi:10.1158/1078-0432.ccr-15-2412 (2016).

332 Damuzzo, V. *et al.* Clinical implication of tumor-associated and immunological parameters in melanoma patients treated with ipilimumab. O*ncoimmunology* 5**,** e1249559, doi:10.1080/2162402x.2016.1249559 (2016).

333 Husain, Z., Huang, Y., Seth, P. & Sukhatme, V. P. Tumor-derived lactate modifies antitumor immune response: effect on myeloid-derived suppressor cells and NK cells. J *Immunol* 1**91,** 1486-1495, doi:10.4049/jimmunol.1202702 (2013).

334 Loeffler, D. A., Juneau, P. L. & Heppner, G. H. Natural killer-cell activity under conditions reflective of tumor micro-environment. I*nt J Cancer* 4**8,** 895-899, doi:10.1002/ijc.2910480617 (1991).

335 Errea, A. *et al.* Lactate Inhibits the Pro-Inflammatory Response and Metabolic Reprogramming in Murine Macrophages in a GPR81-Independent Manner. P*LoS One* 1**1,** e0163694, doi:10.1371/journal.pone.0163694 (2016).

336 Chirasani, S. R. *et al.* Diclofenac inhibits lactate formation and efficiently counteracts local immune suppression in a murine glioma model. I*nt J Cancer* 1**32,** 843-853, doi:10.1002/ijc.27712 (2013).

337 Nasi, A. *et al.* Dendritic cell reprogramming by endogenously produced lactic acid. J *Immunol* 1**91,** 3090-3099, doi:10.4049/jimmunol.1300772 (2013).

338 Longo, D. L. *et al.* A general MRI-CEST ratiometric approach for pH imaging: demonstration of in vivo pH mapping with iobitridol. J *Am Chem Soc* 1**36,** 14333-14336, doi:10.1021/ja5059313 (2014).

339 Longo, D. L. *et al.* In Vivo Imaging of Tumor Metabolism and Acidosis by Combining PET and MRI-CEST pH Imaging. C*ancer Res* 7**6,** 6463-6470, doi:10.1158/0008-5472.CAN-16-0825 (2016).

340 Chen, L. Q. *et al.* Evaluations of Tumor Acidosis Within In Vivo Tumor Models Using Parametric Maps Generated with Acido CEST MRI. M*ol Imaging Biol* 1**7,** 488-496, doi:10.1007/s11307-014-0816-2 (2015).

341 Chen, M. *et al.* Extracellular pH is a biomarker enabling detection of breast cancer and liver cancer using CEST MRI. O*ncotarget* 8**,** 45759-45767, doi:10.18632/oncotarget.17404 (2017).

342 Zhang, L. *et al.* Imaging Extracellular Lactate In Vitro and In Vivo Using CEST MRI and a Paramagnetic Shift Reagent. C*hemistry* 2**3,** 1752-1756, doi:10.1002/chem.201604558 (2017).

343 Madan, A. *et al.* Proton T2 measurement and quantification of lactate in brain tumors by MRS at 3 Tesla in vivo. M*agn Reson Med* 7**3,** 2094-2099, doi:10.1002/mrm.25352 (2015).

344 Semenza, G. L. Tumor metabolism: cancer cells give and take lactate. J *Clin Invest* 1**18,** 3835-3837, doi:10.1172/JCI37373 (2008).

345 Corrò, C. & Moch, H. Biomarker discovery for renal cancer stem cells. J *Pathol Clin Res* 4**,** 3-18, doi:10.1002/cjp2.91 (2018).

346 Peiris-Pagès, M., Martinez-Outschoorn, U. E., Pestell, R. G., Sotgia, F. & Lisanti, M. P. Cancer stem cell metabolism. B*reast Cancer Res* 1**8,** 55, doi:10.1186/s13058-016-0712-6 (2016).

347 Sancho, P., Barneda, D. & Heeschen, C. Hallmarks of cancer stem cell metabolism. B*r J Cancer* 1**14,** 1305-1312, doi:10.1038/bjc.2016.152 (2016).

348 DeBerardinis, R. J. & Chandel, N. S. Fundamentals of cancer metabolism. S*ci Adv* 2**,** e1600200, doi:10.1126/sciadv.1600200 (2016).

349 Gershenwald, J. E. *et al.* Melanoma staging: Evidence-based changes in the American Joint Committee on Cancer eighth edition cancer staging manual. C*A Cancer J Clin* 6**7,** 472-492, doi:10.3322/caac.21409 (2017).

350 Kelderman, S. *et al.* Lactate dehydrogenase as a selection criterion for ipilimumab treatment in metastatic melanoma. C*ancer Immunol Immunother* 6**3,** 449-458, doi:10.1007/s00262-014-1528-9 (2014).

351 Li, G. *et al.* The prognostic value of lactate dehydrogenase levels in colorectal cancer: a meta-analysis. B*MC Cancer* 1**6,** 249, doi:10.1186/s12885-016-2276-3 (2016).

352 Liu, R. *et al.* Overall survival of cancer patients with serum lactate dehydrogenase greater than 1000 IU/L. T*umour Biol* 3**7,** 14083-14088, doi:10.1007/s13277-016-5228-2 (2016).

353 Rizwan, A. *et al.* Relationships between LDH-A, lactate, and metastases in 4T1 breast tumors. C*lin Cancer Res* 1**9,** 5158-5169, doi:10.1158/1078-0432.ccr-12-3300 (2013).

354 Baumann, F. *et al.* Lactate promotes glioma migration by TGF-beta2-dependent regulation of matrix metalloproteinase-2. N*euro Oncol* 1**1,** 368-380, doi:10.1215/15228517-2008-106 (2009).

355 Koltai, T. Cancer: fundamentals behind pH targeting and the double-edged approach. O*nco Targets Ther* 9**,** 6343-6360, doi:10.2147/OTT.S115438 (2016).

356 Morais-Santos, F. *et al.* Targeting lactate transport suppresses in vivo breast tumour growth. O*ncotarget* 6**,** 19177-19189, doi:10.18632/oncotarget.3910 (2015).

357 Schneiderhan, W. *et al.* CD147 silencing inhibits lactate transport and reduces malignant potential of pancreatic cancer cells in in vivo and in vitro models. G*ut* 5**8,** 1391-1398, doi:10.1136/gut.2009.181412 (2009).

358 Beloueche-Babari, M. *et al.* MCT1 Inhibitor AZD3965 Increases Mitochondrial Metabolism, Facilitating Combination Therapy and Noninvasive Magnetic Resonance Spectroscopy. C*ancer Res* 7**7,** 5913-5924, doi:10.1158/0008-5472.CAN-16-2686 (2017).

359 Vishvakarma, N. K. & Singh, S. M. Immunopotentiating effect of proton pump inhibitor pantoprazole in a lymphoma-bearing murine host: Implication in antitumor activation of tumor-associated macrophages. I*mmunol Lett* 1**34,** 83-92, doi:10.1016/j.imlet.2010.09.002 (2010).

360 Vishvakarma, N. K. & Singh, S. M. Augmentation of myelopoiesis in a murine host bearing a T cell lymphoma following in vivo administration of proton pump inhibitor pantoprazole. B*iochimie* 9**3,** 1786-1796, doi:10.1016/j.biochi.2011.06.022 (2011).

361 Calcinotto, A. *et al.* Modulation of microenvironment acidity reverses anergy in human and murine tumor-infiltrating T lymphocytes. C*ancer Res* 7**2,** 2746-2756, doi:10.1158/0008-5472.CAN-11-1272 (2012).

362 Noma, N. *et al.* Impact of Acetazolamide, a Carbonic Anhydrase Inhibitor, on the Development of Intestinal Polyps in Min Mice. I*nt J Mol Sci* 1**8,** doi:10.3390/ijms18040851 (2017).

363 Parkkila, S. *et al.* Carbonic anhydrase inhibitor suppresses invasion of renal cancer cells in vitro. P*roc Natl Acad Sci U S A* 9**7,** 2220-2224, doi:10.1073/pnas.040554897 (2000).

364 Pilon-Thomas, S. *et al.* Neutralization of Tumor Acidity Improves Antitumor Responses to Immunotherapy. C*ancer Res* 7**6,** 1381-1390, doi:10.1158/0008-5472.CAN-15-1743 (2016).

365 Robey, I. F. *et al.* Bicarbonate increases tumor pH and inhibits spontaneous metastases. C*ancer Res* 6**9,** 2260-2268, doi:10.1158/0008-5472.CAN-07-5575 (2009).

366 Sethumadhavan, S. *et al.* Hypoxia and hypoxia-inducible factor (HIF) downregulate antigen-presenting MHC class I molecules limiting tumor cell recognition by T cells. P*LoS One* 1**2,** e0187314, doi:10.1371/journal.pone.0187314 (2017).

# 9 Eigenständigkeitserklärung

Hiermit erkläre ich an Eides statt, dass ich die vorliegende Dissertation selbstständig und ausschließlich unter Verwendung der angegebenen Quellen und Hilfsmittel angefertigt habe. Wörtlich oder inhaltlich entnommene Literaturstellen sind als solche gekennzeichnet. Diese Arbeit wurde bisher weder an der Martin-Luther-Universität Halle-Wittenberg, noch an einer anderen Bildungseinrichtung zur Erlangung eines akademischen Grades eingereicht.

Schkeuditz, 10. März 2021 _____

Sandra Leisz

# 10 Lebenslauf

## 10.1 Persönliche Daten

| | |
|---|---|
| Name, Vorname: | Leisz, Sandra (Dipl.-Biol.) |
| Geburtsdatum, -ort: | 02.09.1983, Schkeuditz |
| Familienstand: | verheiratet |
| Kinder: | 2 Töchter, 1 Sohn |

## 10.2 Wissenschaftlicher Werdegang

| | |
|---|---|
| Seit 09/17 | Laborleiterin der Klinik für Neurochirurgie, Medizinische Fakultät, Martin-Luther-Universität Halle-Wittenberg, Themenschwerpunkte: Analyse neuroprotektiver Substanzen; Identifizierung von Tumormarkern im Vestibularisschwannom |
| 09/18 bis 07/19 | Mutterschutz und Elternzeit |
| 05/16 bis 08/17 | Mutterschutz und Elternzeit |
| 08/10 bis 04/16 | Promotionsstudium am Institut für Medizinische Immunologie, Medizinische Fakultät, Martin-Luther-Universität Halle-Wittenberg mit dem Thema: „Von Hippel-Lindau-, cAMP-responsives Element-bindendes Protein- und Hypoxie-abhängige Veränderungen im Metabolismus des Nierenzellkarzinoms“ unter der Leitung von Frau Prof. Dr. Seliger |
| 05/10 bis 07/10 | Wissenschaftliche Hilfskraft am Institut für Medizinische Immunologie, Medizinische Fakultät, Martin-Luther-Universität Halle-Wittenberg |
| 05/09 bis 04/10 | Diplomarbeit: „Bedeutung der Biglycanexpression für die K-RAS- und HER-2/neu-induzierte onkogene Transformation“ am Institut für Medizinische Immunologie unter der Leitung von Frau Prof. Dr. Seliger |
| 10/05 bis 04/10 | Hauptstudium Biologie, Martin-Luther-Universität Halle-Wittenberg<br>Hauptfach: Genetik<br>Nebenfächer: Immunologie, Biotechnologie, Pflanzenphysiologie |
| 08/08 bis 10/08 | Studentische Hilfskraft am Institut für Pflanzengenetik, Naturwissenschaftliche Fakultät I, Martin-Luther-Universität Halle-Wittenberg, Themenschwerpunkt: Identifizierung von *avrBs3*-ähnlichen Genen in *Ralstonia solanacearum* |
| 10/06 bis 09/07 | Mutterschutz und Elternzeit |
| 10/03 bis 09/05 | Grundstudium Biologie, Georg-August-Universität Göttingen |
| 10/02 bis 09/03 | Chemiestudium, Universität Leipzig |

### 10.3 Schulausbildung

| | |
|---|---|
| 09/94 bis 06/02 | Gymnasium Schkeuditz |
| | Allgemeine Hochschulreife |
| | Leistungskursfächer: Biologie, Deutsch |
| 09/90 bis 08/94 | Thomas-Müntzer-Grundschule Schkeuditz |

Schkeuditz, 10. März 2021 _____

Sandra Leisz

# 11 Publikationen, Vorträge und Fortbildungen

## 11.1 Publikationen

Scheller C, Rampp S, **Leisz S**, Tatagiba M, Gharabaghi A, Ramina KF, Ganslandt O, Matthies C, Westermaier T, Antoniadis G, Pedro MT, Rohde V, von Eckardstein K, Scheller K, Strauss C. Prophylactic nimodipine treatment improves hearing outcome after vestibular schwannoma surgery in men: a subgroup analysis of a randomized multicenter phase III trial. *Neurosurg Rev*. 2020 Aug 22.

**Leisz S**, Trutschel ML, Mäder K, Scheller C, Strauss C, Simmermacher S. Tabotamp®, Respectively, Surgicel®, Increases the Cell Death of Neuronal and Glial Cells In Vitro. *Materials* (Basel). 2020 May 28;13(11):2453.

Zech J, **Leisz S**, Göttel B, Syrowatka F, Greiner A, Strauss C, Knolle W, Scheller C, Mäder K. Electrospun Nimodipine-loaded fibers for nerve regeneration: Development and in vitro performance. *Eur J Pharm Biopharm*. 2020 Jun;151:116-126.

**Leisz S**, Simmermacher S, Prell J, Strauss C, Scheller C. Nimodipine-Dependent Protection of Schwann Cells, Astrocytes and Neuronal Cells from Osmotic, Oxidative and Heat Stress Is Associated with the Activation of AKT and CREB. *Int J Mol Sci*. 2019 Sep 16;20(18):4578.

Steven A, **Leisz S**, Fussek S, Nowroozizadeh B, Huang J, Branstetter D, Dougall WC, Burchardt M, Belldegrun AS, Seliger B, Pantuck A, Kroeger N. Receptor activator of NF-κB (RANK)-mediated induction of metastatic spread and association with poor prognosis in renal cell carcinoma. *Urol Oncol*. 2018 Nov;36(11):502.e15-502.e24.

Subbarayan K, **Leisz S**, Wickenhauser C, Bethmann D, Massa C, Steven A, Seliger B. Biglycan-mediated upregulation of MHC class I expression in HER-2/neu-transformed cells. *Oncoimmunology*. 2018 Jan 16;7(4):e1373233.

Steven A, **Leisz S**, Wickenhauser C, Schulz K, Mougiakakos D, Kiessling R, Denkert C, Seliger B. Linking CREB function with altered metabolism in murine fibroblast-based model cell lines. *Oncotarget*. 2017 Oct 27;8(57):97439-97463.

Steven A, **Leisz S**, Synchra K, Hiebl B, Wickenhauser C, Mougiakakos D, Kiessling R, Denkert C, Seliger B. Hypoxia-mediated alterations and their role in the HER-2/neu regulated CREB status and localization. *Oncotarget*. 2016 Aug 9;7(32):52061-52084.

Stehle F, **Leisz S**, Schulz K, Schwurack N, Weber N, Massa C, Kalich J, Fahldieck C, Seliger B. VHL-dependent alterations in the secretome of renal cell carcinoma: Association with immune cell response? *Oncotarget*. 2015 Dec 22;6(41):43420-37.

**Leisz S**, Schulz K, Erb S, Oefner P, Dettmer K, Mougiakakos D, Wang E, Marincola FM, Stehle F, Seliger B. Distinct von Hippel-Lindau gene and hypoxia-regulated alterations in gene and protein expression patterns of renal cell carcinoma and their effects on metabolism. *Oncotarget*. 2015 May 10;6(13):11395-406.

Steven A, **Leisz S**, Massa C, Iezzi M, Lattanzio R, Lamolinara A, Bukur J, Müller A, Hiebl B, Holzhausen HJ, Seliger B. HER-2/neu mediates oncogenic transformation via altered CREB expression and function. *Mol Cancer Res*. 2013 Nov;11(11):1462-77.

Recktenwald CV*, **Leisz S***, Steven A, Mimura K, Müller A, Wulfänger J, Kiessling R, Seliger B. HER-2/neu-mediated down-regulation of biglycan associated with altered growth properties. *J Biol Chem*. 2012 Jul 13;287(29):24320-9.

*Both authors contributed equally to this manuscript.

### 11.2 Ausgewählte Poster

**Leisz S**, Schulz K, Erb S, Oefner P, Dettmer K, Mougiakakos D, Wang E, Marincola FM, Stehle F, Seliger B. Von Hippel-Lindau gene and hypoxia-regulated alterations in gene and protein expression patterns of renal cell carcinoma and their effects on cell metabolism. Keystone Symposia “Hypoxia: From Basic Mechanisms to Therapeutics”, 2015, Dublin, Irland

**Leisz S**, Schulz K, Oefner P, Dettmer K, Mougiakakos D, Wang E, Marincola FM, Stehle F, Seliger B. Von Hippel-Lindau gene and hypoxia-regulated alterations in gene and protein expression patterns of renal cell carcinoma and their effects on cell metabolism and immune cell response. Doktorandenkongress 2015, Halle (Saale)

Seliger B, **Leisz S**, Schulz K, Erb, Wang E, Marincola FM, Stehle F. Discrimination between Von Hippel-Lindau gene and hypoxia-regulated alterations in the metabolism and protein expression in renal cell carcinoma using ome-based strategies. ASCO 2014 Genitourinary Cancers Symposium, San Francisco, DOI: 10.1200/jco.2014.32.4_suppl.447

**Leisz S**, Schulz K, Oefner P, Dettmer K, Mougiakakos D, Wang E, Marincola FM, Stehle F, Seliger B. VHL- and hypoxia-mediated alterations in the metabolism of renal cell carcinoma, Forschungstag 2014, Halle (Saale)

**Leisz S**, Stehle F, Schulz K, Erb S, Seliger B. VHL and the Warburg effect in renal cell carcinoma. Symposium „Tumor Metabolism meets Immunology“, 2013, Regensburg

**Leisz S**, Stehle F, Erb S, Schulz K, Seliger B. Characterization of the altered metabolism in renal cell carcinoma. International Meeting GRK1591 - Posttranscriptional Control of Gene Expression: Mechanisms and Role in Pathogenesis, 2012, Halle (Saale)

**Leisz S**, Erb S, Leich F, Müller A, Seliger B. Hypoxia-induced alterations of renal cell carcinoma and their modulation by tyrosine kinase inhibitors, AACR 2012, Chicago, DOI: 10.1158/1538-7445.AM2012-1799

### 11.3 Ausgewählte Vorträge

**Leisz S**, Seliger B. Von Hippel-Lindau-mediated alterations in the metabolism of renal cell carcinoma. Retreat GRK1591 - Posttranscriptional Control of Gene Expression: Mechanisms and Role in Pathogenesis, 2015, Freyburg

Steven A, **Leisz S**, Hiebl B, Bedognetti D, Wickenhauser C, Kiessling R, Seliger B. Alterations Of The Tumor Microenvironment By Her-2-neu-induced Creb Activation And Localization And Hypoxia, Qatar Foundation Annual Research Conference 2014, Doha, Katar, DOI: 10.5339/qfarc.2014.HBOP0794

**Leisz S**, Recktenwald CV, Seliger B. Impact of biglycan on HER-2/neu-driven oncogenic transformation. Symposium „Tumor Immunology meets Oncology VIII“, 2012, Halle (Saale)

### 11.4 Auszeichnung

ImmunoTools Award Gewinner 2013
(http://www.immunotools.de/html/award/SandraLeisz.pdf)

### 11.5 Fortbildungen

| | |
|---|---|
| 01/12 bis 04/16 | Assoziiertes Mitglied des Graduiertenkollegs 1591 “Posttranskriptionelle Regulation der Genexpression: Mechanismen und Rolle in der Pathogenese“ unter der Leitung von Prof. Dr. Stefan Hüttelmaier, |

| | |
|---|---|
| | Zentrum für Angewandte Medizinische und Humanbiologische Forschung (ZAMED), Martin-Luther-Universität Halle-Wittenberg |
| 04/16 | Retreat GRK 1591, Quedlinburg |
| 04/15 | Retreat GRK 1591, Freyburg |
| 12/14 | Workshop GRK1591 „Writing paper“, Halle (Saale) (mit Zertifikat) |
| 11/14 | Retreat GRK 1591, Freyburg |
| 07/14 | Erlernen von metabolischen Analysen mittels des „Seahorse Analyzer“, Institut für Hämatologie und internistische Onkologie, Universitätsklinikum Erlangen |
| 11/13 | Workshop Serva Electrophoresis GmbH „Theoretische Grundlagen und praktische Aspekte der Proteinelektrophorese“, Halle (Saale) |
| 07/13 | Workshop GRK1591 „Scientific writing“, Halle (Saale) |
| 05/13 | Workshop GRK1591 „A programmable DNA-binding domain", Halle (Saale) |
| 12/12 | Retreat GRK 1591, Halle (Saale) |
| 09/12 | Workshop GRK1591 „Breath control“, Halle (Saale) |
| 09/12 | Workshop GRK1591 „Protein purification“, Halle (Saale) |
| 08/12 | Workshop GRK1591 „Flow cytometry“, Halle (Saale) |
| 05/12 | Teilnahme am Kurs „Einführung in die Statistiksoftware SPSS“, Institut für Epidemiologie, Martin-Luther-Universität Halle-Wittenberg |
| 04/12 | Erfolgreicher Abschluss der Weiterbildungsveranstaltung „Tierschutz/Versuchstierkunde“ für tierexperimentell tätige Mitarbeiter und Doktoranden (Sachkundenachweis), Tierschutzkommission des Rektorates, Martin-Luther-Universität Halle-Wittenberg |
| 02/12 | Retreat GRK 1591, Oppurg |
| 06/11 | Workshop GRK1591 „Good scientific practice", Halle (Saale) |
| 12/10 | Workshop GRK1591 „How to give an oral presentation", Halle (Saale) |

# 12 Danksagung

Die Arbeiten zu den zusammengefassten Manuskripten wurden in der Zeit von September 2010 bis April 2016 am Institut für Medizinische Immunologie durchgeführt.

Dabei möchte ich zuerst Frau Prof. Barbara Seliger, für die sehr gute wissenschaftliche Betreuung, die stetige Unterstützung während dieser Zeit sowie die Möglichkeit diese Dissertation anfertigen zu können, danken. Ich bin sehr dankbar für das vielfältige Methodenspektrum, welches ich vorwiegend im Institut und auch durch die Assoziation mit dem GRK 1591 unter der Leitung von Prof. Stefan Hüttelmaier erlernen durfte.

Mein besonderer Dank geht an Herrn Prof. Hans-Hinrich Kaatz, der auch nach dieser langen Zeit bereit war das Gutachten zu übernehmen und mich gerade in der letzten Phase dieser Arbeit sehr unterstützt hat. Vielen Dank für Ihre unkomplizierte Bereitschaft und ihr offenes Ohr.

Frau Prof. Marina Kreutz danke ich für die Übernahme des externen Gutachtens und für die Publikationen ihrer spannenden Daten, welche für die Diskussion dieser Arbeit sehr hilfreich waren.

Ich danke allen ehemaligen Kolleginnen und Kollegen, die mich begleitet haben und mit denen ich bis heute freundschaftlich verbunden bin. Vor allem danke ich Christian, Susanne, André und Jens für ihre Mentorentätigkeit, die Weitergabe ihres Wissens und die stetige Motivation. Franzi, Rudi und Kristin danke ich für die Unterstützung bei den 2D-Gel-Analysen.

Ein zusätzlicher Dank geht an Diana W., Björn, Nicole, Anja T., Maria, Nancy und Sven, Jürgen und Diana H., Anja M., Katha und Sylvi für die lustige Zeit, auch außerhalb des Institutes.

Weiterhin danke ich allen Beteiligten für die Geduld, die mir mit dieser Arbeit entgegengebracht wurde, vor allem danke ich diesbezüglich Prof. Christian Strauss und apl. Prof. Christian Scheller (steter Tropfen höhlt den Stein).

Den Studenten und Doktoranden, vor allem Karthik, Elena, Lasse, Sabrina und Sandra, die ich während meiner Promotionszeit selbst betreuen durfte, danke ich für das Interesse an den Projekten und das entgegengebrachte Vertrauen.
Das größte Dankeschön geht allerdings an meine Eltern, meine Schwiegereltern, meinen Mann Sven und meine Kinder Sarah, Sina und Karl. Ihr wisst, ich bin kein Mensch der großen Worte! Deswegen kurz und knapp: Ohne **Euch** hätte ich das nicht geschafft!!! Danke!

# 13 Anhang

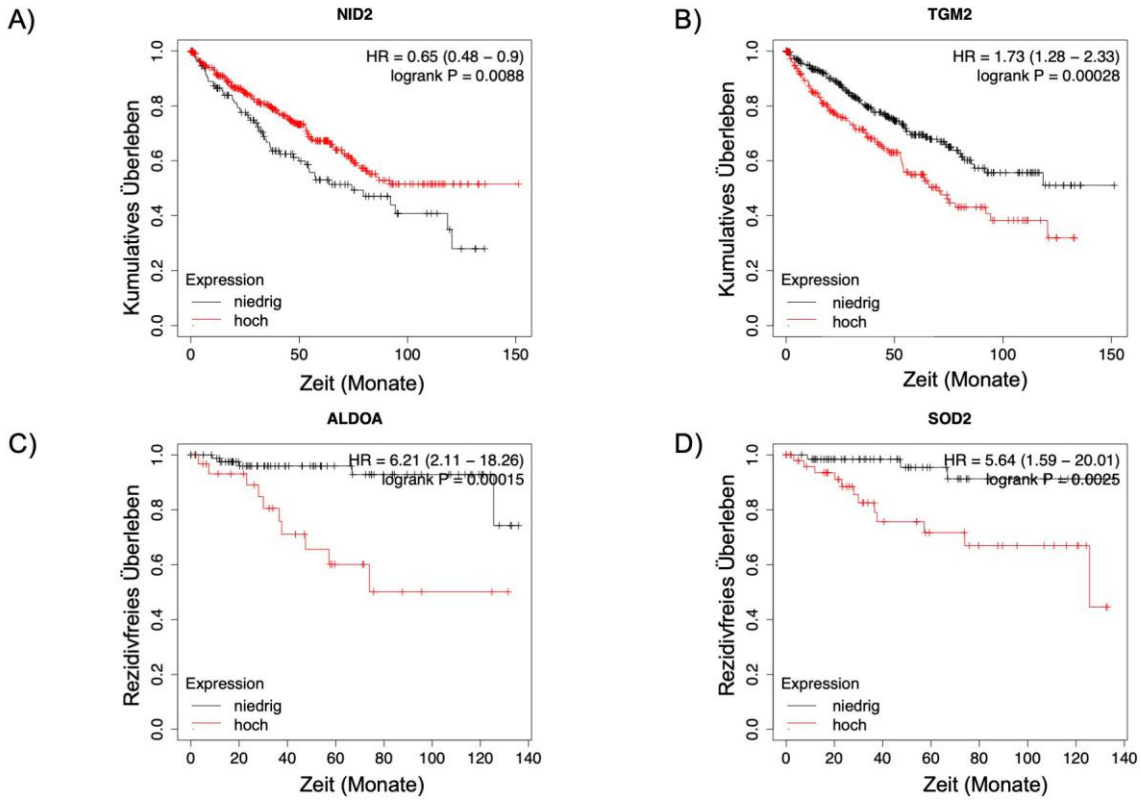


**Anhang Abbildung 1: Kaplan-Meier-Überlebenskurven**
Erstellt mit Kaplan-Meier Plotter

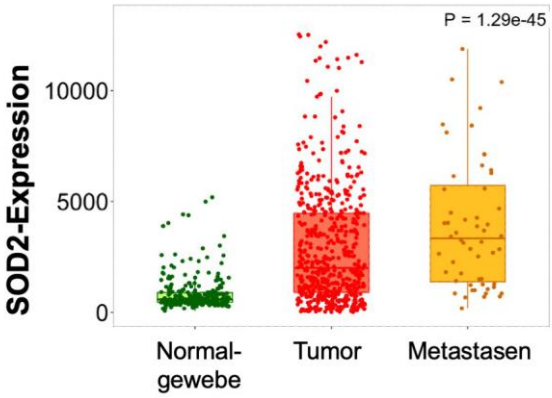


**Anhang Abbildung 2: SOD2-Expressionsanalyse**
Erstellt mit TNMplot.com